Nuclear reactions in the Gamow shell model and solutions of the pairing Hamiltonian based on the rational Gaudin model

Alexis Mercenne

Normandie Université

THESE

Pour obtenir le diplôme de doctorat

Spécialité : Physique

Préparée au sein de l'Université de Caen - Normandie

Réactions nucléaires dans le modèle en couches de Gamow et solutions de l'Hamiltonien d'appariement basées sur le modèle rationnel de Gaudin

Présentée et soutenue par
Alexis Mercenne

Thèse soutenue publiquement le 28 novembre 2016 devant le jury composé de		
M. Morten Hjorth-Jensen	Professeur, University of Oslo, Norway and Michigan State University, East Lansing, MI, USA	Rapporteur
M. Denis Lacroix	Directeur de recherche CNRS, IPNO, Orsay, France	Rapporteur
Me. Francesca Gulminelli	Professeure, Université de Caen - Normandie, LPC Caen, France	Examinateur
M. Marek Płoszajczak	Directeur de recherche CEA, GANIL, Caen, France	Directeur de thèse

Thèse dirigée par Marek PLOSZAJCZAK, GANIL

GANIL T 2016 04

UNIVERSITÉ CAEN NORMANDIE

GANIL laboratoire commun CEA/DSM spiral2 CNRS/IN2P3

Université de Caen-Normandie
U.F.R. de Sciences
ÉCOLE DOCTORALE SIMEM

Thèse de doctorat

présentée et soutenue le : 28 Novembre 2016
par

M. Alexis Mercenne

pour obtenir le

DOCTORAT de l'UNIVERSITÉ de CAEN-NORMANDIE

Spécialité : Constituants élémentaires et physique théorique

Réactions nucléaires dans le modèle en couches de Gamow et solutions de l'Hamiltonien d'appariement basées sur le modèle rationnel de Gaudin

MEMBRES du JURY :

M. Morten Hjorth-Jensen (***Rapporteur***)
Professeur, University of Oslo, Norway and Michigan State University, East Lansing, MI, USA

M. Denis Lacroix (***Rapporteur***)
Directeur de recherche CNRS, IPNO, Orsay, France

Me. Francesca Gulminelli
Professeure, Université de Caen-Normandie, LPC Caen, France

M. Marek Płoszajczak (***Directeur de thèse***)
Directeur de recherche CEA, GANIL, Caen, France

Remerciements

Et voilà, voici la dernière partie à écrire, et qui par ailleurs sera certainement la première à être lue par les futurs lecteurs. Donc je vais essayer de faire court. Mettre sur papier mes remerciements ne devrait pas être la partie la plus difficile de cette thèse, je pense, même s'il me semble que l'un de mes prédécesseurs est toujours en train d'y travailler.

Mes premiers remerciements, formels mais sincères, vont aux membres du jury, Francesca Gulminelli, Denis Lacroix et Morten Hjorth-Jensen, pour leur travail de lecture et d'évaluation de mon manuscrit, mais aussi pour leurs chaleureux encouragements.

Ensuite, je tiens à remercier mon directeur de thèse Marek Płoszajczak, pour le sérieux de son indéfectible encadrement, mais aussi pour sa gentillesse et sa bonne humeur constante au cours de ces dernières années passées à travailler avec lui. Travailler avec Marek sur le continuum signifie aussi intégrer un groupe de personnes, principalement composé de ses anciens étudiants, avec qui j'ai pu nouer des liens. Ainsi, merci à Kévin et Nicolas qui m'auront initié, chacun à leur manière, à ce domaine de recherche mais aussi apporté une aide indispensable lors des moments difficiles. Je salue également Yannen et Jimmy pour les quelques instants qu'on a pu passer ensemble lorsqu'ils étaient de retour en France. Une pensée aussi pour Guoxiang qui aura passé une année à travailler avec nous.

Un grand merci aussi à mes deux lapins Bart et Fabien, qui auront grandement participé à rendre cette dernière année de thèse moins pénible qu'elle n'aurait dû l'être. Je souhaite au premier, bonne chance (oui, il en faut) et surtout bon courage pour sa dernière année, et au second tous mes meilleurs souhaits de réussite pour ce qu'il entreprendra.

Au GANIL, je souhaite également remercier l'équipe des physiciens, dont notamment François De Oliveira Santos, Piet Van Isacker, Beyhan Bastin, David Boilley, Abdelhouahad Chbihi, et le tout nouveau directeur du GANIL, Navin Alahari. Merci aussi au personnel technique et administratif du GANIL qui m'aura beaucoup aidé sur certaines tâches annexes durant ma thèse : merci à Guillaume Lalaire, Nicolas Ménard, Virginie Lefebvre, Sabrina Lecerf-Rossard, Michel Lion, et ceux que j'ai pu oublier.

Un grand merci aussi aux autres doctorants et post-docs croisés au GANIL : Mark, Pierre, Aldric, Benoît, Florent, José, Haïfa, Hongliang, Quentin, Kim, Coralie, Catherina, Marine, Carme, Giacomo, Guillaume, Diego et tous ceux que j'ai pu oublier.

Enfin je souhaite aussi remercier ceux qui m'auront beaucoup influencé au cours de ma scolarité, et qui sont en partie "responsables" de ce manuscrit. Merci à Georges Kaisa pour ses très bons conseils, Mme Rondeau et M Lebaillon qui m'auront guidé vers les sciences physique, et bien entendu, Olivier Juillet, qui aura aussi eu une influence sur moi non négligeable, notamment lors de mon choix de poursuivre mes études vers un doctorat, et plus spécialement en physique théorique.

À présent, je termine avec mes remerciements, certainement les plus importants, pour mes proches. À mes amis, Pierre-Alexandre, Vincent et Jonathan, Benj, Solène, Nilgün, Gerbold, et Thomas, qui m'auront de près ou de loin accompagné durant ces trois dernières années. Un grand merci aussi à Patrick et Robert, que je n'aurais sans doute jamais eu l'occasion de rencontrer si mon anglais n'était pas aussi naze au début de ma thèse. Merci aussi à ma belle-famille, pour beaucoup de choses, Manu, Martine, Anne, François et Aline. À mes parents, pour leur soutien inconditionnel et, forcément, sans qui je ne serais pas arrivé jusqu'ici, à mon frère qui aura sans doute à vivre cette expérience d'ici quelques années, et au reste de ma famille.

Et pour terminer un grand merci tout à fait spécial et singulier à Camille, qui m'aura apporté son soutien et son aide indispensable au vécu de cette thèse.

Contents

Chapter 1

Introduction

110 years after the discovery of atomic nucleus by Ernest Rutheford [1], the theory of atomic nucleus, simple in its fundamental ideas and explaining large amount of experimental facts, is still missing. The field is governed by often disconnected approaches, and the best what one may expect at present is building the comprehensive links between them. This realistic look should not prevent us from stressing the importance of the 'silent revolution', which started at the turn of the century and led to the rapid change of objectives of the nuclear theory and the evolution of its paradigms. Several new ideas and approaches were born at around the same time, which strongly influenced the evolution of nuclear theory for almost two decades. These are: (i) the new many-body approaches, such as the no-core shell model [2–4], the Gamow shell model (GSM) [5–7], the no-core shell model combined with the resonating group method [8,9], the no-core Gamow shell model [10], the no-core shell model with continuum [11,12], the lattice effective field theory [13–15], etc., (ii) the old many-body approaches revisited, such as the density functional theory [16], the shell model embedded in the continuum (SMEC) [17–20], the coupled-cluster theory in Berggren basis [21–25], the density-matrix renormalization group method [26–28], etc., (iii) the new approaches to effective interactions, such as the chiral effective field theory [29], the in-medium similarity renormalization group approach [30–33], etc. This impressive list of achievements, given here in the historic 'order of appearance', is by far not exhaustive and confirms the vitality of the nuclear theory.

The present situation reminds the glorious period from the end of forties to the end of sixties, which gave birth to the nuclear shell model (SM), the microscopic optical potential, the unified (Copenhagen) model of nucleus, the continuum shell model (CSM), the pairing interaction, the G-matrix, the coupled-cluster theory, the Skyrme force, and many others. Is the present-day renaissance of nuclear theory going to last longer than the previous renaissance of fifties? Is it going to lead to the lasting change of the paradigms in nuclear theory? or it will dry up, evolving into the period of innumerable precision calculations, as experienced before?

The evolution of paradigms in nuclear theory is seen mainly: (i) in the approach to in-medium nucleon-nucleon interaction, with developments in connecting QCD with nuclear structure, and affirmation of the significance of three (and higher) -body interactions, (ii) in the development of new *ab initio* many-body theories for structure and reactions, and (iii) in the extension of nuclear shell model for open quantum systems, with attempts to reconcile description of structure and reactions in low-energy continuum.

The first two items are closely related, *i.e.* both aim at solving the same fundamental questions: how the strong interaction described by QCD is responsible for binding protons and neutrons into

nuclei?, how the shell structure arises from fundamental interactions and how it evolves across the nuclear landscape?, what is the origin of simple patterns and collective excitations in nuclei?, how the phenomenologically successful nuclear SM derives from the modern *ab initio* theories?, etc.

The third item reaffirms the role of continuum in structure aspects of nuclei by means of the configuration interaction approach which is valid for bound and unbound nuclei, hence completing and validating the standard nuclear SM. In this formulation, comprehensive and validated theory of nuclei is on the horizon, allowing for the shell model treatment of both weakly bound/unbound states and reaction channels, or an investigation of the collectivization of nuclear wave functions as a result of interplay between internal mixing by interactions and external mixing via the decay channels. Moreover, the unification of structure and reaction aspects of nuclei became possible, and several crucial questions can be now addressed meaningfully, such as: how are the near-threshold cluster configurations born in nuclei?, what is the interplay between continuum and isospin-breaking effects?, what is the role of coalescence of eigenfunctions in the continuum?, what is the common origin of resonance trapping and super-radiance phenomenon?, is the random matrix theory justified?, what is the essential input for developing the "universal" optical model potential?, how to take consistently into account breakup and transfer channels?, and how far can surrogate reactions take us?, *i.e.* is (d,p) going to inform us about (n,γ)?, etc.

The work presented in this manuscript is a part of the latter efforts to describe the atomic nucleus as an open quantum system. The immense richness of the nuclear many-body problem stems from its genuine multi-scale character and underlying effective many-body interactions that are strongly mediated by the nuclear medium. Further complexity is added by the open quantum system nature of the atomic nucleus, which requires a treatment of bound states, resonances, and the continuum of scattering states within a unified framework. To formulate the shell model for open quantum systems, two frameworks have been proposed. The first one, the real-energy CSM in the Hilbert space [34–41], is based on the Feshbach's projection formalism [42, 43]. The second one, which will be discussed in this manuscript, is the GSM [5–7], which is the complex-energy CSM based on the Berggren ensemble [44–46]. The GSM, which is conveniently formulated in the rigged Hilbert space [47–49], offers a fully symmetric treatment of bound, resonance, and scattering states.

At low excitation energies, well-bound nuclei can be considered as closed quantum systems, well described by the standard SM or its modern versions such as the no-core shell model. Moving towards drip lines, or higher in excitation energy, the continuum coupling becomes gradually more important, changing the nature of weakly bound states. In this regime, the chemical potential has a similar magnitude as the pairing gap; hence, the system is dominated by many-nucleon correlations which no longer cannot be considered as small perturbations atop the average potential. Many-body states in neighboring nuclear systems with different proton and neutron numbers become interconnected via continuum, forming correlated domains of quantum states.

Exact numerical simulation of a complex many-body system is not equivalent to understanding its properties. The understanding of specific nuclear properties is often improved by considering exactly solvable models, motivated by a symmetry of the many-body system. Many such simple models have been discussed for bound atomic nuclei. However, no such models exist for nuclei considered as open quantum systems. In the first part of the thesis, we will generalize the rational Gaudin pairing model [50] to include the continuous part of the single-particle (s.p.) spectrum, and then derive a reliable algebraic solution which generalizes exact Richardson solution for bound states [51, 52]. In future, numerous applications of these generalized Richardson equations are

possible (i) to study spectra and transition probabilities in different conditions of binding, (ii) to study the spectroscopy in a long chain of isotopes, or (iii) to calculate pairing properties of unstable ultra-small superconducting grains.

The formulation of reaction theory rooted in GSM will be discussed in the second part of the manuscript. For that the GSM will be expressed in the basis of reaction channels and generalized for multi-nucleon projectiles. Our aim is to develop the microscopic approach which will be capable to describe the transfer reactions. This reaction theory respects the antisymmetrization of target and projectile wave functions, as well as the wave function of the combined system. The application will be presented for the reaction ^{14}O(p,p')^{14}O, where the combined system ^{15}F is a proton emitter.

The manuscript is organized as follows. In Secs. 2.1 and 2.2, we discuss the basic features of the GSM, the construction of the s.p. basis, the choice of the optimal coordinate system, and the regularization of diverging integrals involving continuum states. Sec. 2.3 is devoted to the formulation of the pairing model in the space of discrete and continuum states and solving it by generalizing the Richardson equations for fermions and bosons.

Chapter 3 is devoted to the discussion of the application of GSM approach to nuclear reactions. In Sec. 3.1, the real-energy CSM/SMEC approach for structure and reactions is shortly discussed. In the next section (Sec. 3.2), the coupled-channel (CC) formulation of GSM is discussed in details. This GSM-CC formulation enables to formulate the unified theory of nuclear structure and reactions. Sec. 3.3 collects the presentation of different numerical methods to solve CC equations of the GSM-CC approach for both local and non-local potentials calculated microscopically for a given Hamiltonian. More technical parts of this thesis and some derivations concerning the material of chapters 2 and 3 are contained in the appendices.

Finally, main conclusions of this work and a list of future perspectives are given in chapter 4.

Chapter 2

Structure description of bound, weakly bound and unbound systems in nuclear physics

One of the early observation of the atomic nuclei concerns fluctuations in the relative abundances and masses/separation energies in the periodic table. It has been shown that these fluctuations are associated with particular values of the neutron N and proton numbers Z, called the "magic numbers" [53–55]. This relation is at the origin of the first version of the shell model (SM) [56] wherein independent protons and neutrons fill orbitals associated with the specific quantum numbers. Magic numbers of nucleons in this model always correspond to the gain in binding energy. This 'atomic' version of the SM failed to reproduce magic numbers of nucleons and binding energies of nuclei [57]. Later, following the suggestion of Enrico Fermi, the SM was modified by Göppert-Mayer [58,59] and independently by Haxel, Jensen and Suess [60] to include the spin-orbit coupling term. In this version, the SM succeeded to reproduce the magic numbers of nucleons and the order of shells.

The interaction between nucleons in this independent particle nuclear SM is approximated by the average potential and the spin-orbit coupling term. The description of nuclear spectra was achieved in the SM by introducing the configuration interaction between various arrangements of nucleons in different shells, respecting the Pauli exclusion principle [61–63]. The model was completed by Brueckner [64] who reconciled the picture of independent nucleons moving in the shells of an average potential with the picture of strongly interacting nucleons obeying Pauli principle. (More about the history of nuclear SM can be found in Ref. [65]. A recent review of SM applications for complex spectra is given in Refs. [66, 67].) In spite of the formidable development of *ab initio* approaches, such as the no-core (Gamow) shell model [2, 3, 10, 68], the coupled cluster theory [69, 70], the self-consistent Green's functions approach [71–77], or the in-medium similarity renormalization group method [30–33], the nuclear SM still remains the cornerstone of our understanding of atomic spectra.

The tremendous success of SM in the description of well-bound nuclei lead to the separation of nuclear structure and nuclear reactions. The drawbacks of this separation have been pointed out early [78] as it became clear that the microscopic description of nuclear reactions depends on internal structure of colliding nuclei, and the SM fails to describe resonances and near-threshold states. We know now that the coupling to the continuum can deeply affect the many-body dynamics

and gives rise to new phenomena, such as the two-proton [79–82] and two-neutron [83, 84] decays, the formation of halo structures and Borromean systems [85–87], the appearance of doorway states [88, 89] and trapped resonances [90], or the clusterization in the vicinity of the corresponding cluster emission threshold [91–93]. In the past two decades, these exotic phenomena became important topics of the experimental investigations.

The recent developments of new radioactive ion beam facilities provide the strong impulse for the development of new theoretical approaches dealing with the continuum. Early attempts based on the Feshbach projection formalism [94], led to the continuum shell model (CSM) [34–41] and the shell model embedded in the continuum (SMEC) [17–20, 95] which have been successful to describe exotic phenomena involving at most the two-nucleon decay channels. An alternative approach, which will be discussed in this chapter, is the SM in the complex-energy plane, the so-called Gamow shell model (GSM) [5–7]. This model combines all advantages of the standard nuclear SM with the possibility to deal with any number of particles in the scattering continuum. The GSM is using Berggren ensemble [44–46] to build Slater determinants and henceforth, the many-body wave functions. Wave functions in this approach are the quasi-stationary solutions of the time-dependent Schrödinger equation with the outgoing boundary conditions.

The GSM provides a comprehensive description of the many-body wave functions in all regimes of the binding energy. Eigenfunctions of the resonant states are the poles of the scattering matrix, and in that sense, GSM contains the necessary ingredients to unify the theory of nuclear structure and reactions. One should mention also other approaches which attempt to describe nucleus as an open quantum system. These are the coupled cluster theory [21–25] in Berggren basis, and the no-core shell model with continuum [11, 12] which resembles the SMEC approach and relies on the resonating group method [8, 9] to calculate channel wave functions.

The first part of this chapter is devoted to the discussion of the GSM, the configuration interaction approach for weakly bound and unbound nuclei. In Sec. 2.1, we remind shortly the SM formalism. The following section (Sec. 2.2) is devoted to the open quantum system generalization of the SM; we present the GSM and discuss limitations of the Hilbert space description of open quantum systems. In Sec. 2.2.1, an extension of Hilbert space, the so-called rigged Hilbert space or Gel'fand triple, is briefly presented. Then in Sec. 2.2.2, we introduce Gamow states. Different methods to regularize Gamow states and their application in Berggren single particle (s.p.) basis are discussed in Sec. 2.2.3.

The application of cluster orbital shell model (COSM) coordinates in GSM is discussed in Sec. 2.2.4. We will show that the center-of-mass (c.m.) excitations can be approximately removed if the GSM Hamiltonian is expressed in COSM coordinates. The construction of the complete one- and many-body bases is then discussed in Secs. 2.2.5 and 2.2.6, respectively. Finally, in Sec. 2.2.6, we will list previous applications of the GSM.

In the second part of this chapter (Sec. 2.3), we will present the generalized Richardson equations for fermions and bosons which are interacting with a pairing interaction in bound and unbound s.p. levels. The mathematical framework of these equations, including a short introduction to the Richardson-Gaudin model and the connection between the XXX model of Gaudin and the pairing model, are discussed in Secs. 2.3.1 and 2.3.2. In Sec. 2.3.3, we generalize the pairing Hamiltonian in Berggren basis and derive the generalized Richardson equations which provide the approximate solution for this model (Sec. 2.3.4). The numerical method to solve the generalized Richardson equations are then discussed in Sec. 2.3.5.

In Sec. 2.3.6, results obtained using the generalized Richardson equations are compared with

the exact GSM solutions of the pairing problem. Our aim is to estimate the reliability of the generalized Richardson equations in different regimes of the pairing interaction for different s.p. bases and number of particles. In the following section (Sec. 2.3.7.1), we apply these equations to calculate binding energies and spectra of carbon isotopes. In these studies, we compare results obtained with and without continuum couplings to see effects of the continuum in the spectra of the pairing Hamiltonian. Finally, a possible application of the generalized Richardson equations for the studies of unstable ultra-small superconducting grains will be shortly discussed in Sec. 2.3.7.2.

2.1 Nuclear shell model

The one-body part of the SM Hamiltonian consists of an isotropic harmonic oscillator potential plus a spin-orbit coupling term:

$$U(r) = \frac{1}{2}m\omega^2 r^2 + V_{\rm so}\vec{\ell}.\vec{s} \tag{2.1}$$

where here m is the mass of physical object which generates the mean potential, and $\vec{\ell}, \vec{s}$ the orbital angular momentum and intrinsic spin, respectively. Even if this potential (2.1) is sufficient to reproduce observed magic numbers of nucleons, it fails to explain nuclear spectra. For that, one should consider the configuration interaction, *i.e.* introduce the two-body interaction. In laboratory coordinates, the Hamiltonian reads :

$$\hat{H} = \sum_{i=1}^{A} \hat{t}_i + \sum_{i<j}^{A} \hat{V}_{ij} \tag{2.2}$$

where $\hat{t}_i$ is the kinetic energy operator, and $\hat{V}_{ij}$ is the residual two-body interaction. In most cases, we can limit ourselves to the two-body interaction in (2.2), but many recent studies stress the importance of the three-body interaction [96–103].

In standard SM calculations, completely filled shells form an inert core, so that the configuration mixing involves only nucleons in the valence shells. In such a description, the Hamiltonian can be written as:

$$\hat{H} = \underbrace{\hat{H}_c + \sum_{i\in \rm val} \left(\hat{t}_i + \hat{U}_i^{\rm core}\right)}_{\hat{H}_{\rm basis}} + \underbrace{\sum_{(i<j)\in \rm val} \hat{V}_{ij}}_{\hat{V}} \tag{2.3}$$

where $\hat{H}_{\rm basis}$ is the one-body Hamiltonian which generates the s.p. basis, and $\hat{V}$ the two-body interaction which generates the configuration mixing. In Eq. (2.3), $\hat{H}_c$ is the Hamiltonian of the core, and $\hat{U}_i^{\rm core}$ the one-body potential generated by the core and felt by the valence nucleons. They are defined as :

$$\hat{H}_c = \sum_{i\in \rm core} \hat{t}_i + \sum_{(i<j)\in \rm core} \hat{V}_{ij} \quad \text{and} \quad \sum_{j\in \rm core} \hat{V}_{ij} \to \hat{U}_i^{\rm core} \tag{2.4}$$

The one-body potential $\hat{U}_i^{\rm core} = U(\hat{r}_i)$ is the same as in Eq. (2.1).

Well bound many-body states of a nucleus can be conveniently described in the harmonic oscillator basis. For weakly bound or unbound states, an explicit consideration of continuum states in the many-body framework is mandatory. For example, an understanding of the near-threshold

correlations [91, 92] is missing in SM due to the absence of branch points singularities associated with the particle emission thresholds [104]. The standard procedure to break this deadlock is to include effects of the continuum effectively by adjusting the matrix elements of the Hamiltonian. We will discuss this point in Sec. 2.3.7.1. The application of this recipe became an obstacle in learning about the role of the continuum coupling and the three- (many-) body interaction, or the salient features of the near-threshold collectivity. In the following sections of this chapter, we present the open quantum system formulation of the SM, the GSM, and in the next chapter we will show how to formulate the comprehensive reaction theory which is rooted in this general nuclear structure approach.

2.2 Gamow shell model

In this previous section, we have reminded main features of the SM. We have stressed that this model is adapted for the description of well bound many-body states. The open quantum system extension of SM in the rigged Hilbert space, the GSM, and mathematical details of its formulation will be contained in this section.

2.2.1 Rigged Hilbert space

The mathematical apparatus of the Hilbert space $\mathcal{H}$ is sufficient to describe discrete states of a bounded quantum system. Problems arise if the spectrum of the quantum system contains both discrete and continuous parts. Resonances, which appear in this case, neither belong to the Hilbert space nor they are solutions of the hermitian eigenvalue problem.

Resonances are genuine intrinsic properties of quantum systems, associated with their natural frequencies, and describing preferential decays of unbound states. The standard formulation of quantum mechanics in Hilbert space does not allow the description of state vectors with exponential growth and exponential decay, such as resonance states. Since the spectrum of an observable in the Hilbert space is real, the usual procedure for treating resonance states is either to extract the trace of resonances from the real-energy continuum level density or to describe the resonances by joining the bound state solution in the interior region with an asymptotic solution, *e.g.*, within the R-matrix approach [105–107].

The deficiency of the Hilbert space formulation of quantum mechanics is obvious if one considers the operators, like the position $\hat{Q}$ and momentum $\hat{P}$ operators, which have the continuous spectrum:

$$\begin{aligned} \hat{P}\,|\vec{p}\rangle &= \vec{p}\,|\vec{p}\rangle \quad \text{with} \quad -\infty < ||\vec{p}|| < +\infty \\ \hat{Q}\,|\vec{r}\rangle &= \vec{r}\,|\vec{r}\rangle \quad \text{with} \quad -\infty < ||\vec{r}|| < +\infty \end{aligned} \tag{2.5}$$

Their wave functions: $\langle\vec{r}|\vec{p}\rangle = \frac{1}{(2\pi\hbar)^{3/2}} e^{\frac{i}{\hbar}\vec{p}.\vec{r}}$ and $\langle\vec{r}'|\vec{r}\rangle = \delta(\vec{r}' - \vec{r})$, are not square integrable and hence, do not belong to the Hilbert space.

In the twenties of the last century, Dirac introduced a new mathematical formalism for quantum mechanics, with objects such as bras and kets. As noticed by Dirac and von Neumman [108, 109], this formalism is not compatible with the standard formulation of quantum mechanics.

All these different difficulties of the standard quantum mechanics could be overcome using an extension of the Hilbert space, the so-called rigged Hilbert space. Mathematical apparatus of the

rigged Hilbert space has been formulated in sixties by Gel'fand, Maurin and Böhm [47–49]. The rigged Hilbert space, also called the Gel'fand triplet or equipped Hilbert space, is a triad of spaces:

$$\Phi \subset \mathcal{H} \subset \Phi^{\times} \tag{2.6}$$

The subspace Φ is the set of physical wave functions on which any expectation value, any uncertainty and any commutator can be computed. The dual space $\Phi^{\times}$ contains eigenvectors associated with the continuous spectrum of the observables. These eigenvectors are defined as functionals over the subspace Φ, and they can be used to expand any elements of Φ. Mathematically, Φ is the subspace of test functions, and $\Phi^{\times}$ is the space of distributions.

The Hilbert space $\mathcal{H}$ does not play any particular role in the rigged Hilbert space formalism, *i.e.* in all considered cases one needs only the dual pair of spaces $\Phi \subset \Phi^{\times}$ which characterize the quantum system. The rigged Hilbert space provides a better framework than $\mathcal{H}$ to capture features of quantum systems. It provides a convenient setting for Dirac brackets as well as for vectors and wave functions associated with the continuous spectra. Moreover, the rigged Hilbert space provides a natural framework for a quantum-mechanical description of Gamow states because $\Phi^{\times}$ may contain the generalized eigenvectors for observables having complex eigenvalues. Hence the open quantum system generalization of the SM, the GSM, finds a natural place in the rigged Hilbert space.

2.2.2 Gamow states

Experimentally, resonances often appear as peaks in the cross section. For isolated resonances, their shape resembles the well-known Breit-Wigner distribution which has two parameters: the centroid, which defines the resonance energy E_n, and the width Γ_n at half-maximum. In 1928, George Gamow proposed the quasi-stationary formalism based on quantum tunneling to describe the spontaneous particle emission [110]. In this model, decaying states (Gamow states) are characterized by the complex-energy eigenvalues:

$$\tilde{E}_n = E_n - i\frac{\Gamma_n}{2} \tag{2.7}$$

Let us now show the connection between the width of a decaying state and its half life. Let the number of nuclei at $t = 0$ before the decay takes place is N_0. Then, the number of remaining nuclei at a time $t > 0$ is given by:

$$N(t) = N_0 S(t) \tag{2.8}$$

where $S(t)$ is the survival probability, *i.e.* the probability to find the nucleus at a time $t > 0$, which is defined as:

$$S(t) = \int \left| \langle \vec{r} | e^{-\frac{i}{\hbar} E_n t} | \Psi_n \rangle \right|^2 d^3\vec{r} = e^{-\frac{\Gamma_n}{\hbar} t} \int |\Psi(\vec{r})|^2 d^3\vec{r} = e^{-\frac{\Gamma_n}{\hbar} t} \tag{2.9}$$

where $|\Psi_n\rangle$ is the eigenstate and $\tilde{E}_n$ the associated eigenvalue. This shows that the Gamow states decay exponentially, and one can identify the parameter Γ with the decay width which defines the half-life of the state:

$$T_{1/2} = \frac{\hbar \ln(2)}{\Gamma} \tag{2.10}$$

One should stress that the counterpart of this exponential temporal decrease is the exponential growth of the radial wave function at large distances to ensure the flux conservation [110]. Although

resonances have a finite lifetime and their radial wave function diverges, it is possible to assign the standard labels of stationary eigenstates, like angular momentum, charge, spin, parity, *etc.* to them.

Resonances represented by Gamow states are also poles of the scattering matrix (S-matrix). The S-matrix was introduced in the scattering theory to connect the asymptotic behavior of the scattered wave function between the past and the future. Various poles of the S-matrix in the complex energy plane can be identified with bound states, antibound (virtual) states, capturing and decaying resonances.

The (complex) eigenenergy $\tilde{E}_n$ of the system, corresponds to the wave number:

$$\tilde{k}_n = \sqrt{\frac{2m\tilde{E}_n}{\hbar^2}} = k_n - i\gamma_n \tag{2.11}$$

where m is the particle mass. For a decaying resonance, $k_n, \gamma_n > 0$. At long distances, the radial part of the wave function is proportional to:

$$e^{i\tilde{k}_n r} = e^{ik_n r} e^{\gamma_n r} \tag{2.12}$$

and increases exponentially. The pole of the S-matrix corresponding to the decaying resonance is situated in the forth quadrant of the k-plane.

The states with $\tilde{k}_n = -k_n - i\gamma_n$ and $k_n, \gamma_n > 0$ are called the capturing resonances. They are situated in the third quadrant of the k-plane, and their radial wave function has the following asymptotic behavior:

$$e^{i\tilde{k}_n r} = e^{-ik_n r} e^{-\gamma_n r} \tag{2.13}$$

Capturing resonances are obtained by a time reversal operation $t \to -t$ applied to decaying resonances [49].

States with $\tilde{k}_n = -i\gamma_n$ and $\gamma_n > 0$ are called antibound or virtual states [111–114]. Asymptotically, the radial wave function of an antibound state grows exponentially:

$$u_n(r) \sim e^{i\tilde{k}_n r} = e^{\gamma_n r} \tag{2.14}$$

The physical interpretation of the antibound state is not so straightforward. In the standard quantum mechanics, antibound state can be considered as a feature of the system rather than a state. In the rigged Hilbert space, the antibound state can be interpreted both as a vector in the rigged Hilbert space and as a pole of the S-matrix. Consequently, the antibound state near the decay threshold increases the cross section of the low-energy scattering process [111, 113, 115, 116], and has an appreciable influence on the scattering length. Classic examples is the low-energy $\ell = 0$ nucleon-nucleon scattering characterized by a large and negative scattering length [113, 115]. Related to this is an increased localization of real-energy scattering states just above the decay threshold [117].

A study of the energies of antibound states as a function of potential parameters was done by Nussenzveig [118] (see also [119] for a discussion of the one-dimensional case). In these studies, radius and surface diffuseness of the potential were fixed and the trajectories of bound and antibound states were calculated as a function of the potential depth V_0. For s-wave neutrons, no narrow resonance appears because there is no potential barrier. Thus, by increasing V_0 from the minimal value at which the antibound state appears, the pole crosses $k = 0$ and becomes the

bound state. For protons or for neutrons with $l > 0$, the potential barrier assures the existence of resonant poles. In this case, decaying and capturing poles move toward the imaginary k-axis with increasing V_0. At certain values of V_0, the twin capturing and decaying poles meet at $k = 0$ forming a double-pole singularity. For still larger values of V_0, one of these poles becomes the bound state while the other one moves down along the negative imaginary axis as the antibound state.

2.2.3 Normalization of Gamow states and the Berggren basis

To describe physical systems conveniently, the Hamiltonian and its eigenstates have to be expressed in a suitable basis. For unbound and weakly bound systems, Gamow states and non-resonant continuum states become relevant, and have to be included in the basis. However, due to the complex energy of Gamow states, the probability density of resonances increases exponentially in space, making their normalization and the proof of their orthogonality problematic.

A first method to normalize these states has been proposed by Zel'dovitch [120] who introduced a convergence factor $\epsilon > 0$ to regularize matrix elements:

$$\langle \phi_f | \hat{O} | \phi_i \rangle = \int_0^\infty e^{-\epsilon r^2} \phi_f(r) O(r) \phi_i(r) \tag{2.15}$$

where ϕ_f and ϕ_i are s.p. Gamow states, and $\hat{O}$ is a bounded operator.

Later, Tore Berggren used the method of Zel'dovitch to prove that Gamow states for neutral particles are mutually orthogonal [44]. In the same paper, the first s.p. basis has been proposed, now called the Berggren basis, which includes bound states, resonances, and scattering states. The completeness of the Berggren basis for charged particles has been proved by Michel, Nazarewicz and Płoszajczak [121, 122].

The Berggren basis is an extension of the Newton basis [111], wherein the real-energy continuum is deformed through an analytic continuation into the complex plane. This complex energy contour L^+ in the k-plane encompasses selected resonances and joins the real-k axis to continue toward $k \to \infty$. Hence, using the residue theorem we can write down the completeness relation:

$$\sum_{n \in (b,r)} |\phi_n\rangle \langle \phi_n| + \int_{L^+} |\phi_k\rangle \langle \phi_k| \, dk = \hat{\mathbb{1}} \tag{2.16}$$

where the sum runs over bound and resonance states.

The contour L^+ lies in the fourth quadrant, as shown in Fig. 2.1, and surrounds selected decaying resonances ($\tilde{k}_n = k_n - i\gamma_n$ and $k_n > \gamma_n > 0$). Due to the Cauchy integral theorem, the precise form of the contour L^+ is not important. Usually, only decaying resonances which satisfy: $\arg(k_n) > -\pi/4$, are included. Vertse [123] proposed the generalization of the Berggren completeness relation (2.16) to include the antibound states, whereby extending the applicability of the Berggren ensemble [124–126]. However, this generalized completeness relation is less efficient in practical applications [125] since it requires a significantly denser discretization of the contour in the complex k-plane.

In standard quantum mechanics, the mean value of the hermitian operator $\hat{O}$ associated with an observable in an eigenstate $|\phi_k\rangle$ is always real:

$$\langle \phi_k | \hat{O} | \phi_k \rangle = \langle \hat{O} \rangle_{\phi_k} \in \mathbb{R} \tag{2.17}$$

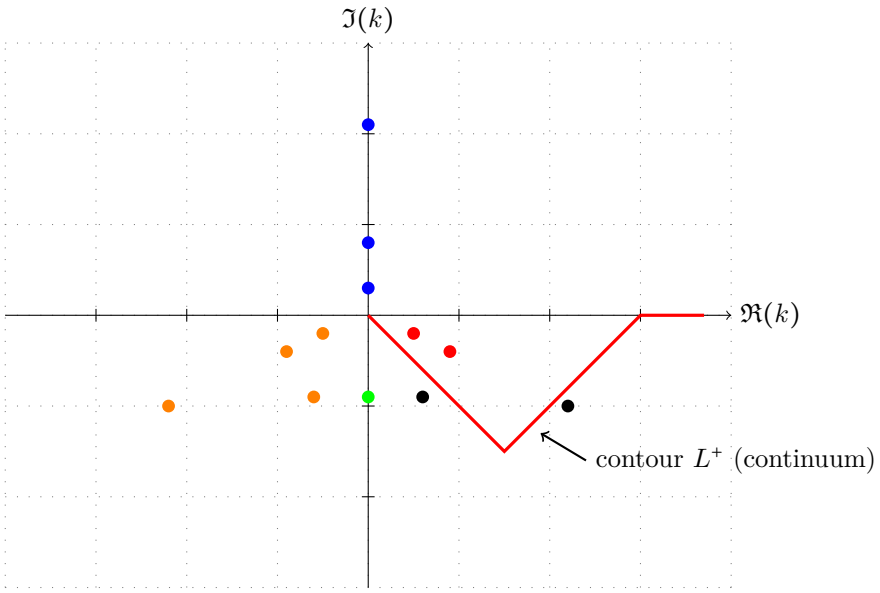

Figure 2.1 – (Color online) Schematic illustration of the complete Berggren basis in k-plane. Blue and red dots represent bound states and decaying resonances which are included in Berggren basis. Decaying resonances which are omitted from the basis are shown with black dots. The antibound or virtual state is represented by a green dot. Orange dots show capturing resonances. Non-resonant continuum states which enter the Berggren completeness relation (2.16) belong to the contour L^+ (in red) which surrounds selected decaying resonances (red dots).

This is not the case in the rigged Hilbert space formulation of quantum mechanics. For the resonance, the mean value of an operator $\hat{O}$ is:

$$\langle \hat{O} \rangle_{\phi(k)} = \Re \langle \hat{O} \rangle_{\phi(k)} + i \Im \langle \hat{O} \rangle_{\phi(k)} \tag{2.18}$$

The interpretation of real and imaginary parts of the mean value for a given observable has been discussed by Berggren [44–46]. The real part can be interpreted as the measured value of an observable, and the imaginary part which is due to the interferences between the resonance and the scattering continuum, corresponds to the uncertainty of the measured value. This interpretation holds for the root mean square radius as well [127].

The regularization method proposed by Zel'dovich was essential to prove the completeness of Berggren ensemble of s.p. states [44]. However, this method turned out to be impractical in numerical applications and had been abandoned in favor of the methods proposed by Hokkyo [128] and Romo [129]. The approach of Romo is based on using the Green's function and its analytic continuation in the complex energy plane. Hokkyo on the contrary, employed the uniform complex-scaling approach to regularize diverging integrals.

In the uniform complex-scaling method, one applies the unitary transformation $\mathcal{U}$, represented by an operator $\hat{U}(\theta)$, which is defined by the uniform rotation $\vec{r} \to e^{i\theta}\vec{r}$ of the coordinates, applied on the s.p. wave functions [130, 131]:

$$\hat{U}(\theta)\phi(\vec{r}) = e^{i\frac{3}{2}\theta}\phi\left(\vec{r}e^{i\theta}\right) \tag{2.19}$$

The factor $e^{i\frac{3}{2}\theta}$ in this expression comes from the dimension of the space [132]. The above transformation guarantees that the selected wave functions associated with the resonances become square integrable [133–135].

Applying the uniform complex-scaling method to the s.p. Hamiltonian, one obtains:

$$\hat{h}(\vec{r}) \rightarrow \hat{h}_\theta(\vec{r}) = \hat{U}(\theta)\hat{h}(\vec{r})\hat{U}^{-1}(\theta) \tag{2.20}$$

The transformed potential $\hat{h}_\theta(\vec{r})$ is no longer hermitian. For a wide class of dilatation-analytic potentials, the spectrum of bound states of $\hat{h}(\vec{r})$ and $\hat{h}_\theta(\vec{r})$ are the same [136]. Properties of the transformed Hamiltonian $\hat{h}_\theta(\vec{r})$ and its spectrum for the dilation-analytic potentials have been studied by the Aguilar, Balslev and Combes [133, 134]. The equivalence between the Zel'dovich's regularization method and the uniform complex-scaling has been proved by Gyarmati and Vertse [137].

As most of the s.p. potentials used in nuclear physics are not dilatation-analytic, the applicability of the uniform complex-scaling for nuclear physics problems is limited. To circumvent this problem, Gyarmati and Vertse introduced the exterior complex-scaling method [137]. The method consists of applying the complex rotation of coordinates only from a certain radius r_a [138]:

$$\begin{aligned} \hat{U}_a(\theta)\phi(r) &= \phi(r) && \text{if} \quad r \le r_a \\ &= \phi(r_a + |r - r_a|e^{i\theta}) && \text{if} \quad r > r_a \end{aligned} \tag{2.21}$$

The exterior complex-scaling method can be applied to any potential and the results do not depend on the parameters a and θ. The existence of a norm for charged particle resonances was proved by Gyarmati and Vertse [137]. In 2002, Michel et al. [5] applied the exterior complex-scaling method in GSM.

In practical applications the truncations are required so that we define the maximum value k_{max} of k on the contour L^+. To ensure the completeness of the s.p. Berggren basis, one has to discretize the contour L^+. The N-point quadrature of the integral along the contour reads:

$$\int_{L^+} |\phi_k\rangle \langle\phi_k| \, dk \simeq \sum_{j=1}^{N} w_j \, |\phi_{k_i}\rangle \langle\phi_{k_j}| \tag{2.22}$$

where the k_j and w_j are values and weights given by the Gauss-Legendre quadrature method. Normalizing the kets $|\phi_{k_j}\rangle$ with a factor $\sqrt{w_j}$:

$$\sum_{j=1}^{N} w_j \, |\phi_{k_j}\rangle \langle\phi_{k_j}| \rightarrow \sum_{j=1}^{N} |\phi_{k_j}\rangle \langle\phi_{k_j}| \quad , \tag{2.23}$$

one obtains the discretized Berggren basis:

$$\begin{aligned} \sum_{n\in(b,r)} |\phi_n\rangle \langle\phi_n| + \int_{L^+} dk \, |\phi_k\rangle \langle\phi_k| &\approx \sum_{n\in(b,r)} |\phi_n\rangle \langle\phi_n| + \sum_{j=1}^{N} |\phi_{k_j}\rangle \langle\phi_{k_j}| \\ &\approx \sum_{n\in(b,r,k_j)} |\phi_n\rangle \langle\phi_n| \end{aligned} \tag{2.24}$$

which is similar to any other discrete s.p. basis.

The many-body basis for fermions consists of the Slater determinants $\{|\Phi_n\rangle\}$ constructed from the s.p. states $\{|\phi_n\rangle\}$ of the complete Berggren basis, like in the case of the HO basis. The completeness of the Berggren ensemble guarantees the following closure relation for the many-body basis [7]:

$$\sum_n |\Phi_n\rangle \langle\Phi_n| = \hat{\mathbb{1}} \tag{2.25}$$

which is used to formulate the GSM.

2.2.4 COSM coordinates and GSM Hamiltonian

In the standard SM, the center-of-mass (c.m.) excitations are removed using the Lawson method [139]. In GSM, this method can no longer be used because Berggren states are not eigenstates of the HO potential. Thus in order to eliminate the c.m. excitations, and also to avoid numerical difficulties in describing nuclei with many valence nucleons in the Jacobi coordinates, the GSM Hamiltonian is expressed in the core plus valence particle approximation using relative nucleon-core coordinates of the COSM [140].

Let us introduce the COSM coordinates:

$$\vec{r}_i = \vec{r}_{i,\text{lab}} - \vec{R}_{\text{c.m.,core}} \quad \text{if} \quad i \in \text{val} \tag{2.26}$$

$$\vec{r}_i = \vec{r}_{i,\text{lab}} \quad \text{if} \quad i \in \text{core} \tag{2.27}$$

where $\vec{r}_{i,\text{lab}}$ is the coordinate of a nucleon in the laboratory system and

$$\vec{R}_{\text{c.m.,core}} = \frac{1}{M_{\text{core}}} \sum_{i\in\text{core}} m_i \, \vec{r}_{i,\text{lab}} \tag{2.28}$$

is the coordinate of the c.m. of the core, where m_i is the mass if the i$^{\text{th}}$ particle and $M_{\text{core}} = \sum_{i\in\text{core}} m_i$ is the mass of the core. The COSM momentum reads:

$$\vec{p}_i = -i\hbar\vec{\nabla}_i \tag{2.29}$$

where $\vec{\nabla}_i$ is the gradient associated to $\vec{r}_i$. The expression of the momentum $\vec{p}_{i,\text{lab}}$ and the total momentum $\vec{P}_{\text{lab}}$ in the laboratory system is:

- For $i \in$ core:

$$\vec{p}_{i,\text{lab}} = \vec{p}_i - \sum_{j\in\text{val}} \frac{m_i}{M_{\text{core}}} \vec{p}_j \tag{2.30}$$

- For $i \in$ val:

$$\vec{p}_{i,\text{lab}} = \vec{p}_i \tag{2.31}$$

and

$$\begin{aligned} \vec{P}_{\text{lab}} &= \sum_{i\in\text{core}} \vec{p}_{i,\text{lab}} + \sum_{i\in\text{val}} \vec{p}_{i,\text{lab}} = \sum_{i\in\text{core}} \vec{p}_i - \sum_{\substack{i\in\text{core} \\ j\in\text{val}}} \frac{m_i}{M_{\text{core}}} \vec{p}_j + \sum_{i\in\text{val}} \vec{p}_i \\ &= \sum_{i\in\text{core}} \vec{p}_i - \sum_{j\in\text{val}} \vec{p}_j + \sum_{i\in\text{val}} \vec{p}_i = \sum_{i\in\text{core}} \vec{p}_i \end{aligned} \tag{2.32}$$

One may notice that $\vec{P}_{\rm lab}$ is only a function of the core linear momenta in COSM coordinates. Thus, the kinetic part of the Hamiltonian in the COSM frame with the c.m. kinetic part taken into account properly is written as:

$$\sum_{i=1}^{A} \frac{\vec{p}_{i,\rm lab}^2}{2m_i} - \frac{\vec{P}_{\rm lab}^2}{2M} = \sum_{i\epsilon \rm val} \frac{\vec{p}_i^2}{2\mu_i} + \frac{1}{M_{\rm core}} \sum_{i<j\epsilon \rm val} \vec{p}_i \cdot \vec{p}_j + \sum_{i\epsilon \rm core} \frac{\vec{p}_i^2}{2\mu'_i} - \frac{1}{M} \sum_{i<j\epsilon \rm core} \vec{p}_i \cdot \vec{p}_j - \frac{1}{M_{\rm core}} \sum_{i\epsilon \rm core} \vec{p}_i \cdot \sum_{j\epsilon \rm val} \vec{p}_j \tag{2.33}$$

where M is the total mass, and μ_i, μ'_i are reduced masses given by:

$$\frac{1}{\mu_i} = \frac{1}{m_i} + \frac{1}{M_{\rm core}} \tag{2.34}$$

and

$$\frac{1}{\mu'_i} = \frac{1}{m_i} - \frac{1}{M} \ . \tag{2.35}$$

Note that the residual coupling between core and valence spaces vanishes as the core is coupled to 0^+ and $\sum_{i\epsilon \rm core} \vec{p}_i$ is of rank one.

Interaction matrix elements involving many-body states built either from core s.p. states or valence s.p. states pose no problem, as Eqs. (2.26,2.27,2.30,2.31) imply that:

$$\vec{r}_{i,\rm lab} - \vec{r}_{j,\rm lab} = \vec{r}_i - \vec{r}_j \tag{2.36}$$

$$\vec{p}_{i,\rm lab} - \vec{p}_{j,\rm lab} = \vec{p}_i - \vec{p}_j \ , \tag{2.37}$$

so that the standard methods can be used to calculate the associated two-body matrix elements. Problems would arise if one considered interaction matrix elements in which one valence state $|i\rangle$ and one core state $|j\rangle$ occur in both bra and ket states of the nuclear interaction. Indeed, in this case, Eqs. (2.26,2.27,2.30,2.31) imply that:

$$\vec{r}_{i,\rm lab} - \vec{r}_{j,\rm lab} = \vec{r}_i - \vec{r}_j + \vec{R}_{\rm c.m.,core} \tag{2.38}$$

$$\vec{p}_{i,\rm lab} - \vec{p}_{j,\rm lab} = \vec{p}_i - \vec{p}_j + \sum_{j'\epsilon \rm val} \frac{m_j}{M_{\rm core}} \vec{p}_{j'} \ . \tag{2.39}$$

It is then clear that a two-body interaction in laboratory coordinates becomes a N-body interaction in COSM coordinates, where core and valence degrees of freedom are coupled. One can avoid these problems by defining an effective interaction with core and valence parts calculated in the laboratory frame, so that couplings between core and valence spaces vanish.

Let us now write the GSM Hamiltonian. We will consider an effective Hamiltonian: $\hat{H} = \hat{T} + \hat{U} + \hat{V}$, where $\hat{T}$ is the kinetic operator, $\hat{U}$ is a s.p. potential, and $\hat{V}$ is a two-body interaction, calculated from a realistic interaction in the laboratory frame. The core part of the Hamiltonian is not considered as the core is inert. We will express it with COSM coordinates:

$$\hat{H} = \hat{T} + \hat{U} + \hat{V} = \sum_{i\epsilon \rm val} \left(\frac{\vec{p}_i^2}{2\mu_i} + U(\hat{\vec{r}}_i) \right) + \sum_{(i<j)\epsilon \rm val} \left(\frac{\hat{\vec{p}}_i \cdot \hat{\vec{p}}_j}{M_{\rm core}} + \hat{V}_{i,j} \right) \tag{2.40}$$

where $M_{\rm core}$ is the mass of the core, and :

$$\frac{1}{\mu_i} = \frac{1}{M_{\rm core}} + \frac{1}{m_i} \tag{2.41}$$

is the reduced mass of the i-th nucleon. The s.p. potential $U(\hat{\vec{r}})$ describes the field of the core and $V(\hat{\vec{r}}_i - \hat{\vec{r}}_j)$ is the two-body interaction. Due to Eqs. (2.36,2.37), the sum involving $\hat{V}_{i,j}$ in Eq. (2.40) does not change from the laboratory frame to the COSM frame.

To see that the substitution of $U(\vec{r}_{i,\rm lab})$ by $U(\vec{r}_i)$ in Eq. (2.40) leads to a very small error, let us separate U in central and spin-orbit parts:

$$U(\vec{r}_{i,\rm lab}) = U^{(\rm c)}(\vec{r}_{i,\rm lab}) + U^{(\rm ls)}(\vec{r}_{i,\rm lab})(\vec{\ell}_{i,\rm lab} \cdot \vec{s}_i) \tag{2.42}$$

For the central part, one has:

$$U^{(\rm c)}(\vec{r}_{i,\rm lab}) = U^{(\rm c)}(\vec{r}_i) + \vec{R}_{\rm c.m.,core} \cdot \nabla U^{(\rm c)}(\vec{r}_i) + \vec{R}_{\rm c.m.,core} \cdot \Delta U^{(\rm c)}(\vec{r}_i) \cdot \vec{R}_{\rm c.m.,core} + \text{rest}, \tag{2.43}$$

where $\Delta U^{(\rm c)}$ is the Hessian matrix associated to $U^{(\rm c)}$. The first-order term of Eq. (2.43) vanishes because the core is coupled to 0^+ and $\vec{R}_{\rm c.m.,core}$ is of rank 1.

One obtains a similar equation for the spin-orbit part of U:

$$\begin{aligned} U^{(\rm ls)}(\vec{r}_{i,\rm lab})(\vec{\ell}_{i,\rm lab)} \cdot \vec{s}_i) &= U^{(\rm ls)}(\vec{r}_{i,\rm lab}) \left[\left(\vec{r}_i + \vec{R}_{\rm c.m.,core} \right) \times \vec{p}_i \right] \cdot \vec{s}_i \\ &= U^{(\rm ls)}(\vec{r}_i)(\vec{\ell}_i \cdot \vec{s}_i) \\ &+ (\vec{R}_{\rm c.m.,core} \cdot \nabla U^{(\rm ls)}(\vec{r}_i))(\vec{\ell}_i \cdot \vec{s}_i) + U^{(\rm ls)}(\vec{r}_i) \left[\left(\vec{R}_{\rm c.m.,core} \times \vec{p}_i \right) \cdot \vec{s}_i \right] \\ &+ (\vec{R}_{\rm c.m.,core} \cdot \Delta U^{(\rm ls)}(\vec{r}_i) \cdot \vec{R}_{\rm c.m.,core})(\vec{\ell}_i \cdot \vec{s}_i) \\ &+ (\vec{R}_{\rm c.m.,core} \cdot \nabla U^{(\rm ls)}(\vec{r}_i)) \cdot \left[\left(\vec{R}_{\rm c.m.,core} \times \vec{p}_i \right) \cdot \vec{s}_i \right] \\ &+ \text{rest} \end{aligned} \tag{2.44}$$

where the first-order terms of Eq. (2.44) also vanish.

The error made is small even for the α-particle core, as it is of the order of $\Delta U / M_{\rm core}$. Indeed, the core matrix elements involving $R_{\rm c.m.,core}$ are of the order of $1/\sqrt{M_{\rm core}}$, the Laplacian of a Woods-Saxon potential is about 5 times smaller than the potential itself, and the derivative of the spin-orbit part of the Woods-Saxon potential is even smaller, so that the relative error made is of the order of 5% or less for an arbitrary core. The Hamiltonian $\hat{H}$ can then be recast with a one-body potential $\hat{U}_{\rm basis}$:

$$\hat{H} = \hat{U}_{\rm basis} + \hat{T} + \hat{V}_{\rm res} \tag{2.45}$$

where $\hat{U}_{\rm basis}$ is the potential which generates the basis, and $\hat{V}_{\rm res} = \hat{V} + \hat{U} - \hat{U}_{\rm basis}$ is the residual interaction. The introduction of $\hat{U}_{\rm basis}$ is a convenient way to remove approximately the long-range component in $\hat{V}_{\rm res}$.

2.2.5 Construction of the s.p. Berggren basis

Let us start by defining the s.p. Hamiltonian: $\hat{h} = \hat{U}_{\rm basis} + \hat{T}$. The s.p. potential generating the basis: $\hat{U}_{\rm basis} = U_{\rm basis}(\hat{\vec{r}})$, can be chosen either as a self-consistent potential like the Hartree-Fock potential, or a phenomenological potential like the Wood-Saxon potential plus a Coulomb and

spin-orbit terms. Hence, Berggren basis states are discrete solutions of the one-body Schrödinger equation:

$$\frac{\partial^2 u_l(k,r)}{\partial r^2} = \left(\frac{l(l+1)}{r^2} + \frac{2m}{\hbar^2} U_{\text{basis}}(r) - k^2 \right) u_l(k,r) \quad \text{with} \quad E = \frac{\hbar^2 k^2}{2m} \tag{2.46}$$

where m is the mass of the nucleon, and l its orbital angular momentum. The reduced radial solutions $u_l(k,r)$ are regular at the origin:

$$u_l(k,r) \underset{r\sim 0}{\sim} C_0(k) r^{l+1} \tag{2.47}$$

At large distances, *i.e.* in the region where the nuclear part of the potential is negligible, the Berggren basis states $u_l(k,r)$ are the solutions of the equation:

$$\frac{\partial^2 u_l(k,r)}{\partial r^2} = \left(\frac{l(l+1)}{r^2} + \frac{2\eta k}{r} - k^2 \right) \tag{2.48}$$

where η is the Sommerfeld parameter:

$$\eta = \frac{mZ}{\hbar^2 k} \tag{2.49}$$

Solutions of Eq. (2.48) are linearly independent, and they can be identified as regular $F_{l,\eta}(kr)$ and irregular $G_{l,\eta}(kr)$ Coulomb functions.

In order to introduce the concepts of incoming and outgoing solutions, it is more convenient to write Coulomb functions as:

$$H^{\pm}_{l,\eta}(kr) = G_{l,\eta}(kr) \pm i F_{l,\eta}(kr) \tag{2.50}$$

The Berggren basis states $u_l(k,r)$ have thus the following asymptotic form:

$$u_l(k,r) \underset{r\to\infty}{\sim} C_+ H^+_{l,\eta}(kr) + C_-(k) H^-_{l,\eta}(kr) \tag{2.51}$$

For bound and resonance states, $C_-(k) = 0$ and $C_+(k) \neq 0$, and for scattering states $C_-(k) \neq 0$ and $C_+ \neq 0$. Hence, due to the boundary conditions (2.47) and (2.51), the solutions $u_l(k,r)$ are unique and can be written as:

$$u_l(k,r) = C_+(k) u^+_l(k,r) + C_-(k) u^-_l(k,r) \tag{2.52}$$

Here, $u^+_l(k,r)$ and $u^-_l(k,r)$ are the two linearly independent solutions of Eq. (2.46).

The $C_0(k)$, $C_+(k)$ and $C_-(k)$ constants in Eqs. (2.52,2.47) are determined by the normalization of the Berggren basis states. The normalization to the Dirac delta is straightforward since it is equivalent to the following condition [121, 122] (see Appendix A.4):

$$C_+(k) C_-(k) = \frac{1}{2\pi} \quad \forall k \tag{2.53}$$

In practice, constants $C_+(k)$ and $C_-(k)$ are determined by the matching condition between the radial wave function $u_l(k,r)$ and its asymptotic form at a given point $R >> 0$:

$$\begin{aligned} &\frac{d}{dr}\left(C_+(k) H^+_{l,\eta}(kR) + C_-(k) H^-_{l,\eta}(kR) \right) = \frac{du_l(k,R)}{dr} \\ &C_+(k) H^+_{l,\eta}(kR) + C_-(k) H^-_{l,\eta}(kR) = u_l(k,R) \end{aligned} \tag{2.54}$$

$C_0(k)$ is then obtained by normalizing the Berggren basis state such that:

$$\int_0^\infty u_l^2(k,r) = 1 \tag{2.55}$$

For bound states and resonances: $C_-(k) = 0$, while for scattering states $C_-(k)$ satisfies Eq. (2.53). Consequently, conditions (2.54) and (2.55) guarantee the continuity of radial wave functions for bound states and resonances. Their differentiability is achieved using the Jost functions [111]:

$$\mathcal{J}^\pm = W(u_l^\pm(k,r), u_l(k,r)) = u_l^\pm(k,r)\frac{du_l(k,r)}{dr} - u_l(k,r)\frac{du_l^\pm(k,r)}{dr} \tag{2.56}$$

Here, $W(f,g)$ is the Wronskian. Jost functions do not depend on r, because $u_l(k,r)$ and $u_l^+(k,r)$ are linearly independent. Thus, the differentiability condition for $u_l(k,r)$:

$$\mathcal{J}^+(k) = 0 \tag{2.57}$$

can be satisfied by varying k.

2.2.6 Determination of the many-body states

Once the s.p. basis is determined, we can diagonalize the full GSM Hamiltonian (2.40). This Hamiltonian is complex-symmetric in the N-body basis (2.25):

$${}^t\hat{H} = \hat{H} \quad \text{with} \quad H_{ij} \in \mathbb{C} \tag{2.58}$$

where $\hat{H}$ is the Hamiltonian matrix and H_{ij} an element of $\hat{H}$. In standard SM calculations, the Hamiltonian is usually diagonalized using the Lanczos method [141]. However, as this method determines the eigenstates by selecting the lowest energies, it fails to identify resonances as eigenvalues associated to scattering states can be lower than those associated to resonances.

The problem of the identification of resonances can be solved with the so-called overlap method [5,142]. This method consists of determining the resonances among all eigenstates $|\Psi\rangle$ by selecting the one having the biggest overlap with a pivot state $|\Psi_0\rangle$. In practice, the pivot state $|\Psi_0\rangle$ is determined by diagonalizing the Hamiltonian (2.40) in a smaller space consisting of Slater determinants composed by s.p. bound states and resonances only. In this space, the diagonalization can be achieved using the Lanczos algorithm or some variant of this method. This is called the pole approximation, and this space is called the pole space. The resulting spectrum is a zero-order approximation of the full spectrum which includes the scattering continuum. Then each eigenstate found in the pole approximation is used as a pivot for the Davidson method [143] which is more precise for excited states. Eigenstates $|\Psi\rangle$ with an overlap greater than 70% with pivots are then selected.

Very large matrices, encountered for example in the no-core GSM [10], require the application of the density matrix renormalization group method in GSM [26–28] to deal with the huge dimensionality of the many-body basis. The main idea of the density matrix renormalization group in GSM, is to gradually consider different s.p states of the discretized non-resonant continuum, and retain only optimal states governed by the eigenvalues of the density matrix with the largest modulus. Indeed, the method is based on the fact that Slater determinants involving many non-resonant continuum s.p states do not play a significant role.

2.2.7 GSM applications

The GSM has been applied in the description of various bound and unbound systems like $^{18-22}$O [5, 142], ^{80}Ni [6, 144], $^{5-10}$He [142, 145], or $^{5-11}$Li [121, 145]. In several applications, in addition to the energy spectra, other relevant quantities have been studied like the radial overlap integrals [146], spectroscopic factors [147], the asymptotic normalization coefficients [148], the charge radii and the neutron-neutron correlations [149].

In Refs. [125, 126, 150] the role of antibound states has been studied. A detailed comparison between the GSM and the Gaussian expansion method has been done for ^{6}He and ^{6}Be [151].

The use of Lee-Suzuki regularization method [152] in GSM has been discussed in Ref. [153] for schematic interactions, and in Refs. [154, 155] for realistic chiral N^{3}LO interactions [156].

The *ab initio* formulation of GSM, the no-core Gamow shell model, has been proposed to study well bound and unbound states of Helium isotopes with a realistic N^{3}LO chiral interaction [10]. In these studies, the density matrix renormalization group method [26–28] has been employed. The no-core Gamow shell model has also been applied to study the existence of a tetraneutron [157] and the unbound isotopes of heavy hydrogen nuclei [158].

2.3 On the solution of pairing problem in the continuum

All even-even nuclei in the ground state are coupled to $J = 0$ angular momentum and are more tightly bound than the neighboring even-odd nuclei. Moreover, in the even-even nuclei there is an energy gap of 1-2 MeV between the ground state and the lowest two quasi-particle excitations. These experimental observations suggest an important role of the residual interactions beyond mean-field in atomic nuclei.

One of the important residual interaction is the pairing interaction. The seniority pairing model has been proposed in 1942 by Racah to provide the classification of electron excitations in atoms [159]. This model has been also applied to understand various inconsistencies of the independent particle model in the description of binding energies and spectra of atomic nuclei.

The Hamiltonian of the seniority pairing model is too simple to offer a satisfactory framework for nuclear studies. In 1957, an extension of this model was proposed by Bardeen, Cooper and Schrieffer (BCS) [160] to explain the superconductivity. Soon afterwards, it was realized that pairing is an important component of the effective interaction, responsible for nuclear superfluidity from finite nuclei to neutron stars [161]. In the BCS model, the Hamiltonian consists of a one-body part determined by either a phenomenological or self-consistent potential, and a two-body part similar to the interaction introduced by Racah. A reliable solution of the BCS theory has been given in terms of the independent quasiparticles. This was a beginning of the long 'success story' of BCS in nuclear physics.

In 1960 Richardson derived an exact solution of the BCS Hamiltonian for a constant pairing strength and a discrete set of s.p. levels [51, 52]. Recently, exact solutions of the pairing model were discussed anew to quantify the error of number projected BCS approach, and to study the superfluid ultra-small grains [162–168]. In 2001, Dukelsky et al. showed that by combining the Richardson solution with the integrable model proposed by Gaudin for quantum spin systems [169], one can derive three classes of exactly solvable pairing Hamiltonian for fermions and bosons [170]. In these models, the pairing Hamiltonian appears as a particular combination of the integrals of motion within the rational class of integrable models. This finding allowed to find many exactly

solvable pairing models by taking arbitrary combinations of the integrals of motion within each class. In particular, the hyperbolic family of Gaudin models, has been proposed in [171] to describe pairing in heavy nuclei. More recently, Gaudin models have been extended to larger Lie algebras including the SO(5) for $T = 1$ isovector pairing [172] and the SO(8) for $T = 0, 1$ spin-isospin pairing [173] allowing for the exact treatment of proton-neutron pairing correlations.

Exactly solvable models have always played an important role in understanding properties of strongly correlated quantum systems, both in condensed matter and nuclear physics. In nuclear physics, the exactly solvable pairing models gave a deeper insight into the superfluid correlations in well bound nuclei. In weakly bound or unbound nuclei, we are missing an insight that could be provided by simple models. An understanding of the pairing correlations in these nuclei is still the "chasse gardée" of advanced numerical simulations, such as the GSM or the coupled-cluster theory. Recently, there have been several attempts to find an exact solution of the pairing model in the continuum. Hasegawa and Kaneko studied effects of s.p. resonances (Gamow states) on pairing correlations [168]. Id Betan attempted to solve Richardson equations with the real-energy continuum [174] but no proof was given that this approach is reliable. An exact solution of pairing Hamiltonian in the continuum can be obtained in GSM though only systems with a small number of active particles can be studied in practice.

In this section, we start with a short presentation of the generalized Gaudin algebra which leads to the Gaudin family of models. Then, we present the formulation of the rational Gaudin pairing model in the Berggren ensemble. In the following subsection, we derive the generalized Richardson solution for the rational Gaudin model with the continuum which is exact in three distinct limits: (i) in the pole approximation [7], (ii) for the discrete spectrum of real energy s.p. levels, and (iii) in the non-resonant s.p. continuum.

By comparing the generalized Richardson solution of the rational Gaudin pairing model with the exact GSM solutions, we will assess the reliability of the generalized Richardson solution in the most general cases of s.p. spectrum, including s.p. bound states, resonances, and the non-resonant continuum.

Finally, we discuss the first application of the generalized Richardson equations for the description of binding energies and spectra of carbon isotopes. We will also point out a possible application of these equations for the studies of unstable ultra-small superconducting grains.

2.3.1 Generalized Gaudin algebra

Exactly solvable quantum integrable models are defined by the Yang-Baxter equation [175–177] which allows to replace an eigenvalue problem by a much simpler algebraic problem. This interesting feature is associated with the existence of hidden symmetries. In condensed matter, the most important exactly solvable models are those developed in the context of one-dimensional systems, such as the Heisenberg model [178, 179], the Tomonaga-Luttinger models [180, 181], and the models with the long-range interactions [182, 183]. The Hamiltonian of an exactly solvable problem is written as a linear combination of the Casimir operators of the group decomposition chain representing relevant symmetries. Some examples of such exactly solvable models are: the Racah's seniority model [159], the Elliott's SU(3) rotational model [184], or the three dynamical limits of the U(6) interacting boson model [185].

The constant pairing Hamiltonian has exact solutions which were derived by Richardson [51,52]. Independently, these solutions were discussed by Gaudin [186] and applied much later to ultra-

small superconducting grains [163]. The connection found between the Richardson's solution and the Gaudin model [169] was followed by the proof of integrability of the pairing model [187]. By establishing the relation between the integrals of motion of the pairing model and those of the Gaudin model, it became possible to derive three classes of integrable pairing models for fermions and bosons [50, 170]. Recent studies of the relation between level crossings and exceptional points in the integrable and non-integrable limits of the pairing model allowed to establish the criterion to distinguish between chaotic and regular dynamics in the quantum regime, for finite systems in low-dimensional Hilbert spaces [188] .

Gaudin algebra	Representation	**l**	Model
XXX	$\oplus_l$(SU(2)-F-P)	N	BCS Richardson Nuclear pairing BCS ($\mathbf{k}\uparrow, \mathbf{k}\downarrow$)
	$\oplus_l$(SU(2)-F-S)	N	Particle-hole-like
	$\oplus_l$(SU(1,1)-B)	N	Bosonic BCS
	$\oplus_l$(SU(2)$\oplus$SU(2))	N	Central spin
	$\oplus_l$(SU(1,1)$\oplus$SU(1,1))	N	Bosonic central spin
XXZ	$\oplus_l$(SU(2)-F-S)	2	Suhl-Matthias-Walker Lipkin-Meshkov-Glick
	$\oplus_l$(SU(1,1)-B)	2	Interacting Boson Model 1 Two-Josephon-coupled BECs
	$\oplus_l$(SU(2)$\oplus h_4$)	N	Generalized Dicke, fermionic atom molecule
	$\oplus_l$(SU(1,1)$\oplus h_4$)	N	Bosonic atom molecule
	$\oplus_l$(SU(2)-F-S $\oplus$SU(2))	N	Kondo-like impurity
	$\oplus_l(h_4\oplus$SU(2)-F-S)	N	Special spin-boson
XYZ	$\oplus_l$su(2)	N	Generalized XYZ Gaudin

Table 2.1 – Exactly solvable models which can be derived from different representations of the generators of the generalized Gaudin algebra. Here, **l** refers to the number of copies of the algebra used to write down the model. The notation F, B, S, P, and h_4 stands for Fermionic, Bosonic, Spin, Pseudospin, and Heisenberg-Weyl algebra respectively. This figure comes from Ref. [50] where more informations about these model can be found. Note that the BCS Hamiltonian belongs to the XXX Gaudin algebra.

The generalized Gaudin algebra can be introduced as a set of operators $\{\hat{S}^k_m \equiv \hat{S}^k(E_m)\}$, where

$k = x, y, z$, satisfying the commutation relations:

$$\begin{aligned}
\left[\hat{S}^k_m, \hat{S}^k_\ell\right] &= 0 \\
\left[\hat{S}^x_m, \hat{S}^y_\ell\right] &= i\left(Y_{m\ell}\hat{S}^z_m - X_{m\ell}\hat{S}^z_\ell\right) \\
\left[\hat{S}^y_m, \hat{S}^z_\ell\right] &= i\left(Z_{m\ell}\hat{S}^x_m - Y_{m\ell}\hat{S}^x_\ell\right) \\
\left[\hat{S}^z_m, \hat{S}^x_\ell\right] &= i\left(X_{m\ell}\hat{S}^y_m - Z_{m\ell}\hat{S}^y_\ell\right)
\end{aligned} \tag{2.59}$$

where $m \neq \ell$, $X_{m\ell} = X(E_m, E_\ell)$, $Y_{m\ell} = Y(E_m, E_\ell)$, and $Z_{m\ell} = Z(E_m, E_\ell)$ are antisymmetric complex functions of two arbitrary complex variables: E_m, E_ℓ, labelled by the positive integers m and ℓ, respectively. Equivalently, in terms of the $k = +, -, z$ basis and for $E_m \neq E_\ell$, one obtains:

$$\begin{aligned}
\left[\hat{S}^\pm_m, \hat{S}^\pm_\ell\right] &= \pm 2V^-_{m\ell}\left(\hat{S}^z_m + \hat{S}^z_\ell\right) \\
\left[\hat{S}^-_m, \hat{S}^+_\ell\right] &= -2V^+_{m\ell}\left(\hat{S}^z_m - \hat{S}^z_\ell\right) \\
\left[\hat{S}^z_m, \hat{S}^\pm_\ell\right] &= \pm\left(V^+_{m\ell}\hat{S}^\pm_m - Z_{m\ell}\hat{S}^\pm_\ell - V^-_{m\ell}\hat{S}^\mp_m\right)
\end{aligned} \tag{2.60}$$

where $\hat{S}^\pm_m = \hat{S}^x_m \pm i\hat{S}^y_m$, and $V^\pm_{m\ell} = \left(X_{m\ell} \pm Y_{m\ell}\right)/2$. Notice that $\hat{S}^{+(-)}_m$ and $\hat{S}^{+(-)}_\ell$ are non-commuting operators, unless $X_{m\ell} = Y_{m\ell}$.

The complex functions $X_{m\ell}, Y_{m\ell}$ and $Z_{m\ell}$ in (2.59) have the following boundary condition:

$$\begin{aligned}
\lim_{\epsilon\to 0} \epsilon X(x, x+\epsilon) &= f(x) \\
\lim_{\epsilon\to 0} \epsilon Z(x, x+\epsilon) &= h(x) \\
\lim_{\epsilon\to 0} \epsilon Y(x, x+\epsilon) &= g(x)
\end{aligned} \tag{2.61}$$

where $f(x), g(x)$, and $h(x)$ are the nonsingular functions. Indeed, X, Y, and Z are complex meromorphic functions having poles of order one. In particular, when $f(x) = g(x) = h(x)$ the above commutations relations (2.59) can be analytically continued to the case $m = \ell$, *i.e.* $E_m \to E_\ell$. For example:

$$\begin{aligned}
\left[\hat{S}^x_m, \hat{S}^y_m\right] &= \lim_{\epsilon\to 0} i(Y(E_m, E_m+\epsilon)\hat{S}^z(E_m) - X(E_m, E_m+\epsilon)\hat{S}^z(E_m+\epsilon)) \\
&= -if(E_m)\frac{\partial \hat{S}^z_m}{\partial E_m}
\end{aligned} \tag{2.62}$$

Then, the commutation relations:

$$\begin{aligned}
\left[\hat{S}^k_m, \hat{S}^k_m\right] &= 0 \\
\left[\hat{S}^x_m, \hat{S}^y_m\right] &= -if(E_m)\frac{\partial \hat{S}^z_m}{\partial E_m} \\
\left[\hat{S}^y_m, \hat{S}^z_m\right] &= -if(E_m)\frac{\partial \hat{S}^x_m}{\partial E_m} \\
\left[\hat{S}^z_m, \hat{S}^x_m\right] &= -if(E_m)\frac{\partial \hat{S}^y_m}{\partial E_m}
\end{aligned} \tag{2.63}$$

together with Eqs. (2.59) form an infinite-dimensional Lie algebra. From the Jacobi identities for the generators of the Lie algebra:

$$\left[\hat{S}_n^x,\left[\hat{S}_m^x,\hat{S}_\ell^y\right]\right]+\left[\hat{S}_\ell^y,\left[\hat{S}_n^x,\hat{S}_m^x\right]\right]+\left[\hat{S}_m^x,\left[\hat{S}_\ell^y,\hat{S}_n^x\right]\right]=0 \tag{2.64}$$

and considering the antisymmetry of the functions X, Y, Z, we obtain the Gaudin equation [169]:

$$Z_{m\ell}X_{\ell n}+Z_{nm}Y_{\ell n}+X_{nm}Y_{m\ell}=0 \tag{2.65}$$

This equation defines the XYZ model of Gaudin.

Let us now consider the XXZ model defined by: $X_{m\ell}=Y_{m\ell}$. The Gaudin equation (2.65) in this case reduces to:

$$Z_{m\ell}X_{\ell n}+Z_{nm}X_{\ell n}+X_{nm}X_{m\ell}=0 \tag{2.66}$$

The condition (2.66) was discussed by Gaudin [169] who found three solutions which can be written in the compact form as:

$$\begin{aligned} X_{ij} &= \frac{\gamma}{\sin\left(\gamma(\eta_i-\eta_j)\right)} \\ Z_{ij} &= \gamma\cot\left(\gamma(\eta_i-\eta_j)\right) \end{aligned} \tag{2.67}$$

Different classes of integrable models correspond to specific values of γ:

- The rational class for $\gamma\to 0$:
$$X_{ij}=Z_{ij}=\frac{1}{\eta_i-\eta_j} \tag{2.68}$$
- The trigonometric class for $\gamma=1$:
$$X_{ij}=\frac{1}{\sin\left(\eta_i-\eta_j\right)}\quad,\quad Z_{ij}=\cot\left(\eta_i-\eta_j\right) \tag{2.69}$$
- The hyperbolic class for $\gamma=i$:
$$X_{ij}=\frac{1}{\sinh\left(\eta_i-\eta_j\right)}\quad,\quad Z_{ij}=\coth\left(\eta_i-\eta_j\right) \tag{2.70}$$

$\eta_{i,j}$ in the above expressions are arbitrary, non-equal real numbers. It is interesting to notice that the rational class corresponds to the XXX model, while the trigonometric and hyperbolic classes correspond to the XXZ model.

Now, let us present the standard method to derive an integrable Hamiltonian for the XXZ model with a realization in terms of the $\bigoplus_{\mathbf{l}}\mathrm{SU}(2)$ algebra. This realization leads to a pairing model. It was demonstrated [187] that any Hamiltonian of a system of fermions interacting through a pairing force can be written as a linear combination of the integrals of motion $\hat{R}_i$:

$$\hat{H}=2\sum_i \epsilon_i\hat{R}_i+C \tag{2.71}$$

where the ϵ_i are the s.p. energies, and C is an arbitrary constant.

Let us consider a possible realization of the generalized Gaudin algebra operators $\hat{S}_m^{\pm}$ and $\hat{S}_m^z$ in terms of generators $\hat{A}_i^{\pm}$ and $\hat{A}_i^z$ of the $\oplus_{\mathbf{I}}\mathrm{SU}(2)$ algebra. These generators satisfy the commutation relations:

$$\left[\hat{A}_i^+, \hat{A}_j^-\right] = 2\delta_{ij}\hat{A}_j^z \quad , \quad \left[\hat{A}_i^z, \hat{A}_j^{\pm}\right] = \pm\delta_{ij}\hat{A}_j^{\pm} \tag{2.72}$$

with $(\hat{A}_j^+)^\dagger = \hat{A}_j^-$. Defining the operators $\hat{S}_m^{\pm}$ and $\hat{S}_m^z$ in terms of the $\oplus_{\mathbf{I}}\mathrm{SU}(2)$ operators:

$$\hat{S}_m^{\pm} = \sum_j X_{mj}\hat{A}_j^{\pm} \quad , \quad \hat{S}_m^z = -\frac{1}{2}\hat{\mathbb{1}} - \sum_j Z_{mj}\hat{A}_j^z \tag{2.73}$$

one obtains a possible realization of the generators of the generalized Gaudin algebra (2.59). The $\hat{R}_i$ operators can be written in terms of both the X, Z functions and the $\hat{A}$ operators as:

$$\hat{R}_i = \hat{A}_i^z - 2\sum_{j\neq i}\left(\frac{X_{ij}}{2}(\hat{A}_i^+\hat{A}_j^- + \hat{A}_i^-\hat{A}_j^+) - Z_{ij}\hat{A}_i^z\hat{A}_j^z\right) \tag{2.74}$$

Any combination of the $\hat{R}_i$ operators (2.74) yields an integrable Hamiltonian. The pairing Hamiltonian belongs to the rational class $\gamma \to 0$.

2.3.2 Representation of the rational XXX model : The pairing Hamiltonian

The pairing Hamiltonian is given in the second quantization formulation by:

$$\hat{H} = \sum_{\alpha}^{D}\epsilon_\alpha\hat{c}_\alpha^\dagger\hat{c}_\alpha - G\sum_{\alpha,\beta}^{D}\hat{c}_\alpha^\dagger\hat{c}_{\bar{\alpha}}^\dagger\hat{c}_{\bar{\beta}}\hat{c}_\beta \tag{2.75}$$

where ϵ_α are the the energies of bound s.p. levels, and G is the pairing strength. Operators $\hat{c}_\alpha^\dagger(\hat{c}_\alpha)$ stand for the particle creation (annihilation) operators, and $\alpha \equiv \{a, m_\alpha\} = \{n_a, \ell_a, j_a, m_\alpha\}$, $\bar{\alpha} = \{a, \bar{m}_\alpha\}$. $\hat{c}_{\bar{\alpha}}^\dagger$ is defined as $\hat{c}_{\bar{\alpha}}^\dagger = (-)^{j_a - m_\alpha}\hat{c}_{\alpha,-m_\alpha}^\dagger$. The degeneracy of a s.p. level a is $\Omega_a = 2j_a + 1$.

Let us define the operators:

$$\hat{n}_a = \sum_{m_\alpha=-j_a}^{j_a}\hat{c}_\alpha^\dagger\hat{c}_\alpha \quad ; \quad \hat{b}_a^\dagger = \sum_{m_\alpha>0}\hat{c}_\alpha^\dagger\hat{c}_{\bar{\alpha}}^\dagger = (\hat{b}_a)^\dagger \tag{2.76}$$

which obey the commutator algebra:

$$\begin{aligned}\left[\hat{n}_a, \hat{b}_{a'}^\dagger\right] &= 2\delta_{aa'}\hat{b}_a^\dagger \\ \left[\hat{b}_a, \hat{b}_{a'}^\dagger\right] &= 2\delta_{aa'}\left(\frac{\hat{\Omega}_a}{4} \pm \frac{\hat{n}_a}{2}\right)\end{aligned} \tag{2.77}$$

where $\hat{\Omega}_a = \Omega_a\hat{\mathbb{1}}$. From now on, whenever there are different signs in the equation, the upper (lower) sign stands for bosons (fermions).

The complete set of states of N particles in $\mathcal{N}$ s.p. states, spanned by the operators $\hat{n}_a$, $\hat{b}_a$, $\hat{b}_a^\dagger$ is given by:

$$|n_1, n_2, \cdots, n_{\mathcal{N}}, \nu\rangle = \frac{1}{\bar{N}}\hat{b}_1^{\dagger n_1}\hat{b}_2^{\dagger n_2}\cdots\hat{b}_{\mathcal{N}}^{\dagger n_{\mathcal{N}}}|\nu\rangle \tag{2.78}$$

where $|\nu\rangle = |\nu_1, \nu_2 \cdots \nu_{\mathcal{N}}\rangle$ is a state of the unpaired particles which satisfy:

$$\hat{b}_a|\nu\rangle = 0 \quad ; \quad \hat{n}_a|\nu\rangle = \nu_a|\nu\rangle \tag{2.79}$$

$\bar{N}$ in Eq. (2.78) is the normalization constant, ν is the total number of the unpaired particles: $\nu = N - 2N_{\text{pair}}$, where N_{pair} is the number of pairs, and ν_a the number of unpaired particles in the level a.

The pairing Hamiltonian (2.75) expressed in the operators $\hat{n}_a$, $\hat{b}_a$, $\hat{b}_a^\dagger$ reads:

$$\hat{H} = \sum_a^{\mathcal{N}} \epsilon_a \hat{n}_a - G \sum_{a,a'}^{\mathcal{N}} \hat{b}_a^\dagger \hat{b}_{a'} \tag{2.80}$$

Defining the three generators of SU(2):

$$\hat{A}_a^+ = \frac{1}{2}\hat{b}_a^\dagger = (\hat{A}_a^-)^\dagger \ , \qquad \hat{A}_a^z = \frac{1}{2}\hat{n}_a - \frac{1}{4}\hat{\Omega}_a \tag{2.81}$$

which satisfy Eq. (2.72) and the rational parametrization: $X_{\eta a} = Z_{ia} = 2G/(2\epsilon_a - E_i)$, with E_i the pair energies, it is possible to show that the pairing Hamiltonian (2.75) stands for an integrable model (see Eq. (2.71)). In this model, any eigenvalue $\tilde{\mathcal{E}}$ of the pairing Hamiltonian (2.80) can be written as:

$$\tilde{\mathcal{E}}^{(K)} = \sum_{i=1}^{N_{\text{pair}}} E_i^{(K)} + \sum_{a=1}^{\mathcal{N}} \epsilon_a \nu_a \quad , \quad K = 0, 1, \cdots, K_{\text{max}} \tag{2.82}$$

where the index K enumerates the eigenstates in an ascending order of the excitation energy, and K_{max} is the total number of eigenstates. In general, $\tilde{\mathcal{E}}^{(K)}$ can be complex and then $\mathcal{R}(\tilde{\mathcal{E}}^{(K)}) = \mathcal{E}^{(K)}$ is the energy, and $2\mathcal{I}(\tilde{\mathcal{E}}^{(K)}) = \Gamma^{(K)}$ is the corresponding width of the K^{th} eigenstate.

Now, considering the Bethe ansatz for the eigenstate of $\hat{H}$:

$$|\Psi\rangle = \prod_i^{N_{\text{pair}}} \hat{S}_i^+ |\nu\rangle \tag{2.83}$$

with $\hat{S}_i^\dagger$, the generator of the generalized Gaudin algebra (2.59) defined in Eq. (2.73), it is possible to show that the eigenvalue problem of the Schrödinger equation can be reduced to an algebraic problem, i.e the Richardson equations [51, 52], given by :

$$1 \pm 2G \sum_a^{\mathcal{N}} \frac{d_a}{2\epsilon_a - E_i^{(K)}} \mp 2G \sum_{j\neq i}^{N_{\text{pair}}} \frac{1}{E_j^{(K)} - E_i^{(K)}} = 0 \tag{2.84}$$

where the pair energies $E_i^{(K)}$ are solutions of N_{pair} coupled non-linear equations, and $d_a = \Omega_a/4 \pm \nu_a/2$.

2.3.3 Generalization of the rational Gaudin model to include the continuum

Generalization of the rational Gaudin model to include the continuum part of a s.p. spectrum, can be formulated in the Berggren s.p. ensemble [44] which includes bound states (b), resonances

(r), and non-resonant (c) continuum states. In this representation, the pairing Hamiltonian of the rational Gaudin model is:

$$\begin{aligned}\hat{H} &= \sum_{i\epsilon b,r}\epsilon_i\hat{n}_i + \sum_c\int_{L_c^+}\epsilon_{k_c}\hat{n}_{k_c}dk_c \\ &- G\sum_{i,i'\epsilon b,r}\hat{b}_i^\dagger\hat{b}_{i'} - G\sum_{c,c'}\int_{L_c^+}\hat{b}_{k_c}^\dagger\hat{b}_{k'_{c'}}dk_c dk'_{c'} \\ &- G\sum_{(i\epsilon b,r),c}\int_{L_c^+}\left(\hat{b}_{k_c}^\dagger\hat{b}_i + \hat{b}_i^\dagger\hat{b}_{k_c}\right)dk_c \end{aligned} \tag{2.85}$$

Sums over c, c' denote summations over different partial waves (ℓ, j) until $(\ell_{\max}, j_{\max})$. k_c is related to the energy of a s.p. state c in the non-resonant continuum: $\epsilon_c = \hbar^2k_c^2/2m$, and m is the particle mass. The discrete sums run over the real energy bound s.p. states and the complex energy s.p. resonances enclosed in between the contour L_c^+ and the real k-axis. All resonances of the same quantum numbers (ℓ, j) have the same contour $L^+_{c(\ell,j)}$ in the complex k-plane. More about the complete Berggren s.p. ensemble and its application in many-body systems can be found in Sec. 2.2.5.

The pair creation (annihilation) operators satisfy the commutator relations (2.77) for the discrete (bound states and resonances) s.p. states, and

$$\begin{aligned}\left[\hat{n}_{k_c}, \hat{b}_{k'_{c'}}^\dagger\right] &= 2\delta(k_c - k'_c)\delta_{cc'}\hat{b}_{k_c}^\dagger \\ \left[\hat{b}_{k_c}, \hat{b}_{k'_{c'}}^\dagger\right] &= \delta(k_c - k'_c)\delta_{cc'}\frac{\hat{\Omega}_{k_c}}{2} \pm \delta_{k_ck'_c}\delta_{cc'}\hat{n}_{k_c}\end{aligned} \tag{2.86}$$

for the non-resonant scattering s.p. states.

In all practical applications, the continuum has to be discretized. It is convenient to define new pair and number operators:

$$\hat{\tilde{n}}_q = w_q\hat{n}_q \quad ; \quad \hat{\tilde{b}}_q^\dagger = \sqrt{w_q}\hat{b}_q^\dagger = (\hat{\tilde{b}}_q)^\dagger \tag{2.87}$$

where index q runs over all bound, resonance and discretized scattering states in the Berggren basis. w_q is a Gaussian weight of the integration procedure. For bound and resonance states, $w_q = 1$. With this definition, all states of the pairs of particles are normalized to unity and treated on the same footing. The new operators $\hat{\tilde{n}}_q, \hat{\tilde{b}}_q, \hat{\tilde{b}}_q^\dagger$ satisfy similar commutation relations as the operators $\hat{n}_i, \hat{b}_i, \hat{b}_i^\dagger$ in discrete levels (Eq. (2.77)):

$$\begin{aligned}\left[\hat{\tilde{n}}_q, \hat{\tilde{b}}_{q'}^\dagger\right] &= 2\delta_{qq'}\hat{\tilde{b}}_q^\dagger \\ \left[\hat{\tilde{b}}_q, \hat{\tilde{b}}_{q'}^\dagger\right] &= 2\delta_{qq'}\left(\frac{\hat{\Omega}_q}{4} \pm \frac{\hat{\tilde{n}}_q}{2}\right)\end{aligned} \tag{2.88}$$

The Hamiltonian of the generalized rational Gaudin model (2.85) expressed in the operators $\hat{\tilde{n}}_q, \tilde{b}_q, \tilde{b}_q^\dagger$ reads:

$$\hat{H} = \sum_q^{\mathcal{N}}\epsilon_q\hat{\tilde{n}}_q - \sum_{q,q'}^{\mathcal{N}}G_{qq'}\hat{\tilde{b}}_{q'}^\dagger\hat{\tilde{b}}_q \quad ; \quad G_{qq'} = \sqrt{w_q}\sqrt{w_{q'}}G \tag{2.89}$$

where $\mathcal{N}$ is the total number of bound, resonance and discretized continuum s.p. states.

In general, pairing models with the state-dependent pairing interaction are not integrable. The exception from this rule is the hyperbolic model [171, 189] where Gaussian weights w_q are linear functions of s.p. energies ϵ_q. Trying to find a good ansatz for the eigenstate, one has then to look for reliable approximations of the Hamiltonian (2.89) and/or the commutation relations (2.86) for the non-resonant scattering states which break the SU(2) commutator algebra.

It is important to note that if we want to diagonalize the Hamiltonian (Eq. (2.89)) we have to be careful applying the new normalized operators $\hat{\hat{n}}_q$ and $\hat{\hat{b}}_q^\dagger, \hat{\hat{b}}_q$. As the Hamiltonian (2.85) is expressed in a certain basis of Slater determinants, the contour discretization leads not only to new normalized operators but also to new normalized Slater determinants, so that the action of $\hat{\hat{n}}_q, \hat{\hat{b}}_q^\dagger$ and $\hat{\hat{b}}_q$ on these Slater determinants is defined as in the discrete case.

2.3.4 Approximate solution for the rational Gaudin model with the continuum

An approximate solution for the generalized rational pairing model (2.89) can be found by replacing the Kronecker delta by the Dirac delta in the commutator (2.86) for states in the non-resonant continuum:

$$\left[\hat{b}_{k_c}, \hat{b}^\dagger_{k'_{c'}}\right] = 2\delta(k_c - k'_c)\delta_{cc'}\left(\frac{\hat{\Omega}_{k_c}}{4} \pm \frac{\hat{n}_{k_c}}{2}\right) . \tag{2.90}$$

With this change, the pair operators $\hat{\hat{b}}_q^\dagger(\hat{\hat{b}}_q)$ for bound, resonance and discretized scattering states satisfy:

$$\begin{aligned}\left[\hat{\hat{n}}_q, \hat{\hat{b}}^\dagger_{q'}\right] &= 2\delta_{qq'}\hat{\hat{b}}^\dagger_q \\ \left[\hat{\hat{b}}_q, \hat{\hat{b}}^\dagger_{q'}\right] &= 2\delta_{qq'}\left(\frac{\hat{\Omega}_q}{4} \pm \frac{\hat{\hat{n}}_q}{2w_q}\right)\end{aligned} \tag{2.91}$$

Note that the difference between Eqs.(2.91) and (2.88) is the presence of the weight w_q. The transformation presented in Eq. (2.91) is mathematically undefined. Due to this choice, we cannot have a proper definition of these new operators and, hence, the direct diagonalization of a Hamiltonian (2.89) using deformed operators (2.91) is not possible. In the following, we suppose that the deformed operators act like those in Eq. (2.76).

Let us derive the eigenvalue of the pairing Hamiltonian (2.89). Similarly as in the Richardson solution [51, 52], we take the product of pair states

$$|\Psi_{\rm norm}\rangle = \prod_{\eta=1}^{N_{\rm pair}} \hat{S}^\dagger_{\eta;{\rm norm}}|\nu\rangle \tag{2.92}$$

as an ansatz for the many-body state, where

$$\hat{S}^\dagger_{\eta;{\rm norm}} = c_\eta G \sum_q^{\mathcal{N}} \frac{\hat{\hat{b}}^\dagger_q \sqrt{w_q}}{2\epsilon_q - E_\eta} \tag{2.93}$$

and E_η are the pair energies (here we removed the index K to simplify the notation). The normalization constants c_η are determined by solving:

$$\frac{1}{(c_\eta G)^2} = \frac{1}{{C_\eta}^2} = \sum_q^{\mathcal{N}} \frac{w_q}{(2\epsilon_q - E_\eta)^2} \tag{2.94}$$

It is convenient to define: $\hat{S}^\dagger_\eta = \hat{S}^\dagger_{\eta;\mathrm{norm}}/C_\eta$, so that

$$|\Psi_{\mathrm{norm}}\rangle = \prod_{\eta=1}^{N_{\mathrm{pair}}} C_\eta \hat{S}^\dagger_\eta |\nu\rangle = C|\Psi\rangle \tag{2.95}$$

and

$$C = \prod_{\eta=1}^{N_{\mathrm{pair}}} C_\eta \quad \text{and} \quad |\Psi_n\rangle = \prod_{\eta=1}^{N_{\mathrm{pair}}} \hat{S}^\dagger_\eta |\nu\rangle \ .$$

The operators $\hat{\tilde{n}}, \hat{S}_\eta$ and $\hat{S}_0$:

$$\hat{S}^\dagger_0 = \sum_q^{\mathcal{N}} \hat{\tilde{b}}^\dagger_q \sqrt{w_q} \tag{2.96}$$

satisfy the commutator relations:

$$\begin{aligned}
\left[\hat{\tilde{n}}_q, \hat{S}^\dagger_\eta\right] &= \frac{2\hat{\tilde{b}}^\dagger_q \sqrt{w_q}}{2\epsilon_q - E_\eta} \\
\left[\hat{\tilde{n}}_q, \hat{S}^\dagger_0\right] &= 2\sqrt{w_q}\hat{\tilde{b}}^\dagger_q \\
\left[\hat{S}_\eta, \hat{S}^\dagger_{\eta'}\right] &= \sum_q^{\mathcal{N}} \frac{2w_q(\hat{\Omega}_q/4 \pm \hat{\nu}_q/2)}{(2\epsilon_q - E_\eta)(2\epsilon_q - E_{\eta'})} \\
\left[\hat{S}_0, \hat{S}^\dagger_\eta\right] &= \sum_q^{\mathcal{N}} \frac{w_q\hat{\Omega}_q/2 \pm \hat{\tilde{n}}_q}{2\epsilon_q - E_\eta} \\
\left[\hat{S}^\dagger_0, \hat{S}^\dagger_\eta\right] &= 0
\end{aligned} \tag{2.97}$$

which can be derived from the commutation relations for operators $\hat{\tilde{n}}_q, \hat{\tilde{b}}^\dagger_q, \hat{\tilde{b}}_q$ (Eq. (2.91)).

The Hamiltonian of the generalized rational Gaudin model (2.89) expressed in these operators is:

$$\hat{H} = \sum_q^{\mathcal{N}} \epsilon_q \hat{\tilde{n}}_q - G\hat{S}^\dagger_0 \hat{S}_0 \tag{2.98}$$

and the pair energies for boson and fermion systems are given by:

$$1 \pm 2G \sum_q^{\mathcal{N}} \frac{w_q\,(\Omega_q/4 \pm \nu_q/2)}{2\epsilon_q - E_\eta} \mp 2G \sum_{\mu\neq\eta}^{N_{\mathrm{pair}}} \frac{1}{E_\mu - E_\eta} = 0 \tag{2.99}$$

The first sum in these generalized Richardson equations can be split into separate terms coming from from the resonant states and the discretized scattering states.

In the continuum limit, the generalized Richardson equations are:

$$\begin{aligned} 1 \quad &\pm \quad 2G \sum_{i\in b,r}^{\mathcal{N}} \frac{d_i}{2\epsilon_i - E_\eta} \\ &\pm \quad 2G \sum_{c}^{\ell_{\max},j_{\max}} \int_{L_c^+} \frac{d_{k_c}}{\hbar^2 k_c^2/m - E_\eta} dk_c \\ &\mp \quad 2G \sum_{\mu\neq\nu}^{N_{\text{pair}}} \frac{1}{E_\mu - E_\eta} = 0 \end{aligned} \tag{2.100}$$

where $d_i = \Omega_i/4 \pm \nu_i/2$ and similarly for d_{k_c}.

Equations (2.99) provide the approximate solution of rational Gaudin model with continuum which is obtained by replacing exact commutator relations (2.86) by approximate ones (2.90) (see Appendix A.2 for details of the derivation of Eq. (2.99)). In certain limiting situations this solution is however exact. For a discrete set of bound s.p. levels, all weights w_q are equal to 1 and, hence, Eq. (2.99) reduces to an exact solution for the rational Richardson-Gaudin model [51,52]. By the same argument, Eq. (2.99) provides an exact solution in the pole approximation, *i.e.* neglecting the non-resonant continuum states. Eq. (2.99) is also exact if the Berggren ensemble contains only states of the non-resonant continuum because in this case one may take the same weights $w_q \equiv w$ for all continuum states q and renormalize the pairing strength $G' = Gw$ accordingly. In this particular case, the third sum in Eq. (2.99) goes to 0 and one obtains:

$$1 \pm 2G \sum_{c}^{\ell_{\max},j_{\max}} \int \frac{d_{k_c}}{2\epsilon_{k_c} - E_\eta} dk_c = 0 \ . \tag{2.101}$$

2.3.5 Numerical solution of the rational Gaudin model with the continuum

Numerical solution of (generalized) Richardson equations (2.99) is plagued by divergencies if two or more pair energies coincide with twice a s.p. energy. In the weak coupling limit ($G \to 0$), the standard way to approach this problem is to start with an educated guess for pair energies E_i and then evolve them by iteratively solving the (generalized) Richardson equations for increasing values of G. At each step, the solution for pair energies is updated with the Newton-Raphson method using the solution of the previous step as the new starting point [190].

This initial guess is determined by solving the generalized Richardson equations in the limit $G \to 0$. The general expression for pair energies E_i in this limit is:

$$\lim_{G\to 0} E_i = 2\epsilon_q \quad \text{with} \quad i = 1,\cdots,N_{\text{pair}} \quad \text{and} \quad q = 1,\cdots,\mathcal{N} \tag{2.102}$$

The analytical determination of pair energies becomes difficult if many pairs occupy the same s.p. level q. In a general case of N_{pair} pairs occupying the same s.p. state of energy ϵ_q, the starting pair energies E_i are found by solving the set of N_{pair} coupled equations:

$$1 \pm \frac{2Gd_q}{2\epsilon_q - E_i} \mp 2G \sum_{j\neq i}^{N_{\text{pair}}} \frac{1}{E_j - E_i} = 0 \qquad i = 1,\cdots,N_{\text{pair}} \tag{2.103}$$

Notice that the non-resonant continuum states in the weak coupling limit $G << 1$ are not occupied and, hence, the corresponding terms in generalized Richardson equations are absent in this limit.

It is possible to write the analytic solution of Eq. (2.103) for one or two pairs of particles on the same level q. If a degeneracy of the s.p. level q is $\Omega_q = 2$, *i.e.* at most one pair of particles can occupy this level, the solution of Eq. (2.103) is:

$$E_i = 2\epsilon_q - 2Gd_q \tag{2.104}$$

For higher degeneracy of s.p. states q ($\Omega_q \geq 4$), the analytical solution of Eq. (2.103) for two pairs of particles is:

$$\begin{aligned} E_i &= 2\epsilon_q - G(d_q + 1) + iG\sqrt{2d_q + 1} \\ E_{i'} &= 2\epsilon_q - G(d_q + 1) - iG\sqrt{2d_q + 1} \end{aligned} \tag{2.105}$$

Derivations of Eq. (2.104) and Eq. (2.105) are given in Appendix A.3. For three pairs occupying the same level q at $G << 1$, we can use a combination of the solutions (2.104) and (2.105), *i.e.* one pair is initiated with Eq. (2.104) while the two others are initiated with Eq. (2.105).

It is interesting to notice that if two pairs at $G \to 0$ occupy the same s.p. state q, then their energies are complex conjugate. If the s.p. spectrum is real then this symmetry of the pair energies at $G \to 0$ is preserved by the iterative procedure of solving the generalized Richardson equations for any G. This special symmetry of pair energies in the weak coupling limit is broken for finite G if the non-resonant continuum states are included in the basis. Indeed, continuum states are absent in Eq. (2.103) but become occupied for finite values of the pairing strength G and hence, the initial symmetry of pair energies is broken in the course of solving the generalized Richardson equations.

For systems with an odd number particles, *i.e.* with unpaired particles and seniority $\nu \neq 0$, we have to use Eqs. (2.104), (2.105) to initiate the pair energies, and set ν_q in Eq. (2.99). Setting the ν_q gives the information of how many of unpaired particles occupy the level q.

Numerical solutions of (generalized) Richardson equations exhibit singularities also for finite G [191]. Formally, they cancel out and the total energy (the sum of pair energies) is always a continuous function of G. However, these singularities generate instabilities in numerical applications which are hard to deal with. Those which occur at specific values of the pairing strength G_c, are seen in the convergence of different pair energies to the same energy $2\epsilon_q$. Consequently, the derivative of pair energies with respect to G becomes very large and the Newton-Raphson method becomes unstable.

The practical solution of this problem has been proposed by Richardson for doubly degenerate levels [192]. In this case, two pair energies E_λ and $E_{\lambda'}$ converge to the same energy $2\epsilon_q$, thus it is convenient to use a new set of variables:

$$\begin{aligned} \lambda_+ &= 4\epsilon_q - E_\lambda - E'_\lambda \\ \lambda_- &= \left(E_\lambda - E'_\lambda\right)^2 \end{aligned} \tag{2.106}$$

for $G \simeq G_c$. The particularity of these new variables is that their derivative with respect to G does not diverge at $G = G_c$. Thus, it is possible to perform a polynomial fit of $\lambda_+(G)$ and $\lambda_-(G)$ in the vicinity of G_c, and extrapolate the pair energies E_λ and $E_{\lambda'}$ across G_c.

The reference solution for the rational Gaudin model with the continuum is provided by the exact diagonalization of the pairing Hamiltonian (2.85). We discretize the contour L_c^+ using the

Gauss-Legendre quadrature method and build the s.p. spectrum which is used both in the generalized Richardson equations (2.99) and in the GSM.

2.3.5.1 Numerical solution of pairing Hamiltonian in the GSM

Exact solutions of the pairing Hamiltonian (2.85) are obtained by diagonalizing the Hamiltonian matrix using the Davidson method. This matrix is sparse with only ~0.4% of non-zero matrix elements. The calculation of eigenvalues in this case is efficient because matrix-vector multiplications are fast and the storage of a matrix can be optimized.

2.3.5.2 Calculation of the pairing gap

A useful measure of pairing correlations in a given eigensate $|\Psi^{(K)}\rangle$ is the pairing gap:

$$\Delta^{(K)} = G \sum_{q}^{\mathcal{N}} \sqrt{n_q^{(K)}(1 - n_q^{(K)})} \tag{2.107}$$

where the sum runs over s.p. states, and $n_q^{(K)}$ is the occupation probability of the state q. Determination of the occupation probability $n_q^{(K)}$ can be done exactly through the diagonalization of GSM Hamiltonian.

Let us write the eigenstate $|\Psi^{(K)}\rangle$ of a pairing Hamiltonian (2.80) as an expansion in a basis of Slater determinants $|\Phi_\alpha\rangle$:

$$|\Psi^{(K)}\rangle = \sum_{\alpha} C_\alpha^{(K)} |\Phi_\alpha\rangle \tag{2.108}$$

The expectation value of the particle number operator $\hat{N}$ is:

$$\begin{aligned} N = \langle\Psi^{(K)}|\,\hat{N}\,|\Psi^{(K)}\rangle &= \sum_{\alpha,\alpha'} C_\alpha^{(K)} C_{\alpha'}^{(K)} \langle\Phi_\alpha|\,\hat{N}\,|\Phi_{\alpha'}\rangle \\ &= \sum_{q} 2n_q^{(K)} \end{aligned} \tag{2.109}$$

Hence, the occupation probability can be determined numerically as:

$$n_q^{(K)} = \sum_{\alpha} g(\alpha, q; K)\, \left(C_\alpha^{(K)}\right)^2 \tag{2.110}$$

where $g(\alpha, q; K)$ is equal to 1 or 0 depending on whether the s.p. state q is occupied or unoccupied in the Slater determinant α of an eigenstate K.

In the generalized Richardson equations, we have no access to the expansion of the N-body state in terms of Slater determinants. Therefore, the s.p. occupation probabilities in an eigenstate K are determined by [191, 193]:

$$n_q^{(K)} = \frac{\partial \tilde{\mathcal{E}}^{(K)}}{\partial \epsilon_q}\ , \tag{2.111}$$

where $\tilde{\mathcal{E}}^{(K)}$ is the total energy of the eigenstate K, and ϵ_q is the energy of the s.p. state q.

G (MeV)	Nb of pairs	9pts	15pts	21pts	30pts	45pts
0.01	2 pairs	$7.2138e^{-13}$	$7.7698e^{-13}$	$8.0458e^{-13}$	$8.2666e^{-13}$	$8.4342e^{-13}$
	3 pairs	$2.3513e^{-12}$	$2.5342e^{-12}$	$2.6134e^{-12}$	$2.6800e^{-12}$	$2.7341e^{-12}$
	4 pairs	$6.7547e^{-12}$	$7.2574e^{-12}$	$7.4856e^{-12}$	$7.6711e^{-12}$	$7.8102e^{-12}$
	5 pairs	$2.5847e^{-11}$	$2.7248e^{-11}$	$2.8080e^{-11}$	$2.8722e^{-11}$	$2.9235e^{-11}$
0.3	2 pairs	$1.2957e^{-6}$	$1.3994e^{-6}$	$1.4467e^{-6}$	$1.4840e^{-6}$	$1.5142e^{-6}$
	3 pairs	$3.7227e^{-6}$	$4.0202e^{-6}$	$4.1560e^{-6}$	$4.2630e^{-6}$	$4.3496e^{-6}$
	4 pairs	$9.3104e^{-6}$	$1.0038e^{-5}$	$1.0375e^{-5}$	$1.0642e^{-5}$	$1.0858e^{-5}$
	5 pairs	$2.8099e^{-5}$	$2.9908e^{-5}$	$3.0917e^{-5}$	$3.1709e^{-5}$	$3.2352e^{-5}$
0.5	2 pairs	$1.4789e^{-5}$	$1.5996e^{-5}$	$1.6549e^{-5}$	$1.6985e^{-5}$	$1.7339e^{-5}$
	3 pairs	$4.1116e^{-5}$	$4.4524e^{-5}$	$4.6087e^{-5}$	$4.7321e^{-5}$	$4.8322e^{-5}$
	4 pairs	$9.6271e^{-5}$	$1.0434e^{-4}$	$1.0810e^{-4}$	$1.1109e^{-4}$	$1.1351e^{-4}$
	5 pairs	$2.5972e^{-4}$	$2.8007e^{-4}$	$2.9096e^{-4}$	$2.9961e^{-4}$	$3.0670e^{-4}$
0.7	2 pairs	$6.8983e^{-5}$	$7.4729e^{-5}$	$7.7371e^{-5}$	$7.9457e^{-5}$	$8.1148e^{-5}$
	3 pairs	$1.9074e^{-4}$	$2.0725e^{-4}$	$2.1486e^{-4}$	$2.2089e^{-4}$	$2.2579e^{-4}$
	4 pairs	$4.3862e^{-4}$	$4.7885e^{-4}$	$4.9771e^{-4}$	$5.1275e^{-4}$	$5.2507e^{-4}$
	5 pairs	$1.1595e^{-3}$	$1.2756e^{-3}$	$1.3361e^{-3}$	$1.3849e^{-3}$	$1.4254e^{-3}$

Table 2.2 – Comparison between exact GSM diagonalization and generalized Richardson calculation (2.99). The relative error of the total energy calculated using Eqs. (2.99) is shown for various values of the pairing strengths G, different number of fermion pairs and different number of discretization points along the real-energy contour.

2.3.6 Comparison between solutions of GSM and generalized Richardson equations

2.3.6.1 Bound single particle states

In this subsection, we compare results obtained by solving the generalized Richardson equations (2.99) for fermions with the exact GSM results for a spectrum of well bound s.p. levels: $\epsilon_q = \{-5, -4, -3, -2, -1\}$ MeV. Each level is doubly degenerate. To assure the completeness of a s.p. basis, the set of s.p. states from the discretized real-energy contour is added.

The contour is composed of three segments: $[k_0; k_1] = [0.0; 0.5]$, $[k_1; k_2] = [0.5; 1.0]$, and $[k_2; k_{\max}] = [1.0; 2.0]$, and the calculations are performed for different strengths G of the pairing interaction: $G = 0.01$ MeV, $G = 0.3$ MeV, $G = 0.5$ MeV and $G = 0.7$ MeV. The Gauss-Legendre method is used to select optimal discretized s.p. levels along the real-energy contour for each given number of the discretization points. The same set of s.p. levels and the corresponding Gaussian weights are then used to find the total energy of the system by solving both, the generalized Richardson equation (2.99) and the GSM.

The relative error of the total energy $\mathcal{E}$ (2.82) calculated using generalized Richardson equations (2.99) with respect to the exact GSM energy: $\delta(\mathcal{E}) = (\mathcal{E}_{\rm GSM} - \mathcal{E})/\mathcal{E}_{\rm GSM}$, is shown in Table 2.2 for different total number of the discretization points. Each segment of the contour L_c^+ is discretized with the same number of points. One may notice that the discrepancy between GSM and generalized Richardson results grows with increasing pairing strength and number of fermion pairs. Due to the approximation made in the commutator relations (2.86), the expression (2.99) for pair energies does not account exactly for the pair-pair interaction. For a single pair, as expected,

the energy obtained by solving generalized Richardson equations (2.99) coincides with the exact GSM result.

2.3.6.2 Weakly bound and resonances states

The evolution of the relative error of the generalized Richardson equations (2.99) for weakly bound and resonance double degenerate s.p. levels will be discussed in this subsection as a function of the pairing strength for 2 and 3 pairs of fermions. Different spectra of s.p. states used in these calculations are shown in Table 2.3. To construct complete s.p. Berggren basis, we take a

Spectrum	S.p. energies (MeV)
1	{ -2.5 , -1.5 , -0.5 }
2	{ -1.5 , -0.5 , (0.5 , -0.05) }
3	{ -0.5 , (0.5 , -0.05) , (1.5 , -0.15) }
4	{ -2.5 , -1.5 , -0.5 , (0.5 , -0.05) }

Table 2.3 – The s.p. levels used in the studies of the relative error of the generalized Richardson approach (2.99).

different contour in the complex k-plane for each considered resonance state. The contour used for the spectrum 1 in Table 2.3 is divided into three segments along the real-k axis: $[k_0; k_1]$ = $[0.0; 0.5]$, $[k_1; k_2]$ = $[0.5; 1.0]$, and $[k_2; k_{\max}]$ = $[1.0; 2.0]$. The parametrization of contours for different resonances is shown in Table 2.4. Each contour is discretized with 30 points selected by the Gauss-Legendre quadrature procedure and all segments are discretized with 10 points.

Resonance	k_0 (fm^{-1})	k_1 (fm^{-1})	k_2 (fm^{-1})	$k_{\max}$ (fm^{-1})
$(0.5, -0.05)$	0.0	(0.1549 , -0.14)	1.0	2.0
$(1.5, -0.15)$	0.0	(0.2682 , -0.2)	1.0	2.0

Table 2.4 – Parameters of the contours in the complex-k plane associated with the resonances.

The dependence of the relative error of ground state energy and width calculated using the generalized Richardson equations (2.99) is plotted in Figs. 2.2 to 2.5 as a function of the pairing strength G for different s.p. spectra shown in Table 2.3. The relative error depends strongly on both the pairing strength and the number of fermion pairs. One may also notice (see Figs. 2.3 - 2.5) spikes of the relative error at certain values of the pairing strength. At these discrete values of G, either real or imaginary part of the complex total energy calculated using the generalized Richardson equations (2.99) is equal to the GSM energy. We found these spikes in $\delta(\mathcal{E})$ and/or $\delta(\Gamma)$ only in the cases of s.p. spectra with at least one resonance.

Table 2.5 shows the relative error of the total energy for all discrete states in the space spanned by 3 fermion pairs in five doubly degenerate levels with energies:
$\epsilon_i = \{-2.5, -1.5, -0.5, (0.5, -0.05), (1.5, -0.15)\}$ in units of MeV. The s.p. contours in the k-plane are given in Table 2.4. Results are shown for two values of the pairing strength: $G = 0.4$ MeV and $G = 0.7$ MeV. One can see that the precision of the calculation using the generalized Richardson equations (2.99) can vary by two orders of magnitude from one state to another. As a rule, the

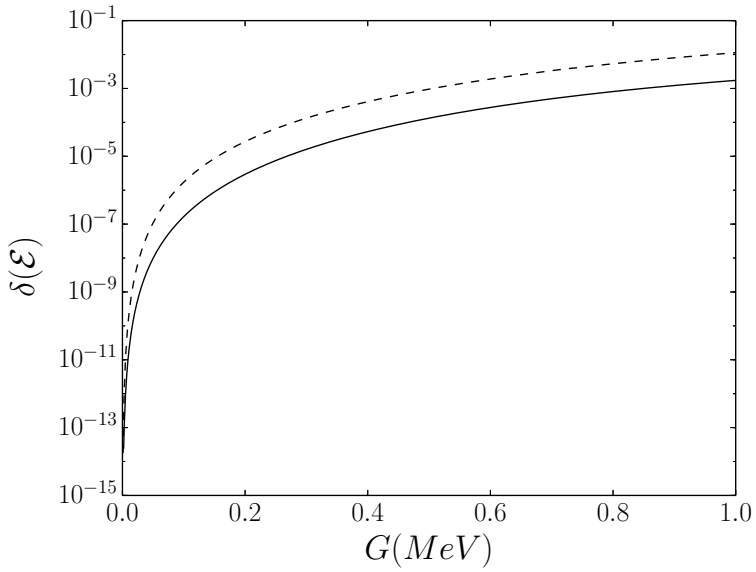

Figure 2.2 – Spectrum 1 (Table 2.3): The relative error $\delta(\mathcal{E})$ of the ground state energy calculated using solutions of the generalized Richardson equations (2.99) for the pair energies E_i, is plotted as a function of the pairing strength G. Results for two (three) pairs of fermions are shown with the solid (dashed) line.

		G = 0.4MeV		G = 0.7MeV	
State	Conf	$\delta(\mathcal{E})$	$\delta(\Gamma)$	$\delta(\mathcal{E})$	$\delta(\Gamma)$
1	11100	$8.2900e^{-4}$	$1.6856e^{-2}$	$6.3687e^{-3}$	$2.0974e^{-2}$
2	11010	$5.8954e^{-4}$	$4.9297e^{-2}$	$3.9907e^{-3}$	$2.9677e^{-1}$
3	11001	$7.6322e^{-5}$	$1.5083e^{-3}$	$7.0742e^{-4}$	$1.3266e^{-2}$
4	10110	$2.5319e^{-3}$	$5.1784e^{-2}$	$2.3193e^{-2}$	$1.3863e^{-1}$
5	01110	$6.2516e^{-3}$	$6.1601e^{-2}$	$4.3516e^{-2}$	$1.7037e^{-2}$
6	10101	$1.5258e^{-4}$	$1.3426e^{-3}$	$1.7037e^{-2}$	$1.2335e^{-1}$
7	10011	$2.2406e^{-4}$	$1.7029e^{-4}$	$8.7716e^{-4}$	$5.7504e^{-3}$
8	01101	$2.2482e^{-4}$	$1.5166e^{-3}$	$1.1971e^{-4}$	$6.1501e^{-3}$
9	01011	$2.4802e^{-2}$	$1.2426e^{-3}$	$1.3286e^{-2}$	$7.7301e^{-3}$
10	00111	$6.9734e^{-4}$	$7.9498e^{-4}$	$1.6944e^{-2}$	$5.6188e^{-3}$

Table 2.5 – The relative error of the complex energy for all excited states of a pairing Hamiltonian (2.85) with three pairs of fermions distributed over five doubly degenerate levels and three discretized continua. The pole space configuration for each state, *i.e.* the occupation by pairs of fermions of each discrete s.p. level, is indicated in the second column for $G = 0$. For more details, see the description in the text.

relative error for the imaginary part of the total energy is bigger than the corresponding error of the real part.

In Figs. 2.6, 2.7, and 2.8, we present the relative error for other relevant quantities: the

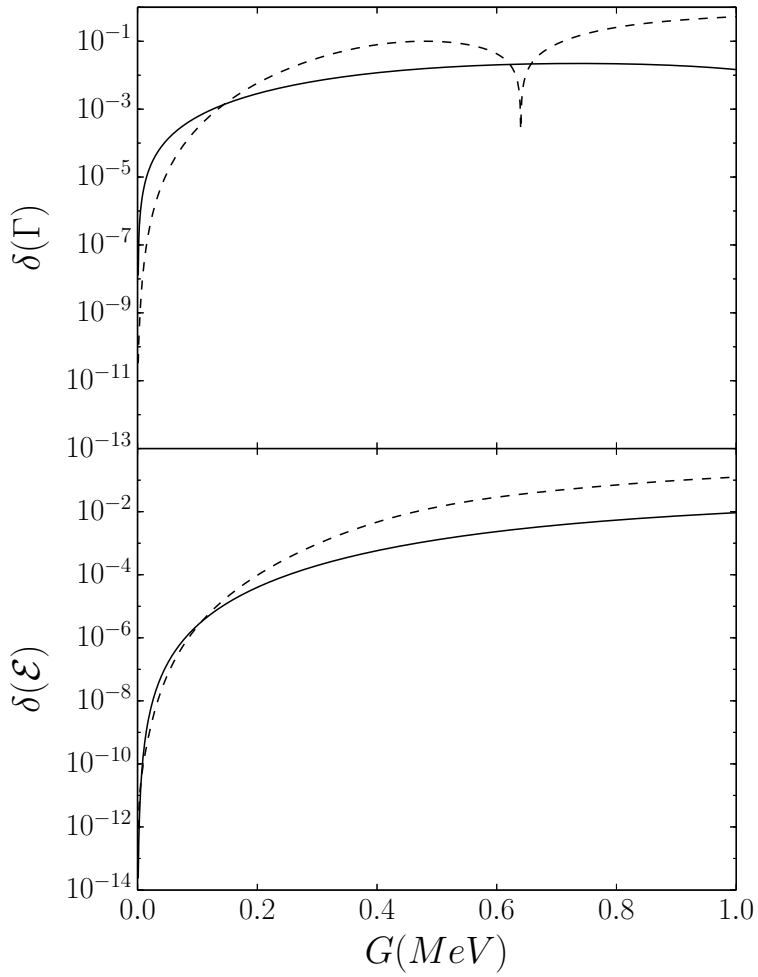

Figure 2.3 – Spectrum 2 (Table 2.3): The relative error of the ground state energy $\delta(\mathcal{E})$ and width $\delta(\Gamma)$ which are calculated using solutions of the generalized Richardson equations (2.99) for the pair energies E_i, is plotted as a function of the pairing strength G. For more details, see the caption of Fig. 2.2.

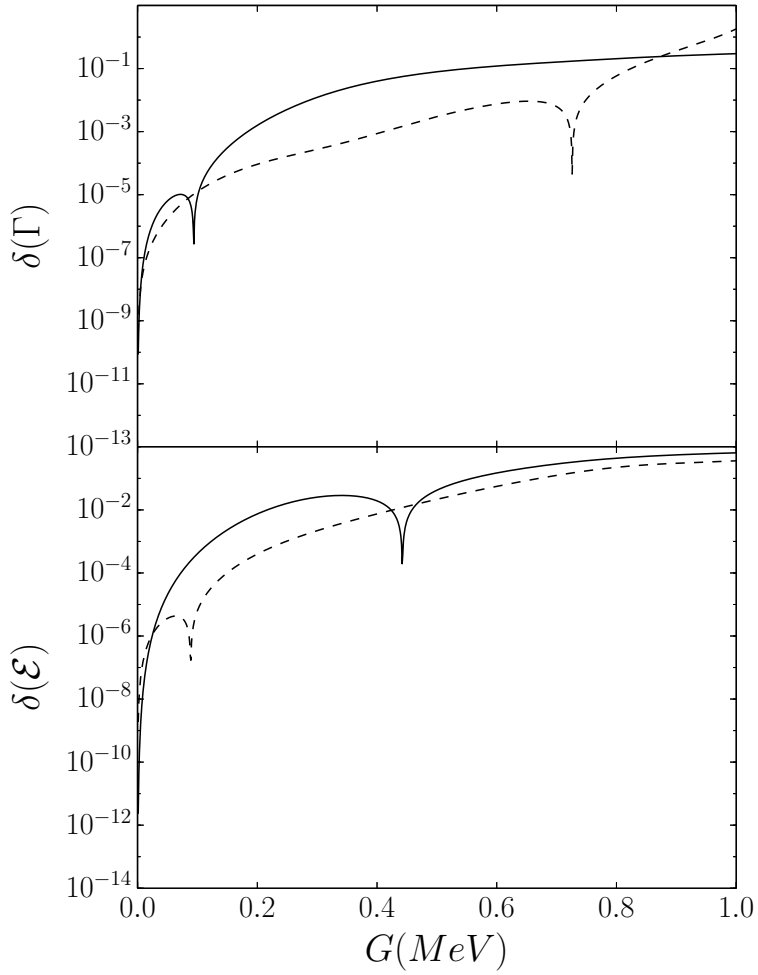

Figure 2.4 – The same as in Fig. 2.3 but for spectrum 3 in Table 2.3.

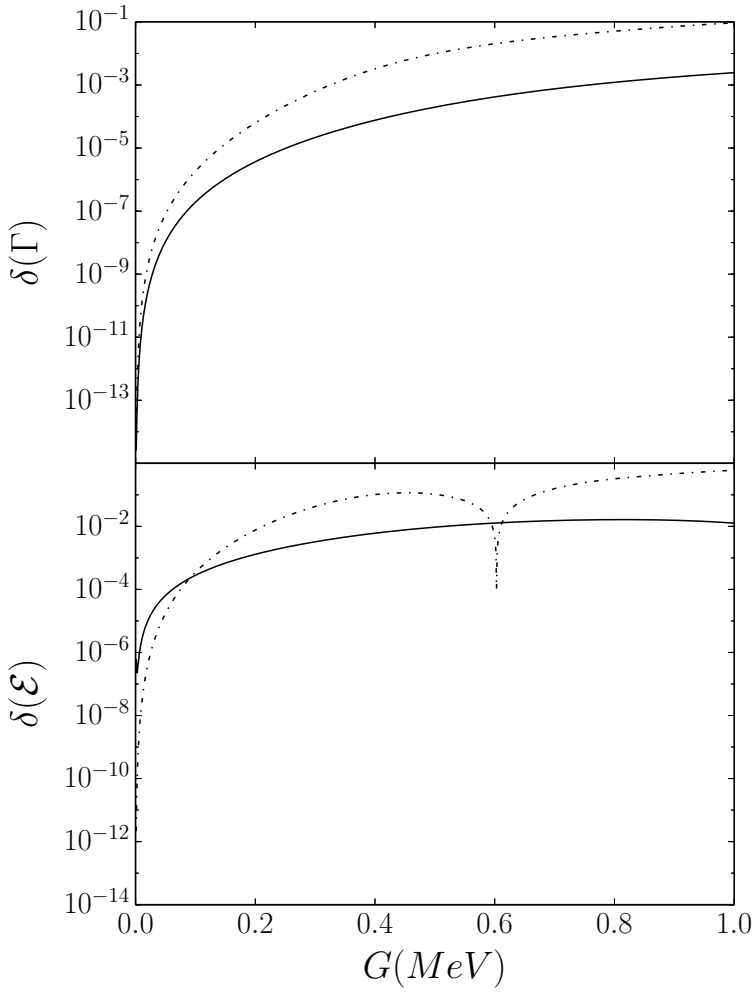

Figure 2.5 – The same as in Fig. 2.3 but for spectrum 4 in Table 2.3. The contour in the complex-k plane for the resonance pole at (0.5 MeV, –0.05 MeV) is: $[k_0; k_1] = [0.0; (0.1549, -0.2)]$, $[k_1; k_2] = [(0.1549, -0.2); 1.0]$, and $[k_2; k_{\max}] = [1.0; 2.0]$ in fm^{-1}. Results for two (four) pairs of fermions are shown with solid (dashed-dotted) line.

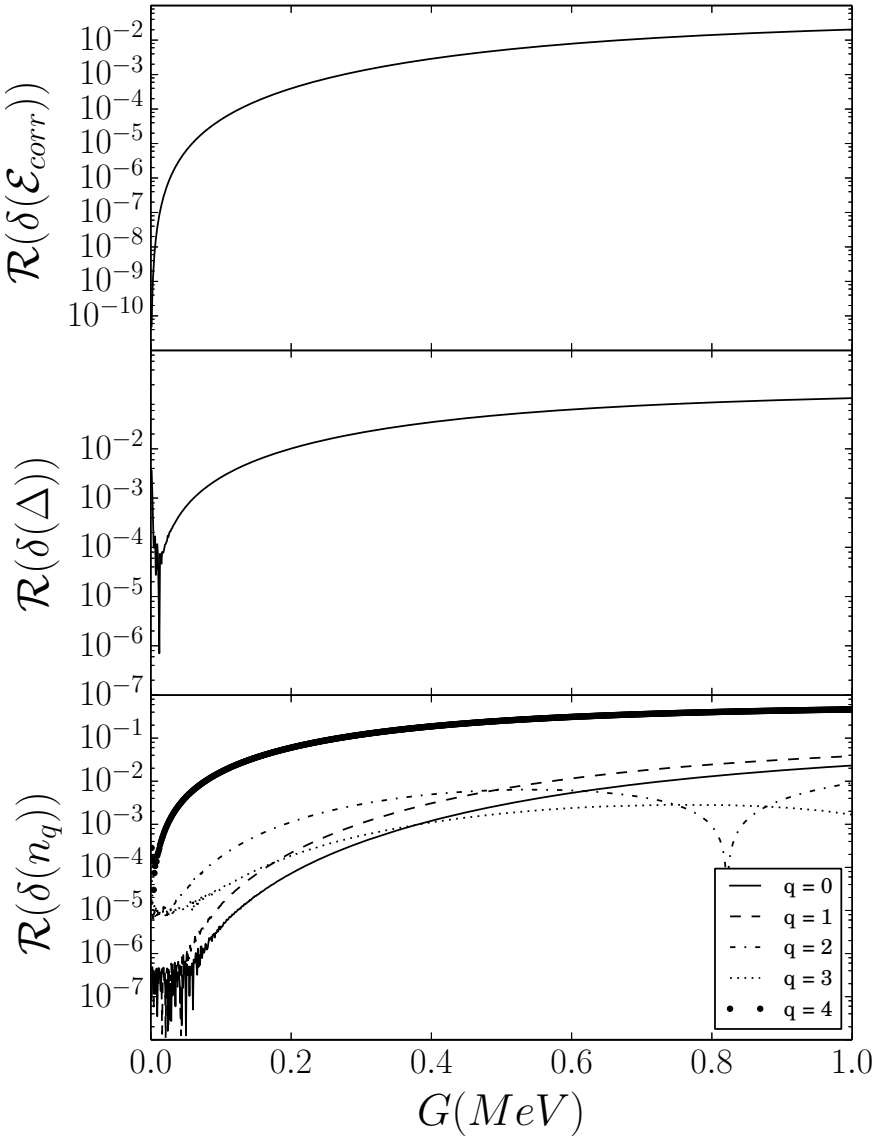

Figure 2.6 – Spectrum 2 (Table 2.3): The relative error of the generalized Richardson solution for real parts of: (i) the correlation energy $\mathcal{E}_{corr}$ (the upper part), (ii) the pairing gap Δ (the middle part), and (iii) the occupation probability n_q for 5 lowest s.p. states $q = 0 \ldots, 4$ (the lower part). These calculations have been performed for the ground state of the spectrum 2.

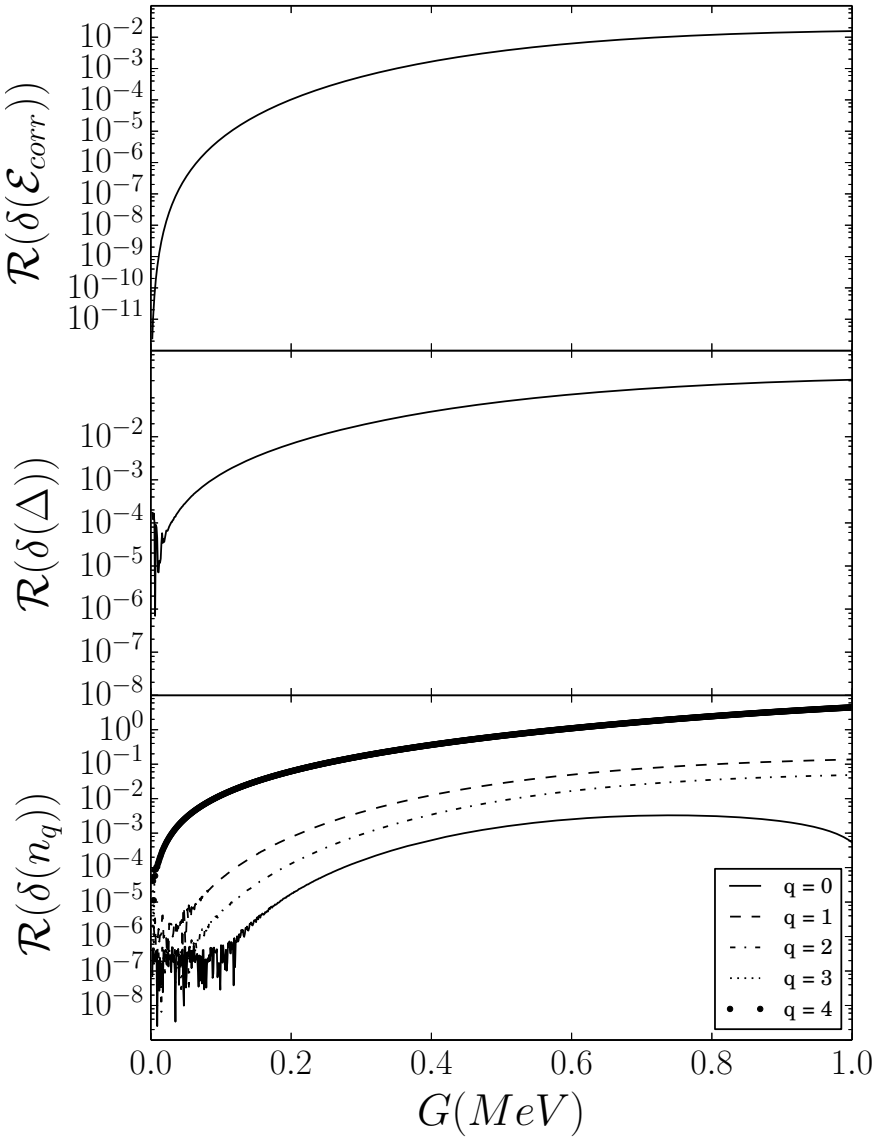

Figure 2.7 – The same as in Fig. 2.6 but for the first excited state.

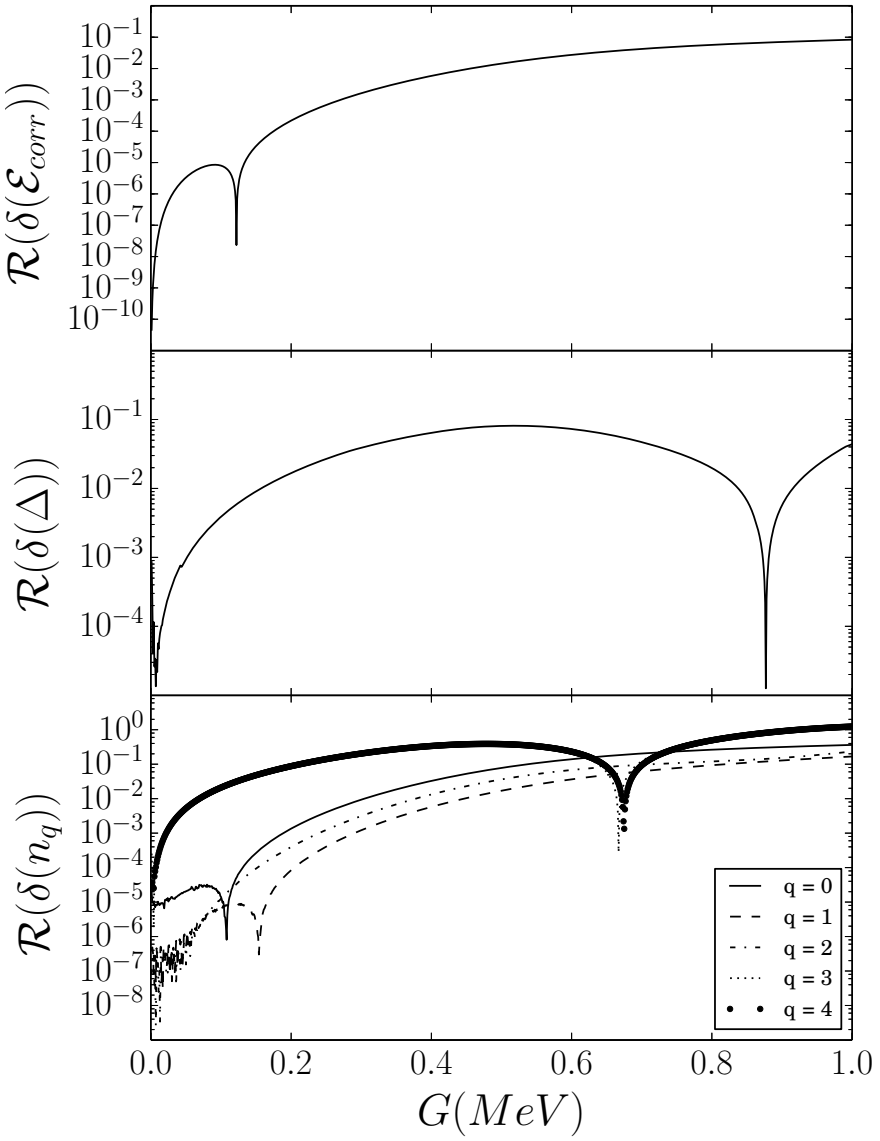

Figure 2.8 – The same as in Fig. 2.6 but for the second excited state.

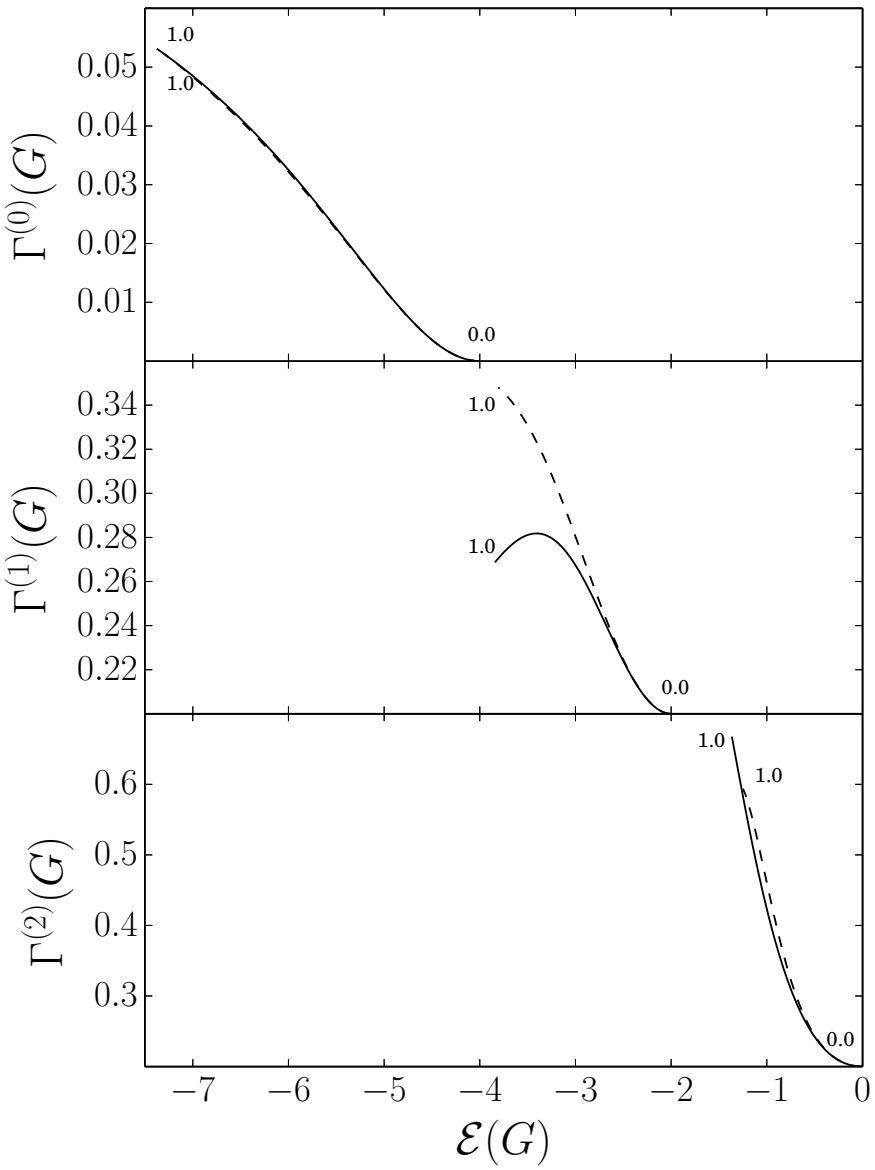

Figure 2.9 – Spectrum 2 (Table 2.3): The evolution of the three lowest complex eigenvalues $((\mathcal{E}^{(i)}, \Gamma^{(i)})$; $i = 0, 1, 2)$ of the pairing Hamiltonian is plotted as function of the pairing strength for 2 pairs of fermions. The upper most (lowest) figure shows results for the second excited (ground) state, whereas the figure in the middle is for the first excited state. The solid and dashed lines show the exact GSM solution, and the solution of the generalized Richardson approach (2.99), respectively. Numbers at the curves denote limiting values of the pairing strength (in MeV).

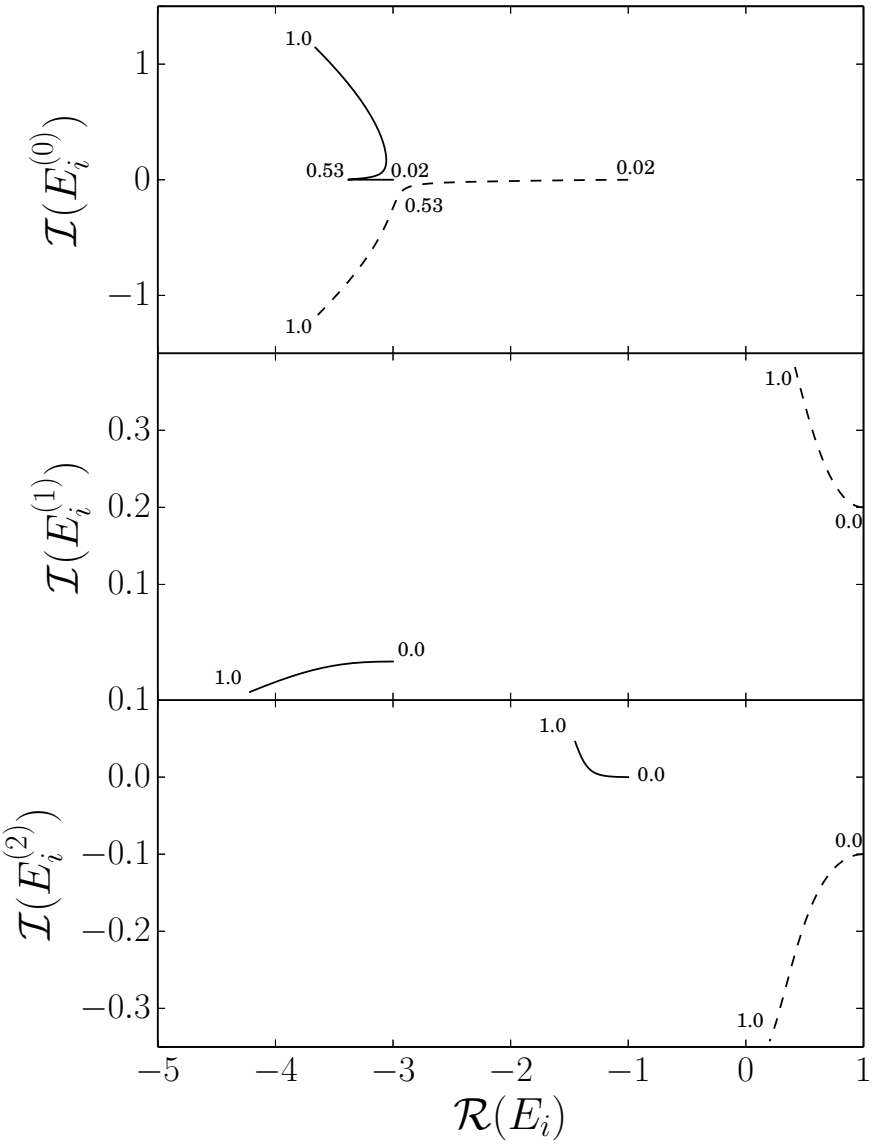

Figure 2.10 – Spectrum 2 (Table 2.3): The evolution of the lowest two (complex) pair energies $E_i^{(K)}$ $(i = 0, 1)$ with the pairing strength for 2 pairs of fermions. The pair energies are obtained by solving the generalized Richardson equations (2.99) for the ground state $(K = 0)$, and for the two lowest excited states $(K = 1, 2)$. Numbers at the curves show limiting values of the pairing strength (in MeV).

correlation energy $\mathcal{E}_{corr}$, the pairing gap Δ, and the occupation probability n_q for 5 lowest s.p. states ($q = 0, \ldots, 4$). The calculations are performed for two pairs of fermions. Results are shown for the ground state, and the next two excited states. The correlation energy is calculated as: $\mathcal{E}_{corr} = \mathcal{E}_{G=0} - \mathcal{E}$. The pairing gap Δ is calculated according to Eq. (2.107). In GSM, the occupation probabilities are determined using Eq. (2.110), whereas in the generalized Richardson equations approach we use Eq. (2.111). One can see that deeps in the relative error of different quantities shown in Figs. 2.6-2.8, do not appear at the same values of the pairing strength.

The trajectory of complex eigenvalues ($\mathcal{E} - \Gamma$) of the pairing Hamiltonian in the energy-width plane is plotted in Fig. 2.9 as a function of the pairing strength G in the interval from 0 to 1 MeV for the ground state ($K = 0$) (the upper part), the first excited state ($K = 1$) (the middle part), and the second excited state ($K = 2$) (the lower part) excited state. The solid (dashed) lines show the solutions of GSM (generalized Richardson equations). One may notice that the relative discrepancy between exact and approximate results is largest for the first excited state at large values of the pairing strength G .

In Fig. 2.10, the trajectory of pair energies in the complex energy plane is plotted for the ground state ($K = 0$) (the upper part), the first excited state ($K = 1$) (the middle part), and the second excited state ($K = 2$) as a function of the pairing strength G in the interval from 0 to 1 MeV. In the upper part of the figure, one can see that the pair energies in an interval $0 < G < 0.53$ MeV tend to approach each other along the real-energy axis. At $G \sim 0.53$ MeV, these two pair energies exhibit an avoided crossing and then move rapidly into the complex-energy plane with increasing value of the pairing strength. The pattern of avoided crossings, *i.e.* mixing pair energies, is a general pattern and can be seen for excited states ($K = 1, 2$) as well.

2.3.7 Application of generalized Richardson equations to physical systems

In the previous sections, we solved the generalized Richardson equation for the rational Gaudin model with the continuum. In order to obtain the Richardson-like solution for this generalized pairing problem, we had to compromise commutation relations for the non-resonant continuum states. Therefore, whenever the occupation of non-resonant continuum states becomes important, one might expect that the solution of the generalized Richardson equation is less accurate. This happens for strong pairing correlations.

To test this expectation, we compared solutions of the generalized Richardson equation with exact GSM solutions. We have shown that even though the relative error of the generalized Richardson solution grows with the number of fermion pairs and the pairing strength, nevertheless it remains rather accurate, especially in the limit of weak pairing correlations. One can use this model to simulate various situations involving pairing correlations and continuum in weakly bound or unbound states. In particular, one can use this model to test the common strategy of nuclear SM to replace effects of continuum couplings by the phenomenological adjustment of both s.p. energies and two-body matrix elements.

Like many well-known group theoretical models developed in nuclear physics, the rational Gaudin model with the continuum can be applied to calculate not only energy spectra but also transitions probabilities in the long series of isotopes. One should stress however that the absence of particle-hole interaction makes this model unrealistic, as the essential element of the competition between pairing and quadrupole interaction is missing.

Below, we will apply generalized Richardson equations to calculate spectra of carbon isotopes

and investigate the role of the continuum in these spectra. We will also comment on a possibility to investigate the weak-pairing limit of the ultra-small superconducting grains which is characterized by strong fluctuations of the pairing field.

2.3.7.1 Chain of carbon and oxygen isotopes

To illustrate possible applications of the generalized Richardson equations, we will now calculate spectra of carbon isotopes with $14 \leq A \leq 24$. The choice of parameters in the Hamiltonian (2.89) is motivated by the experimental spectrum of ^{13}C and the binding energy of ^{14}C. In this calculation, we assume the core of ^{12}C and calculate energies of all states in $^{14-20}$C with respect to the energy of this core.

Berggren basis consists of the pole s.p. states: $0p_{1/2}$, $1s_{1/2}$, $0d_{5/2}$, $0d_{3/2}$, $0f_{7/2}$, and the two non-resonant continua: $\{d_{3/2}\}$, $\{f_{7/2}\}$. S.p. energies of bound states $0p_{1/2}$, $1s_{1/2}$, $0d_{5/2}$ are given by experimental energies of $1/2^-_1, 1/2^+_1$ and $5/2^+_1$ states in ^{13}C: $\epsilon_{0p_{1/2}} = -4.946$ MeV, $\epsilon_{1s_{1/2}} = -1.857$ MeV, and $\epsilon_{0d_{5/2}} = -1.093$ MeV. The energy of resonances $0d_{3/2}$ and $0f_{7/2}$ are [174]: $\epsilon_{0d_{3/2}} = (2.267\ \text{MeV}; -0.416\ \text{MeV})$ and $\epsilon_{0f_{7/2}} = (9.288\ \text{MeV}; -3.040\ \text{MeV})$. The complex contours $\{d_{3/2}\}$ and $\{f_{7/2}\}$ associated with $0d_{3/2}$ and $0f_{7/2}$ resonance are given in Table 2.6. They are discretized with 10 points per segment, *i.e.* 30 points per contour. For the pairing strength, we take: $G = \chi/A$, where $\chi = 11.13$ MeV. The constant χ is adjusted to reproduce the experimental binding energy of ^{14}C with respect to ^{12}C.

Resonance	k_0 (fm^{-1})	k_1 (fm^{-1})	k_2 (fm^{-1})	$k_{\max}$ (fm^{-1})
$d_{3/2}$	0.0	(0.332 , -0.03)	0.66	2.0
$f_{7/2}$	0.0	(0.678 , -0.1)	1.24	2.0

Table 2.6 – Parameters of the contours L^+ in the complex k-plane, associated with $0d_{3/2}$ and $0f_{7/2}$ resonance poles. Each contour consists of three segments: $[k_0, k_1]$, $[k_1, k_2]$, $[k_2, k_{\max}]$, and each segment is discretized with 10 points.

To evaluate the role of the continuum in the spectra of carbon isotopes, we compare results of the generalized Richardson equations (2.99) with results of the standard Richardson calculations (2.84) without continuum couplings and with real s.p. energies. In the latter case, the s.p. energies of the bound states: $0p_{1/2}$, $1s_{1/2}$, $0d_{5/2}$, are the same as given above, and energies of $0d_{3/2}$ and $0f_{7/2}$ resonances are real: $\epsilon_{0d_{3/2}} = 2.267$ MeV and $\epsilon_{0f_{7/2}} = 9.288$ MeV. To reproduce the experimental binding energy of ^{14}C in this SM-like basis, the pairing strength is increased $\chi = 15.064$ MeV.

In Table 2.7, we compare experimental binding energies (B_{exp}) with binding energies calculated using either generalized Richardson equations (B_{GR}) or standard Richardson equations which neglect continuum effects (B_{R}). All energies are given with respect to the energy of ^{12}C. One can see that continuum changes the A-dependence of binding energies. Interestingly, B_{GR} is equal to B_{exp} both in ^{14}C and in ^{20}C.

Fig. 2.11 presents the spectrum of ^{14}C calculated using either the generalized Richardson equations for the rational Gaudin model with the continuum, or the standard Richardson equations for the same model but without the continuum. The experimental spectrum for this nucleus is shown for a comparison. The pairing strength in both calculations is adjusted to reproduce the experimental ground state energy of ^{14}C with respect to ^{12}C. The calculated spectra in both

Isotope	B_{exp} (MeV)	B_{GR} (MeV)	B_{R} (MeV)
^{14}C	13.123	13.124	13.124
^{16}C	18.590	20.814	20.477
^{18}C	23.505	25.130	24.386
^{20}C	27.013	27.170	25.886

Table 2.7 – Binding energy in the chain of carbon isotopes $^{14-20}$C. B_{GR} and B_{R} give results of the generalized Richardson equations (2.99) and standard Richardson equations (2.84), respectively. B_{exp} gives the experimental binding energy. All energies are given with respect to the energy of ^{12}C.

Conf	State	E_{GR}(MeV)	E_{R}(MeV)
$(1)^2$	0^+	0	0
$(2)^2$	0^+	5.805	6.173
$(1)^1(2)^1$	$0^-, 1^-$	6.321	6.321
$(1)^1(3)^1$	$2^-, 3^-$	7.085	7.085
$(3)^2$	0^+	9.821	9.871
$(2)^1(3)^1$	2^+	10.174	10.174
$(3)^1(3)^1$	$2^+, 4^+$	12.031	12.031

Table 2.8 – The initial configuration (G = 0) and excitation energies of different states of ^{14}C calculated using both the generalized Richardson equations (E_{GR}) and the standard Richardson (E_{R}) equations. The initial configuration is denoted by the index of an occupied level ($1 \equiv 0p_{1/2}, 2 \equiv 1s_{1/2}, 3 \equiv 0d_{5/2}$) and the number of particles in a given level (1 or 2).

Conf	State	E_{GR}(MeV)	E_{R}(MeV)
$(1)^2(2)^2$	0^+	0	0
$(1)^2(3)^2$	0^+	5.996	5.646
$(1)^2(2)^1(3)^1$	$2^+, 3^+$	6.337	5.946
$(1)^2(3)^1(3)^1$	$2^+, 4^+$	7.051	6.655
$(2)^2(1)^1(3)^1$	$2^-, 3^-$	7.392	7.947
$(2)^2(3)^2$	0^+	7.719	8.304
$(2)^2(3)^1(3)^1$	$2^+, 4^+$	12.923	12.913

Table 2.9 – The initial configuration (G = 0) and energies of different states of ^{16}C calculated using both the generalized Richardson equations (E_{GR}) and the standard Richardson (E_{R}). For details, see the caption of Fig. 2.8.

models are identical, except for the excited 0^+ states which are shifted down by the coupling to the continuum. The first excited 0^+ state is shifted by almost 400 keV with respect to the ground state even though the experimental one- and two-neutron separation energies in this nucleus are large. Identical energy for other states is an artifact of having ^{12}C as a core, namely, these states can be

Conf	State	E_{GR}(MeV)	E_{R}(MeV)
$(1)^2(2)^2(3)^2$	0^+	0	0
$(1)^2(2)^2(3)^1(3)^1$	$2^+, 4^+$	5.788	5.328
$(1)^2(3)^2(2)^1(3)^1$	$2^+, 3^+$	5.730	5.459
$(1)^2(3)^4$	0^+	–	–
$(2)^2(3)^2(1)^1(3)^1$	$2^-, 3^-$	7.668	7.820
$(3)^4(1)^1(2)^1$	$0^-, 1^-$	7.744	8.096
$(2)^2(3)^4$	0^+	9.161	9.846
$(1)^2(3)^2(3)^1(3)^1$	$2^+, 4^+$	9.166	8.449
$(2)^2(3)^2(3)^1(3)^1$	$2^+, 4^+$	14.041	14.059

Table 2.10 – The initial configuration (G = 0) and energies of different states of ^{18}C calculated using both the generalized Richardson equations (E_{GR}) and the standard Richardson equations (E_{R}). The second 0_2^+ state could not be calculated due to a singularity problem arising at a finite G. For other details, see the caption of Fig. 2.8.

Config	State	E_{GR} (MeV)	E_{R} (MeV)
$(1)^2(2)^2(3)^4$	0^+	0	0
$(1)^2(2)^2(3)^2(3)^1(3)^1$	$2^+, 4^+$	5.168	4.613
$(1)^2(3)^4(2)^1(3)^1$	$2^+, 3^+$	5.578	5.289
$(2)^2(3)^4(1)^1(3)^1$	$2^-, 3^-$	8.054	8.183
$(3)^6(1)^1(2)^1$	$0^-, 1^-$	8.452	8.848

Table 2.11 – The initial configuration (G = 0) and energies of different states of ^{20}C calculated using both the generalized Richardson equations (E_{GR}) and the standard Richardson (E_{R}) equations is compared with the experimental spectrum. We omitted configurations with more than 2 pairs on a level.

created only by breaking a pair of valence neutrons in ^{14}C. The pairing correlations in this case are absent and so are the continuum effects. For each calculated state of ^{14}C, initial configurations and excitation energies are shown in Table 2.8. The initial configuration (G=0) is defined by an index of an occupied level, *e.g.* $1 \equiv 0p_{1/2}, 2 \equiv 1s_{1/2}, 3 \equiv 0d_{5/2}$, etc. and the number of particles in a given level (n = 1, 2, ...). n = 1 means an unpaired particle. n = 2 or 4, denotes 1 or 2 pairs of particles, respectively.

Fig. 2.12 presents the spectrum of ^{16}C. Both the generalized Richardson equations and the standard Richardson equations for the same model without the continuum fail to reproduce an experimental sequence of states. This is a failure of the schematic two-body interaction in this model. Comparing the spectra of ^{16}C obtained in the two variants of the rational Gaudin model, one may notice significant relative energy shifts which depend strongly on the configuration of a given state. The individual shifts due to the continuum couplings in this model can be as large as 600 keV. Similar conclusions can be made by comparing results of the rational Gaudin model, with and without the continuum couplings, for ^{18}C (Fig. 2.13) and ^{20}C (Fig. 2.14).

Fig. 2.15 shows the evolution of the pairing gap (2.107) with the mass number in the ground state of even-even carbon isotopes. The pairing gap is calculated either neglecting the continuum ($\Delta_{\rm R}$) by solving the standard Richardson equations, or including the continuum ($\Delta_{\rm GR}$) and solving the generalized Richardson equations. Parameters in these calculations have been described in Sect. 2.3.7.1. One can see that the pairing gap in ^{14}C and ^{16}C is strongly reduced by the presence of $0d_{3/2}$ and $0f_{7/2}$ resonances and their associated $\{d_{3/2}\}$ and $\{f_{7/2}\}$ non-resonant continuum states in the complex k-plane. The A-dependence of the pairing gap is also significantly changed by the presence of the continuum. $\Delta_{\rm GR}$ is more robust than $\Delta_{\rm R}$, and at the $0d_{5/2}$ subshell closure in ^{24}C is almost 2 times bigger than $\Delta_{\rm R}$.

The A-dependence of the ground state energy in even-even carbon isotopes is shown in Fig. 2.16. The energies are given with respect to the energy of ^{12}C. The solid line shows experimental data, whereas the dashed and dashed-dotted lines exhibit results of Richardson calculations with ($\mathcal{E}_{\rm GR}$) and without ($\mathcal{E}_{\rm R}$) the continuum. One can see that both $\mathcal{E}_{\rm GR}$ and $\mathcal{E}_{\rm R}$ have incorrect A-dependence for $14 \leq A \leq 20$ what is due to an absence of the particle-hole component of the two-body interaction in the Hamiltonian (2.85) of the rational Gaudin model. In view of the simplicity of this Hamitonian, it may be considered as surprising that $\mathcal{E}_{\rm GR}$ describes well both the binding energy of ^{20}C, ^{22}C isotopes, and the experimental position of the neutron dripline. The magnitude of a rapid increase of the energy at $A = 24$ depends on the $0d_{5/2}$-$0d_{3/2}$ spin-orbit splitting and the $\{d_{3/2}\}$ non-resonant continuum.

Fig. 2.17 compares experimental and calculated A-dependence of the ground state energy in even-even oxygen isotopes. In this calculation, we assume a core of ^{16}O and calculate energies of all states in $^{18-28}$O with respect to the energy of this core. Berggren basis consists of the pole s.p. states: $0d_{5/2}$, $1s_{1/2}$, $0d_{3/2}$, $0f_{7/2}$, and the two non-resonant continua: $\{d_{3/2}\}$, $\{f_{7/2}\}$. S.p. energies of bound states and resonances $0d_{5/2}$, $1s_{1/2}$, $0d_{3/2}$ and $0f_{7/2}$ are given by experimental energies of $5/2^+_1, 1/2^+_1$, $3/2^+_1$, and $7/2^-_1$ states in ^{17}O: $\epsilon_{0d_{5/2}} = -4.143$ MeV, $\epsilon_{1s_{1/2}} = -3.273$ MeV, $\epsilon_{0d_{3/2}} = (0.944 - 0.048i)$ MeV, and $\epsilon_{0f_{7/2}} = (1.557 - 0.002i)$. The complex energy contours $\{d_{3/2}\}$ and $\{f_{7/2}\}$ associated with $0d_{3/2}$ and $0f_{7/2}$ resonances are given in Table 2.12. They are discretized with 10 points per segment, *i.e.* 30 points per contour. For the pairing strength, we take: $G = \chi/A$, with

Resonance	k_0 (fm^{-1})	k_1 (fm^{-1})	k_2 (fm^{-1})	$k_{\rm max}$ (fm^{-1})
$d_{3/2}$	0.0	(0.224 , -0.05)	0.448	2.0
$f_{7/2}$	0.0	(0.274 , -0.01)	0.548	2.0

Table 2.12 – Parameters of the contours L^+ in the complex k-plane, associated with $0d_{3/2}$ and $0f_{7/2}$ resonance poles. Each contour consists of three segments: $[k_0, k_1]$, $[k_1, k_2]$, $[k_2, k_{\rm max}]$, and each segment is discretized with 10 points.

$\chi = 10.602$ MeV for generalized Richardson calculation and $\chi = 13.338$ MeV for SM-like, standard Richardson calculation. The constant χ is adjusted to reproduce the experimental binding energy of ^{18}O with respect to ^{16}O.

It can be seen in Fig. 2.17 that the non-resonant continuum does not play a significant role for $^{18-24}$O and, consequently, $\mathcal{E}_{\rm GR}$ (the dashed line) and $\mathcal{E}_{\rm R}$ (the dashed-dotted line) are almost equal. Continuum plays a significant role only in the vicinity of the neutron dripline, for $A \geq 26$. The A-dependence of both $\mathcal{E}_{\rm GR}$ and $\mathcal{E}_{\rm R}$ differs significantly from the experimental dependence (see the solid line in Fig. 2.17), however the experimental position of the neutron dripline at ^{24}O in oxygen

is reproduced by the generalized Richardson calculation. On the contrary, the dripline predicted by the SM-like calculation without the continuum ($\mathcal{E}_{\mathrm{R}}$) is at ^{26}O.

These examples show that the continuum couplings in the rational Gaudin model have significant and non-trivial effects on the spectra of studied systems. Adjusting parameters of the SM Hamiltonian in one nucleus, ^{14}C in the studied chain of isotopes, to include effectively neglected continuum effects does not solve the problem in heavier isotopes of the same chain for which significant state and configuration dependent energy shifts due to the continuum couplings are found. On the other hand, this simple pairing Hamiltonian reproduce correctly an experimental position of the neutron dripline in carbon and oxygen isotopes if the continuum states are included. At this point, it is difficult to asses if this encouraging result is generic and can be associated with the predominance of pairing correlations close to the two-nucleon driplines [7].

Even though the rational Gaudin model is not a realistic approximation of nuclear SM Hamiltonian, one is tempted to conclude that results of this model are more general than the model itself, *i.e.* the coupling between discrete and continuum states cannot be replaced by simply fitting the two-body matrix elements to the observed spectra in a certain mass region. This standard procedure in many practical applications leads to wrong conclusions about the nature of effective interactions and the structure of many-body states. This is particularly worrisome if one wants to study states in long chains of isotopes from the valley of stability towards the drip lines.

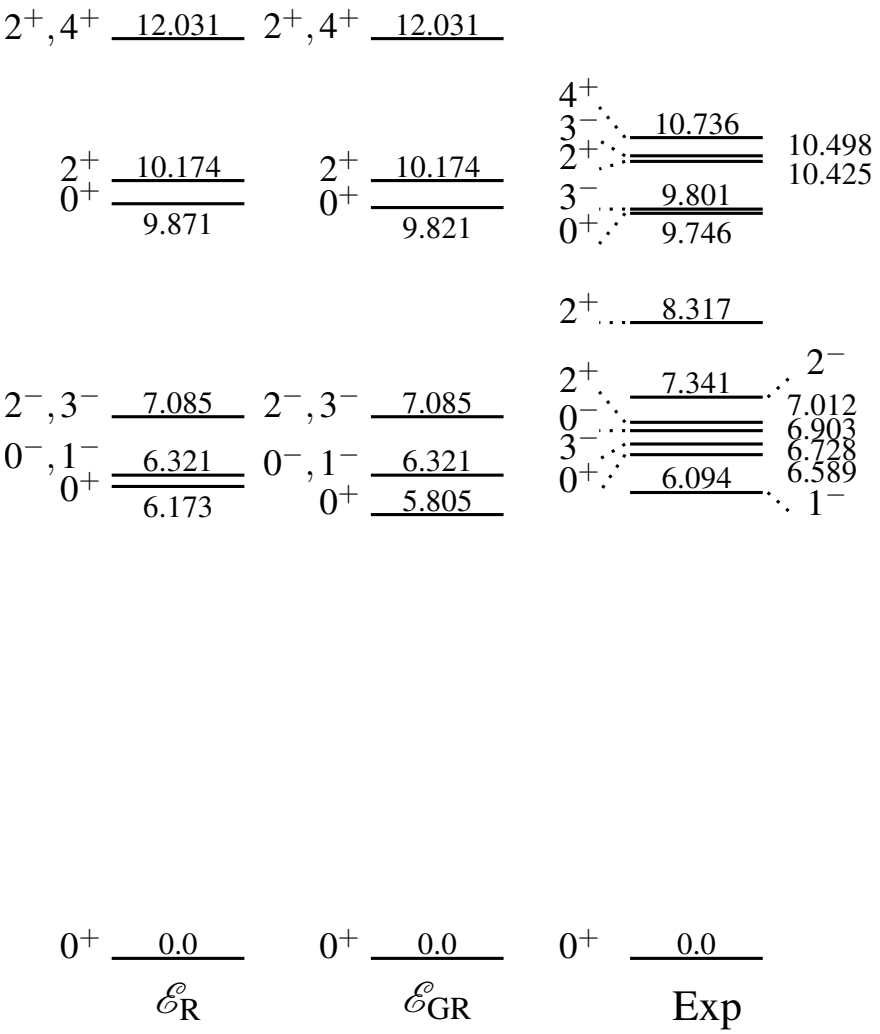

Figure 2.11 – The experimental spectrum of ^{14}C is compared with the spectra calculated using either the standard Richardson equations (no continuum) ($\mathcal{E}_{\mathrm{R}}$), or and generalized Richardson equations ($\mathcal{E}_{\mathrm{GR}}$). For more details, see the discussion in the text.

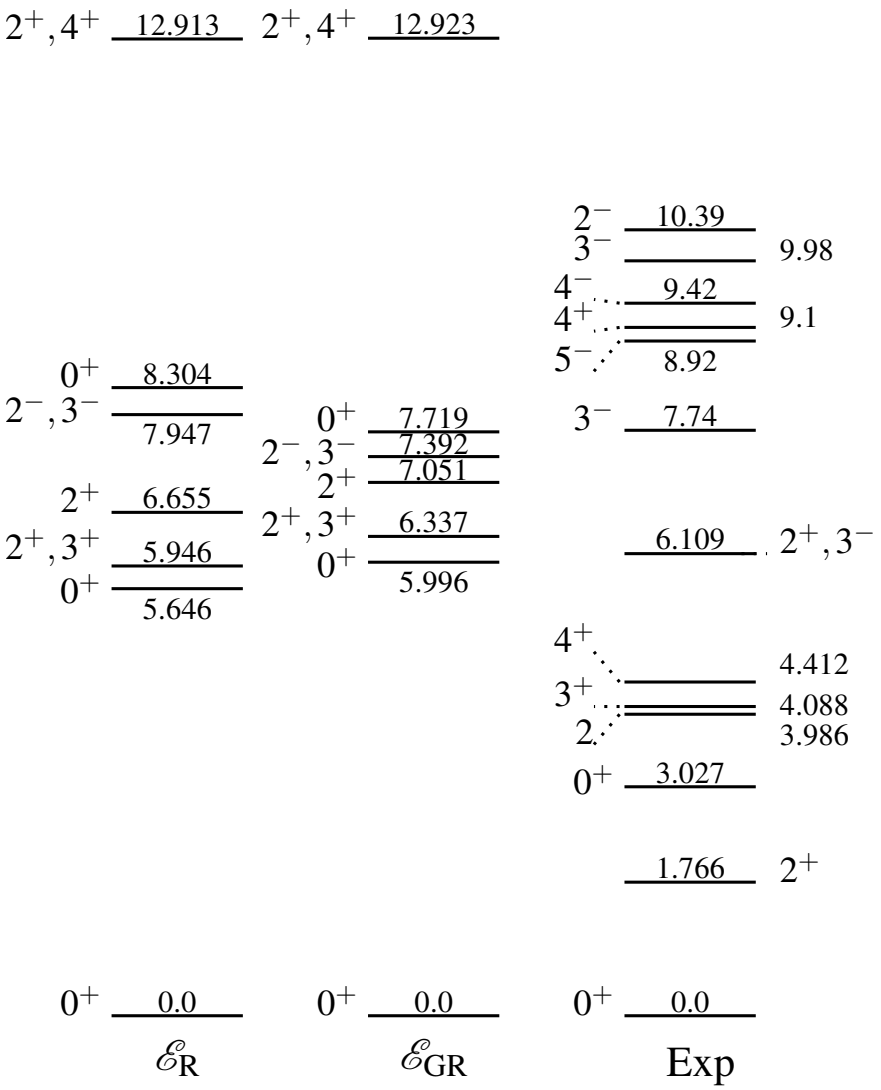

Figure 2.12 – Experimental spectrum of ^{16}C is compared with the spectra calculated using either the standard Richardson equations (no continuum) ($\mathcal{E}_{\rm R}$), or and generalized Richardson equations ($\mathcal{E}_{\rm GR}$). For more details, see the discussion in the text.

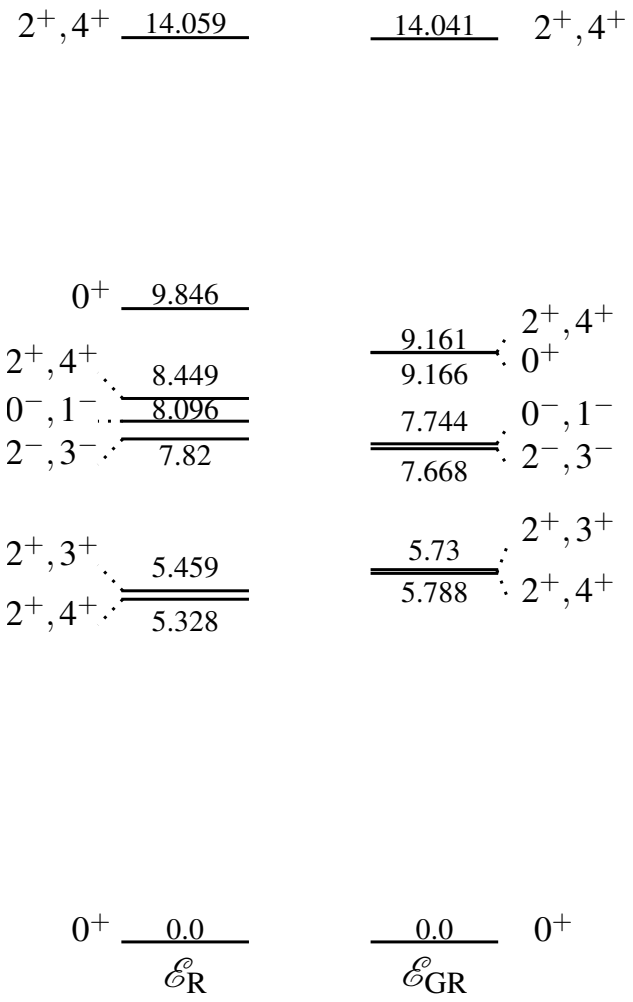

Figure 2.13 – The spectrum of ^{18}C calculated using either the standard Richardson equations (no continuum) ($\mathcal{E}_{\mathrm{R}}$), or the generalized Richardson equations ($\mathcal{E}_{\mathrm{GR}}$). For more details, see the discussion in the text. We omitted the second 0^+ as mentioned in Tab. 2.10

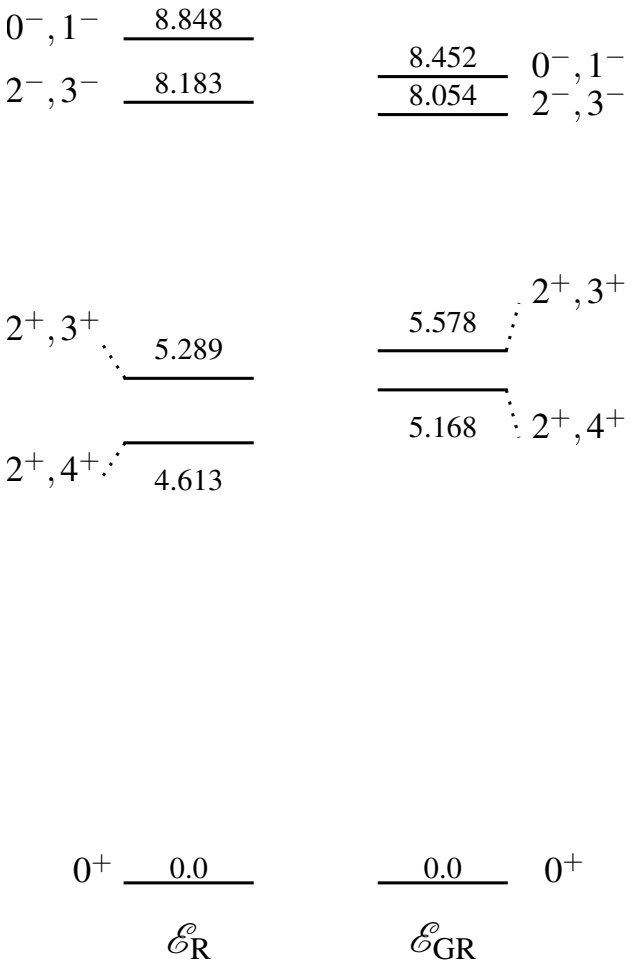

Figure 2.14 – The spectrum of ^{20}C calculated using the standard Richardson equations (no continuum) ($\mathcal{E}_{\mathrm{R}}$) is compared with the spectrum obtained by solving the generalized Richardson equations ($\mathcal{E}_{\mathrm{GR}}$). For more details, see the discussion in the text. No excited states are known experimentally for this nucleus.

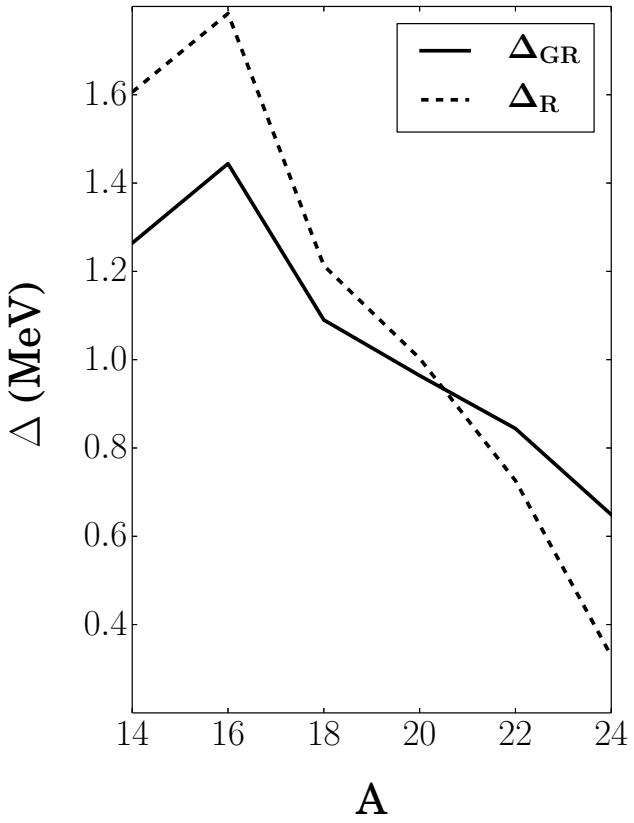

Figure 2.15 – The pairing gap (2.107) in even-even carbon isotopes. The dashed line shows results obtained by solving the standard Richardson equations, *i.e.* neglecting the continuum. The solid line depicts solutions of the generalized Richardson equations. For more details, see the discussion in the text.

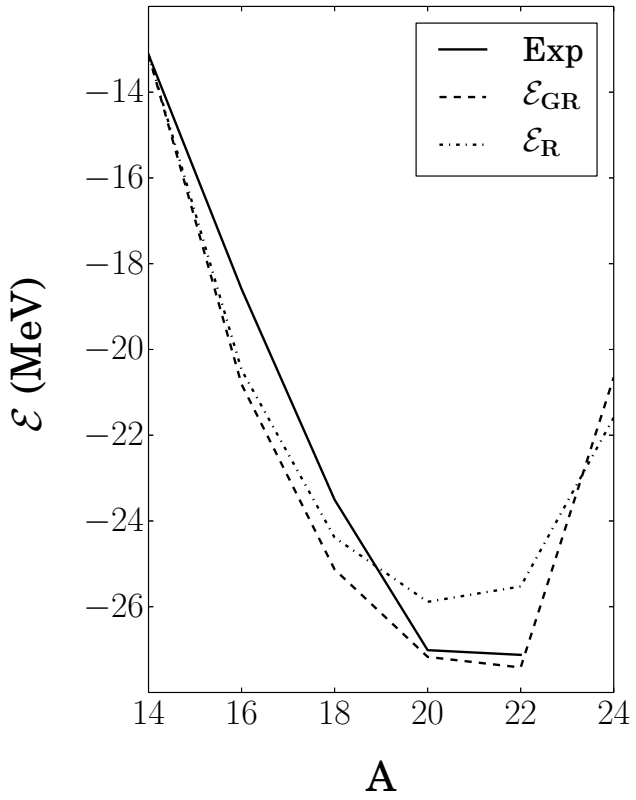

Figure 2.16 – The energy of even-even carbon isotopes with respect to ^{12}C, calculated using either the standard Richardson equations $\mathcal{E}_{\mathrm{R}}$ (the dashed-dotted line), *i.e.* neglecting the continuum, or the generalized Richardson equations $\mathcal{E}_{\mathrm{GR}}$ (the dashed line). Experimental energies are shown with a solid line. For more details, see the discussion in the text.

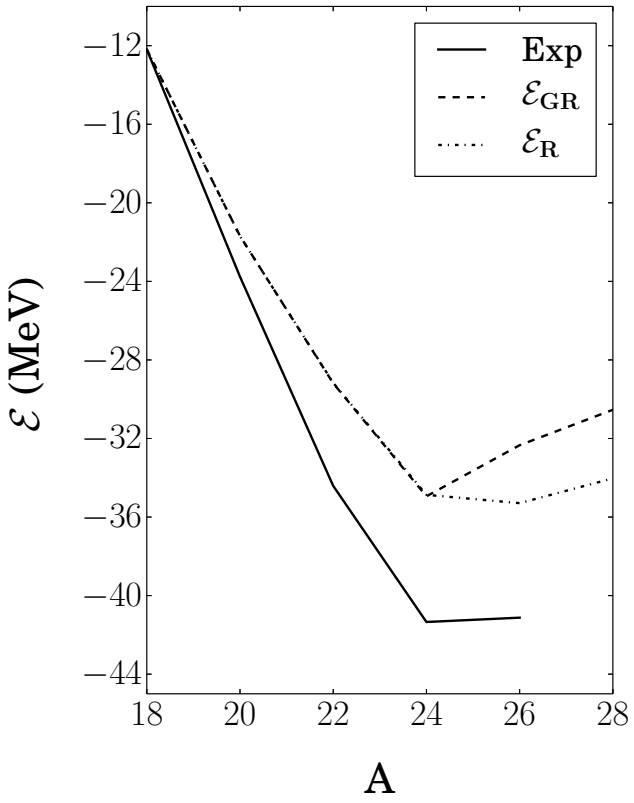

Figure 2.17 – The same as in Fig. 2.16 but for even-even oxygen isotopes.

2.3.7.2 Ultra-small superconducting grains

In 1959, Anderson [194] claimed that the phenomenon of superconductivity must disappear for metallic grains if the mean level spacing d, which is inversely proportional to the volume, is of the order of the superconducting gap in bulk $\tilde{\Delta}$. A simple argument supporting this conjecture is that the ratio $\tilde{\Delta}/d$ measures the number of electronic levels involved in the formation of Cooper pairs, so that if $\tilde{\Delta}/d \leq 1$ then there are no active levels accessible to build the pair correlations. Apart from some theoretical studies, this conjecture remained largely unexplored until the recent fabrication of ultra-small metallic grains.

Ralph, Black and Tinkham [195, 196], in a series of experiments, studied the superconducting properties of aluminum grains at the nanoscale. Giaever and Zeller [197] were among the first to probe the Anderson's criterion experimentally. Studying tunneling through granular thin films containing electrically insulated Sn grains, they demonstrated the existence of an energy gap for grain sizes right down to the critical size estimated by Anderson, but were unable to prove that smaller particles are always normal. Later, Ralph, Black, and Tinkham [195, 196] succeeded to study transport through individual nanometer-scale aluminium grains. These experiments revealed the existence of a spectroscopic gap larger than d which could be driven to zero by applying a suitable magnetic field. It was found in these studies, that the mean level spacings is $d \sim 0.45$ MeV, whereas the bulk gap is $\tilde{\Delta} \sim 0.38$ MeV which satisfies the Anderson's condition $d \geq \tilde{\Delta}$.

These experimental observations produced intense theoretical activity focused on the study of

the pairing Hamiltonian with equally spaced s.p. levels [198–202]. The pairing Hamiltonian used in the studies:

$$\hat{H} = \sum_{\alpha}^{D}(\epsilon_\alpha - \mu)\hat{c}_\alpha^\dagger \hat{c}_\alpha - \lambda d \sum_{\alpha,\beta}^{D} \hat{c}_\alpha^\dagger \hat{c}_{\bar{\alpha}}^\dagger \hat{c}_{\bar{\beta}} \hat{c}_\beta \tag{2.112}$$

belongs to the class of rational Richardson-Gaudin models. Here, the s.p. levels are given by: $\epsilon_\alpha = \alpha d$, d is the average level spacing, μ is the chemical potential, and λ is the dimensionless coupling constant. The Hamiltonian (2.112) has two regimes depending on the ratio $d/\tilde{\Delta} = 2\sinh(1/\lambda)/N$, with N the number of electrons, between the equidistant spacing and the bulk superconductivity [203]. In the weak coupling limit: $(d/\tilde{\Delta} >> 1)$, which corresponds to small grains or small coupling constants, the system is in a regime with strong pairing fluctuations above the Fermi sea. In the strong coupling limit: $(d/\tilde{\Delta} << 1)$, which corresponds to large grains or strong coupling constants, the bulk BCS wave function describes correctly the ground state properties of the grains.

The role of continuum couplings in these two regimes of the pairing Hamiltonian (2.112) is unknown but could be easily studied using the generalized Richardson equations for the picket fence set of bound states, resonances, supplemented by the non-resonant continuum states. Generally, two types of quantities are calculated as functions of increasing $d/\tilde{\Delta}$, *i.e.* increasing N: the even and odd ($b = 0$ and 1, respectively) condensation energy E_b^C, and the Matveev-Larkin parameter [204]. The condensation energy is given by:

$$E_b^{(\mathrm{C})} = E_b^{\mathrm{g.s}} - \langle FS|\,\hat{H}\,|FS\rangle \tag{2.113}$$

the difference between the ground state energy of the pairing Hamiltonian Eq. (2.112) and the energy of the Fermi state (FS) which is the Slater determinant obtained by simply filling all levels up to the Fermi surface. The Matveev-Larkin parameter:

$$\Delta_{\mathrm{ML}} = E_1(N) - \frac{1}{2}\left[E_0(N+1) + E_0(N-1)\right] \tag{2.114}$$

measures the difference between the ground state energy of an odd grain and the mean energy of the neighboring even grains obtained by adding and removing one electron. Both the condensation energy $E_b^{(\mathrm{C})}$ and the Matveev-Larkin parameter Δ_{ML} can be easily investigated for different both s.p. spectra and numbers of electrons. In particular, one expects that the continuum coupling may have an influence on the ultra-small grains in the weak coupling regime of the pairing Hamiltonian.

Chapter 3

Towards a unified model of nuclear structure and reaction

Nuclear reactions are used to probe properties of the atomic nuclei and understand various astrophysical processes from the Big Bang nucleosynthesis to the evolution of stars and the relative abundances of different isotopes/nuclei in the Universe. Reaction cross sections are one of the most important observables which provide information not only about the reaction probabilities but also about the structure of the nucleus. Indeed, many structural properties of the nucleus are determined by means of nuclear collisions. For example, direct nuclear reactions can select the final state of the reaction process. The transfer or knockout of one nucleon probes the single particle (s.p.) states, the inelastic scattering excites collective states and the transfer of two nucleons brings information about the pairing correlations. Single neutron transfer using the (p,d)-reaction became a common tool to explore neutron capture reactions at stellar energies (see Ref. [205]). In general, complex projectiles such as deuteron, triton, alpha, or even heavier nuclei are involved in transfer reactions and hence their theoretical modeling is difficult.

Nuclear elastic scattering processes can be described using the complex one-body potential [206–208] (the optical potential) where the imaginary part takes into account an absorption of the wave function, in analogy to the absorptive imaginary part of the index of refraction in wave optics. This approach reached its maturity in the works of Feshbach and others [209–211] on the generalized optical potential which effectively takes into account couplings to the inelastic channels. Later, Mahaux and Sartor [212] developed the dispersive optical model which uses the dispersion relation to link the imaginary and real parts of the optical potential and hence, the elastic scattering cross sections with the properties of bound s.p. states [213].

A more general formalism is required to describe the inelastic scattering or transfer reactions. In these reactions, one has to introduce additional quantum numbers to label internal states of colliding nuclei and different partitions of nucleons in the collision process. For this purpose, it is convenient to introduce reaction channels [214–216] to define the asymptotic states of the quantum system before and after the collision. Any partition of nucleons among collision partners defines an arrangement channel. The particle transfer process becomes then the quantum hopping process in the space of arrangement channels.

Narrow resonances are observed in various nuclear reaction cross sections. According to Niels Bohr [217], the long lifetime of these states is related to their complexity which arises because the available energy is shared among many nucleons. Accordingly, it was for a long time considered

almost hopeless to approach nuclear reaction theory from a microscopic point of view. Many earlier formulations of the reaction theory [218–220] proposed an expression for the collision matrix with no explicit reference to the nuclear Hamiltonian. These formulations were devised to provide a convenient framework for the analysis of the resonance processes.

Nuclear reaction theory received a considerable impetus from Feshbach [42,43] who emphasized the dynamical origin of resonances and of the optical model. In his work, the collision matrix is expressed in terms of the matrix elements of the nuclear Hamiltonian [42, 43, 221]. In its first formulation, the Feshbach's formalism neglected the antisymmetrization of the A-body wave function which is a serious challenge to any nuclear reaction theory [94, 222, 223].

At higher energies, the precise knowledge of the structure of projectile and target nuclei is not always mandatory for the quantitative description of nuclear reactions. On the contrary, details of the shell structure of colliding nuclei and their many-body wave functions are essential for understanding the low energy radiative capture or transfer reactions, and this cries out for a unified framework. The attempts in this direction led to various formulations of the CSM/SMEC [34, 35, 38, 39, 41, 104, 224] which are based on the Feshbach projection formalism [42, 43]. These models were the first to provide a truly unifying picture of nuclear structure and reactions but their applications for processes involving more than two nucleons in the non-resonant continuum were too complicate to be pursued. The CSM is formulated in the coupled-channel (CC) framework which is well suited for decay processes and reactions. On the other hand, the description of spectroscopy requires the reformulation of the CSM to include the discrete part of the continuum spectrum (the s.p. resonances) in the configuration mixing [225].

Recently, the GSM has been proposed which uses the Berggren basis [44–46] and the external complex scaling method [137] to regularize the resonance wave functions. Contrary to the CSM, the GSM is not limited by the number of particles in the scattering continuum. On the other hand, the GSM is the configuration interaction approach and as such it is the tool of choice for nuclear structure studies. To reconcile the GSM with the reaction theory, a reformulation of the GSM in terms of the coupled channels is mandatory [226]. The first applications of the GSM in the CC framework (GSM-CC) have been achieved for the elastic and inelastic scattering of protons on ^{6}He [226], ^{18}Ne [227], and ^{14}O [228]. The GSM-CC has also been applied to study proton/neutron radiative capture reactions [229, 230].

Our aim in this chapter is to formulate the GSM-CC approach for transfer/knockout reactions and extend its applicability for reactions involving complex (multi-nucleon) projectiles. Moreover, since GSM-CC describes reactions in the COSM coordinates, the resulting theory can be applied to study elastic and various inelastic reactions involving also medium- and heavy-mass nuclei. However before approaching this goal, in the next section (Sec. 3.1) we will recall basic features of the CSM/SMEC which were the first theoretical approaches to bring together the configuration interaction approach (the SM) and the reaction theory (the S-matrix, the optical model potential).

In Sec. 3.2 we discuss the CC formulation of the GSM. In subsection 3.2.1 we remind general features of the Schrödinger equation in the channel representation. In the following subsections, we discuss the Hamiltonian of the projectile (Sec. 3.2.2) and the Slater determinant expansion of the states of the composed system projectile+target (Sec. 3.2.3 - 3.2.4). The orthogonalization condition for states of the composed system with respect to the occupied states in the core is discussed in Sec. 3.2.5 . The following subsections (Sec. 3.2.6 - 3.2.7) concentrate on discussing matrix elements of the Hamiltonian, approximations in the treatment of antisymmetry in the system projectile-target at large c.m. energies, and details of the actual calculation of the matrix

elements of the Hamiltonian and the norm.

Sec. 3.3 is devoted to the discussion of the numerical resolution of the CC equations. Among many things, we discuss the Green's function approach to obtain the solution of the CC equations.

The next section (Sec. 3.4) is devoted to the presentation of some applications of the GSM-CC approach to nuclear reactions. After giving few practical tips concerning the GSM-CC calculations, we will present results of the calculation for the reaction ^{14}O(p,p') and properties of the intermediate system ^{15}F in this reaction.

3.1 From Feshbach projection formalism to the CSM

The basic idea of CSM is to use a finite depth potential to generate the s.p. basis. This potential is generally a Wood-Saxon potential, plus a spin-orbit and Coulomb term, and it generates s.p. bound states and resonances. Both bound states and resonances have an outgoing asymptotics but the resonance wave function is not square integrable. To overcome this problem, one should separate the localized part of the resonance wave function inside the Coulomb and centrifugal barriers from its tail at large distances [225]. The localized part of resonance, properly normalized and orthogonalized to all bound states, is then put in the subspace of discrete s.p. states, whereas the resonance tail remains in the non-resonant continuum. The scattering states are taken along the positive real-k axis. By construction, the CSM is formulated in Hilbert space. The many-body states are Slater determinants made of bound s.p. states and anamneses of the s.p. resonances.

At this point, the Feshbach projection formalism is used. The idea is to separate Hilbert space into the two subspaces $\mathcal{Q}$ and $\mathcal{P}$ such that : $\mathcal{H} = \mathcal{Q} \cup \mathcal{P}$, where $\mathcal{H}$ is a Hilbert space. The subspace $\mathcal{Q}$ is the subspace of Slater determinants with only discrete states occupied, while the subspace $\mathcal{P}$ is the complement subspace which includes the non-resonant continuum states. In the following, we will only consider a simpler case where $\mathcal{P}$ stands for the set of configuration with only one nucleon in the continuum.

The projection operator $\hat{Q}$ and $\hat{P}$ on the subspaces $\mathcal{Q}$ and $\mathcal{P}$, are defined as :

$$\hat{Q} = \sum_n |SD_n\rangle \langle SD_n| \quad , \quad \hat{P} = \hat{\mathbb{1}} - \hat{Q} \tag{3.1}$$

where the Slater determinants $|SD_n\rangle$ are build of the discrete s.p. states generated by the mean potential. Using Eq. (3.1), one can rewrite the Hamiltonian $\hat{H}$ of the A-nucleon system as:

$$\begin{aligned} \hat{H} = (\hat{P}+\hat{Q})\hat{H}(\hat{P}+\hat{Q}) &= \hat{P}\hat{H}\hat{P} + \hat{Q}\hat{H}\hat{P} + \hat{P}\hat{H}\hat{Q} + \hat{Q}\hat{H}\hat{Q} \\ &= \hat{H}_{PP} + \hat{H}_{QP} + \hat{H}_{PQ} + \hat{H}_{QQ} \end{aligned} \tag{3.2}$$

with:

$$\hat{H}_{QQ}\,|\Phi_i\rangle = E_i\,|\Phi_i\rangle \tag{3.3}$$

$$\hat{H}_{PP}\,|\xi\rangle = E\,|\xi\rangle \tag{3.4}$$

Here Eq. (3.3) is an eigenvalue problem, where $|\Phi_i\rangle = \sum_n c_n\,|SD_n\rangle$, while Eq. (3.4) is a CC equation with:

$$|\xi\rangle = \sum_c \int_0^\infty \frac{u_c(r)}{r} r^2\,|(c,r)\rangle\,dr \tag{3.5}$$

where $|(c,r)\rangle = \left[|\Psi_{\mathrm{T}}^{J_{\mathrm{T}}}\rangle \otimes |r,\ell,j,\tau\rangle\right]^{J}$ are the channel states and $ru_c(r) = \langle(c,r)|\xi\rangle$. Here, $|\Psi_{\mathrm{T}}^{J_{\mathrm{T}}}\rangle$ is the target state with J_{T} its angular momentum, $|r,\ell,j,\tau\rangle$ is the projectile state with j its angular momentum, and J is the total angular momentum. The boundary conditions defining the $u_c(r)$ are: (i) the outgoing wave behavior in all channels c, and (ii) the incoming wave behavior in the entrance channel c_0. The correlations between the projectile and the target are taken into account through the microscopically calculate coupling potentials between different channels.

Let us consider the state: $|\Psi\rangle = (\hat{P}+\hat{Q})|\Psi\rangle = |\Psi_P\rangle + |\Psi_Q\rangle$, of the A-nucleon system. The Schrödinger equation $\hat{H}|\Psi\rangle = E|\Psi\rangle$ can be rewritten using Eq. (3.2), and then projected on the subspaces $\mathcal{Q}$ and $\mathcal{P}$ as follows:

$$(\mathcal{Q}) \; : (E - \hat{H}_{QQ})|\Psi_Q\rangle = \hat{H}_{QP}|\Psi_P\rangle \tag{3.6}$$

$$(\mathcal{P}) \; : (E - \hat{H}_{PP})|\Psi_P\rangle = \hat{H}_{PQ}|\Psi_Q\rangle \tag{3.7}$$

Introducing the resolvent operator:

$$\hat{G}_P^{+} = (E^{+} - \hat{H}_{PP})^{-1} = \lim_{\eta\to 0}(E + i\eta - \hat{H}_{PP})^{-1} \; ,$$

the solution $|\Psi_P\rangle$ of Eq. (3.7) can be written as:

$$|\Psi_P\rangle = |\xi\rangle + \hat{G}_P^{+}(E)\hat{H}_{PQ}|\Psi_Q\rangle \tag{3.8}$$

Note that $|\Psi_P\rangle$ is a sum of the unperturbed solution $|\xi\rangle$ in $\mathcal{P}$, *i.e.* the scattering part, plus a term taking into account the coupling with $\mathcal{Q}$. Using Eq. (3.8) in Eq. (3.6), one obtains the following expression for $|\Psi_Q\rangle$:

$$(E - \hat{H}_{QQ} - \hat{H}_{QP}G_P^{+}(E)\hat{H}_{PQ})|\Psi_Q\rangle = \hat{H}_{QP}|\xi\rangle \tag{3.9}$$

Using expressions (3.8), (3.9), and the completeness relation:

$$\sum_i |\Phi_i\rangle\langle\Phi_i| = \hat{\mathbb{1}} \; ,$$

one obtains the solution for $|\Psi\rangle$ in the whole space $\mathcal{Q}\cup\mathcal{P}$:

$$|\Psi\rangle = |\xi\rangle + \sum_{ij}\left[|\Phi_i\rangle + |w_i^{(+)}\rangle\right]\langle\Phi_i|\frac{1}{E - \hat{H}_{QQ}^{\mathrm{eff}}}|\Phi_j\rangle\langle\Phi_j|\hat{H}_{QP}|\xi\rangle \tag{3.10}$$

The state $|\Psi\rangle$ is thus written as a sum of a direct part $|\xi\rangle$ and a resonant part. Here $|w_i^{(+)}\rangle$ is the extension of $|\Phi_i\rangle$ in $\mathcal{P}$:

$$|w_i^{(+)}\rangle = G_p^{(+)}(E)\hat{H}_{PQ}|\Phi_i\rangle \tag{3.11}$$

and $\hat{H}_{QQ}^{\mathrm{eff}}$ is the effective Hamiltonian in $\mathcal{Q}$:

$$\hat{H}_{QQ}^{\mathrm{eff}} = \hat{H}_{QQ} + \hat{H}_{QP}G_P^{+}(E)\hat{H}_{PQ} \tag{3.12}$$

In general, the effective Hamiltonian $\hat{H}_{QQ}^{\mathrm{eff}}(E)$ is non-hermitian and energy dependent. It contains an "internal interaction" in $\hat{H}_{QQ}$ which makes the configuration mixing like in SM, but it contains also an "external interaction" $\hat{H}_{QP}\hat{G}_P^{+}(E)\hat{H}_{PQ}$ which couples the states in $\mathcal{Q}$ and $\mathcal{P}$ and generates the energy correction to the $\mathcal{Q}$-space eigenvalues.

Let us now discuss the description of bound states and resonances of the A-nucleon system. In this case, $|\Psi\rangle$ is a set of discrete states: $\hat{H}|\Psi_n\rangle = E_n|\Psi_n\rangle$, and $|\Psi_n\rangle = |\Psi_Q^n\rangle + |\Psi_P^n\rangle$. Removing the scattering part $|\xi\rangle$ in $|\Psi_P^n\rangle$, one can see that the states $|\Psi_Q^n\rangle$ are the eigenvectors of the effective Hamiltonian:

$$(E - \hat{H}_{QQ}^{\text{eff}}(E))|\Psi_Q\rangle = 0 \ ,$$

with the eigenvalues $E_n(E) + i\Gamma_n(E)/2$. Then, it is possible to define $|\tilde{w}_n^{(+)}\rangle$ the extension of $|\Psi_Q\rangle$ in $\mathcal{P}$ as:

$$|\tilde{w}_n^{(+)}\rangle = \hat{G}_P^+(E)\hat{H}_{PQ}|\Psi_Q\rangle \ .$$

The states $|\Psi_Q^n\rangle$ and $\tilde{w}_n^{(+)}$ can be expressed in a basis of $|\Phi_i\rangle$ and $|w_i^{(+)}\rangle$, respectively:

$$\begin{aligned} |\Psi_Q^n\rangle &= \sum_i \alpha_i^n |\Phi_i\rangle \\ |\tilde{w}_n^{(+)}\rangle &= \sum_i \alpha_i^n |w_i^{(+)}\rangle \end{aligned} \tag{3.13}$$

Now, defining

$$|\Omega_n^{(+)}\rangle = |\Psi_Q^n\rangle + |\tilde{w}_n^{(+)}\rangle$$

and inserting in Eq. (3.10) twice the following two completeness relations:

$$\begin{aligned} \sum_n |\Psi_Q^n\rangle\langle\Psi_Q^n| &= \hat{\mathbb{1}} \\ \sum_n |\Omega_n^{(+)}\rangle\langle\Omega_n^{(+)}| &= \hat{\mathbb{1}} \end{aligned} \tag{3.14}$$

one obtains the final expression for $|\Psi\rangle$:

$$|\Psi\rangle = |\xi\rangle + \frac{1}{\sqrt{2\pi}} \sum_n |\Omega_n^{(+)}\rangle \frac{\gamma_n}{E - E_n(E) + i\frac{\Gamma_n(E)}{2}} \tag{3.15}$$

where

$$\tilde{\gamma}_n^c = \sqrt{2\pi}\langle\Psi_Q^n|\hat{H}_{QP}|\xi\rangle \tag{3.16}$$

are the coupling matrix elements between the pure scattering states lying in $\mathcal{P}$ and the bound states and resonances $|\Psi_Q^n\rangle$ lying in $\mathcal{Q}$.

It is interesting to notice that the states $|\Psi\rangle$ and $|\Omega_n^{(+)}\rangle$ are equivalent in the following sense: $|\Psi\rangle$ is a scattering state which takes into account corrections from the discrete states while $|\Omega_n^{(+)}\rangle$ is the resonance state which takes into account corrections from the scattering states. The corrections from the discrete states to the scattering states $|\Psi\rangle$ are contained in the sum over these states (the second term in Eq. (3.15)), while the corrections from the decay channels to the wave function $|\Omega_n^{(+)}\rangle$ are contained in $|\tilde{w}_n^{(+)}\rangle$.

For a given incoming channel c_0 and an exit channel c, the S-matrix is expressed as:

$$S_{cc_0} = S_{cc_0}^{(0)} - ie^{i(\delta_c^{(0)} + \delta_{c_0}^{(0)})} \sum_n \frac{\tilde{\gamma}_c^n \tilde{\gamma}_{c_0}^n}{E - E_n(E) + i\frac{\Gamma_n}{2}} \tag{3.17}$$

Here, $\delta_c^{(0)}$ is the scattering phase shift for the same incoming and exit channels, $S_{cc_0}^{(0)}$ is the matrix element for the non-resonant part of the scattering process, and $\tilde{\gamma}_n^c$ is defined as:

$$\tilde{\gamma}_n^c = -e^{i\delta_c^{(0)}} \frac{\sqrt{4\mu}}{\hbar k_c} \sum_{ic'} \int_0^\infty r u_{c'}(r) w_i^{c'}(r) dr \tag{3.18}$$

with μ the reduced mass of the collision partners, $ru_{c'}(r) = \langle (c', r)|\xi\rangle$ and $w_i^{c'}(r) = \langle (c', r)|w_i\rangle$.

Finally, the cross section describing the wave scattered from an incoming channel c_0 to an exit channel c is given by:

$$\frac{d\sigma}{d\Omega}(c_0 \to c) = \frac{\pi}{k_{c_0}^2} \left| \sum_{\ell,\ell',m'} i^{\ell-\ell'} \sqrt{2\ell+1} Y_{\ell'}^{m'}(\theta,\phi)(S_{cc_0} - \delta_{cc_0}) \right|^2 \tag{3.19}$$

By construction, CSM considers the configuration interaction for Slater determinants build by harmonic oscillator wave functions for bound s.p. states and anamneses of s.p. resonances [34–41] in the internal subspace ($\mathcal{Q}$-space). The external subspace ($\mathcal{P}$-space) is supposed to include only non-resonant continuum states what implies that the special procedure to extract the localized part of the resonance wave functions has to be defined. The coupling between the internal SM-like states, and the external subspace ($\mathcal{P}$-space) is evaluated by solving the CC equations. The quality of the CSM approach depends on the goodness of the separation method between $\mathcal{Q}$ and $\mathcal{P}$ subspaces. In the future, one could envisage the variant of Feshbach projection formalism in which GSM instead of SM is used to build the subspace of discrete many-body states, leaving the selected channel wave functions in $\mathcal{P}$.

3.2 Coupled channel formulation of the GSM

GSM is the generalization of SM to the resonant and non-resonant continuum. Like in SM, the many-body states in GSM are written in terms of Slater determinants and hence, the GSM is a tool *par excellence* for the nuclear structure studies. The fundamental problem which will be discussed in this chapter is how to reconcile the GSM with the reaction theory. A similar problem challenged already the forefathers of the microscopic reaction theory, like Feshbach, Kerman, Mahaux, and others, who were preoccupied by the (in)compatibility of the SM with the reaction theory. This fundamental problem returns again because we know now that the SM is not a satisfactory formulation of the configuration interaction in all binding and boundary conditions.

The reaction theory deals with scattering wave functions which are solutions of the Schrödinger equation with the appropriate boundary conditions. This scattering state could be provided by the GSM, but the Slater determinant representation of a GSM wave function is not suitable for a description of reactions because the entrance and exit channels cannot be easily identified. Furthermore, the determination of constants C_+ and C_- (see Eq. (2.52)), which are associated with the A-body scattering wave function and allow to calculate the S-matrix, is not possible using the Slater determinants.

To break this deadlock, one may formulate GSM in the CC representation. In general, the scattering state in such a formulation is a combination of different reaction channels. The coupling between different reaction channels is then given by the coupling potentials which are calculated microscopically using the GSM wave functions. The expansion of the radial wave function gives an access to the S-matrix [231] which provides the whole information about the reaction process.

3.2.1 Coupled channel problem in Berggren basis

As discussed in the introduction of this chapter, to go beyond elastic scattering one has to take into account the internal structure of the collision partners and consider different reaction channels. In this formulation, the nucleus is seen as consisting of different cluster partitions of the projectile and target nuclei. The wave function of an A-body system in any of its cluster partition is fully antisymmetrized. A similar view on the reaction dynamics has been put forward by the resonating group method [232, 233]. With this assumption, the channel state is written as:

$$|(c,r)\rangle = \hat{\mathcal{A}}\Big[|\Psi_{\rm T}^{J_{\rm T}}\rangle \otimes |\Psi_{\rm P}^{J_{\rm P}}\rangle\Big]^{J_A}_{M_A} \ , \tag{3.20}$$

with $|\Psi_{\rm T}^{J_{\rm T}}\rangle$ and $|\Psi_{\rm P}^{J_{\rm P}}\rangle$ the state of the target and the projectile respectively, and $J_{\rm T}$ and $J_{\rm P}$ their are the associated total angular momenta. J_A is the total angular momentum $\vec{J}_A = \vec{J}_{\rm T} + \vec{J}_{\rm P}$, and M_A its projection. Here r denotes the relative distance between the c.m. of the projectile and the target. This relative distance is contained in $|\Psi_{\rm P}^{J_{\rm P}}\rangle$ with all the other quantum numbers defining the projectile state:

$$|\Psi_{\rm P}^{J_{\rm P}}\rangle = |r, \ell, J_{\rm int}, J_{\rm P}\rangle \tag{3.21}$$

In this expression, ℓ is the orbital angular momentum, $J_{\rm int}$ the intrinsic angular momentum, and $\vec{J}_{\rm P} = \vec{\ell} + \vec{J}_{\rm int}$. Note that $|r,\ell\rangle$ stands for the c.m. part of the projectile. Hence channel index c stands for the $\{A-a, J_{\rm T}; a, \ell, J_{\rm int}, J_{\rm P}\}$ quantum number, with $(A-a)$ and a the number of nucleons in the target and projectile respectively. The channel states $|(c,r)\rangle$ form a complete basis:

$$\sum_c \int_0^\infty |(c,r)\rangle \langle (c,r)| \, dr = \hat{\mathbb{1}} \tag{3.22}$$

so that the A-body state $|\Psi\rangle$ can be expanded in this basis as:

$$|\Psi_{M_A}^{J_A}\rangle = \sum_c \int \frac{u_c(r)}{r} r^2 \, |(c,r)\rangle \, dr \ , \tag{3.23}$$

with $\langle (c,r)|\Psi\rangle = r\, u_c(r)$. The state $|\Psi\rangle$ describes the scattering process in relative coordinates, as the c.m. part of the target-projectile system is neglected since it reduces to a plane wave. Thus, the $u_c(r)$ is the radial wave function describing the relative motion between the target and the projectile. Using Eq. (3.23), the Schrödinger equation becomes:

$$\sum_c \int_0^\infty r^2 \, (H_{cc'} - E N_{cc'}) \, \frac{u_c(r)}{r} = 0 \ , \tag{3.24}$$

where:

$$\begin{aligned} H_{cc'}(r',r) &= \langle (c',r')| \, \hat{H} \, |(c,r)\rangle \\ N_{cc'}(r,r') &= \langle (c',r')|(c,r)\rangle \end{aligned} \tag{3.25}$$

Eqs. (3.24) are the CC equations which determine the radial wave function $u_c(r)$.

The projectile state $|\Psi_{\rm P}^{J_{\rm P}}\rangle = |r, \ell, J_{\rm int}, J_{\rm P}\rangle$ can be split into radial and internal parts:

$$|r, \ell, J_{\rm int} \ , J_{\rm P}\rangle = |r\rangle \otimes |\ell, J_{\rm int} \ , J_{\rm P}\rangle \ .$$

Using a one-body Berggren basis $\{|n\rangle\}$, one can write:

$$|r\rangle = \sum_n \frac{u_n(r)}{r} |n\rangle \tag{3.26}$$

where $\langle n|r\rangle = u_n(r)/r$. Then, the expansion of the projectile state in Berggren basis of the c.m. states reads:

$$|r, \ell, J_{\text{int}}\ , J_{\text{P}}\rangle = \sum_n \frac{u_n(r)}{r} |n, \ell, J_{\text{int}}\ , J_{\text{P}}\rangle \tag{3.27}$$

Note that n refers here to the (cluster) c.m. Berggren state of the projectile nucleus, while it refers to a standard one-body Berggren state for one-nucleon projectiles. Finally, one obtains the expression for the channel state in the Berggren basis:

$$\begin{aligned} |(c,r)\rangle = \hat{\mathcal{A}}\Big[|\Psi_{\text{T}}^{J_{\text{T}}}\rangle \otimes |r, \ell, J_{\text{int}}\ , J_{\text{P}}\rangle\Big]_{M_A}^{J_A} &= \hat{\mathcal{A}}\left[|\Psi_{\text{T}}^{J_{\text{T}}}\rangle \otimes \left(\sum_n \frac{u_n(r)}{r} |n, \ell, J_{\text{int}}\ , J_{\text{P}}\rangle\right)\right]_{M_A}^{J_A} \\ &= \sum_n \frac{u_n(r)}{r} \hat{\mathcal{A}}\Big[|\Psi_{\text{T}}^{J_{\text{T}}}\rangle \otimes |n, \ell, J_{\text{int}}\ , J_{\text{P}}\rangle\Big]_{M_A}^{J_A} \\ &= \sum_n \frac{u_n(r)}{r} |(c,n)\rangle \end{aligned} \tag{3.28}$$

Using these expressions, the matrix elements $H_{cc'}(r,r')$ can be formally expanded in a basis of $|n\ \ell\ J_{\text{int}}\ J_{\text{P}}\ M_{\text{P}}\rangle$ states as:

$$H_{cc'}(r,r') = \sum_{n,n'} H_{cc'}(n,n') \frac{u_n(r)}{r} \frac{u_{n'}(r')}{r'} \tag{3.29}$$

In the following subsection, we will provide useful details on how to compute matrix elements of $H_{cc'}(r,r')$.

3.2.2 Hamiltonian of the projectile

The determination of $H_{cc'}(r,r')$ involves the projectile Hamiltonian $\hat{H}_{\text{P}}$ which has not been defined until now. This Hamiltonian generates states of the projectile $|n, \ell, J_{\text{int}}\rangle$. We start by writing the Hamiltonian of the A-nucleons system in the laboratory coordinates:

$$\hat{H} = \sum_i \frac{\vec{\text{P}}_{i,\text{lab}}^2}{2m_i} + \sum_{i<j} \hat{V}_{ij}\ , \tag{3.30}$$

where i,j runs over all nucleons, and $\hat{V}_{ij}$ is the nucleon-nucleon interaction in the laboratory coordinates.

In the following, we want to separate the projectile Hamiltonian into the c.m. and intrinsic parts. Let $\hat{U}_i^{\text{target}}$ be the mean-field created by all target nucleons and acting on projectile nucleons i:

$$\sum_{j\in\text{target}} \hat{V}_{ij} \to \hat{U}_i^{\text{target}} \tag{3.31}$$

We assume that the one-body potential $\hat{U}_i^{\text{target}}$ is spherically symmetric and spin-independent. Neglecting couplings between the target and the projectile, *i.e.* at large distances, the projectile Hamiltonian $\hat{H}_{\text{P}}$ can be written as:

$$\hat{H}_{\text{P}} = \sum_{i\in\text{proj}} \left(\frac{\vec{\text{P}}_{i,\text{lab}}^2}{2m_i} + \hat{U}_i^{\text{target}} \right) + \sum_{i<j\in\text{proj}} \hat{V}_{ij} \tag{3.32}$$

As linear momenta of valence particles are identical in laboratory and COSM coordinates, and as R_{core} corrections are second-order when one goes from laboratory to COSM coordinates (see Sec. 2.2.4), $\hat{H}_{\text{P}}$ in COSM coordinates is the same as in Eq. (3.32). Hence, from now on, we will use COSM coordinates only. We can write:

$$\begin{aligned} \hat{H}_{\text{P}} &= \sum_{i\in\text{proj}} \left(\frac{\vec{\text{P}}_{i,\text{lab}}^2}{2m_i} + \hat{U}_i^{\text{target}} \right) + \sum_{i<j\in\text{proj}} \hat{V}_{ij} \\ &= \sum_{i\in\text{proj}} \frac{\left(\vec{\text{P}}_i - \frac{1}{a}\vec{\text{P}}_{\text{c.m.}}\right)^2}{2m_i} + \sum_{i<j} \hat{V}_{ij} + \frac{\vec{\text{P}}_{\text{c.m.}}^2}{2M_{\text{eff}}} + \sum_{i\in\text{proj}} \hat{U}_i^{\text{target}} \end{aligned} \tag{3.33}$$

where $\vec{\text{P}}_{\text{c.m.}} = \sum_{i\in\text{proj}} \vec{\text{P}}_i$. In this expression, a is the number of nucleons in the projectile, m the nucleon mass, and M_{eff} the reduced mass which is defined as:

$$\frac{1}{M_{\text{eff}}} = \frac{1}{M_{\text{P}}} + \frac{1}{M_{\text{T}}} \tag{3.34}$$

with M_{P} and M_{T} the masses of the projectile and target, respectively. Assuming the cluster approximation, *i.e.* implying $\vec{r}_i \simeq \vec{R}_{\text{c.m.}}$ and replacing $R_{\text{c.m.}}$ by r for the sake of simplicity, the average field created by all targets nucleons can be approximated by:

$$U_{\text{c.m.}}(r,r') = \sum_{i\in\text{proj}} U_i^{\text{target}}(r,r') = a_p\, U_p^{\text{target}}(r,r') + a_n\, U_n^{\text{target}}(r,r') \ , \tag{3.35}$$

where a_p and a_n are the number of protons and neutrons in the projectile, respectively. Consequently, $\hat{H}_{\text{P}}$ reads:

$$\hat{H}_{\text{P}} = \hat{H}_{\text{int}} + \hat{H}_{\text{c.m.}} \tag{3.36}$$

with:

$$\hat{H}_{\text{int}} = \sum_{i\in\text{proj}} \frac{\left(\vec{\text{P}}_i - \frac{1}{a}\vec{\text{P}}_{\text{c.m.}}\right)^2}{2m} + \sum_{i<j\in\text{proj}} \hat{V}_{ij} \tag{3.37}$$

$$\hat{H}_{\text{c.m.}} = \frac{\vec{\text{P}}_{\text{c.m.}}^2}{2M_{\text{eff}}} + \hat{U}_{\text{c.m.}} \tag{3.38}$$

$\hat{H}_{\text{int}}$ is the intrinsic Hamiltonian of the projectile and $\hat{H}_{\text{c.m.}}$ only involves the c.m. coordinates of the projectile and bears the spherical symmetry. Clearly, $\hat{H}_{\text{P}}$ generates the $|n,\ell,J_{\text{int}}\rangle$ states (3.27). Here $|n,\ell\rangle$ are the eigenstates of $\hat{H}_{\text{c.m.}}$, and $|J_{\text{int}}\rangle$ is the exact ground state of the projectile and the eigenstate of $\hat{H}_{\text{int}}$.

3.2.3 About the harmonic oscillator basis in the expansion of projectile states

The determination of $H_{cc'}(r,r')$ involves the calculation of matrix elements of the interaction for target and projectile states expanded in a basis of Slater determinants. The procedure is straightforward for the target states which are calculated in GSM. The construction of projectile states as the linear combination of Slater determinants requires the separation of c.m. and intrinsic parts.

Let us start with the definition of projectile states (3.21) in k-space:

$$|\Psi_{\rm P}^{J_{\rm P}}\rangle = |k,\ell,J_{\rm int},J_{\rm P}\rangle \ , \tag{3.39}$$

where k and ℓ are the relative momentum and angular momentum of the c.m., respectively. In order to use implement targets and projectile within a GSM picture, we should be expand the projectile state in a complete basis of Slater determinants:

$$|\Psi_{\rm P}^{J_{\rm P}}\rangle = \sum_{\alpha} C_{\alpha}^{a}|\Phi_{\alpha}^{a}\rangle \ , \tag{3.40}$$

where the Slater determinants are built from the s.p. states of the Berggren ensemble. To ensure the exact numerical reproduction of the Dirac's delta:

$$\langle\Psi_{\rm P}^{J_{\rm P}}|\Psi_{\rm P}^{J'_{\rm P}}\rangle = \delta(k-k') \ ,$$

one should consider an infinite set of Slater determinants $|\Phi_{\alpha}^{a}\rangle$ with an extremely fine discretization of the one-body continuum. The exact reproduction of $\delta(k-k')$ ensures the separation of c.m. and intrinsic parts of $|\Psi_{\rm P}^{J_{\rm P}}\rangle$.

To circumvent this numerical problem, we will use the harmonic oscillator basis. As the nuclear reactions are localized close to the target, the wave function of the projectile can be approximated by the bound state wave function, so that we can use the harmonic oscillator basis to expand it.

Let us define the harmonic oscillator expansion of the projectile state as:

$$|\Psi_{\rm P}^{J_{\rm P}}\rangle = \sum_{\gamma} B_{\gamma}^{a}|\Omega_{\gamma}^{a}\rangle \equiv \Big[|N,L\rangle^{\rm HO}\otimes|J_{\rm int}\rangle\Big]_{M_{\rm P}}^{J_{\rm P}} \tag{3.41}$$

with $|\Omega_{\gamma}^{a}\rangle$ a Slater determinants made of the one-body harmonic oscillator states. The many-body state $|N,L,J_{\rm int}\rangle_{M_{\rm P}}^{J_{\rm P}}$ has to be computed. For this, we begin by calculating the ground state of the cluster with a $0s$ c.m. part:

$$|N=0,\ L=0,\ M=0\rangle\,|J_{\rm int},M_{\rm int}\rangle \tag{3.42}$$

In order to calculate the c.m. harmonic oscillator many-body states efficiently, we introduce the rang 1 tensor ladder operator:

$$\hat{A}_{\mu}^{\dagger} = \sqrt{\frac{M\omega}{2\hbar}}\hat{R}_{\mu}^{(1)} - i\sqrt{\frac{1}{2M\hbar\omega}}\hat{\rm P}_{\mu}^{(1)} \ , \tag{3.43}$$

where $\mu=-1,0,+1$, and $\hat{R}_{\mu}^{(1)}$, $\hat{\rm P}_{\mu}^{(1)}$ represent the position and momentum of the projectile in c.m. system, respectively:

$$\hat{R}_{\mu}^{(1)} = \frac{1}{a}\sum_{i=1}^{a}\hat{r}_{i,\mu}^{(1)} \quad , \quad \hat{\rm P}_{\mu}^{(1)} = \sum_{i=1}^{a}\hat{\rm P}_{i,\mu}^{(1)} \tag{3.44}$$

$\hat{r}^{(1)}_{i,\mu}$, and $\hat{\mathrm{P}}^{(1)}_{i,\mu}$ in (3.44) are respectively the position and momentum of each nucleon of the projectile in the c.m. system, and a is the number of nucleons in the projectile. In practice, the action of $\hat{A}^\dagger$ on $|\Omega^a_\gamma\rangle$ is calculated using:

$$\hat{R}^{(1)}_\mu = \frac{1}{a}\sum_{\alpha,\beta}\langle\alpha|\,\hat{r}^{(1)}_\mu\,|\beta\rangle\,\hat{c}^\dagger_\alpha\hat{c}_\beta \quad , \quad \hat{\mathrm{P}}^{(1)}_\mu = \sum_{\alpha,\beta}\langle\alpha|\,\hat{p}^{(1)}_\mu\,|\beta\rangle\,\hat{c}^\dagger_\alpha\hat{c}_\beta \tag{3.45}$$

with $|\alpha\rangle, |\beta\rangle$ the one-body harmonic oscillator states, and $\hat{c}^\dagger_\alpha(\hat{c}_\beta)$ the particle creation (annihilation) operators. If we apply the $\hat{A}^\dagger_\mu$ tensor operator on the $|N,L,M\rangle$ state, we increase the $2N+L$ by one harmonic oscillator c.m. quantum:

$$2N+L \to 2N+L+1 \equiv 2N'+L' \,. \tag{3.46}$$

At this point, we couple the tensor operator $\hat{A}^\dagger$ acting on $|N,L,J_{\mathrm{int}},M_{\mathrm{int}}\rangle$:

$$\left[\hat{A}^\dagger\,|N,L,J_{\mathrm{int}},M_{\mathrm{int}}\rangle\right]^{L'}_{M'} = C^{N',L'}_{N,L}\,|N',L',M',J_{\mathrm{int}},M_{\mathrm{int}}\rangle \tag{3.47}$$

where the coefficient $C^{N',L'}_{N,L}$ does not depend of M' because it can be expressed as:

$$\begin{aligned} C^{N',L'}_{N,L} &= \langle N',L',M'|\left[\hat{A}^\dagger\,|N,L,J_{\mathrm{int}},M_{\mathrm{int}}\rangle\right]^{L'}_{M'}\rangle \\ &= \frac{1}{\sqrt{2L'+1}}\,\langle N',L'||\hat{A}^\dagger||N,L\rangle \end{aligned} \tag{3.48}$$

using the Wigner-Eckart theorem. Note that $\hat{A}^\dagger_\mu$ does not act on $|J_{\mathrm{int}},M_{\mathrm{int}}\rangle$. Therefore, we can build the set of states

$$\{|N,L,M_L,J_{\mathrm{int}},M_{\mathrm{int}}\rangle\} \tag{3.49}$$

because the harmonic oscillator degeneracy induced by $\hat{A}^\dagger_\mu$ is lifted by the L coupling. Then using Clebsch-Gordan coefficients, we couple the many-body state in Eq. (3.47) to J_{P}:

$$\langle N,L,M_L,J_{\mathrm{int}},M_{\mathrm{int}}|N,L,J_{\mathrm{int}}\rangle^{J_{\mathrm{P}}}_{M_{\mathrm{P}}} \tag{3.50}$$

As we already mentioned in (3.41), each state $|N,L,J_{\mathrm{int}}\rangle$ has to be expanded in the basis of harmonic oscillator Slater determinants $|\Omega^a_\gamma\rangle$. For that, we used (3.45) in:

$$\hat{A}^\dagger\,|N,L,J_{\mathrm{int}},M_{\mathrm{int}}\rangle = C^{N'L'}_{NL}\,|N',L',J_{\mathrm{int}},M_{\mathrm{int}}\rangle = \sum_\gamma B^a_\gamma\hat{A}^\dagger\,|\Omega^a_\gamma\rangle \tag{3.51}$$

which allows to determine all coefficients B^a_γ of each state $|N,L,J_{\mathrm{int}},M_{\mathrm{int}}\rangle$.

We now express the projectile state in the Berggren basis:

$$|\Psi^{J_{\mathrm{P}}}_{\mathrm{P}}\rangle = \sum_\alpha C^a_\alpha\,|\Phi^a_\alpha\rangle \tag{3.52}$$

The C^a_α coefficients are readily obtained:

$$C^a_\alpha = \langle\Phi^a_\alpha|N,L,J_{\mathrm{int}}\rangle^{J_{\mathrm{P}}}_{M_{\mathrm{P}}} = \sum_\gamma B^a_\gamma\langle\Phi^a_\alpha|\Omega^a_\gamma\rangle \tag{3.53}$$

As $|\Phi^a_\alpha\rangle$ and $|\Omega^a_\gamma\rangle$ are built from different one-body basis states, the overlap $\langle\Phi^a_\alpha|\Omega^a_\gamma\rangle$ must be calculated using the definition of SD as a linear combination of non-antisymmetrized tensor products:

$$\langle\Phi^a_\alpha|\Omega^a_\gamma\rangle = \sum_{\mathrm{P}} (-1)^{\mathrm{P}} \langle s_1 ... s_a| \hat{\mathrm{P}} |\sigma_1 ... \sigma_a\rangle \ , \tag{3.54}$$

where $\hat{\mathrm{P}}$ is the permutation operator. In this expression, $|s_i\rangle$ are s.p. states of the Berggren basis occupied in $|\Phi^a_\alpha\rangle$, and $|\sigma_i\rangle$ are s.p. states of the harmonic oscillator basis occupied in $|\Omega^a_\gamma\rangle$.

3.2.4 Expansion of nuclear states in a basis of Slater determinants

In the previous section, we have discussed how the projectile states are expanded in a basis of Slater determinants made of the one-body Berggren states. In this section, we will calculate the expansion of the A-body $|\Psi\rangle$:

$$|\Psi\rangle = \{C^\dagger_{|n,\ell,J_{\mathrm{int}}\rangle^{J_{\mathrm{P}}}_{M_{\mathrm{P}}}} |\Psi^{J_{\mathrm{T}}}_{\mathrm{T}}\rangle\}^{J_A}_{M_A} = \sum_\alpha C_\alpha |\Phi_\alpha\rangle \ , \tag{3.55}$$

where $C^\dagger_{|n,\ell,J_{\mathrm{int}}\rangle}$ is the projectile creation operator. For that, we use the expansion of $|\Psi^{J_{\mathrm{T}}}_{\mathrm{T}}\rangle$ in $(A-a)$-body Slater determinants and $|n,\ell,J_{\mathrm{int}}\rangle^{J_{\mathrm{P}}}_{M_{\mathrm{P}}}$ in a-body Slater determinants, which are obtained from the diagonalization of the GSM Hamiltonian $\hat{H}$:

$$|\Psi^{J_{\mathrm{T}}}_{\mathrm{T}}\rangle = \sum_\beta C^{A-a}_\beta |\Phi^{A-a}_\beta\rangle \tag{3.56}$$

$$|n,\ell,J_{\mathrm{int}}\rangle^{J_{\mathrm{P}}}_{M_{\mathrm{P}}} = \sum_\gamma C^a_\gamma |\Phi^a_\gamma\rangle \tag{3.57}$$

One may notice the a and $(A-a)$-body character of expansion coefficients and Slater determinants in the above expression. Applying the creation operator of Eq. (3.55) on the state (3.56) with a given angular momentum projection M_p, and using Eq. (3.57), the following uncoupled fully antisymmetrized A-body wave function appears:

$$\begin{aligned}
\{C^\dagger_{|n,\ell,J_{\mathrm{int}}\rangle^{J_{\mathrm{P}}}_{M_{\mathrm{P}}}} |\Psi^{J_{\mathrm{T}}}_{\mathrm{T}}\rangle\} &= \sum_\beta C^{A-a}_\beta C^\dagger_{|n,\ell,J_{\mathrm{int}}\rangle^{J_{\mathrm{P}}}_{M_{\mathrm{P}}}} |\Phi^{A-a}_\beta\rangle \\
&= \sum_{\beta\gamma} C^{A-a}_\beta C^a_\gamma \ \mathcal{A}\{|\Phi^{A-a}_\beta\rangle |\Phi^a_\gamma\rangle\} \\
&= \sum_\alpha C_\alpha |\Phi_\alpha\rangle
\end{aligned} \tag{3.58}$$

where the Slater determinants:

$$|\Phi_\alpha\rangle = (-1)^{\varphi_\alpha} \ \hat{\mathcal{A}}\{|\Phi^{A-a}_\beta\rangle |\Phi^a_\gamma\rangle\}$$

are A-body basis functions, and the expansion coefficients:

$$C_\alpha = (-1)^{\varphi_\alpha} b^{A-a}_\beta b^a_\gamma$$

include the rearrangements phase: $(-1)^{\varphi_\alpha}$. The angular momentum projection M_p verifies: $M + M_p = M_A$. The Slater determinants $|\Phi_\alpha\rangle$ vanish if $|\Phi^{A-a}_\beta\rangle$ and $|\Phi^a_\gamma\rangle$ have at least one s.p. state in common. The expansion of A-body wave function (3.55) can then be determined by coupling the wave function (3.58) to a given angular momentum.

3.2.5 Orthogonalization condition model in GSM-CC approach

If we act with $C^{\dagger}_{|n,\ell,J_{\rm int}\rangle^{J_{\rm P}}_{M_{\rm P}}}$ on $|\Psi^{J_{\rm T}}_{\rm T}\rangle$, we have to ensure that all calculated wave functions are orthogonal to the occupied states in the core, as demanded by the orthogonalization condition model. In principle, this should be assured by handling all states in the basis of Slater determinants. However, the orthogonalization condition model does not work in the finite model space, as in this case formally exact cancellations become numerically inexact and generate large unphysical couplings. Thus, we have to use a different procedure to avoid the occupation of core states.

We will introduce projectors defined with c.m. and relative coordinates:

$$\hat{Q} = \sum_{n\leq n_{\rm min}} |n,\ell,J_{\rm int},J_{\rm P},M_{\rm P}\rangle\langle n,\ell,J_{\rm int},J_{\rm P},M_{\rm P}| \tag{3.59}$$

$$\hat{\rm P} = 1 - Q_{\rm c.m.} \tag{3.60}$$

where $n_{\rm min}$ is chosen so as to remove the cluster eigenstates of $\hat{H}_{\rm P}$ sizably occupying the core. Using Eqs. (3.59) and (3.60), $\hat{H}_{\rm c.m.}$ is redefined :

$$\hat{H}_{\rm c.m.} \to \hat{\rm P}\hat{H}_{\rm c.m.}\hat{\rm P} = \hat{H}_{\rm c.m.} - \hat{Q}\hat{H}_{\rm c.m.} - \hat{H}_{\rm c.m.}\hat{Q} + \hat{Q}\hat{H}_{\rm c.m.}\hat{Q} \tag{3.61}$$

The new operator generates an additional short-range interaction which should be added to $\hat{H}_{\rm P}$ in Eq. (3.32). The modification of $\hat{H}_{\rm P}$ also generates a modification of the coupling part between the target and the projectile, while $\hat{H}$ (3.30) remains the same. This orthogonalization procedure has been checked to be reliable and numerically stable.

3.2.6 Matrix elements and approximations

Let us define the projectile state as a product:

$$|\Psi^{J_{\rm P}}_{\rm P}\rangle = \hat{\mathcal{A}}\prod_{k_{\rm rel}\leq k_{\rm max}} |k_{\rm rel}\rangle\,|k_{\rm c.m.}\rangle \tag{3.62}$$

involving the low relative momentum state $|k_{\rm rel}\rangle$, which embodies its compact cluster structure, and the c.m. part $|k_{\rm c.m.}\rangle$. Here $k_{\rm max}$ stands for a maximal linear momentum allowed for pairs of nucleons, related to the average relative velocity of nucleons inside the cluster. The Hamiltonian is written as: $\hat{H} = \hat{\rm T} + \hat{U}_{\rm core} + \hat{V}_{\rm res}$, where $\hat{U}_{\rm core}$ is the potential of the core and $\hat{V}_{\rm res}$ is the two-body residual interaction.

In order to evaluate the matrix elements:

$$\langle\hat{\mathcal{A}}\{\langle\Psi^{J_{{\rm T}_f}}_{{\rm T}_f}|\otimes\langle r_f\ \ell_f\ J_{{\rm int},f}\ J_{{\rm P},f}|\}^{J_A}_{M_A}|\,\hat{H}\,|\hat{\mathcal{A}}\{|\Psi^{J_{{\rm T}_i}}_{{\rm T}_i}\rangle\otimes|r_i\ \ell_i\ J_{{\rm int},i}\ J_{{\rm P},i}\rangle\}^{J_A}_{M_A}\rangle \tag{3.63}$$

we separate the Hamiltonian $\hat{H}$ into a part which generates the basis, and the residual part:

$$\hat{H} = \hat{\rm T} + \hat{U}_{\rm basis} + (\hat{V}_{\rm res} - \hat{U}_0) \tag{3.64}$$

where $\hat{U}_{\rm basis}$ is the optimal potential of A-particle system and $\hat{U}_0 = \hat{U}_{\rm basis} - \hat{U}_{\rm core}$. The advantage of this decomposition is that $\hat{V} = \hat{V}_{\rm res} - \hat{U}_0$ is finite-range.

The two-body matrix elements $\langle a,b|\hat{V}|c,d\rangle$ involved in the target-projectile coupling at high $k_{\text{c.m.}}$ energy are negligible (see Appendix A.1):

$$\langle a,b|\hat{V}|c,d\rangle \to 0 \text{ unless } \begin{cases} k_a, k_b \le k_{\max} & \text{and} \quad k_{\text{core}}, k_d \le k_{\max} \\ k_a, k_b > k_{\max} & \text{and} \quad k_{\text{core}}, k_d > k_{\max} \end{cases} \tag{3.65}$$

$|a\rangle, |b\rangle, |c\rangle$ and $|d\rangle$ in (3.65) are Berggren states of momentum k_a, k_b, k_{core} and k_d, respectively. $k_{\max}$ is an arbitrarily large momentum of the one-body state. Another way to formulate Eq. (3.65) is:

$$\langle a,b|\hat{V}|c,d\rangle \to 0 \text{ if } \exists (i,j) \in \{a,b,c,d\} \mid k_i \le k_{\max} \text{ and } k_j > k_{\max} \tag{3.66}$$

where $i,j \in \{a,b,c,d\}$. This property of $\langle a,b|\hat{V}|c,d\rangle$ is useful to derive the analytic form of the CC equations.

3.2.6.1 The antisymmetry of a target-projectile system at large c.m. energies

Results obtained in Sec. (A.1.1) imply that assuming $k_{\text{c.m.}} > k_{\text{c.m.max}}$, with $k_{\text{c.m.max}} = 2k_{max}$ the only non-vanishing two-body matrix elements $\langle a,b|\hat{V}|c,d\rangle$ are those for which $k_i > k_{\max}\ \forall i \in \{a,b,c,d\}$. Therefore, an important consequence of the decoupling between target and projectile is that the antisymmetry can be suppressed between projectile and target if $k_{\text{c.m.}} > k_{\text{c.m.max}}$, as in this case linear momenta of the occupied states verify: $k \le k_{\max}$ in the target and $k > k_{\max}$ in the projectile.

We will use in practice a basis of harmonic oscillator states to expand c.m. states whereas all previous results implied the use of Bessel and Berggren basis states (see Appendix A.1). However, the overlap $\langle k_{\text{c.m.}}|N\rangle$ is small at large momentum $k_{\text{c.m.}}$ unless $N > N_{\max}$ for $N_{\max}$ sufficiently large, because for Bessel functions of momentum $k_{\text{c.m.}}$: $\langle k_{\text{c.m.}}|N\rangle = U_N^{\text{HO}}(k_{\text{c.m.}})$. Hence, all previous results remain valid if we replace c.m. Berggren states of momentum $k_{\text{c.m.}} > k_{\text{c.m.max}}$ by c.m. harmonic oscillator states of principal quantum number $N > N_{\max}$.

3.2.7 Matrix elements of Hamiltonian $H_{cc'}(r,r')$ and norm $N_{cc'}(r,r')$

In this section, we will discuss the computation of $N_{cc'}(r,r')$ and $H_{cc'}(r,r')$. The calculation of the overlaps $N_{cc'}(r,r')$ is straightforward:

$$\begin{aligned} N_{cc'}(r,r') &= \sum_{n,n'} \frac{u_n(r)}{r}\frac{u_{n'}(r')}{(r')} \\ &= \sum_{n,n'} \frac{u_n(r)}{r}\frac{u_{n'}(r')}{r'} \langle \Psi_{\text{T}}^{J_{\text{T}}}| \hat{C}_{|n,\ell,J_{\text{int}}\rangle} \hat{C}^{\dagger}_{|n,\ell,J_{\text{int}}\rangle} |\Psi_{\text{T}}^{J_{\text{T}}}\rangle \\ &= \sum_{n,n'} \frac{u_n(r)}{r}\frac{u_{n'}(r')}{r'} \sum_{\alpha,\alpha'} C_\alpha C_{\alpha'} \langle \Phi_{\alpha'}|\Phi_\alpha\rangle \end{aligned} \tag{3.67}$$

$|\Phi_\alpha\rangle$ in this equation are given in Eq. (3.58). Due to the decoupling of the target and projectile at high energy, it is more convenient to rewrite the Hamiltonian $\hat{H}$ by introducing the target Hamiltonian $\hat{H}_{\text{T}}$:

$$\hat{H}_{\text{T}} = \hat{\text{T}}_{\text{T}} + \hat{U}^{\text{T}}_{\text{basis}} + (\hat{V}_{\text{res}} - \hat{U}_0)^{A-a}, \tag{3.68}$$

where $(\hat{V}_{\text{res}} - \hat{U}_0)^{A-a}$ is the part of $\hat{V}_{\text{res}} - \hat{U}_0$ acting on the $(A-a)$-body target state, and where $\hat{\text{T}}_{\text{T}}$ and $\hat{U}^{\text{T}}_{\text{basis}}$ are the target kinetic and potential parts of the Hamiltonian $\hat{H}$, respectively. The

Hamiltonian can thus be written as:

$$\hat{H} = \hat{H}_{\mathrm{T}} + \hat{H}_{\mathrm{P}} + \hat{H}_{\mathrm{TP}} \ , \tag{3.69}$$

where $\hat{H}_{\mathrm{TP}} = \hat{H} - \hat{H}_{\mathrm{T}} - \hat{H}_{\mathrm{P}}$ by definition.

The action of target and projectile Hamiltonians $\hat{H}_{\mathrm{T}}$ and $\hat{H}_{\mathrm{P}}$ (3.36) on A-body states is effected by considering non fully antisymmetrized A-body states:

$$\hat{H}_{\mathrm{T}} \left(|\Psi_{\mathrm{T}}\rangle \otimes |\Psi_{\mathrm{P}}\rangle \right) = \left(\hat{H}_{\mathrm{T}} |\Psi_{\mathrm{T}}\rangle \otimes |\Psi_{\mathrm{P}}\rangle \right) \tag{3.70}$$

$$\hat{H}_{\mathrm{P}} \left(|\Psi_{\mathrm{T}}\rangle \otimes |\Psi_{\mathrm{P}}\rangle \right) = \left(|\Psi_{\mathrm{T}}\rangle \otimes \hat{H}_{\mathrm{P}} |\Psi_{\mathrm{P}}\rangle \right) \tag{3.71}$$

Matrix elements $H_{cc'}(r, r')$ (3.29) can be decomposed in four terms using Eq. (3.29):

$$\begin{aligned} H_{cc'}(r,r') \quad = & \sum_{\substack{n \le n_{\max} \\ n' \le n_{\max}}} H_{cc'}(n,n') \frac{u_n(r)}{r} \frac{u_{n'}(r')}{r'} \\ & + \sum_{\substack{n \le n_{\max} \\ n' > n_{\max}}} H_{cc'}(n,n') \frac{u_n(r)}{r} \frac{u_{n'}(r')}{r'} \\ & + \sum_{\substack{n > n_{\max} \\ n' \le n_{\max}}} H_{cc'}(n,n') \frac{u_n(r)}{r} \frac{u_{n'}(r')}{r'} \\ & + \sum_{\substack{n > n_{\max} \\ n' > n_{\max}}} H_{cc'}(n,n') \frac{u_n(r)}{r} \frac{u_{n'}(r')}{r'} \end{aligned} \tag{3.72}$$

The first term is a finite sum and can be calculated using standard shell model formulas.

Sums in the second term will be shown to be equal to zero:

$$\begin{aligned} & H_{cc'}\left(n,n'\right) \\ & = \left[\langle \Psi_{\mathrm{T}}^{J_{\mathrm{T}}}| \otimes \langle n \ \ell \ J_{\mathrm{int}} \ J_{\mathrm{P}} \ M_{\mathrm{P}}| \right] \hat{\mathcal{A}} \hat{H} \hat{\mathcal{A}} \left[|\Psi_{\mathrm{T}}^{J'^{\mathrm{T}}}\rangle \otimes |n' \ \ell' \ J'_{\mathrm{int}} \ J'_{\mathrm{P}} \ M'_{\mathrm{P}}\rangle \right] \\ & = \left[\langle \Psi_{\mathrm{T}}^{J_{\mathrm{T}}}| \otimes \langle n \ \ell \ J_{\mathrm{int}} \ J_{\mathrm{P}} \ M_{\mathrm{P}}| \right] \left(\hat{H}_{\mathrm{T}} + \hat{H}_{\mathrm{P}} + \hat{\mathcal{A}} \hat{H}_{\mathrm{TP}} \hat{\mathcal{A}} \right) \left[|\Psi_{\mathrm{T}}^{J'^{\mathrm{T}}}\rangle \otimes |n' \ \ell' \ J'_{\mathrm{int}} \ J'_{\mathrm{P}} \ M'_{\mathrm{P}}\rangle \right] \qquad (3.73) \\ & = \left[\langle \Psi_{\mathrm{T}}^{J_{\mathrm{T}}}| \otimes \langle n \ \ell \ J_{\mathrm{int}} \ J_{\mathrm{P}} \ M_{\mathrm{P}}| \right] E_{\mathrm{c.m.}} + E_{\mathrm{T}} + E_{\mathrm{int}} \left[|\Psi_{\mathrm{T}}^{J'^{\mathrm{T}}}\rangle \otimes |n' \ \ell' \ J'_{\mathrm{int}} \ J'_{\mathrm{P}} \ M'_{\mathrm{P}}\rangle \right] \\ & + \sum_{\alpha,\beta} C_\alpha C_\beta \langle \Phi_\alpha | \hat{H}_{\mathrm{TP}} | \Phi_\beta \rangle \\ & = \left(E_{\mathrm{c.m.}} + E_{\mathrm{T}} + E_{\mathrm{int}} \right) \delta_{cc'} \delta_{nn'} + \sum_{\alpha,\beta} C_\alpha C_\beta \langle \Phi_\alpha | \hat{H}_{\mathrm{TP}} | \Phi_\beta \rangle \qquad (3.74) \\ & = \sum_{\alpha,\beta} C_\alpha C_\beta \langle \Phi_\alpha | \hat{H}_{\mathrm{TP}} | \Phi_\beta \rangle = \sum_{\substack{\alpha,\beta \\ \gamma,\delta,\epsilon,\zeta \epsilon T,p}} C_\alpha C_\beta \langle \gamma,\delta | \hat{V} | \epsilon,\zeta \rangle \langle \Phi_\alpha | a_\gamma^+ a_\delta^+ a_\epsilon a_\zeta | \Phi_\beta \rangle \qquad (3.75) \end{aligned}$$

because the conditions (3.66) are verified. Indeed, due to Eqs. (3.70) and (3.71), the antisymmetrizers have been suppressed in (3.73) except for $\hat{H}_{\mathrm{TP}}$. In Eq.(3.74), the term involving $E_{\mathrm{c.m.}}$, E_{T}, and E_{int} disappears because we have $n \neq n'$ and $c \neq c'$. Then, only the sum involving the Slater determinants remains in Eq. (3.75). In this equation, $|\gamma\rangle, |\delta\rangle, |\epsilon\rangle, |\zeta\rangle$ stand for s.p. states which are

occupied in target and projectile. As the conditions (3.66) are verified, we have $\langle\gamma,\delta|\,\hat{V}\,|\epsilon,\zeta\rangle = 0$, and Eq.(3.75) is equal to zero.

The third sum in Eq. (3.72) is treated identically for symmetry reasons. The last sum in Eq. (3.72) reads :

$$\begin{aligned}
&H_{cc'}(n,n') \\
&= \left[\langle\Psi_{\mathrm{T}}^{J_{\mathrm{T}}}|\otimes\langle n\ \ell\ J_{\mathrm{int}}\ J_{\mathrm{P}}\ M_{\mathrm{P}}|\right]\left(\hat{H}_{\mathrm{T}}+\hat{H}_{\mathrm{P}}+\hat{\mathcal{A}}\hat{H}_{\mathrm{TP}}\hat{\mathcal{A}}\right)\left[|\Psi_{\mathrm{T}}^{J'_{\mathrm{T}}}\rangle\otimes|n'\ \ell'\ J'_{\mathrm{int}}\ J'_{\mathrm{P}}\ M'_{\mathrm{P}}\rangle\right] \qquad (3.76)\\
&= \left[\langle\Psi_{\mathrm{T}}^{J_{\mathrm{T}}}|\otimes\langle n\ \ell\ J_{\mathrm{int}}\ J_{\mathrm{P}}\ M_{\mathrm{P}}|\right]\hat{H}_{\mathrm{T}}+\hat{H}_{\mathrm{P}}\left[|\Psi_{\mathrm{T}}^{J_{\mathrm{T}}}\rangle\otimes|n'\ \ell'\ J'_{\mathrm{int}}\ J'_{\mathrm{P}}\ M'_{\mathrm{P}}\rangle\right]\\
&= \left[\langle\Psi_{\mathrm{T}}^{J_{\mathrm{T}}}|\otimes\langle n\ \ell\ J_{\mathrm{int}}\ J_{\mathrm{P}}\ M_{\mathrm{P}}|\right]\hat{H}_{\mathrm{T}}+\hat{H}_{\mathrm{int}}+\hat{H}_{\mathrm{c.m.}}\left[|\Psi_{\mathrm{T}}^{J'_{\mathrm{T}}}\rangle\otimes|n'\ \ell'\ J'_{\mathrm{int}}\ J'_{\mathrm{P}}\ M'_{\mathrm{P}}\rangle\right]\\
&= (E_{\mathrm{T}}+E_{\mathrm{int}}+E_{\mathrm{c.m.}})\,\delta_{cc'}\delta_{nn'} \qquad (3.77)
\end{aligned}$$

Here, the matrix elements involving $\hat{H}_{\mathrm{TP}}$ in Eq.(3.76) are equal to zero due to the decoupling between the target and the projectile because we have $n > n_{\max}$ and $n' > n_{\max}$ (see Sec. 3.2.6.1).

Consequently, we can express the matrix elements $H_{cc'}(r,r')$ as:

$$H_{cc'}(r,r') = \sum_{\substack{n\le n_{\max}\\ n'\le n_{\max}}} H_{cc'}(n,n')\frac{u_n(r)}{r}\frac{u_{n'}(r')}{r'} + \delta_{cc'}\sum_{n>n_{\max}}(E_{\mathrm{T}}+E_{\mathrm{int}}+E_{\mathrm{c.m.}})\frac{u_n(r)}{r}\frac{u_n(r')}{r'} \qquad (3.78)$$

The sums in Eq. (3.78) involving $n > n_{\max}$ and $n' > n_{\max}$ can be written as:

$$\begin{aligned}
&\sum_{n>n_{\max}}(E_{\mathrm{T}}+E_{\mathrm{int}}+E_{\mathrm{c.m.}})\frac{u_n(r)}{r}\frac{u_n(r')}{r'}\\
&= \sum_{n}(E_{\mathrm{T}}+E_{\mathrm{int}}+E_{\mathrm{c.m.}})\frac{u_n(r)}{r}\frac{u_n(r')}{r'}\\
&- \sum_{n\le n_{\max}}(E_{\mathrm{T}}+E_{\mathrm{int}}+E_{\mathrm{c.m.}})\frac{u_n(r)}{r}\frac{u_n(r')}{r'} \qquad (3.79)
\end{aligned}$$

where the first sum in Eq. (3.79) can be expressed with Dirac delta's due to completeness properties of $u_n(r)$ states:

$$\begin{aligned}
&\sum_{n}(E_{\mathrm{T}}+E_{\mathrm{int}}+E_{\mathrm{c.m.}})\frac{u_n(r)}{r}\frac{u_n(r')}{r'}\\
&= (E_{\mathrm{T}}+E_{\mathrm{int}})\frac{\delta(r-r')}{rr'} + \mathrm{T}_{\mathrm{c.m.}}\frac{\delta(r-r')}{rr'} + U_{\mathrm{c.m.}}(r,r') \qquad (3.80)
\end{aligned}$$

$\mathrm{T}_{\mathrm{c.m.}}$ and $U_{\mathrm{c.m.}}(r,r')$ in (3.80) stand for the c.m. kinetic and potential parts of Eq. (3.38), respectively. Hence, we can write finally:

$$\begin{aligned}
H_{cc'}(r,r') &= \delta_{cc'}\left[-\frac{\hbar^2}{2M_{\mathrm{eff}}}\frac{\partial^2}{\partial r^2}+\frac{\hbar^2\ell(\ell+1)}{2M_{\mathrm{eff}}r^2}+E_{\mathrm{T}}+E_{\mathrm{int}}\right]\frac{\delta(r-r')}{rr'}\\
&+ \delta_{cc'}U_{\mathrm{c.m.}}(r,r')+\tilde{V}_{cc'}(r,r') \qquad (3.81)
\end{aligned}$$

where $\tilde{V}_{cc'}$ includes the remaining short-range potential terms of the Hamiltonian kernels, *i.e.* the first sum of Eq. (3.72,3.78) and the last sum of Eq. (3.79):

$$\tilde{V}_{cc'} = \sum_{\substack{n\le n_{\max}\\ n'\le n_{\max}}} H_{cc'}(n,n')\frac{u_n(r)}{r}\frac{u_{n'}(r')}{r'} - \sum_{n\le n_{\max}} (E_{\rm T}+E_{\rm int}+E_{\rm c.m.})\frac{u_n(r)}{r}\frac{u_n(r')}{r'} \tag{3.82}$$

$H_{cc'}(n,n')$ in the above expression is:

$$H_{cc'}(n,n') = (E_{\rm c.m.}+E_{\rm T}+E_{\rm int})\,\delta_{cc'}\delta_{nn'} + \sum_{\substack{\alpha,\beta\\ \gamma,\delta,\epsilon,\zeta\epsilon T,p}} C_\alpha C_\beta \langle\gamma,\delta|\hat{V}|\epsilon,\zeta\rangle\langle\Phi_\alpha|a^+_\gamma a^+_\delta a_\epsilon a_\zeta|\Phi_\beta\rangle \tag{3.83}$$

To compute the matrix elements $\langle\gamma,\delta|\hat{V}|\epsilon,\zeta\rangle$, it is necessary to use the harmonic oscillator basis to calculate the last term involving $\hat{V}$ in Eq. (3.83), because it is more convenient and stable numerically. For this, we perform an expansion of the eigenstates $|n,\ell\rangle$ of $\hat{H}_{\rm c.m.}$ into an harmonic oscillator basis : $|n,\ell\rangle = \sum_{N,L}\langle N,L|n,\ell\rangle|N,L\rangle$.

3.2.8 Calculation of the reaction cross sections

In this section, we will discuss the determination of cross sections for elastic, inelastic or transfer reactions. Let us start with the following ansatz for the A-nucleon eigenstate of $\hat{H}$:

$$|\Psi^{e,J_A}_{M_A}\rangle = \sum_c \int_0^\infty \frac{u_c^{e,J_A}(r)}{r} r^2\,|(c,r)\rangle\,dr \tag{3.84}$$

In the above expression, we have introduced additional indices J_A, M_A, and e in the total state and in the relative wave function. These are the total angular momentum J_A defined as $\vec{J}_A = \vec{J}_{\rm T}+\vec{J}_{\rm P}$, its projection M_A, and the entrance channel e. The asymptotic behavior of the radial amplitude $u_c^{e,J_A}(r)$ associated with the channel c is:

$$\begin{aligned} u_c^{eJ_A}(r) \;\longrightarrow\; & -\frac{1}{2i}\left[\delta_{ce}H^-_{\ell_e}(\eta_e,k^e r) - S^{J_A}_{ec}H^+_{\ell_c}(\eta_c,k^c r)\right] \\ & = \delta_{ce}F_{\ell_e}(\eta_e,k^e r) + T^{J_A}_{ec}H^+_{\ell_c}(\eta_c,k^c r)\,, \end{aligned} \tag{3.85}$$

where $F_{\ell_e}(\eta_e,k^e r)$ is the regular Coulomb function, and η the Sommerfeld parameter. The S-matrix and the T-matrix elements are related by the expression:

$$T^{J_A}_{ec} = \frac{(S^{J_A}-1)_{ec}}{2i} \tag{3.86}$$

In the reactions involving light projectiles ($A\le 4$), mostly the target states stand for the actual physical channels. Let us denote by $\tilde{c}$ the set of quantum numbers which completely defines target states, so that $c=\{\tilde{c},\ell,J_{\rm int},J_{\rm P}\}$. The physical scattering wave function, characterized by the entrance state of the target $\tilde{e}$ (usually the ground state), the magnetic quantum numbers $M^{\tilde{e}}_{\rm P}$ and $M^{\tilde{e}}_{\rm T}$ of the projectile and the target, respectively, reads:

$$|\varphi^{\tilde{e}}_{M^{\tilde{e}}_{\rm P}M^{\tilde{e}}_{\rm T}}\rangle = \sum_{\ell_e,J^e_{\rm P},J_A} \frac{A^{\ell_e J_{\rm int}J^{\tilde{e}}_{\rm T}J_A}_{M^{\tilde{e}}_{\rm P}M^{\tilde{e}}_{\rm T}}}{k^{\tilde{e}}}\,|\Psi^{\tilde{e}\ell_e J^e_{\rm P}}_{M_A=M^{\tilde{e}}_{\rm P}+M^{\tilde{e}}_{\rm T}}J_A\rangle \tag{3.87}$$

where the coefficients are given by :

$$A^{\ell_e J_{\rm int} J_{\rm T}^{\tilde{e}} J_A}_{M_{\rm P}^{\tilde{e}} M_{\rm T}^{\tilde{e}}} = \langle J_{\rm P}^{e} M_{\rm P}^{\tilde{e}} | \ell_e m_e J_{\rm int} M_{\rm int} \rangle \, \langle J_A M_A | J_{\rm P}^{e} M_{\rm P}^{\tilde{e}} J_{\rm T}^{\tilde{e}} M_{\rm T}^{\tilde{e}} \rangle \, i^{\ell_e} \sqrt{4\pi(2\ell_e+1)} e^{i\sigma_{\ell_e}} \tag{3.88}$$

Here, σ_ℓ is the Coulomb phase shift defined as $\sigma_\ell = \arg\left(\Gamma(\ell+1+i\eta)\right)$ with Γ the Euler's gamma function. This particular partial wave decomposition in terms of $|\Psi^{e,J_A}_{M_A}\rangle$ confers to the physical scattering state $|\varphi^{\tilde{e}}_{M_{\rm P}^{\tilde{e}} M_{\rm T}^{\tilde{e}}}\rangle$ its correct asymptotic behavior, that is:

$$\begin{aligned} \langle \vec{r} \, | \varphi^{\tilde{e}}_{M_{\rm P}^{\tilde{e}} M_{\rm T}^{\tilde{e}}} \rangle \longrightarrow & \exp\left(i\left[kz + \eta \, \ln(k(r-z))\right]\right) \cdot |J_{\rm int}\rangle \otimes |\Psi^{\tilde{e},J_{\rm T}}_{M_{\rm T}}\rangle \\ + \sum_{\tilde{c} M_{\rm P}^{\tilde{e}} M_{\rm T}^{\tilde{e}}} & f_{\tilde{e} M_{\rm P}^{\tilde{e}} M_{\rm T}^{\tilde{e}} \to \tilde{c} M_{\rm P}^{\tilde{c}} M_{\rm P}^{\tilde{c}}}(\theta,\phi) \cdot \frac{\exp\left(i\left[kr - \eta \, \ln(2kr)\right]\right)}{r} \cdot |J_{\rm int}\rangle \otimes |\Psi^{\tilde{e},J_{\rm T}}_{M_{\rm T}}\rangle \end{aligned} \tag{3.89}$$

In the above expression, we changed notations and replaced c by $\tilde{c}$ defined as $c = \{\tilde{c}, \ell, J_{\rm int}\}$, and e by $\tilde{e}$ with $e = \{\tilde{e}, \ell, J_{\rm int}\}$. These modifications are motivated by the fact that $(\ell, J_{\rm int})$ are not measured experimentally, so the cross section will only depend on $\tilde{c}$ and $\tilde{e}$.

The scattering amplitude in terms of the T-matrix elements is:

$$\begin{aligned} f_{\tilde{e} M_{\rm P}^{\tilde{e}} M_{\rm T}^{\tilde{e}} \to \tilde{c} M_{\rm P}^{\tilde{c}} M_{\rm T}^{\tilde{c}}}(\theta,\phi) = & \, \delta_{\tilde{c}\tilde{e}} \, \delta_{M_{\rm P}^{\tilde{c}} M_{\rm P}^{\tilde{e}}} \delta_{M_{\rm T}^{\tilde{c}} M_{\rm T}^{\tilde{c}}} \, f_C(\theta) \\ + \sum_{\ell^e J_{\rm P}^{e} \ell^c J_{\rm P}^{c} J_A} & \frac{C^{\ell^e J_{\rm P}^{e} J_{\rm T}^{\tilde{e}} \ell^c J_{\rm P}^{c} J_{\rm T}^{\tilde{c}} J_A}_{M_{\rm P}^{\tilde{e}} M_{\rm T}^{\tilde{e}} M_{\rm P}^{\tilde{c}} M_{\rm T}^{\tilde{c}}}}{k^{\tilde{e}}} \, T^{J_A}_{\tilde{e}\ell^e J_{\rm P}^{e}, \tilde{c}\ell^c J_{\rm P}^{c}} Y^{\ell^c}_{M_{\rm P}^{\tilde{e}} + M_{\rm T}^{\tilde{e}} - M_{\rm P}^{\tilde{c}} - M_{\rm T}^{\tilde{c}}}(\theta,\phi) \end{aligned} \tag{3.90}$$

where

$$\begin{aligned} & C^{\ell^e J_{\rm P}^{e} J_{\rm T}^{\tilde{e}} \ell^c J_{\rm P}^{c} J_{\rm T}^{\tilde{c}} J_A}_{M_{\rm P}^{\tilde{e}} M_{\rm T}^{\tilde{e}} M_{\rm P}^{\tilde{c}} M_{\rm T}^{\tilde{c}}} \\ & = \langle J_{\rm P}^{e} M_{\rm P}^{\tilde{e}} | \ell^e 0 M_{\rm int} M_{\rm P}^{\tilde{e}} \rangle \, \langle J_{\rm P}^{c} \, M_{\rm P}^{\tilde{e}} + M_{\rm T}^{\tilde{e}} - M_{\rm T}^{\tilde{c}} | \ell^c \, M_{\rm P}^{\tilde{e}} + M_{\rm T}^{\tilde{e}} - M_{\rm P}^{\tilde{c}} - M_{\rm T}^{\tilde{c}} M_{\rm int} M_{\rm P}^{\tilde{c}} \rangle \\ & \times \langle J_A \, M_{\rm P}^{\tilde{e}} + M_{\rm T}^{\tilde{e}} | J_{\rm P}^{e} M_{\rm P}^{\tilde{e}} J_{\rm T}^{\tilde{e}} M_{\rm T}^{\tilde{e}} \rangle \, \langle J_A \, M_{\rm P}^{\tilde{e}} + M_{\rm T}^{\tilde{e}} | J_{\rm P}^{c} \, M_{\rm P}^{\tilde{e}} + M_{\rm T}^{\tilde{e}} - M_{\rm T}^{\tilde{c}} \, J_{\rm T}^{\tilde{c}} M_{\rm T}^{\tilde{c}} \rangle \\ & \times \, i^{(\ell^e - \ell^c)} \sqrt{4\pi(2\ell^e+1)} e^{i(\sigma_{\ell^e} + \sigma_{\ell^c})} \, . \end{aligned} \tag{3.91}$$

From the expression (3.89) of the physical scattering state, the differential cross section for the scattering process to the channel $(\tilde{c}, M_{\rm P}^{\tilde{c}}, M_{\rm T}^{\tilde{c}})$ at a given angle θ reads:

$$\frac{d\sigma_{\tilde{e} M_{\rm P}^{\tilde{e}} M_{\rm T}^{\tilde{e}} \to \tilde{c} M_{\rm P}^{\tilde{c}} M_{\rm T}^{\tilde{c}}}}{d\Omega}(\theta) \; = \; \frac{k^{\tilde{c}}}{k^{\tilde{e}}} |f_{\tilde{e} M_{\rm P}^{\tilde{e}} M_{\rm T}^{\tilde{e}} \to \tilde{c} M_{\rm P}^{\tilde{c}} M_{\rm T}^{\tilde{c}}}(\theta,\phi)|^2 \tag{3.92}$$

The differential cross sections of the scattering process to a given target state $\tilde{c}$ thus reads:

$$\frac{d\sigma_{\tilde{e} \to \tilde{c}}}{d\Omega}(\theta) \; = \; \frac{1}{2(2J_{\rm T}^{\tilde{e}}+1)} \sum_{M_{\rm P}^{\tilde{e}} M_{\rm T}^{\tilde{e}} M_{\rm P}^{\tilde{c}} M_{\rm T}^{\tilde{c}}} \frac{k^{\tilde{c}}}{k^{\tilde{e}}} |f_{\tilde{e} M_{\rm P}^{\tilde{e}} M_{\rm T}^{\tilde{e}} \to \tilde{c} M_{\rm P}^{\tilde{c}} M_{\rm T}^{\tilde{c}}}(\theta,\phi)|^2 \tag{3.93}$$

3.3 Numerical resolution of the coupled-channel equations

In this section, we present different numerical methods to calculate the A-body scattering states $|\Psi^{J_A}_{M_A}\rangle$ (3.23). These A-body scattering states $|\Psi^{J_A}_{M_A}\rangle$ are expanded in a basis of channels $|(c,r)\rangle$. However, due to the antisymmetrization between the projectile and the target, the channel are not orthogonal among each other. Thus in Sec. 3.3.1 we shall detail the method used to orthogonalize the channel states $|(c,r)\rangle$. Observables can be calculated if we know the radial amplitude $u_c(r)$ for each channel c involved in $|\Psi^{J_A}_{M_A}\rangle$. Hence, in Sec. 3.3.2 and 3.3.3 we shall detail the the boundary conditions that we considered for the radial amplitude. In Sec. 3.3.3 we shall detail the method of the equivalent potential which is used to deal with non-local potential occurring in Eq. (3.81) when we solved the CC equations (3.24) with direct integration. Finally, in Sec. 3.3.5 we present an alternative method of the direct integration, which is based on the use of the Green's functions, to solve the CC equations (3.24).

3.3.1 Orthogonalization of the channel states

The CC formalism leads to a generalized eigenvalue problem because different channel basis states are non-orthogonal. To formulate the GSM-CC equations as the generalized eigenvalue problem, one should express Eq. (3.24) in the orthogonal channel basis $\{|(c,r)\rangle_o\}$:

$$ {}_o\langle(c',r')|(c,r)\rangle_o = \frac{\delta(r-r')}{r^2}\delta_{cc'} \tag{3.94}$$

The transformation from the non-orthogonal channel basis $\{|(c,r)\rangle\}$ to the orthogonal one $\{|(c,r)\rangle_o\}$ is given by the overlap operator $\hat{O}$:

$$ |(c,r)\rangle = \hat{O}^{\frac{1}{2}}\,|(c,r)\rangle_o $$

The CC equations in Eq. (3.24) written in the orthogonal basis are:

$$ \sum_c \int_0^\infty dr\, r^2 ({}_o\langle(c',r')|\hat{H}_o|(c,r)\rangle_o - E_o\,\langle(c,r)|\hat{O}|(c,r)\rangle_o)\,{}_o\langle(c,r)|\Psi_o\rangle = 0\ , \tag{3.95}$$

where : $\hat{H}_o = \hat{O}^{1/2}\hat{H}\hat{O}^{1/2}$, $|\Psi_o\rangle = \hat{O}^{1/2}\,|\Psi\rangle$, $E_o = \hat{O}E$ and :

$$\begin{aligned} {}_o\langle(c',r')|\hat{H}_o|(c,r)\rangle_o &= \langle(c',r')|\hat{H}|(c,r)\rangle \\ {}_o\langle(c',r')|\hat{O}|(c,r)\rangle_o &= \langle(c',r')|(c,r)\rangle \end{aligned} \tag{3.96}$$

The transformation of this generalized eigenvalue problem into a standard eigenvalue problem is achieved with a substitution: $|\Phi\rangle = \hat{O}\,|\Psi\rangle$. One obtains:

$$ \sum_c \int_0^\infty dr\, r^2 ({}_o\langle(c',r')|\hat{H}|(c,r)\rangle_o - E_o\,\langle(c',r')|(c,r)\rangle_o)\,{}_o\langle(c,r)|\Phi\rangle = 0 \tag{3.97}$$

with

$$ {}_o\langle(c,r)|\Phi\rangle = \langle(c,r)|\hat{O}^{\frac{1}{2}}|\Psi\rangle \equiv w_c(r)r\ . $$

In the non-orthogonal channel basis, these CC equations become:

$$ \sum_c \int_0^\infty dr\, r^2\,\langle(c',r')|\hat{H}_{\rm m}|(c,r)\rangle\,\frac{w_c(r)}{r} = E\frac{w_{c'}(r')}{r'} \tag{3.98}$$

with

$$ {}_o\langle (c',r')|\hat{H}|(c,r)\rangle_o \equiv \langle (c',r')|\hat{H}_{\rm m}|(c,r)\rangle \ . $$

$\hat{H}_{\rm m}$ in (3.98) is the modified Hamiltonian: $\hat{H}_{\rm m} = \hat{O}^{-\frac{1}{2}}\hat{H}\hat{O}^{-\frac{1}{2}}$. In practice, the $\hat{O}^{-1/2}$ operator is calculated using the Moore-Penrose pseudoinverse method [234, 235].

In order to have a more precise treatment of antisymmetry in the calculation of matrix elements of $\hat{H}_{\rm m}$, we introduce a new operator $\hat{\Delta}$: $\hat{O}^{-\frac{1}{2}} = \hat{\Delta} + \hat{\mathbb{1}}$, which is associated with the part of $\hat{O}^{-\frac{1}{2}}$ acting on the low-energy channel states. Then, instead of calculating the matrix elements of $\hat{H}_{\rm m}$ directly, it is possible to calculate them as:

$$ \hat{H}_{\rm m} = (\hat{\Delta}+\hat{\mathbb{1}})H(\hat{\Delta}+\hat{\mathbb{1}}) = \hat{H} + \hat{H}\hat{\Delta} + \hat{\Delta}\hat{H} + \hat{\Delta}\hat{H}\hat{\Delta} \tag{3.99} $$

In this formulation, the non-antisymmetrized terms are taken into account exactly with the identity operator. Inserting Eq. (3.99) in CC equations (3.98), one obtains the CC equations for the reduced radial wave functions $w_c(r)/r$:

$$ \left(-\frac{\hbar^2}{2M_{\rm eff}}\left(\frac{\partial^2}{\partial r^2} - \frac{\ell(\ell+1)}{r^2}\right)\right. $$
$$ \left. + \quad V_c^{(\rm loc)}(r)\right)\frac{w_c(r)}{r} + \sum_{c'}\int_0^\infty dr'\, rr'^2 \frac{V_{c,c'}^{(\text{non-loc})}(r,r')}{rr'}\frac{w_{c'}(r')}{r'} = (E - E_T - E_{\rm int})\frac{w_c(r)}{r} \tag{3.100} $$

where $E_{\rm int}$ is the intrinsic energy of the projectile (it is zero in the case of a single-nucleon projectile) and the non-local potential $V_{c',c}^{(\text{non-loc})}(r',r)$ reads:

$$ \frac{1}{r'r}V_{c',c}^{(\text{non-loc})}(r',r) = \tilde{V}_{c',c}(r',r) + \langle r',c'|\hat{H}\hat{\Delta}|r,c\rangle + \langle r',c'|\hat{\Delta}\hat{H}|r,c\rangle + \langle r',c'|\hat{\Delta}\hat{H}\hat{\Delta}|r,c\rangle \ . \tag{3.101} $$

Note that we split the local and non-local part of $U_{\rm c.m.}(r,r')$ and $\tilde{V}_{cc'}(r,r')$ (see 3.81) into $V_c^{(\rm loc)}$ and $V_c^{(\text{non-loc})}$. The radial channel wave functions $u_c(r)/r$ are then obtained from solutions of Eq. (3.100) using the equation:

$$ \frac{u_c(r)}{r} = \frac{w_c(r)}{r} + \sum_{c'}\int_0^\infty dr'\, r'^2 \langle (c,r)|\hat{O}^{\frac{1}{2}}\hat{\Delta}\hat{O}^{\frac{1}{2}}|(c',r')\rangle \frac{w_{c'}(r')}{r'} \ . \tag{3.102} $$

3.3.2 Boundary conditions and basis functions

Boundary conditions for the radial wave functions at $r = 0$ are $w_c(r=0) = 0$ for all channels. For $r \to +\infty$, we have an outgoing wave behavior $w_c(r) = w_c^{(+)}(r)$ for all channels, except for the incoming channel where it is: $w_e(r) = w_e^{(+)}(r) + w_e^{(-)}(r)$. In our problem, the incoming part $w_e^{(-)}$ is fixed, and the outgoing parts $w_c^{(+)}(r)$ and $w_e^{(+)}(r)$ have to be determined. Due to the channel-channel couplings, the radial wave functions $w_c(r)$ for $r \sim 0$ are not always $w_c \sim r^{\ell+1}$, like in the GSM.

To solve this problem, radial wave functions $w_c(r)$ are expanded in the forward basis corresponding to the internal region ($0 \le r \le R$) where the nuclear part of the potential is not negligible,

and in the backward basis corresponding to the asymptotic region ($R \le r \le R_{\max}$) where the nuclear part of the potential can be neglected. The expansion of the CC equations in the forward basis is integrated from $r = 0$ to $r = R$, and the expansion in the backward basis is integrated from $r = R_{\max}$ to $r = R$. Contrary to the radial wave functions $w_c(r)$, these new basis states have the correct boundary conditions. Thus the CC equations can be integrated numerically in each region, with the matching condition at $r = R$.

The expansion is written in the forward basis for $0 \le r \le R$:

$$w_c(r) = \sum_b C_b^{(0)} w_{c,b}^{(0)}(r) \tag{3.103}$$

and in the backward basis for $R \le r \le R_{max}$:

$$w_c(r) = \sum_b C_b^{(+)} w_{c,b}^{(+)}(r) + w_e^{(-)}(r) \tag{3.104}$$

Eq. (3.103) stands for bound states, while Eq. (3.104) is general for scattering states and resonances. Note that for resonances we have: $w_e^{(-)}(r) = 0)$. For $c = b$, the forward basis at $r \sim 0$ is defined by: $w_{c,b}^{(0)}(r) \sim r^{\ell_b+1}$. Other channels ($c \neq b$) are ruled by: $w_{c,b}^{(0)}(r) = o(r^{\ell_b+1})$. The backward basis verifies for $c = b$:

$$w_{c,b}^{(+)}(r) \sim C_b^{(+)} H_{\ell_b}^{+}(\eta_b, k_b r) \tag{3.105}$$

and for other channels ($c \neq b$) :

$$w_{c,b}^{(0)}(r) = 0 \tag{3.106}$$

It should be stressed that in the region $r > R$, the solutions (3.105) and (3.106) are exact, because only the Coulomb+centrifugal interaction remains in this region. However, as the centrifugal potential is singular at $r = 0$, one cannot demand that channels with $c \neq b$ verifying $w_{c,b}^{(0)}(r) = o(r^{\ell_b+1})$ should be put to zero for $r \sim 0$, as it would be not precise numerically. It is therefore necessary to devise their behavior for $r \sim 0$.

For that, one writes the CC differential equations for a channel $c \neq b$ at $r \sim 0$:

$$[w_{c,b}^{(0)}]''(r) = \left(\frac{\ell_c(\ell_c+1)}{r^2} + a_c \right) w_{c,b}^{(0)}(r) + \sum_{c' \neq c} a_{c'} w_{c'}(r) + o(w_{c,b}^{(0)}(r)) \tag{3.107}$$

where $a_c = (2m/\hbar^2) V_{cc}^{(\mathrm{eq})}(0) - k^2$, and $a_{c'} = (2m/\hbar^2) V_{cc'}^{(\mathrm{eq})}(0)$. All terms inside the sum in this equation are $o(r^{\ell_b+1})$, except the one for which $c' = b$. One also has $w_{c,b}^{(0)}(r) = o(r^{\ell_b+1})$. Thus, the Eq. (3.107) becomes:

$$[w_{c,b}^{(0)}]''(r) = \frac{\ell_c(\ell_c+1)}{r^2} w_{c,b}^{(0)}(r) + a_b r^{\ell_b+1} + o(r^{\ell_b+1}) \tag{3.108}$$

It is then immediate to verify that for $c \neq b$:

$$w_{c,b}^{(0)}(r) \sim C_{b,bef}^{(0)} \frac{a_b}{(\ell_b+2)(\ell_b+3) - \ell_c(\ell_c+1)} r^{\ell_b+3} \quad , \quad \ell_c \neq \ell_b + 2 \tag{3.109}$$

$$w_{c,b}^{(0)}(r) \sim C_{b,bef}^{(0)} \frac{a_b}{2\ell_b+5} r^{\ell_b+3} \ln(r) \quad , \qquad \ell_c = \ell_b + 2 \, . \tag{3.110}$$

Note that $C_{b,bef}^{(0)}$ are the constants $C_b^{(0)}$ calculated during the previous iteration. It is necessary to use $C_{b,bef}^{(0)}$ and $C_{b,bef}^{(+)}$ in the asymptotic form of the channel components because the local equivalent equation used is inhomogeneous, *i.e.* the fact that $w(r)$ is a solution of the local CC Schrödinger equation does not imply that const $\times\, w(r)$ is a solution as well.

3.3.3 Components of the basis functions

Matching linear combinations of the two sets of basis wave functions (Eqs. (3.103), (3.104)) and their derivatives, at a given radius r_m, provides the full solution of the CC equations:

$$\sum_b \left[C_b^{(0)} w_{e,b}^{(0)}(r_m) - C_b^{(+)} w_{e,b}^{(+)}(r_m) \right] = w_e^{(-)}(r_m) \quad \text{(scattering)} \tag{3.111}$$

$$\sum_b \left[C_b^{(0)} \frac{dw_{e,b}^{(0)}}{dr}(r_m) - C_b^{(+)} \frac{dw_{e,b}^{(+)}}{dr}(r_m) \right] = \frac{dw_e^{(-)}}{dr}(r_m) \quad \text{(scattering)} \tag{3.112}$$

$$\sum_b \left[C_b^{(0)} w_{c,b}^{(0)}(r_m) - C_b^{(+)} w_{c,b}^{(+)}(r_m) \right] = 0 \quad \text{(all other cases)} \tag{3.113}$$

$$\sum_b \left[C_b^{(0)} \frac{dw_{c,b}^{(0)}}{dr}(r_m) - C_b^{(+)} \frac{dw_{c,b}^{(+)}}{dr}(r_m) \right] = 0 \quad \text{(all other cases)} \tag{3.114}$$

For scattering states, $c = c_0$ in Eqs. (3.111), (3.112), and $c \neq c_0$ in Eqs. (3.113), (3.114). For bound states and resonances, one should use Eqs. (3.113), (3.114) for all cases.
In Eq.(3.111), $w_{e,b}^{(-)}(r) = C_{c_0}^{(-)} H_{\ell_{c_0}}^{-}(\eta_{c_0}, k_{c_0} r)$ for $r > R$, with $C_{c_0}^{(-)} = 0$ for bound states and resonances, and $C_{c_0}^{(-)} \cdot C_{c_0,bef}^{(+)} = 1/2\pi$ for scattering states (see Appendix A.4).

For scattering states, Eqs. (3.111)-(3.114) form a linear system of equations: $AX = B$, which is immediate to solve. For bound states and resonances (Eqs. (3.113), (3.114)), $AX = 0$ as there is no incoming channel. In this case, one has to have $\det A = 0$, and $\det A$ can be considered as a generalization of Jost function for the CC equations. The constants $C_b^{(0)}, C_b^{(+)}$ are given by the eigenvector of zero eigenvalue.

3.3.4 Method of the modified equivalent potential

The CC equations are systems of coupled differential equations function of a single variable r. Using the equivalent potential method, one can include the integro-differential equations in the same class of systems. For this, we define the matrix differential equation:

$$W''(r) = M^{(\mathrm{eq})}(r) W(r) + S^{(\mathrm{eq})}(r) \,, \tag{3.115}$$

where $W(r)$ is a vector where each component is a w_c. Then $M_{cc'}^{(eq)}(r)$ is equal to:

$$M_{cc'}^{(\mathrm{eq})}(r) = (2m/\hbar^2) V_{cc'}^{(\mathrm{eq})}(r) + \left(\frac{\ell_c(\ell_c+1)}{r^2} - k^2 \right) \delta_{cc'} \,, \tag{3.116}$$

and $S_c^{(\mathrm{eq})}(r)$ is the residual source coming from the equivalent potential method. One has then for Eq. (3.100):

$$\begin{aligned} V_{cc'}^{(\mathrm{eq})}(r) &= V_{cc'}^{(\mathrm{loc})}(r) + \frac{(1 - F_{c'}(r)) \int_0^{+\infty} V_{cc'}^{(\mathrm{non-loc})}(r, r') w_{c'}(r') \, dr'}{w_{c'}(r)} \\ S_c^{(\mathrm{eq})}(r) &= \sum_{c'} F_{c'}(r) \int_0^{+\infty} V_{cc'}^{(\mathrm{non-loc})}(r, r') w_{c'}(r') \, dr' \end{aligned} \tag{3.117}$$

where $F_{c'}(r)$ is a function removing the singularities due to the zeros of $w_{c'}(r)$.

3.3.5 Green's function representation of the CC equation

The methods presented in previous sections are iterative and hence can present instabilities if the channel-channel coupling is too strong. In this case, it is preferable to use the Green's function method to obtain the scattering solution of Eq. (3.100).

We start from the A-body scattering state $|\Psi^{J_A}_{M_A}\rangle$, of energy E, which is the solution of the Schrödinger equation:

$$\hat{H}\,|\Psi^{J_A}_{M_A}\rangle = E\,|\Psi^{J_A}_{M_A}\rangle \tag{3.118}$$

The A-body scattering state is decomposed in a channel basis as:

$$|\Psi^{J_A}_{M_A}\rangle = \sum_c \int_0^\infty \frac{u_c(r)}{r} r^2\,|(c,r)\rangle\,dr \tag{3.119}$$

Here, $u_c(r)$ is the radial wave function associated with the channel c. Note that the radial distance r stands for either the distance between the projectile and the target.

In order to see the appearance of the resolvent, we introduce an approximate Hamiltonian $\hat{H}^{(0)}$ and its eigenvector $|\Psi^{(0)}\rangle$:

$$\begin{aligned} \hat{H}^{(0)} &= \hat{t} + \hat{U}_{\text{basis}} \qquad \text{(nucleon)} \\ &= \hat{T}_{\text{CM}} + \hat{U}_{\text{CM}} \qquad \text{(cluster)} \end{aligned} \tag{3.120}$$

$$\hat{H}^{(0)}\,|\Psi^{(0)}\rangle = E\,|\Psi^{(0)}\rangle \tag{3.121}$$

$\hat{H}^{(0)}$ is the matrix with all non-diagonal elements equal to zero, and one non-zero diagonal element for the entrance channel (only c_0 is activated). Eq. (3.121) is straightforward to solve as $\hat{H}^{(0)}$ leads to a one-dimensional differential equation.

Let us separate $\hat{H}$ and $|\Psi^{J_A}_{M_A}\rangle$ in two parts involving $\hat{H}^{(0)}$ and $|\Psi^{(0)}\rangle$, and a remaining part:

$$\hat{H} = \hat{H}^{(0)} + \hat{H}_{\text{rest}} \tag{3.122}$$

$$|\Psi^{J_A}_{M_A}\rangle = |\Psi^{(0)}\rangle + |\Psi_{\text{rest}}\rangle \tag{3.123}$$

Using Eqs. (3.118), (3.121), (3.122), and (3.123), one obtains:

$$(\hat{H} - E)\,|\Psi_{\text{rest}}\rangle = |S\rangle \tag{3.124}$$

$$|S\rangle = -\hat{H}_{\text{rest}}\,|\Psi^{(0)}\rangle \tag{3.125}$$

where the source term $|S\rangle$ has been introduced. One can see from (3.125), that if $\hat{H}_{\text{rest}}$ is of finite range, then $S(r) \to 0$ when $r \to +\infty$. Hence, $|S\rangle$ can be expanded in the Berggren basis generated by $\hat{H}^{(0)}$, so that Eq. (3.124) becomes a linear system in this representation:

$$M_E \Psi_{\text{rest}} = S \tag{3.126}$$

where

$$(\Psi_{\text{rest}})_{n,c} = \langle n,c|\Psi_{\text{rest}}\rangle \tag{3.127}$$

$$(M_E)_{n,c\;n',c'} = \langle n',c'|\hat{H} - E|n,c\rangle \tag{3.128}$$

$$(S)_{n,c} = \langle n,c|S\rangle \tag{3.129}$$

and $|n,c\rangle$ is a Berggren basis state of index n in the channel c.

Similarly to the Lippman-Schwinger equation, the fundamental problem of Eq. (3.126) is the non-invertible character of M_E on the real-energy axis. The standard remedy is to replace E by $E+i\epsilon$, with $\epsilon \to 0^+$. In this way, the linear system of equations (3.126) becomes invertible, and an outgoing asymptotic of $u_c(r)$ in all outgoing channels is imposed.

This method becomes unstable for small ϵ. To circumvent this problem, the contour defining $|n,c\rangle$ Berggren basis states is chosen so that the energy of basis states has always a non-zero imaginary part. Consequently, M_E is invertible along this contour, and Eq.(3.126) is numerically solvable. The outgoing wave character of $|\Psi_{\rm rest}\rangle$ in all channels is guaranteed by the finite norm of $|\Psi_{\rm rest}\rangle$ in the Berggren basis representation. Indeed, as $\||\Psi_{\rm rest}\|$ is finite, we have $\Psi_{\rm rest}(z) \to 0$ if $z \to +\infty$, where $z = r + (R-r)e^{i\theta}$, R is a radius outside of the range of nuclear interaction, and angle θ $(0 < \theta < \pi/2)$ is properly chosen. Once $|\Psi_{\rm rest}\rangle$ is calculated in the Berggren basis, its calculation in the coordinate space becomes straightforward. It has been checked numerically that if the equivalent potential method is numerically stable, then both the Green's function method and the direct integration method provide the same solution $|\Psi^{J_A}_{M_A}\rangle$.

The Berggren basis is also useful to determine bound states and resonances of the CC Hamiltonian $\hat{H}$, in which case the CC problem becomes the matrix diagonalization problem. The application of the Berggren basis for solving the Faddeev equation is discussed in the Appendix A.5.

3.4 Applications of the GSM-CC to nuclear reactions

In this section, we will present some applications of the GSM-CC formalism. In Secs. 3.4.1 and 3.4.2, we will comment on practical aspects of the nuclear reaction calculation. In particular, Sec. 3.4.2.3 is devoted to a study of the importance of deuteron and non-resonant reaction channels for the completeness of the channel basis in GSM-CC calculation of ^{42}Sc. In the following section (Sec. 3.4.3), we will discuss the ^{14}O(p,p')^{14}O reaction and the structure of ^{15}F.

3.4.1 Practical issues involved in GSM-CC calculations

The GSM-CC calculation requires a rigorous approach to produce relevant results. The A-body state of a nucleus in GSM-CC calculation is built using the basis of channel states which includes information about target and projectile nuclei. In the applications presented in this manuscript, we consider one-nucleon projectile (proton or neutron). The computer code for deuteron induced reactions projectile is in progress.

Target states are described in GSM, using different approximations for continuum states. In a typical calculation, we have to define: (i) the core and the valence space in target nucleus, (ii) the truncations, (iii) the mean-field potential and (iv) the residual two-body interaction. The choice of the core fixes the number of active nucleons, *i.e.* the number and the nature of nucleons in the valence shells.

S.p. states in valence space are either harmonic oscillator or Gamow states. In the harmonic oscillator space, one works with the real-energy continuum which is discretized by a finite number of harmonic oscillator states. In this case, one has to fix both the maximum angular momentum $\ell_{\rm max}$ and the maximum energy $n_{\rm max}\,\hbar\omega$, where $n_{\rm max}$ is a positive integer number. For each (ℓ, j) state, the highest oscillator shell $N_{\rm max}$ considered is fixed by the relation: $2N_{\rm max} + \ell = n_{\rm max}$.

Working with the Berggren ensemble, one has to define first the pole states, *i.e.* the s.p. bound states and/or resonances. Decaying resonances lie in the fourth quarter of the complex k-plane and satisfy: $\mathcal{R}(k) > |\mathcal{I}(k)|$. In order to ensure the completeness of the Berggren ensemble, one should include non-resonant states from the contour in k-plane which encompasses resonances included in the valence space. In practice, one performs a partial wave decomposition of the continuum, and choose different complex contour for each (ℓ, j) state. Cauchy theorem guarantees that results of the Berggren basis calculation are independent of the chosen contour if the number of (ℓ, j)-resonances inside of the contour remains the same. Similarly as in the harmonic oscillator calculation, one should choose the maximum angular momentum ($\ell_{\max}$) and the maximum energy or momentum ($k_{\max}$) of s.p. states in the continuum.

Valence shells are defined by s.p. states of the average potential generated by the core and acting on the valence nucleons. This potential can be described either by an infinite depth harmonic oscillator potential:

$$U_{\mathrm{HO}}(r) = \frac{1}{2} M_{\mathrm{core}} \omega^2 r^2$$

or by a finite-depth potential, like the Woods-Saxon potential:

$$U_{\mathrm{WS}}(r) = -V_0 \left[1 + \exp\left(\frac{r - R_0}{a} \right) \right]^{-1}$$

or the Hartree-Fock potential. In the harmonic oscillator potential, M_{core} is the mass of the core and ω is the oscillator frequency. They are put together in the oscillator length parameter: $b = \sqrt{\hbar/(M_{\mathrm{core}}\omega)}$, with a standard value $b \simeq 1.01 A^{1/6}$ fm [236, 237]. Concerning the Woods-Saxon potential, V_0 is the depth, R_0 is the radius, and a is the diffuseness of the potential with a standard value $a \sim 0.67$ fm [236, 237]. Parameters R_0 and V_0 are chosen according to the size of the core: $R_0 = r_0 A^{1/3}$, $V_0 = (51 \pm 33(N - Z)/A)$ MeV, where $r_0 \simeq 1.25 - 1.27$ fm [236, 237]. These formulae provide useful initial values for the optimization of an average potential in each studied case.

In the study of nucleus $A = A_{\mathrm{core}} + A_v$, where A_{core} and A_v are the number of nucleons in the core and valence shells, the first step is to determine the average potential which fits binding energy and excited states in a nucleus $A_{\mathrm{core}} + 1$. In general, we have different average potentials for protons and neutrons, but also for each angular momentum ℓ. The ℓ-dependence can be justified by the non-locality of the nuclear potential.

In the next step, we go to $A_{\mathrm{core}} + 2$ nucleus to fix parameters of the two-body interaction which allows to describe binding energy and spectrum of excited states in this nucleus. These can be readjusted again at a later stage to find the best compromise between the description of nuclei $A_{\mathrm{core}} + 2$ and $A_{\mathrm{core}} + A_v$.

In the calculation of nuclei with $A \geq A_{\mathrm{core}} + 2$, we have to choose the truncation scheme in the space of Slater determinants. In practice, this space is limited by two kinds of truncations: (i) the energy truncation in the s.p. space, and (ii) the limitation of the number of particles excited from the pole space into the non-resonant continuum. The latter truncation is crucial in GSM-CC studies of medium mass and heavy nuclei with the large number of valence nucleons.

GSM can be useful to adjust parameters of the GSM-CC Hamiltonian. The first step consists of fixing the many-body pole states in GSM-CC, *i.e.* many-body bound states and resonances of the composite system of projectile and target (see the discussion at the end of Sec. 3.3.5). In general, the calculation of many-body pole states requires less numerical resources than the complete calculation of the cross section. Moreover, these states are useful to determine important reaction

channels, or estimate the role of the non-resonant channels which are built using scattering states of the target. In some applications, these non-resonant channels are not included to simplify the GSM-CC calculation. Then the correction factors are determined to rescale the two-body part of channel-channel coupling potentials and in this way compensate for missing non-resonant channels. These correction factors ensure that the GSM-CC and GSM spectra of many-body pole states are the same.

One could think that once the relevant reaction channels are identified and the channel-channel coupling potentials are rescaled, if necessary, then the calculation of the reaction cross sections is straightforward. Unfortunately, in the partial wave decomposition of the projectile wave function it might happen that for certain values of ℓ, the associated average potentials are not constrained by the pole states of the composite system. Nevertheless, these partial waves play a role in the partial wave decomposition of the projectile and thus in the reaction cross section calculation. In this weakly constrained problem, the GSM-CC calculation of cross sections or phase shifts for smaller systems, like the nucleon scattering on $(A_{\rm core})$- or the $(A_{\rm core}+1)$-nucleus, can be useful to adjust those unconstrained parameters of the average potential. In this way, one may obtain better average potentials for the description of reactions involving the $(A_{\rm core}+A_v)$ system. We will return to this discussion in Sec. 3.4.2.

3.4.2 Tests of the GSM-CC approach with deuteron and non-resonant reaction channels

In this section, we present various tests of the GSM-CC approach on the examples of the elastic scattering reactions ^{40}Ca(p,p), ^{40}Ca(n,n), the neutron transfer reaction ^{40}Ca(d,p)^{41}Ca, and the spectrum of ^{42}Sc. The role of non-resonant reaction channels, built by the scattering states of target nucleus, on the spectroscopy of bound and resonance states will be discussed by comparing the spectrum of GSM-CC pole states with the GSM spectrum for ^{42}Sc.

3.4.2.1 Parameters of one-body potentials and two-body interaction

To illustrate certain aspects of the GSM-CC approach, we present in this section an example of GSM-CC calculations for systems with one and two nucleons outside of the core of ^{40}Ca . The ^{42}Sc is studied in the basis of reaction channels consisting of ^{40}Ca+d and ^{41}Ca+p, and ^{41}Sc+n. GSM is used to construct target states (3.56) and fix one- and two-body terms of the Hamiltonian. Here, we consider a core of ^{40}Ca with a valence space defined in either a harmonic oscillator basis or a Berggren basis. The harmonic oscillator basis is limited by a maximum energy of $12\hbar\omega$ what implies: $2n+\ell \leq 12$. This means that we have 7 shells for $\ell=0$, 6 shells for $\ell=1$ and $\ell=2$, and 5 shells for $\ell=3$ and $\ell=4$.

The target nucleus (^{40}Ca) is considered as an inert core in a 0^+ state. Low-lying states of ^{41}Ca (^{41}Sc) are described using the Woods-Saxon potential as one neutron (proton) outside of the ^{40}Ca core. Parameters of the potentials for $\ell=1$ and $\ell=3$ are adjusted to reproduce experimental energy of $7/2^-_1$, $3/2^-_1$, $5/2^-_1$ and $1/2^-_1$ states in ^{41}Ca and ^{41}Sc. These states are considered as s.p. states, and their energies determine the position of subshells $0f_{7/2}$, $1p_{1/2}$, $0f_{5/2}$, and $1p_{1/2}$ in the GSM calculation. In the Berggren basis, we consider non-resonant continuum states on a complex-energy contour for each of these real or complex-energy s.p. pole states. In addition, we include complex-energy continua for $s_{1/2}$, $d_{3/2}$, $d_{5/2}$, $g_{7/2}$, and $g_{9/2}$. Each contour is discretized with 21 points, *i.e.* the Berggren basis contains 193 s.p. states which become shells in the multiparticle

calculations. All s.p. continuum states along the chosen contours have a complex energy (see Tab. 3.1) in order to avoid singularities in a calculation of the resolvent in the Green's function method (see the discussion at the end of Sec. 3.3.5).

GSM calculation of the spectrum of ^{42}Sc determines parameters of the two-body FHT interaction [238]. In this calculation we use the Woods-Saxon potential which is adjusted in ^{41}Ca and ^{41}Sc for $\ell = 1$ and $\ell = 3$.

Woods-Saxon potentials for $\ell = 0, 2, 4$ are adjusted using the GSM-CC approach. These ℓ-waves contribute to the reaction cross-sections but are not unambiguously determined by the spectra of ^{41}Ca and ^{41}Sc. Woods-Saxon potentials for $\ell = 0, 2, 4$ are obtained by fitting elastic scattering cross sections for ^{40}Ca(p,p)^{40}Ca and ^{40}Ca(n,n)^{40}Ca reactions calculated in GSM-CC.

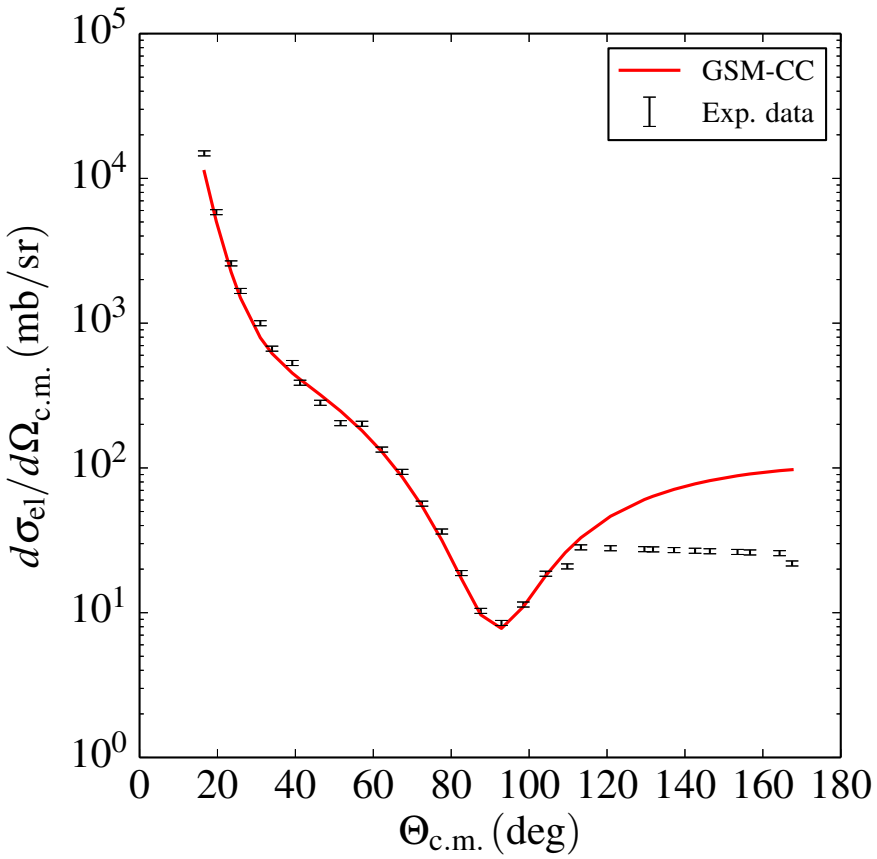

Figure 3.1 – Differential cross section for the reaction ^{40}Ca(p,p)^{40}Ca at 9.61 MeV in the c.m. [239].

The cross sections for ^{40}Ca(p,p)^{40}Ca and ^{40}Ca(n,n)^{40}Ca reactions are presented in Figs. 3.1 and 3.2. The projectile (proton or neutron) is described by partial waves ℓ in the range from 0 to 4. One can see that GSM-CC with fitted Woods-Saxon average potentials fails to reproduce the data at backward angles $\Theta_{c.m.} \geq 120°$. This suggests the deficiency of a simple structure assumed for ^{40}Ca and low-lying states in ^{41}Ca and ^{41}Sc.

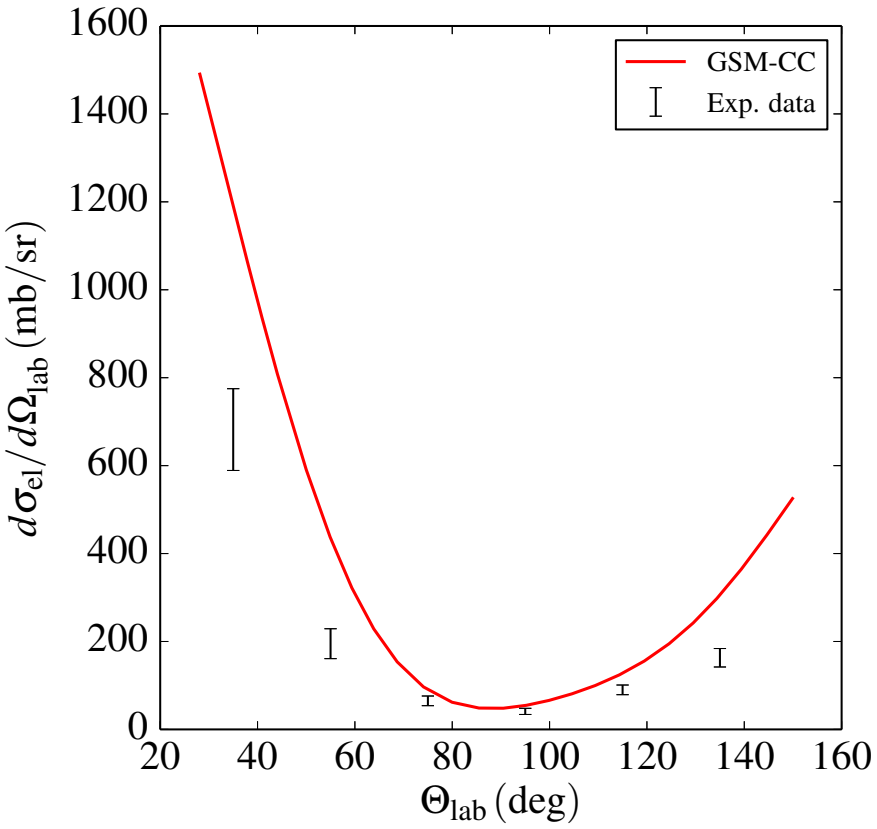

Figure 3.2 – Differential cross section for the reaction ^{40}Ca(n,n)^{40}Ca at 2.69 MeV in the c.m. [240].

3.4.2.2 GSM-CC calculation of the pole states in different approximations for ^{41}Ca, ^{41}Sc, and ^{42}Sc

Calculation of the pole states provides a test of the GSM-CC computational scheme. It consists of diagonalizing the Hamiltonian (3.69) in a basis of the channel states $|(c,n)\rangle$ (3.28). As a test, let us compare the two diagonalization schemes:
(i) the diagonalization where the c.m. part of the projectile $|n,\ell\rangle$ (see Sec.3.2.2) is described with the same basis (*e.g.* the harmonic oscillator basis) as the one used in GSM for the calculation of target states: $|(c,n_{\rm GSM}\rangle$, and
(ii) the diagonalization where the c.m. part of the projectile $|n,\ell\rangle$ is described in Berggren basis and used in the Green's function method (see Sec. 3.3.5).

The GSM space used for $|(c,n_{\rm GSM})\rangle$ is defined by a maximal energy of 12 $\hbar\omega$ (see the discussion above), while the Berggren basis used for $|(c,n_{\rm GF})\rangle$ is defined in Tab. 3.1 for neutron and proton projectiles. The comparison between these two diagonalizations is presented in Tab. 3.2 for ^{41}Sc.

GSM space in Tab. 3.2 is the harmonic oscillator space (GSM – HO) with non-resonant channels described in the harmonic oscillator approximation. One can see an excellent agreement between results of the GSM-CC diagonalization in the space of channels $|(c,n_{\rm GSM})\rangle$ and the GSM diagonalization in the space of Slater determinants. This proves the equivalence of these two formulations in the same model space. A small discrepancy between the two GSM-CC diagonalizations is due to the difference between the harmonic oscillator basis (HO), and the Berggren

States	k_0 (fm^{-1})	k_1 (fm^{-1})	k_2 (fm^{-1})	k_3 (fm^{-1})
$0f_{7/2}$	-	-	-	-
$1p_{1/2}$	-	-	-	-
$0f_{5/2}$	-	-	-	-
$1p_{3/2}$	-	-	-	-
$s_{1/2}$	0.0	(0.5,-0.05)	(1.0,-0.05)	2.0
$p_{3/2}$	0.0	(0.5,-0.05)	(1.0,-0.05)	2.0
$p_{1/2}$	0.0	(0.5,-0.05)	(1.0,-0.05)	2.0
$d_{5/2}$	0.0	(0.5,-0.05)	(1.0,-0.05)	2.0
$d_{3/2}$	0.0	(0.5,-0.05)	(1.0,-0.05)	2.0
$f_{7/2}$	0.0	(0.5,-0.05)	(1.0,-0.05)	2.0
$f_{5/2}$	0.0	(0.5,-0.05)	(1.0,-0.05)	2.0
$g_{9/2}$	0.0	(0.5,-0.05)	(1.0,-0.05)	2.0
$g_{7/2}$	0.0	(0.5,-0.05)	(1.0,-0.05)	2.0

Table 3.1 – Berggren basis of the c.m. state $|n,\ell\rangle$ for the neutron/proton projectile. All pole states which are not presented here, are contained in the core. For each segment of the contour, we consider 7 scattering states.

State	^{41}Sc (GSM-HO)	^{41}Sc (GSM-CC) (HO)	^{41}Sc (GSM-CC) (GF)
$7/2^-$	-1.085	-1.085	-1.099
$3/2^-$	0.632	0.632	0.513
$5/2^-$	1.503	1.503	1.471
$1/2^-$	2.380	2.380	2.090

Table 3.2 – Spectrum of ^{41}Sc calculated in GSM and GSM-CC in different approximations. GSM-CC (HO) denotes the calculation in the harmonic oscillator space including the non-resonant channels. GSM-CC (GF) is the calculation in Berggren basis using the Green's function method. GSM calculation is performed in the harmonic oscillator space with the non-resonant continuum described in the harmonic oscillator approximation. All energies are given with respect to the ^{40}Ca core. For more details, see the text.

basis (GF), namely: (i) the scattering wave functions are different, (ii) the number of continuum states is different, (iii) and the truncation in those bases is different. Note that the Berggren basis used in GSM-CC (GF) (see Tab. 3.1) includes the complex contour. Such a contour is necessary to perform numerically stable Green's function method calculation which avoids the singularities in the resolvent operator (3.128).

In Tab. 3.3 we present the same calculations as in Tab. 3.2 but using the Berggren space for GSM (GSM-B) calculations. This Berggren basis is defined in Tab. 3.1. Here the agreement between the two GSM-CC calculations is excellent. Again, if the same s.p. basis is used in GSM and GSM-CC (GF), one finds identical pole states. This provides a stringent test of the GSM-CC solution using the Green's function method. This method will be used later to calculate reaction cross-sections.

In Tab. 3.4 we present a comparison between the two GSM-CC diagonalizations and the GSM calculation for ^{42}Sc. The GSM space is the harmonic oscillator space (GSM – HO) with

State	^{41}Sc (GSM-B)	^{41}Sc (GSM-CC) (GSM)	^{41}Sc (GSM-CC) (GF)
$7/2^-$	-1.085	-1.085	-1.085
$3/2^-$	0.632	0.633	0.629
$5/2^-$	1.503	1.503	1.502
$1/2^-$	2.380	2.380	2.384

Table 3.3 – The same as in Tab. 3.2 but in the Berggren basis. For more details, see the caption of Tab. 3.2 and text.

State	^{42}Sc (GSM-HO)	^{42}Sc (GSM-CC) (HO)	^{42}Sc (GSM-CC) (GF)
0^+	-12.632	-12.089	-12.112
1^+	-12.172	-11.626	-11.657
7^+	-11.789	-11.669	-11.693
3^+	-11.122	-10.836	-10.870
5^+	-11.044	-10.832	-10.864
2^+	-10.999	-10.740	-10.772

Table 3.4 – Spectrum of ^{42}Sc calculated in GSM and GSM-CC in different approximations. All energies are given with respect to the ^{40}Ca core. For more details, see the text.

non-resonant configurations included in the harmonic oscillator approximation. The GSM-CC solution using the Green's functions method (GSM-CC (GF)) is performed in the Berggren basis $|(c, n_{\rm GF})\rangle$ given in Tab. 3.1. Only channels with one-nucleon projectiles: ^{41}Sc+n and ^{41}Ca+p, are included in this calculation. The channels of ^{42}Sc are built using $7/2^-_1$ bound state, $3/2^-_1$, $5/2^-_1$, $1/2^-_1$ resonances, and non-resonant continua: $\{9/2^+_1\}$, $\{1/2^+_1\}$, $\{5/2^+_1\}$, $\{3/2^+_1\}$, $\{7/2^+_1\}$, $\{3/2^-_1\}$, $\{1/2^-_1\}$, $\{7/2^-_1\}$, and $\{5/2^-_1\}$ in ^{41}Ca, and $7/2^-_1$, $3/2^-_1$, $5/2^-_1$, $1/2^-_1$ bound states and non-resonant continua: $\{9/2^+_1\}$, $\{1/2^+_1\}$, $\{5/2^+_1\}$, $\{3/2^+_1\}$, $\{7/2^+_1\}$, $\{3/2^-_1\}$, $\{1/2^-_1\}$, $\{7/2^-_1\}$, and $\{5/2^-_1\}$ in ^{41}Sc. One can see that the difference between the two GSM-CC calculations is of the order of ~100 keV. This amounts to different s.p. bases, as discussed in Tab. 3.2 and 3.3.

One can also notice a more important difference between the GSM calculation and both the GSM-CC diagonalization in the harmonic oscillator space $|(c, n_{\rm GSM})\rangle$ (GSM-CC (HO)), and the GSM-CC diagonalization in the Berggren space $|(c, n_{\rm GF})\rangle$ (GSM-CC (GF)). This is due to the orthogonalization procedure between many-body channels involved in the description of ^{42}Sc in GSM-CC. Indeed, among all considered reaction channels, there are many redundancies because the same configurations of ^{42}Sc can be generated either by ^{41}Sc+n channels or by ^{41}Ca+p channels. The redundant channels have a nonzero overlap with other channels, but their norm is close to 1. This means that each redundant channel contains a small physical component which is orthogonal to all other channels.

Redundant channels generate numerical instabilities in the Moore-Penrose pseudo-inverse procedure which is used to invert the overlap matrix $\hat{O}$ (see Sec. 3.3.1). To avoid this problem, one could simply remove redundant channels, but this brute force cancellation of small physical components contained in redundant channels would break slightly the completeness of the channel basis and, therefore, would lead to numerical imprecisions. These imprecisions generate differences between the GSM and GSM-CC calculations (see Tab. 3.4).

Redundant channels can be a serious problem for nuclei like ^{42}Sc which are described in a small

s.p. basis and where all states can be generated doubly, either in ^{41}Sc+n or ^{41}Ca+p channels. Fortunately, the spurious effects of redundant channels can be kept under control in most applications by a suitable choice of the model space, they can be kept under control. Their importance can be quantified by making a comparison with the GSM results in the same model space. In the following section, we will discuss the GSM-CC reaction calculation for ^{14}O (p,p) ^{14}O, which is almost free from the spurious effects of the redundant channels.

One should stress that the possibility to compare the GSM eigenvalues with those obtained by diagonalizing the GSM-CC Hamiltonian matrix in the space of channels $|(c,n)\rangle$, gives a control of the numerical precision of GSM-CC reaction calculations, in what concerns the role of both the non-resonant channels and the redundant channels.

3.4.2.3 Deuteron and non-resonant channels in the GSM-CC description of ^{42}Sc

At present, we continue the study of ^{42}Sc by including reaction channels with deuteron projectile and the non-resonant reaction channels. The intrinsic part of the deuteron is a 1^+ state which is calculated in a NCSM formalism using N^{3}LO chiral interaction [241]. The c.m. part of the deuteron which is calculated in Berggren basis with $\ell_{max} = 2$, is defined in Tab. 3.5.

L	$(2S+1)LJ$	pole	scattering	k_0 (fm^{-1})	k_1 (fm^{-1})	k_2 (fm^{-1})	k_3 (fm^{-1})
0	$3S1$	5	30	0.0	(0.2,-0.1)	(1.0,-0.1)	2.0
	$3P0$	4	30	0.0	(0.2,-0.1)	(1.0,-0.1)	2.0
1	$3P1$	4	30	0.0	(0.2,-0.1)	(1.0,-0.1)	2.0
	$3P2$	4	30	0.0	(0.2,-0.1)	(1.0,-0.1)	2.0
	$3D1$	3	30	0.0	(0.2,-0.1)	(1.0,-0.1)	2.0
2	$3D2$	3	30	0.0	(0.2,-0.1)	(1.0,-0.1)	2.0
	$3D3$	3	30	0.0	(0.2,-0.1)	(1.0,-0.1)	2.0

Table 3.5 – Berggren basis describing the c.m. part of the deuteron wave function. The columns "pole" and "scattering" give the number of pole and scattering states, respectively. Here S is the spin of the deuteron, L its angular momentum and $\vec{J} = \vec{L} + \vec{S}$. In the following three columns, we present the complex contour of the Berggren basis for each state.

State	^{42}Sc (GSM-HO)	^{42}Sc (GSM-CC) (HO)	^{42}Sc (GSM-CC) (GF)
0^+	-12.632	-12.088	-12.095
1^+	-12.172	-11.891	-11.966
7^+	-11.789	-11.670	-11.740
3^+	-11.122	-10.973	-11.229
5^+	-11.044	-10.890	-10.969
2^+	-10.999	-10.740	-10.758

Table 3.6 – Spectrum of ^{42}Sc calculated in GSM and GSM-CC in different approximations. As compared to results shown in Tab. 3.4, the deuteron projectile channels have been added.

In Tab. 3.6 we present a comparison between the GSM and GSM-CC spectra of ^{42}Sc. The GSM-CC calculations include deuteron projectile channels. Inclusion of these channels improves the description of ^{42}Sc for 1^+_1 and 3^+_1 states. However, a significant difference between GSM and

GSM-CC remains, *i.e.* significant correlations are still missing in the GSM-CC wave function for discrete states of ^{42}Sc.

State	^{42}Sc (GSM-HO)	^{42}Sc (GSM-CC) (HO)	^{42}Sc (GSM-CC) (GF)
0^+	-12.632	-12.580	-12.549
1^+	-12.172	-12.134	-12.091
7^+	-11.789	-11.788	-11.873
3^+	-11.122	-11.121	-11.42
5^+	-11.044	-10.998	-11.089
2^+	-10.999	-11.043	-11.084

Table 3.7 – Spectrum of ^{42}Sc calculated in GSM and GSM-CC in different approximations. As compared to results shown in Tab. 3.4, the deuteron projectile channels and the non-resonant channels have been included.

The role of non-resonant channels can be seen in Tab. 3.7. Tab. 3.8 we present the non-resonant channels used for ^{41}Ca and ^{41}Sc.

J^π	Nb of scattering states
$7/2^-$	4
$3/2^-$	4
$5/2^-$	4
$1/2^-$	4
$1/2^+$	5
$3/2^+$	5
$5/2^+$	5
$7/2^+$	5
$9/2^+$	5

Table 3.8 – Non-resonant scattering states of ^{41}Ca and ^{41}Sc which are used to build the non-resonant channels in ^{42}Sc.

One can see that taking non-resonant channels into the basis improves significantly the spectrum of ^{42}Sc. One may expect that the non-resonant channels are also indispensable for a comprehensive analysis of the reaction cross sections involving the ^{42}Sc in the intermediate state. Fig. 3.3 compares GSM results with those of the GSM-CC approach which are obtained with (GSM-CC(NRC)) or without (GSM-CC) non-resonant channels. No correction factors have been used in this calculation to compensate for missing reaction channels, *i.e.* the absence of non-resonant channels in the channel basis is a principal reason of the discrepancy between GSM and GSM-CC results.

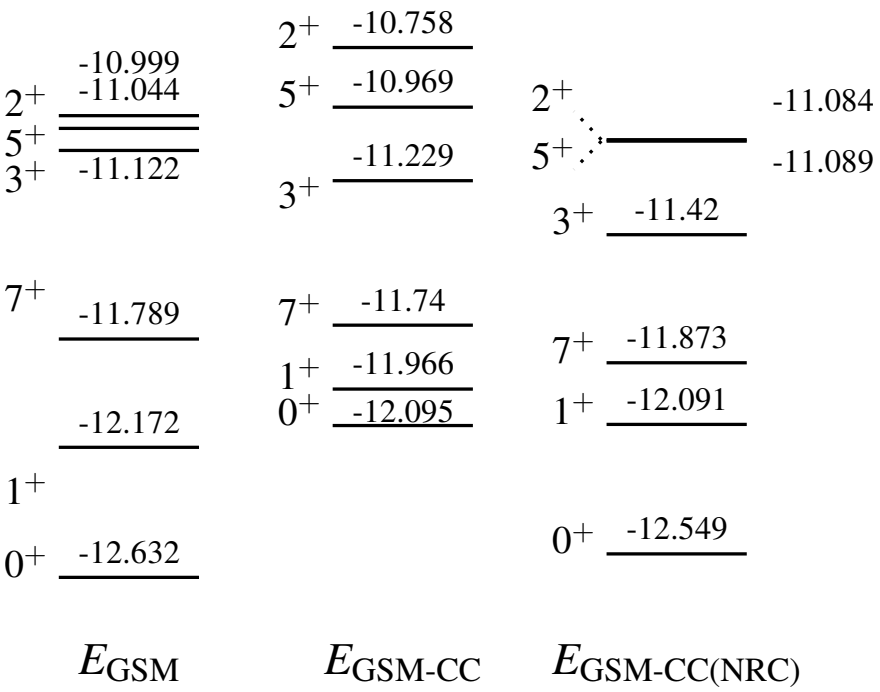

Figure 3.3 – Spectrum of ^{42}Sc calculated in GSM and in GSM-CC without the non-resonant channels (GSM-CC) and with the non-resonants channels (GSM-CC(NRC)).

3.4.2.4 Neutron transfer reaction ^{40}Ca(d,p)^{41}Ca$_{\text{g.s.}}$

Fig. 3.4 presents the GSM-CC calculation of the neutron transfer differential cross section for the reaction ^{40}Ca(d,p)^{41}Ca$_{\text{g.s.}}$ with the deuteron projectile. The one-body Woods-Saxon potential for $\ell = 0, 2, 4$ has been adjusted to describe ^{40}Ca(p,p)^{40}Ca, ^{40}Ca(n,n)^{40}Ca, and ^{40}Ca(d,p)^{41}Ca differential cross-sections. In this exploratory GSM-CC calculation of the transfer reaction, we do not include non-resonant channels to describe the spectrum of ^{42}Sc. Consequently, we apply small corrective factors in the channel-channel coupling potentials which are: 1.05, 1.1, and 0.965, for 1^+, 2^+, and 3^+ states of ^{42}Sc, respectively. One can see that the GSM-CC approach describes satisfactorily the experimental neutron transfer differential cross section ^{40}Ca(d,p)^{41}Ca$_{\text{g.s.}}$. Small deviations with respect to the experimental data [242] are seen at most forward and backward angles.

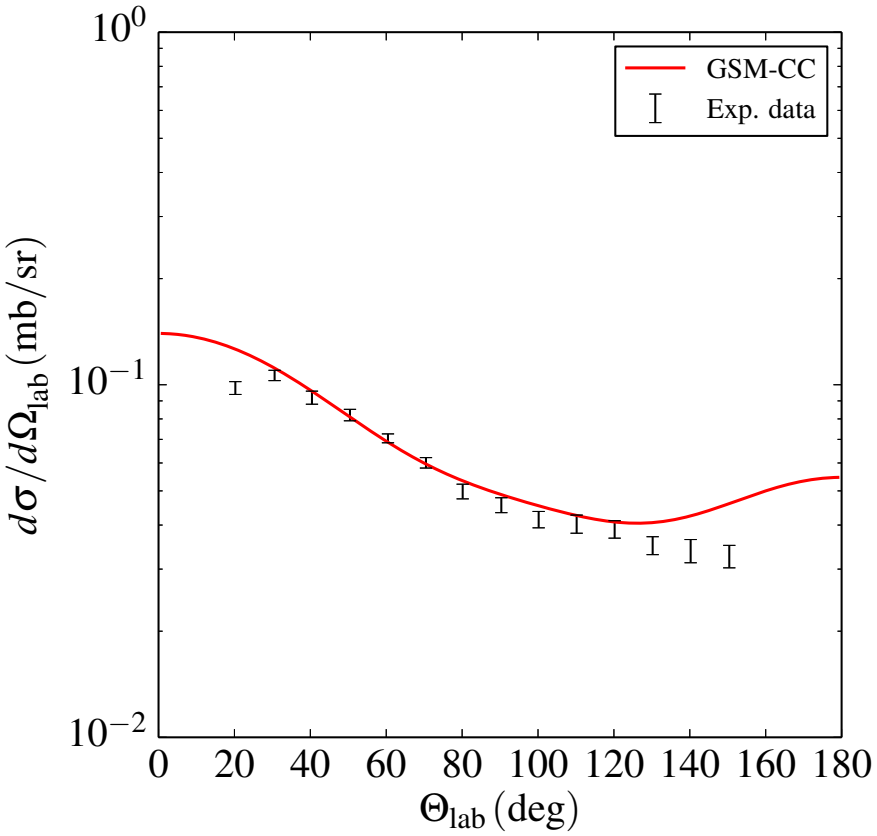

Figure 3.4 – Neutron transfer differential cross section for the reaction ^{40}Ca(d,p)^{41}Ca$_{\rm g.s.}$ at $E_{\rm d}$ = 1.9 MeV incident deuteron energy in the laboratory system, is calculated using the GSM-CC approach without non-resonant reaction channels. Experimental data are taken from [242].

3.4.3 Proton scattering on ^{14}O

In this section, we shall discuss GSM-CC calculation for the reaction: ^{14}O (p,p) ^{14}O. This investigation was stimulated by the recent experimental study of this reaction at GANIL [228].

Properties of the ground state $J^\pi = 1/2^+_1$ and its first excited state $J^\pi = 5/2^+_1$ of ^{15}F were measured several times [243–249] (see Ref. [250] for a recent compilation of the experimental results). Both states $1/2^+_1$ and $5/2^+_1$ are unbound by ~ 1.3 MeV and ~ 2.8 MeV, respectively. The theoretical predictions of the ground state width vary from 0.5 MeV to 1.3 MeV, whereas the first excited state is estimated to have the width $\Gamma \simeq 300$ keV [250–252]. The structure of the ground state (first excited state) of ^{15}F has been interpreted as the $\ell = 0$ ($\ell = 2$) proton coupled to the ^{14}O$^{\rm g.s}$ core [253]. Both states are described well as the s.p. configurations with a spectroscopic factor of $S > 0.5$ [250, 253, 254].

In the mirror nucleus ^{15}C, the second excited state is known at 3.103 MeV with $J^\pi = 1/2^-_1$ with a width $\Gamma = 29(3)$ keV [255]. Canton *et al.* [256] used the multichannel algebraic scattering theory with the Pauli-hindered method to calculate low-lying states in ^{15}F. They predicted a very narrow width $\Gamma = 5$ MeV for the second excited state $J^\pi = 1/2^-_1$.

Fortune and Sherr [257] used a potential model to determine the s.p. widths which they scaled

down to reproduce the measured widths in ^{15}C. The extracted spectroscopic factors was then used to estimate widths of mirror states in ^{15}F. These calculations confirmed that narrow resonances are expected in ^{15}F, but their width for the second excited state is ~ 10 times larger than the one reported in Ref. [256].

Experimentally, a first indication of the second excited state in ^{15}F was obtained in the transfer reaction ^{15}O(^{14}N, ^{15}C)^{15}F [247]. In this experiment, 150(100) keV width was found, but the spin and the parity of this state were not determined. This narrow width is surprising because the second excited state in ^{15}F is ~ 3.5 MeV above the combined Coulomb plus centrifugal barrier in ^{14}O + p. Later, the same state was observed through the angular correlations of decay products in the fragmentation of ^{17}N$_e$ [258].

^{15}F has been studied recently in the reaction ^{14}O(p,p)^{14}O at GANIL SPIRAL1 facility [259]. The excitation function was measured in the inverse kinematics. The excitation function at low energy is dominated by Coulomb scattering, but it also shows peaks and interferences that correspond to the presence of resonances in ^{15}F. Properties of these resonances, *i.e.* resonance energy, width, and spin, have been deduced from the R-matrix analysis of the shape of the peaks [260,261].

Due to the unbound nature of ^{15}F, a proper treatment of continuum couplings is mandatory. The GSM-CC formalism is particularly adapted for the description of ^{15}F. It allows to compare the calculated GSM-CC excitation function for ^{14}O(p,p)^{14}O and the GSM/GSM-CC spectrum of ^{15}F resonances with the experimental data. In this way, one may extract the structural information about unbound states of ^{15}F without recourse to uncontrolled approximations.

	a_0 (MeV)	R_0(fm)	V_0 (MeV)	V_{so}(MeV)
$\ell = 0$	0.65	3.13	59	0
$\ell = 1$	0.65	3.13	60	5
$\ell = 2$	0.65	3.13	56	5.22

Table 3.9 – Parameters of the Woods-Saxon potential for the description of ^{13}N, ^{14}O and ^{15}F.

Parameter	Value (MeV)
$V_{\mathrm{C,odd,t}}$	159.778
$V_{\mathrm{C,even,t}}$	-10
$V_{\mathrm{C,odd,s}}$	2
$V_{\mathrm{C,even,s}}$	9.876
$V_{\mathrm{SO,odd,t}}$	38.644
$V_{\mathrm{SO,even,t}}$	1000
$V_{\mathrm{T,odd,t}}$	34.411
$V_{\mathrm{T,even,t}}$	-10

Table 3.10 – Parameters of the FHT interaction [238] for the description of ^{14}O and ^{15}F

In our studies, the translationally invariant GSM Hamiltonian consists of (i) the Woods-Saxon potential with a spin-orbit term which describes the field of ^{12}C acting on valence nucleons in ^{13}N, ^{14}O, and ^{15}F, (ii) the Furutani-Horiuchi-Tamagaki (FHT) finite-range two-body interaction [238]

	k min (fm^{-1})	k peak (fm^{-1})	k middle (fm^{-1})	$k_{\max}$(fm^{-1})
$L^+_{d_{5/2}}$	0.0	0.3-i0.1	0.6	2.0
$L^+_{s_{1/2}}$	0.0	0.25-i0.1	0.5	2.0

Table 3.11 – Parameters of the contours in the complex k-plane

for valence nucleons, and (iii) the recoil term (for details see Sec. 2.2.4). The Woods-Saxon parameters (see Table 3.9) are adjusted to reproduce the ground state $1/2^-_1$ and the excited states $1/2^+_1$ and $5/2^+_1$ of ^{13}N. Parameters of the FHT interaction (see Table 3.10) are adjusted to reproduce energies of the low-lying states in ^{14}O and ^{15}F, and the one- and two-proton separation energies in ^{15}F.

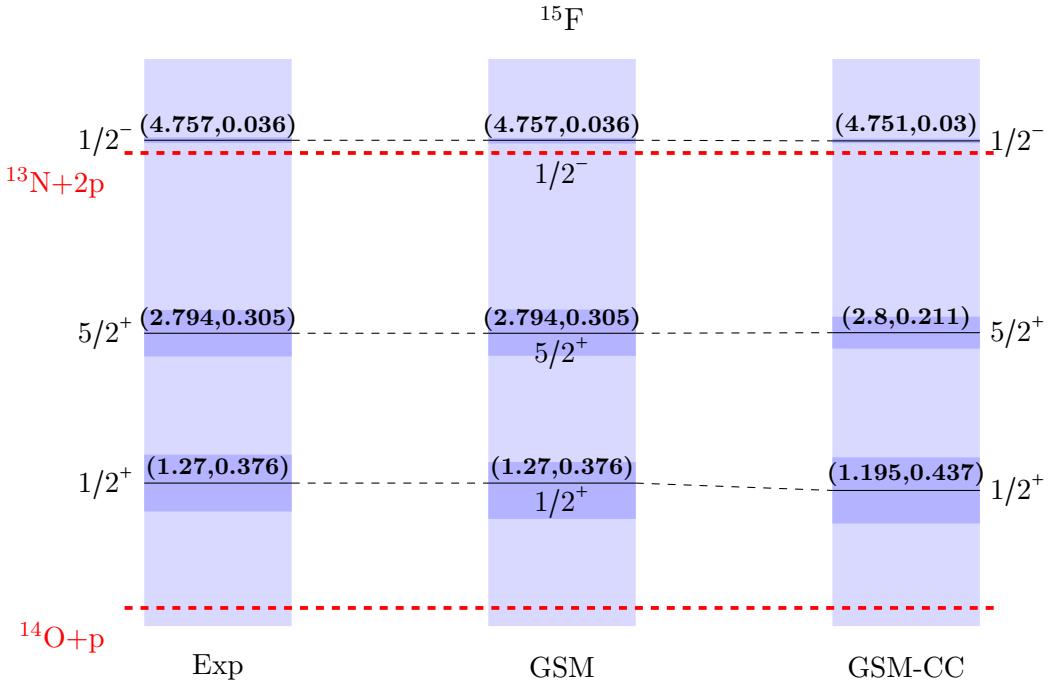

Figure 3.5 – ^{42}Sc spectrum calculated in GSM and GSM-CC, and compared with experimental data.

The s.p. space consists of three resonant shells $0p_{1/2}$, $0d_{5/2}$, $1s_{1/2}$, and several shells in the discretized non-resonant continuum on $L^+_{d_{5/2}}$ and $L^+_{s_{1/2}}$ in the complex k-plane. Each contour consists of three segments (see Table 3.11), and each segment is discretized with 10 points, so altogether $L^+_{d_{5/2}}$ and $L^+_{s_{1/2}}$ contours are discretized with 30 points. Scattering states states along each contour are generated by the same Woods-Saxon potential.

To reduce the size of GSM matrix, the basis of Slater determinants is truncated by limiting the number of particles in the non-resonant continuum to 2 nucleons. Moreover, the $p_{1/2}$ continuum is approximated by 5 lowest harmonic oscillator wave functions. Similarly, the $p_{3/2}$ and $d_{3/2}$ continua are approximated by 5 and 6 harmonic oscillator states, respectively.

The antisymmetric eigenstates of GSM-CC are expanded in the basis of channel states which are built by coupling the GSM wave functions for the ground state 0^+_1, and excited states 1^-_1, 0^+_2, 3^-_1, 2^+_1, 0^-_1, 2^+_2, 2^+_1 with the proton wave functions in partial waves: $s_{1/2}$, $p_{1/2}$, $p_{3/2}$, $d_{3/2}$ and $d_{5/2}$.

The two-body part of the FHT interaction from which the channel-channel coupling potentials are calculated, is rescaled by the multiplicative factors 1.07, 0.96 and 0.95 for $1/2^+_1$, $5/2^+_1$ and $1/2^+_1$ states of ^{15}F, respectively, to compensate for neglected channels built from higher lying resonances and non-resonant continuum states of ^{14}O. We checked the mutual consistency of the GSM and GSM-CC by comparing ^{15}F eigenvalues which are calculated either in the Slater determinant representation (GSM) or in the CC representation (GSM-CC).

The lowest resonances $J^\pi = 1/2^+_1, 5/2^+_1$, and $1/2^-_1$ in ^{15}F, are shown in Fig. 3.5. We compare the experimental spectrum with GSM and GSM-CC calculations. Numbers in the brackets give energy and width of these states. All energies are given with respect to the energy of ^{12}C core.

The narrow resonance $1/2^-_1$ can decay either by one- or two-proton emission. In GSM, this state:

$$\langle \Psi | 0p_{1/2}[1]1s_{1/2}[2] \rangle^2 = 0.97 \quad , \quad \langle \Psi | 0p_{1/2}[1]0d_{5/2}[2] \rangle^2 = 0.02 \tag{3.130}$$

is an almost pure configuration of two protons in $s_{1/2}$ resonant and non-resonant shells coupled to ^{13}N. The non-resonant continuum $s_{1/2}$ plays an important role in the structure of this state. The collectivization of near-threshold state due to the coupling to the nearby two-proton decay channel, helps to increase the weight of this diproton configuration in GSM calculation [92].

The diproton nature of $1/2^-_1$ state implies that the one-proton decay width is suppressed as compared to widths of low-lying levels $1/2^+_1$ and $5/2^+_1$. Indeed, the emission of two protons from this narrow state is energetically possible. Since there is no intermediate state accessible, it should be a direct two-proton emission to the ground state of ^{13}N. However, the available decay energy is only $Q_{2p} = 129$ keV (see Fig. 3.6) and the Wigner limit for ^{2}He cluster emission with $\ell = 0$ is: $\Gamma_{^2\mathrm{He}} = 4.\mathrm{e}^{-11}$ eV ($t_{1/2} = 16.5$ μs) [228].

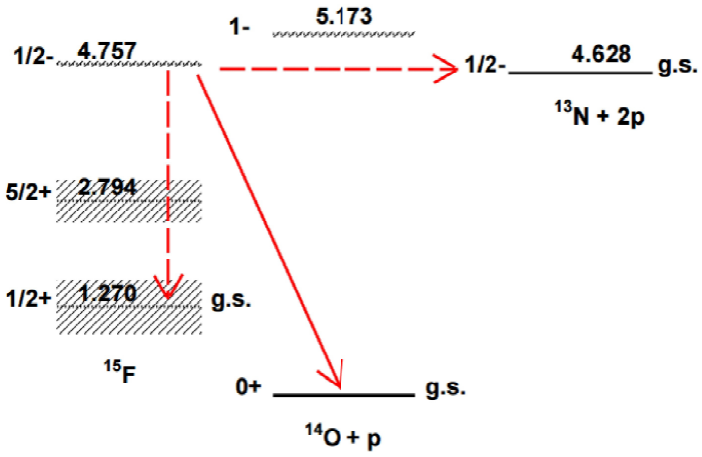

Figure 3.6 – (Color online) Level scheme of ^{15}F. Open decay channels for the $1/2^-_1$ resonance are: the one proton emission (red arrow), the gamma transition and the two proton emission (red dashed arrow). The hatched areas correspond to the width of the resonances $1/2^+_1$ and $5/2^+_1$.

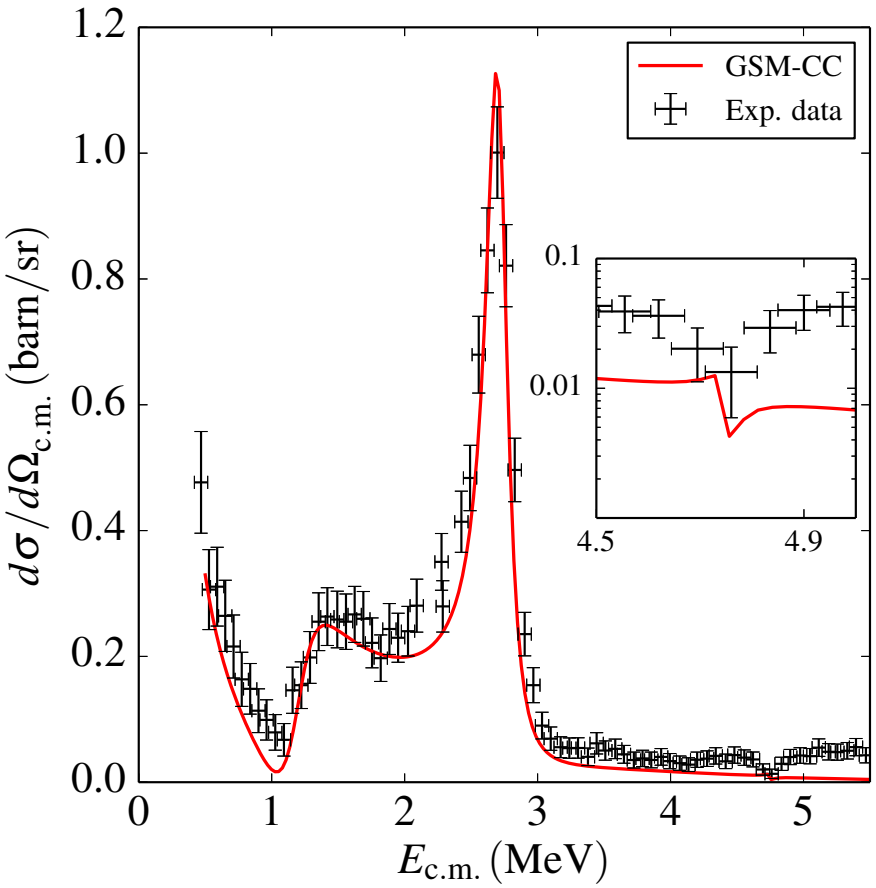

Figure 3.7 – (Color online) Experimental excitation function of the reaction ^{14}O(p,p)^{14}O at 180° in the c.m. system is compared with the GSM-CC results [228]. Inset shows the calculated and measured excitation function at around the narrow resonance $1/2^-_1$.

Even if spectroscopic factors are model dependent, their values within a given theoretical framework provide a useful insight into the structure of the calculated wave functions. The spectroscopic factors make more sense in the unified framework, such as the GSM (GSM-CC), where both the reaction cross sections and the spectra are calculated using the same Hamiltonian.

Table 3.12 presents the one-proton spectroscopic factors calculated in GSM for $1/2^+_1$, $5/2^+_1$, and $1/2^-_1$ resonances in ^{15}F. One can see that the ground state $1/2^+_1$ is mainly the $p_{1/2}$ proton coupled to $J^\pi = 1^-_1$ state of ^{14}O at $E = 5.173$ MeV, and a $1s_{1/2}$ proton coupled to the ground state of ^{14}O. The dominant configuration in the first excited state $5/2^+_1$ is a $0d_{5/2}$ proton coupled to the ground state of ^{14}O. The $1/2^-_1$ state exhibits large one-proton spectroscopic factors to the excited states of ^{14}O: $J^\pi = 1^-_1$ at $E^* = 5.173$ MeV, $J^\pi = 0^+_2$ at $E^* = 7.040$ MeV, and $J^\pi = 3^-_1$ at $E^* = 6.272$ MeV. The $p_{1/2}$ spectroscopic factor to the ground state of ^{14}O is very small, reducing the one-proton decay width significantly. The weight of the non-resonant continuum in these spectroscopic factors is of the order of few percents.

The GSM-CC excitation function for the reaction ^{14}O(p,p)^{14}O at 180° in the c.m. is compared with the experimental data in Fig. 3.7. The overall agreement with the data is excellent. The calculated cross section above $5/2^+_1$ resonance is lower than seen experimentally. This deficiency

$1/2^+_1$		$5/2^+_1$		$1/2^-_1$	
$S(\langle 1/2^+_1 \vert a^\dagger_{p_{1/2}} \vert 1^-_1\rangle)$	0.95	$S(\langle 5/2^+_1 \vert a^\dagger_{d_{5/2}} \vert 0^+_1\rangle)$	0.84	$S(\langle 1/2^-_1 \vert a^\dagger_{s_{1/2}} \vert 1^-_1\rangle)$	0.55
$S(\langle 1/2^+_1 \vert a^\dagger_{s_{1/2}} \vert 0^+_1\rangle)$	0.85	$S(\langle 5/2^+_1 \vert a^\dagger_{d_{5/2}} \vert 0^+_2\rangle)$	0.05	$S(\langle 1/2^-_1 \vert a^\dagger_{p_{1/2}} \vert 0^+_2\rangle)$	0.47
$S(\langle 1/2^+_1 \vert a^\dagger_{s_{1/2}} \vert 0^+_2\rangle)$	0.02			$S(\langle 1/2^-_1 \vert a^\dagger_{d_{5/2}} \vert 3^-_1\rangle)$	0.31
				$S(\langle 1/2^-_1 \vert a^\dagger_{p_{1/2}} \vert 0^+_1\rangle)$	0.05
				$S(\langle 1/2^-_1 \vert a^\dagger_{d_{3/2}} \vert 1^-_1\rangle)$	0.001

Table 3.12 – Real part of spectroscopic factors calculated in GSM for different resonances in ^{15}F.

can be explained by the absence of higher lying resonances and non-resonant continuum states of ^{14}O.

Figs. 3.8, 3.9 and 3.10 show the differential cross section for elastic 0^+, and inelastic 1^-, 3^- channels, respectively. The GSM-CC calculations are done for different c.m. energies of the incident projectile: $E_{\text{c.m.}} = 6.5$ MeV, 8.5 MeV, and 10.5 MeV.

The elastic differential cross section (Fig. 3.8) varies strongly with the excitation energy, mainly at intermediate ($\Theta_{\text{c.m.}} \sim 40$ °) and backward ($\Theta_{\text{c.m.}} \sim 160$ °) angles. One can see a significant increase of the differential cross section for $E_{\text{CM}} \geq 8.5$ MeV at backward angles which is due to the opening of inelastic channels: 1^-_1 and 3^-_1 at 5.17 MeV and 6.27 MeV, respectively.

Figs. 3.9 and 3.10 show the inelastic differential cross section in 1^- and 3^- channels. The magnitude of these differential cross-sections depends strongly on $E_{\text{c.m.}}$.

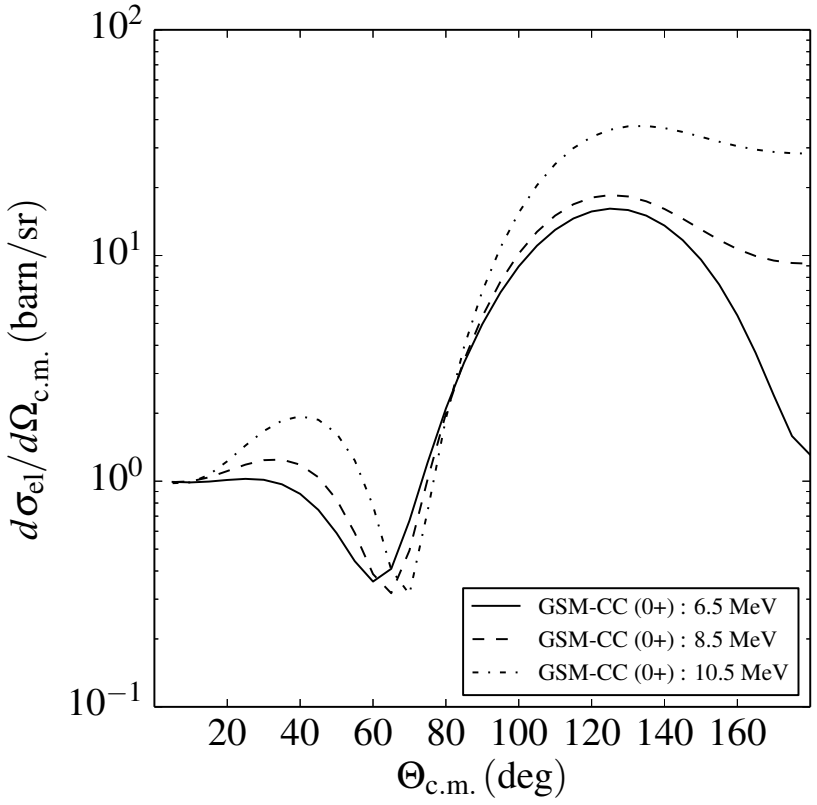

Figure 3.8 – Differential cross section for the elastic channel 0^+ at different c.m. energies.

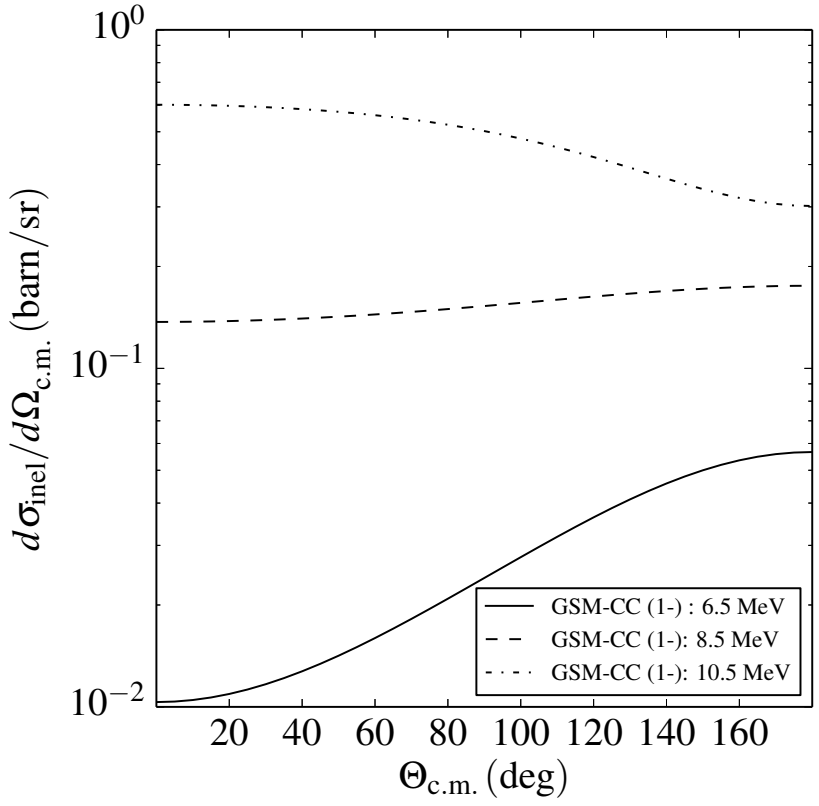

Figure 3.9 – Differential cross section for the inelastic channel 1^- at different c.m. energies.

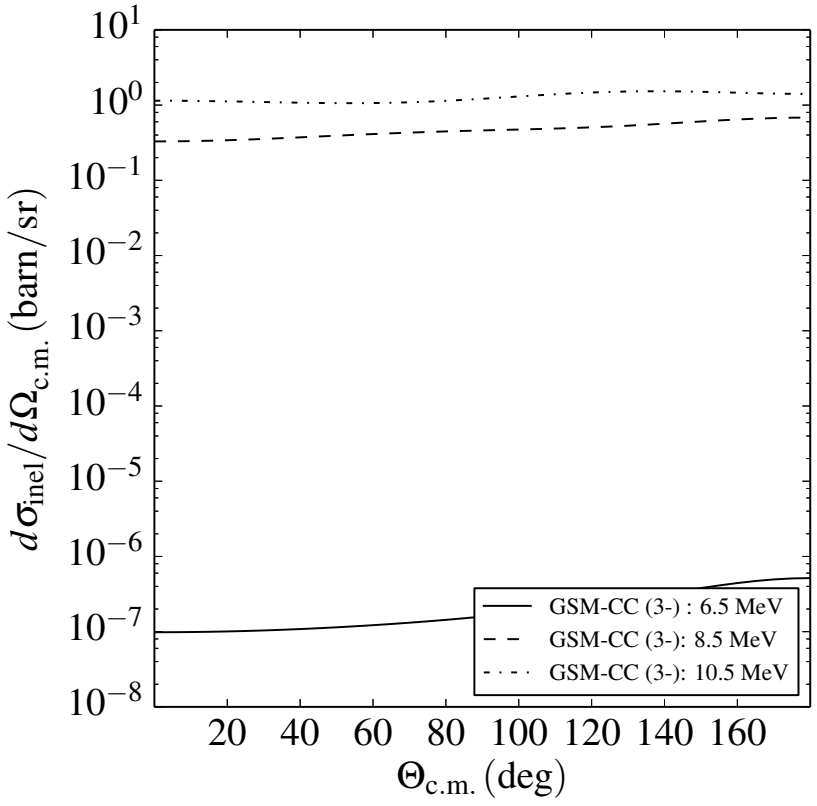

Figure 3.10 – Differential cross section for the inelastic channel 3^- at different c.m. energies.

Chapter 4

Conclusions

Two problems have been addressed in this work. The first one concerned generalization of the Richardson solution for the pairing Hamiltonian of a rational Gaudin model including the continuum. The second one was devoted to the formulation of the GSM-CC approach for nuclear reactions with multi-nucleon projectiles. This paves the way for the applicability of the reaction theory which is rooted in GSM for a broader class of reactions, including the transfer/knockout reactions.

The first objective is related to an urgent need to characterize and understand effects of the continuum coupling on nuclear spectra and binding energy. Algebraic models, based on emergent symmetries of nuclear many-body problem, helped in the past to identify elementary building blocks and essential concepts behind the formation mechanism of rich spectra of excited states. In the domain of weakly bound and/or unbound nuclei, such models do not exist, what hinders the understanding of qualitative features of the continuum. The pairing model plays a special role among the algebraic models. Exact solution for this Hamiltonian was derived by Richardson for a spectrum of bound s.p. levels [51, 52]. In this work, pairing Hamiltonain was generalized in Berggren basis and the generalized Richardson solution was derived for this problem. The comparison between this solution and exact results of GSM, obtained by the diagonalization of the pairing Hamiltonian, confirmed that the generalized Richardson solution is a reliable alternative of an exact GSM diagonalization, in particular in heavy nuclei with large number of valence nucleons. In the problem of ultra-small superconducting grains, the generalized Richardson solution of the pairing Hamiltonian in Berggren basis could help to understand the influence of continuum on pairing properties, in particular in the transitional region of the weak coupling limit.

There is an intense activity to describe the A-dependence of nuclear binding energy in the *ab initio* framework, using the interactions derived in chiral effective field theory [23, 102, 262–264]. In these studies, it was found that the chiral 3-body interaction plays a significant role reducing the over-binding which is found systematically when only 2-body interactions are used. In SMEC studies with the effective 2-body Hamiltonian including the continuum, it was found that the continuum coupling plays an essential role to explain one- and two-neutron separation energies in oxygen and fluorine chains of isotopes, *i.e.* it may change the A-dependence of nuclear binding energies [265]. In this work, the chain of carbon isotopes was studied using the (generalized) Richardson solution for a schematic pairing Hamiltonian in two approximations: (i) in the closed quantum system approximation, *i.e.* with bound s.p. levels and neglecting continuum couplings, and (ii) in the open quantum system approximation using Berggren s.p. ensemble. Fixing in both

approaches the strength of pairing interaction in a nucleus (^{14}C) with 2 nucleons outside of the ^{12}C closed core, it was found that the A-dependence of binding energy and the spectra of $^{14-20}$C depend strongly on the continuum coupling. Of course, the interaction in this model is much too simple to draw definitive conclusions but the qualitative effect is indisputable. Another observation was that the effect of continuum coupling on eigenvalues and structure of their eigenfunctions, depends strongly on the coupling of nucleons and, hence, varies rapidly from one state to another. Again, the interaction in a pairing model is too simple and the coupling to the one-nucleon continuum neglected, in order to draw the quantitative conclusions. Nevertheless, results of this generalized pairing Hamiltonian gives a warning that one should be cautious not to over-interpret results of SM with fitted two-body matrix elements as this model is missing significant physical ingredients.

The development of reaction theory which would be compatible with GSM is a challenge to nuclear theorists and urgent need for the experimental nuclear physics. The analysis of experimental data is done using often unjustified theoretical concepts, such as the local optical potential, because for several decades there was no sufficient progress in the consistent application of dispersion relations in the optical model, or in the derivation of new non-local parameterizations of the optical potential which are based on the GSM or CSM. One should stress that there is also no general acceptation among experimentalists of the fact that the systematic and hence, dull experiments on proton/neutron scattering in the broad range of energies and in long chains of (stable) isotopes, are mandatory to understand the in-medium interactions of nucleons. Instead, the experimentalists concentrate efforts on producing pseudo-data, like the spectroscopic factors, and produce an avalanche of 'exciting' data/conclusions using not well understood experimental techniques. An example of such are transfer and knockout reactions which give contradictory results on the spectroscopic factors and their dependence on the asymmetry of neutron and proton separation energies [266–268]. All that calls for a strong involvement of theorists in the development of reaction theory which would be rooted in GSM and allows for a direct connection between spectroscopic and reaction observables within the unified framework. This is a key problem not only in the physics of exotic nuclei in the vicinity of drip lines, but also in the traditional playground, close to the valley of β-stability.

GSM-CC approach provides the link between experiment and theory which allows to determine spectroscopic information directly from reaction physics observables, such as the (in)elastic scattering cross-section, excitation function, nucleon transfer cross section, etc. In this work, such a consistent application of the nuclear reaction theory (GSM-CC) has been presented on the example of spectrum of low-lying resonances in ^{15}F which was studied experimentally via the excitation function ^{14}O(p,p)^{14}O. Here, combined application of GSM and GSM-CC approaches allowed to link directly the reaction data to the structure of ^{15}F without any inconsistent 'massaging' of the data. Moreover, the exploratory study of the neutron transfer cross-section has been presented for the reaction ^{40}Ca(d,p)^{41}Ca$_{\text{g.s.}}$. Further development of the GSM-CC approach for transfer and knockout reactions is urgent not only to avoid above mentioned hubbub in knockout vs transfer reactions, but also to verify claims that the surrogate reaction, like (d,p), can inform us about the low-energy (n,γ) radiative capture cross-sections of interest in astrophysics.

In this work, we have made a progress by completing the formulation of nuclear reaction theory based on GSM, which allows to describe any binary reaction process with multi-nucleon (nuclear) projectiles. Numerical applications of this consistent microscopic theory are very demanding and offer surprises, like the problem of redundant reaction channels which has to be treated with great caution. The great advantage of the present formulation of reaction theory is that by

comparing the spectrum of eigenvalues calculated in GSM and obtained by diagonalizing the GSM-CC Hamiltonian matrix, one can estimate an importance of redundant channels. In the same way, the lack of non-resonant reaction channels can be judged according to their influence on the spectrum of GSM/GSM-CC eigenvalues. As an interesting by-product of the formal reaction theory based on GSM and Berggren basis, we have also discussed the application of Berggren basis to solve Faddeev equations.

The GSM-CC formulation which has been presented in this thesis uses the COSM coordinates to reduce dimensionality of the Fock space and to remove (approximately) the spurious c.m. excitations. In this way, heavy nuclei with a limited number of valence particles, can be studied systematically. Similarly as the no-core generalization of the standard GSM, one can envisage the studies of reactions in light nuclei using no-core GSM-CC approach with modern interactions derived in chiral effective field theory.

Appendix A

Annexes

A.1 Matrix elements and approximations

A.1.1 Neutron-neutron case

a) Plane waves

Neutron wave functions in the asymptotic region are free wave functions, so that they can always be expanded in a basis of plane waves, even if they are scattering states. Plane waves will be denoted as $|\vec{k}\rangle$, and we will perform a decomposition into relative and c.m. parts, for a moment with the real linear momenta:

$$\langle \vec{r}_a, \vec{r}_b | \vec{k}_a, \vec{k}_b \rangle = e^{i\vec{k}_a \cdot \vec{r}_a} e^{i\vec{k}_b \cdot \vec{r}_b} = e^{i\vec{k}_{\rm rel} \cdot \vec{r}_{\rm rel}} e^{i\vec{k}_{\rm c.m.} \cdot \vec{r}_{\rm c.m.}} \tag{A.1}$$

where:

$$\vec{r}_{\rm rel} = \vec{r}_a - \vec{r}_b \qquad \text{and} \qquad \vec{r}_{\rm c.m.} = \frac{1}{2}\left(\vec{r}_a + \vec{r}_b\right) \tag{A.2}$$

$$\vec{k}_{\rm rel} = \frac{1}{2}\left(\vec{k}_a - \vec{k}_b\right) \qquad \text{and} \qquad \vec{k}_{\rm c.m.} = \vec{k}_a + \vec{k}_b \tag{A.3}$$

The translationally invariant character of V implies that:

$$\langle \vec{k}_a, \vec{k}_b | \hat{V} | \vec{k}_c, \vec{k}_d \rangle = \langle \vec{k}_{\rm rel}, \vec{k}_{\rm c.m.} | \hat{V} | \vec{k'}_{\rm rel}, \vec{k'}_{\rm c.m.} \rangle = \delta(\vec{k}_{\rm c.m.} - \vec{k'}_{\rm c.m.}) \langle \vec{k}_{\rm rel} | \hat{V} | \vec{k'}_{\rm rel} \rangle \ . \tag{A.4}$$

As we are dealing with the effective nuclear interactions, of low-energy character, we can demand V to verify $\langle \vec{k'}_{\rm rel} | \hat{V} | \vec{k}_{\rm rel} \rangle = 0$, unless $k_{\rm rel} \leq k_{{\rm rel}max}$ and $k'_{\rm rel} \leq k_{{\rm rel}max}$. This requirement is clearly consistent with the cluster definition of Eq. (3.62).

Let us write the equation of energy conservation arising from Eq. (A.3):

$$k^2_{c.m.} + 4k^2_{\rm rel} = 2(k^2_a + k^2_b). \tag{A.5}$$

Due to the cluster approximation, $k_{\rm rel} \ll k_{c.m.}$ if $k_{c.m.} > k_{\rm max}$, as the nucleons in the projectiles virtually follow the same trajectory. Thus, Eq. (A.5) becomes:

$$k^2_{c.m.} = 2(k^2_a + k^2_b) \qquad \text{for} \qquad k_a > k_{\rm max} \qquad \text{or} \qquad k_b > k_{\rm max} \tag{A.6}$$

up to an error which can be made arbitrarily small. Moreover, having $k_a > k_{\max}$, $k_b \leq k_{\max}$ or $k_a \leq k_{\max}$, $k_b > k_{\max}$ is also impossible within the cluster approximation, as they correspond to the configurations for which the cluster dislocates. Consequently, from Eqs. (A.5), (A.6) one obtains :

$$k_a \leq k_{\max},\ k_b \leq k_{\max} \Rightarrow k_{c.m.} \leq 2k_{\max} \tag{A.7}$$

$$k_a > k_{\max},\ k_b > k_{\max} \Rightarrow k_{c.m.} > 2k_{\max} \tag{A.8}$$

with other cases leading to vanishing matrix elements of V due to the cluster approximation.

Consequently, the only non-vanishing matrix elements $\langle \vec{k}_a, \vec{k}_b | \hat{V} | \vec{k'}_a, \vec{k'}_b \rangle$ are those for which $k_i \leq k_{\max}$ or $k_i > k_{\max}$ $\forall i \in \{a, b, c, d\}$, because the case for which $k_a \leq k_{\max}$, $k_b \leq k_{\max}$, $k'_a > k_{\max}$ and $k'_b > k_{\max}$ have the Dirac delta function $\delta(k_{\text{c.m.}} - k'_{\text{c.m.}})$ and vanish, and other cases imply that $k_a > k_{\max}$, $k_b \leq k_{\max}$ or $k_a \leq k_{\max}$, $k_b > k_{\max}$ (same for k'_a, k'_b). Hence, $\langle \vec{k}_a, \vec{k}_b | \hat{V} | \vec{k'}_a, \vec{k'}_b \rangle \simeq 0$ when Eq. (3.66) is fulfilled by plane waves.

b) Bessel functions

The matrix elements $\langle \vec{k}_{\text{rel}} | \hat{V} | \vec{k'}_{\text{rel}} \rangle$ will be expanded in a set of Bessel functions $\{|k_{\text{rel}}, \ell_{\text{rel}}, m_{\text{rel}}\rangle\}$. This representation is convenient to handle because of its natural connection to planes waves, and because Berggren basis functions become asymptotically equal to Bessel functions for large linear momenta:

$$\begin{aligned} & \langle k_{\text{rel}}, \ell_{\text{rel}}, m_{\text{rel}} | \hat{V} | k'_{\text{rel}}, \ell'_{\text{rel}}, m'_{\text{rel}} \rangle \\ = & \int \langle \vec{k}_{\text{rel}} | k_{\text{rel}}, \ell_{\text{rel}}, m_{\text{rel}} \rangle \langle k'_{\text{rel}}, \ell'_{\text{rel}}, m'_{\text{rel}} | \vec{k'}_{\text{rel}} \rangle \langle \vec{k}_{\text{rel}} | \hat{V} | \vec{k'}_{\text{rel}} \rangle \ d\Omega_{k_{\text{rel}}} \ d\Omega_{k'_{\text{rel}}} \end{aligned} \tag{A.9}$$

The overlaps in Eq. (A.9) are determined using the plane wave expansion in partial waves arising from the additional theorem:

$$\langle \vec{r} | \vec{k} \rangle = \frac{1}{(2\pi)^{3/2}} e^{i\mathbf{k}.\mathbf{r}} = \frac{1}{(2\pi)^{3/2}} e^{ikr\cos\theta'} = \frac{4\pi}{(2\pi)^{3/2}} \sum_{\ell} \sum_{m=-\ell}^{\ell} i^{\ell} j_{\ell}(kr) Y_{\ell}^{m}(\Omega_r) Y_{\ell}^{m}(\Omega_k)^* \tag{A.10}$$

where θ' stands for the angle between the two vectors $\vec{k}$ and $\vec{r}$. The overlap between plane wave and Bessel function thus reads:

$$\begin{aligned} \langle \vec{k'}_{\text{rel}} | k_{\text{rel}}, \ell_{\text{rel}}, m_{\text{rel}} \rangle &= \int \langle \vec{k'}_{\text{rel}} | \vec{r}_{\text{rel}} \rangle \langle r_{\text{rel}}, \Omega_{r_{\text{rel}}} | k_{\text{rel}}, \ell_{\text{rel}}, m_{\text{rel}} \rangle \ d\vec{r}_{\text{rel}} \\ &= \frac{1}{(2\pi)^{3/2}} \sqrt{\frac{2}{\pi}} \int j_{\ell_{\text{rel}}}(k_{\text{rel}}\ r_{\text{rel}}) Y_{\ell_{\text{rel}}}^{m_{\text{rel}}}(\Omega_{r_{\text{rel}}}) e^{-i\vec{k'}_{\text{rel}}.\vec{r}_{\text{rel}}} \ d\vec{r}_{\text{rel}} \\ &= \frac{4\pi}{(2\pi)^{3/2}} \sqrt{\frac{2}{\pi}} Y_{\ell_{\text{rel}}}^{m_{\text{rel}}}(\Omega_{k_{\text{rel}}}) \int i^{\ell_{\text{rel}}} j_{\ell_{\text{rel}}}(k_{\text{rel}}\ r_{\text{rel}}) j_{\ell_{\text{rel}}}(k'_{\text{rel}}\ r_{\text{rel}})\ r_{\text{rel}}^2 \ dr_{\text{rel}} \\ &= \frac{4\pi}{(2\pi)^{3/2}} i^{\ell_{\text{rel}}} \delta(k_{\text{rel}} - k'_{\text{rel}}) Y_{\ell_{\text{rel}}}^{m_{\text{rel}}}(\Omega_{k_{\text{rel}}}) \end{aligned} \tag{A.11}$$

Inserting Eq. (A.11) in Eq. (A.9), one obtains:

$$\begin{aligned}\langle \vec{k}_{\rm rel}|\hat{V}|\vec{k'}_{\rm rel}\rangle &= \frac{1}{2\pi}\sum_{\substack{\ell_{\rm rel},\ell'_{\rm rel}\\ m_{\rm rel},m'_{\rm rel}}} i^{(\ell_{\rm rel}+\ell'_{\rm rel})} Y^{m_{\rm rel}}_{\ell_{\rm rel}}(\Omega_{k_{\rm rel}}) Y^{m'_{\rm rel}}_{\ell'_{\rm rel}}(\Omega_{k'_{\rm rel}})^* \\ &\times \int \delta(k_{\rm rel}-k''_{\rm rel})\delta(k'_{\rm rel}-k'''_{\rm rel})\,\langle k''_{\rm rel},\ell,m|\hat{V}|k'''_{\rm rel},\ell',m'_{\rm rel}\rangle\, dk''_{\rm rel}\; dk'''_{\rm rel} \\ &= \frac{1}{2\pi}\sum_{\substack{\ell_{\rm rel},\ell'_{\rm rel}\\ m_{\rm rel},m'_{\rm rel}}} i^{(\ell_{\rm rel}+\ell'_{\rm rel})} Y^{m_{\rm rel}}_{\ell_{\rm rel}}(\Omega_{k_{\rm rel}}) Y^{m'_{\rm rel}}_{\ell'_{\rm rel}}(\Omega_{k'_{\rm rel}})^* \,\langle k_{\rm rel},\ell_{\rm rel},m_{\rm rel}|\,\hat{V}\,|k'_{\rm rel},\ell'_{\rm rel},m'_{\rm rel}\rangle\end{aligned} \tag{A.12}$$

c) Berggren basis

In order to treat the general Berggren basis ensemble, we write the asymptotic behavior of the Berggren wave function in terms of Bessel functions, firstly for large r and then in the entire space:

$$u(r) \to C^+ h^+_\ell(kr) + C^- h^-_\ell(kr), \qquad r \to +\infty \tag{A.13}$$

where the functions h^+_ℓ and h^-_ℓ are Hankel functions, and C^+, C^- their associated coefficients. Let us to write Eq. (A.13) in terms of Ricatti-Bessel functions $\hat{j}_\ell(kr) = krj_\ell(kr)$:

$$\hat{j}_\ell(kr) = \frac{h^+_\ell(kr) - h^-_\ell(kr)}{2i} \tag{A.14}$$

Hence:

$$u(r) \to C\hat{j}_l(kr) + Dh^+_\ell(kr), \qquad r \to +\infty \tag{A.15}$$

where $u(r)$ is written in terms of Bessel and purely outgoing parts. Eq. (A.15), valid in the asymptotic region, can be extended to the entire space:

$$|a\rangle = C_a\,|k_a,\ell\rangle + |a^+\rangle \tag{A.16}$$

where $|k_a,\ell\rangle$ is an other Bessel function, and $|a^+\rangle$:

$$|a^+\rangle = \int \langle k,\ell|a^+\rangle\,|j_\ell(k)\rangle\,dk = \int u_{a^+}(k)\,|j_\ell(k)\rangle\,dk \tag{A.17}$$

k_a and k should belong to different contours, as $|k_a\rangle$ must lie above the k-contour so that it can be treated as an integrable state using the complex scaling.

In order to determine the asymptotic behavior of $u_{a^+}(k)$ for $k \to +\infty$, we will use the fact that $u_a(k)$ verifies the following Schrödinger equation $\hat{H}_{\rm P}$ in momentum space:

$$\frac{\hbar^2k^2}{2m}u_a(k) + \int U_{\rm basis}(k,k')u_a(k')dk' = \frac{\hbar^2k_a^2}{2m}u_a(k)\,. \tag{A.18}$$

Due to the low energy character of $U_{\rm basis}$, Eq. (A.18) implies that $u_a(k) \to 0$ faster than any inverse power of k_a when $k \to +\infty$ (same for k fixed and $k_a \to +\infty$). Eq. (A.16) implies that:

$$\langle k'_a,\ell_a|a\rangle = u(k'_a) = \delta(k'_a - k_a) + \langle k'_a,\ell_a|a^+\rangle\,. \tag{A.19}$$

Thus, $\langle a^+|k'_a, \ell_a\rangle \to 0$ for $k'_a \to +\infty$ and k_a fixed (same for k'_a fixed and $k_a \to +\infty$).

If $k'_i > k_{max}$ or $k'_i \leq k_{max}$, then there is at least one $k_i \leq k_{max}$ or $k_i > k_{max}$, respectively (conditions from Eq. (3.66)). Thus, if we have for example $k'_a \leq k_{max}$ and $k_a > k_{max}$ then the r.h.s. of the Eq. (A.18) is unbounded while the l.h.s. is bounded, and $u(k'_a) = O(1)$.

By injecting this in Eq. (A.18), one obtains:

$$u(k'_a) = O\left(\frac{1}{k_a^2}\right)$$

Repeating this n times, one obtains:

$$u(k'_a) = O\left(\frac{1}{k_a^{2n}}\right) \ ,$$

and with Eq. (A.19) we have: $\langle k'_a, \ell_a|a^+\rangle = 0$. Finally, if we have either $k'_i > k_{max}$ or $k'_i \leq k_{max}$ then there is at least one product $\langle k'_i, \ell_i|i^+\rangle$ which vanishes. Hence, the matrix elements $\langle f_a, f_b|\hat{V}|f_c, f_d\rangle$ always vanish if we have the conditions (3.66).

Let us write the matrix elements of $\hat{V}$ using Eq. (A.15):

$$\langle a, b|\hat{V}|c, d\rangle = \sum_{f_a, f_b, f_c, f_d} \langle f_a, f_b|\hat{V}|f_c, f_d\rangle \ , \tag{A.20}$$

where $|f_i\rangle = \{|k_i, \ell_i, m_i\rangle, |i^+\rangle\}$ with $i = \{a, b, c, d\}$. We express the matrix elements $\langle f_a, f_b|\hat{V}|f_c, f_d\rangle$ using the Bessel function expansion of $|f_i\rangle$ states:

$$\begin{aligned}\langle f_a, f_b|\hat{V}|f_c, f_d\rangle \quad = \quad & \int \langle f_a|k'_a, \ell_a, m_a\rangle \langle f_b|k'_b, \ell_b, m_b\rangle \langle f_c|k'_c, \ell_c, m_c\rangle \langle f_d|k'_d, \ell_d, m_d\rangle \\ \times \quad & \langle k'_a, \ell_a, m_a, k'_b, \ell_b, m_b|\hat{V}|k'_c, \ell_c, m_c, k'_d, \ell_d, m_d\rangle \, dk'_a dk'_b dk'_c dk'_d\end{aligned} \tag{A.21}$$

where Eq. (3.66) is supposed to be verified. Note that a product in the integrand of Eq. (A.21) is negligible if only one of its factor is negligible, because all factors therein are bounded, due to the normalizations of basis states and the low-energy character of $\hat{V}$.

Let us first consider $k'_i \leq k_{max}\ \forall i \in \{a, b, c, d\}$ or $k'_i > k_{max}\ \forall i \in \{a, b, c, d\}$, so that $\langle k'_a, \ell_a, k'_b, \ell_b|\hat{V}|k'_c, \ell_c, k'_d, \ell$ Thus, there is at least one $|f_i\rangle$ whose associated linear momentum k_i is far from k'_i, *i.e.* $k_i \leq k_{\max}$ and $k'_i > k_{\max}$, or $k_i > k_{\max}$ and $k'_i \leq k_{\max}$. Due to $k_i \neq k'_i$, we have $\langle f_i|k'_i, \ell_i, m_i\rangle$ equal to zero if $|f_i\rangle$ is equal to $|k_i, \ell_i, m_i\rangle$. If $|f_i\rangle$ is equal to $|i^+\rangle$, $\langle f_i|k'_i, \ell_i, m_i\rangle$ is negligible (see Eq. (A.19) and below).

The last case to consider is that of the k'_i verifying Eq. (3.66) $\forall i \in \{a, b, c, d\}$. For this, we will expand $\langle k'_a, \ell_a, m_a, k'_b, \ell_b, m_b|\hat{V}|k'_c, \ell_c, m_c, k'_d, \ell_d, m_d\rangle$ in relative and c.m. basis states, so that the

demonstrated properties of the relative two-body matrix elements of $\hat{V}$ at high energy can be used:

$$\begin{aligned}
& \langle k'_a, \ell_a, m_a, k'_b, \ell_b, m_b | \hat{V} | k'_c, \ell_c, m_c, k'_d, \ell_d, m_d \rangle \\
= & \int \langle k'_a, \ell_a, m_a, k'_b, \ell_b, m_b | \vec{k}_a, \vec{k}_b \rangle \langle \vec{k}_c, \vec{k}_d | k'_c, \ell_c, m_c, k'_d, \ell_d, m_d \rangle \\
\times & \langle \vec{k}_a, \vec{k}_b | \hat{V} | \vec{k}_c, \vec{k}_d \rangle \, d\vec{k}_a d\vec{k}_b \vec{k}_c \vec{k}_d \\
= & \int \langle \ell_a, m_a | \Omega_{k_a} \rangle \langle \ell_b, m_b | \Omega_{k_b} \rangle \langle \ell_c, m_c | \Omega_{k_c} \rangle \langle \ell_d, m_d | \Omega_{k_d} \rangle \\
\times & \delta(\vec{k}_{\text{c.m.}} - \vec{k}'_{\text{c.m.}}) \langle \vec{k}_{\text{rel}} | \hat{V} | \vec{k}'_{\text{rel}} \rangle \, d\vec{k}_a d\vec{k}_b d\vec{k}_c d\vec{k}_d \\
= & \frac{1}{2\pi} \sum_{\ell,m,\ell',m'} i^{\ell+\ell'} \int Y_\ell^m(\Omega_k) Y_{\ell'}^{m'}(\Omega_{k'})^* \\
\times & \langle \ell_a, m_a | \Omega_{k_a} \rangle \langle \ell_b, m_b | \Omega_{k_b} \rangle \langle \ell_c, m_c | \Omega_{k_c} \rangle \langle \ell_d, m_d | \Omega_{k_d} \rangle \\
\times & \langle k_{\text{rel}}, \ell, m | \hat{V} | k'_{\text{rel}}, \ell', m' \rangle \, d\Omega_{k_a} d\Omega_{k_b} d\Omega_{k_c} d\Omega_{k_d}
\end{aligned} \tag{A.22}$$

To derive the above expression, Eqs. (A.4) and (A.12) have been used.

As we have at least one $k'_i \leq k_{max}$ and $k'_j > k_{max}$ with $i, j \in \{a, b, c, d\}$, we have either k_{rel} bounded and k'_{rel} unbounded, or vice versa, so that $\langle k_{\text{rel}}, \ell, m | \hat{V} | k'_{\text{rel}}, \ell', m' \rangle$ is always negligible. Hence, $\langle a, b | \hat{V} | c, d \rangle \to 0$ when Eq. (3.66) is fulfilled for all cases.

The Berggren basis possesses in general the complex-energy states, so that Eq. (3.66) has to be extended to this case, with the inequalities related to k_{max} now verified by the real parts of linear momenta. For this, one can see that we can apply analytic continuation on linear momenta in Eq. (A.22), because radial and angular parts are well separated therein. Thus, $\langle a, b | \hat{V} | c, d \rangle \to 0$ when Eq. (3.66) stands is also fulfilled for complex linear momenta.

A.1.2 Proton-proton and proton-neutron case

For the cases involving protons in $\{a, b, c, d\}$, we will consider the screening method in order avoid divergences due to the infinite-range of the Coulomb potential arising from the proton generating potential. This is justified by the fact that reactions of importance always occur relatively close to the target, all the others reducing to pure Rutherford scattering. Hence, we can consider that the Coulomb Hamiltonian acts up to a radius R. Consequently, proton wave functions become proportional to neutron wave functions at large distances. We then have to prove that normalization of screened and unscreened proton wave functions is asymptotically the same for $R \to +\infty$ so that the plane wave decomposition method elaborated for neutrons in the previous paragraph can be applied in the proton case as well.

For $r \leq R$, but nevertheless sufficiently large to be outside of the nuclear region, the asymptotic behavior of the screened Berggren proton wave function as $r \to +\infty$ is that of Coulomb wave functions:

$$\begin{aligned}
u_e(r) = u_c(r) \quad \to \quad & C'_+ H^+_{\ell\eta}(kr) + C'_- H^-_{\ell\eta}(kr) \\
= \quad & C^+ e^{ikr - i\eta \ln(2kr)} + C^- e^{-ikr + i\eta \ln(2kr)} + O\left(\frac{1}{kr}\right)
\end{aligned} \tag{A.23}$$

where $H^+_{\ell\eta}$ and $H^-_{\ell\eta}$ are the incoming and outgoing Coulomb wave functions. For $r > R$, the asymptotic behavior of proton wave functions goes back to that of neutrons:

$$u_s(r) \to C^+_s e^{ikr} + C^-_s e^{-ikr} + O\left(\frac{1}{kr}\right) \tag{A.24}$$

where the index s stands for "screening". Constants in Eqs. (A.23) and (A.24) are determined using the continuity of the wave function and of its derivative:

$$\begin{cases} C^+ e^{ikR - i\eta \ln(2kR)} + C^- e^{-ikR + i\eta \ln(2kR)} + O\left(\frac{1}{kR}\right) &= C_s^+ e^{ikR} + C_s^- e^{-ikR} \\ C^+ e^{ikR - i\eta \ln(2kR)} - C^- e^{-ikR + i\eta \ln(2kR)} + O\left(\frac{1}{kR}\right) &= C_s^+ e^{ikR} - C_s^- e^{-ikR} \end{cases} \tag{A.25}$$

so that for $R \to +\infty$, knowing that $C_s^+ C_s^- = \frac{1}{2\pi}$, we have the normalization:

$$C^+ C^- = \frac{1}{2\pi} + O\left(\frac{1}{R}\right) \tag{A.26}$$

and we have proved that screened functions have the same normalization as unscreened functions.

Therefore, if protons are present in $\{a, b, c, d\}$, Eq. (A.26) implies that:

$$\langle a, b | \hat{V} | c, d \rangle = \langle a_s, b_s | \hat{V} | c_s, d_s \rangle + O\left(\frac{1}{R}\right). \tag{A.27}$$

Consequently, as R can be arbitrarily large, one can consider that $\langle a, b | \hat{V} | c, d \rangle = 0$ in Eq. (A.27) when the conditions embedded in Eq. (3.65) are verified.

A.2 Derivation of the generalized Richardson equations

An approximate solution for the pairing Hamiltonian in Berggren basis (2.89) can be found by replacing the Kronecker delta by Dirac delta in the commutation relation:

$$\left[\hat{b}_k, \hat{b}_{k'}^\dagger\right] = 2\delta(k - k') \left(\frac{\hat{\Omega}_k}{4} \pm \frac{\hat{n}_k}{2}\right) \tag{A.28}$$

With this change, the new pair operators satisfy:

$$\begin{aligned} \left[\hat{\hat{n}}_q, \hat{\hat{b}}_{q'}^\dagger\right] &= 2\delta_{qq'} \hat{\hat{b}}_q^\dagger \\ \left[\hat{\hat{b}}_q, \hat{\hat{b}}_{q'}^\dagger\right] &= 2\delta_{qq'} \left(\frac{\hat{\Omega}_q}{4} \pm \frac{\hat{\hat{n}}_q}{2w_q}\right) \end{aligned} \tag{A.29}$$

where the index q runs over bound, resonance and discretized continuum states. In this approximation, let us now derive the solution of the Schrödinger equation for both the fermion and boson system: $\hat{H} |\Psi_{\text{ norm}}\rangle = E |\Psi_{\text{ norm}}\rangle$, with $E = \sum_{\nu=1}^{N_{\text{pair}}} E_\nu + \sum_q^{\mathcal{N}} \nu_q \epsilon_q$ where E_ν are the pair energies, N_{pair} the number of pairs and $\mathcal{N}$ the total number of bound, resonance and discretized continuum states, *i.e.* $\mathcal{N} = 2N + \nu$ with $\nu = \sum_q^{\mathcal{N}} \nu_q$ the number of unpaired particles. As an ansatz for the many-body state we take:

$$|\Psi_{\text{ norm}}\rangle = \prod_{\nu=1}^{N_{\text{pair}}} \hat{S}_{\nu;\,\text{norm}}^\dagger |0\rangle \quad ; \quad \hat{S}_{\nu;\,\text{norm}}^\dagger = c_\nu G \sum_q^{\mathcal{N}} \frac{\hat{\hat{b}}_q^\dagger \sqrt{w_q}}{2\epsilon_q - E_\nu} \tag{A.30}$$

where the normalization constants c_ν are given by:

$$\frac{1}{(c_\nu G)^2} = \frac{1}{{C_\nu}^2} = \sum_q \frac{w_q}{(2\epsilon_q - E_\nu)^2} \tag{A.31}$$

In order to simply the derivation, it is more convenient to define $\hat{S}^\dagger_\nu = \hat{S}^{\text{norm},\dagger}_\nu / C_\nu$ so that:

$$|\Psi_{\text{ norm}}\rangle = \prod_{\nu=1}^{N_{\text{pair}}} C_\nu \hat{S}^\dagger_\nu |0\rangle = C|\Psi\rangle \tag{A.32}$$

where

$$C = \prod_{\nu=1}^{N_{\text{pair}}} C_\nu$$

and

$$|\Psi\rangle = \prod_{\nu=1}^{N_{\text{pair}}} \hat{S}^\dagger_\nu |0\rangle$$

Let us begin by evaluating the commutator:

$$\left[\hat{H}, \prod_{\nu=1}^{N_{\text{pair}}} \hat{S}^\dagger_\nu\right] = \sum_{\nu=1}^{N_{\text{pair}}} \left(\left(\prod_{\eta=1}^{\nu-1} \hat{S}^\dagger_\eta \right) \left[\hat{H}, \hat{S}^\dagger_\nu\right] \left(\prod_{\mu=\nu+1}^{N_{\text{pair}}} \hat{S}^\dagger_\mu \right) \right) \tag{A.33}$$

It is convenient to rewrite the Hamiltonian (2.89) in a discretized form:

$$\hat{H} = \sum_q^{\mathcal{N}} \epsilon_q \hat{\hat{n}}_q - G \hat{S}^\dagger_0 \hat{S}_0 \quad ; \quad \hat{S}^\dagger_0 = \sum_q^{\mathcal{N}} \hat{\hat{b}}^\dagger_q \sqrt{w_q} \quad , \tag{A.34}$$

where $\mathcal{N}$ is the total number of bound, resonance and discretized continuum states. Thus, knowing the following commutation relations:

$$\hat{\hat{b}}^{\dagger 2}_q = 0 \quad , \quad [\hat{\hat{b}}_q, \hat{\hat{b}}^\dagger_{q'}] = 2\delta_{qq'} \left(\frac{\hat{\Omega}_q}{4} \pm \frac{\hat{\hat{n}}_q}{2w_q} \right) \quad , \quad [\hat{\hat{n}}_q, \hat{\hat{b}}^\dagger_{q'}] = 2\delta_{qq'} \hat{\hat{b}}^\dagger_q \tag{A.35}$$

we get:

$$\left[\hat{\hat{n}}_q, \hat{S}^\dagger_\nu\right] = \frac{2\hat{\hat{b}}^\dagger_q \sqrt{w_q}}{2\epsilon_q - E_\nu} \quad , \quad \left[\hat{S}_0, \hat{S}^\dagger_\nu\right] = \sum_q^{\mathcal{N}} \frac{w_q \hat{\Omega}_q / 2 \pm \hat{\hat{n}}_q}{2\epsilon_q - E_\nu} \tag{A.36}$$

and with $\left[\hat{S}^\dagger_0, \hat{S}^\dagger_\nu\right] = 0$ we have:

$$\begin{aligned} \left[\hat{H}, \hat{S}^\dagger_\nu\right] &= \sum_q^{\mathcal{N}} \epsilon_q \left[\hat{\hat{n}}_q, \hat{S}^\dagger_\nu\right] - G \left[\hat{S}^\dagger_0 \hat{S}_0, \hat{S}^\dagger_\nu\right] \\ &= E_\nu \hat{S}^\dagger_\nu + \hat{S}^\dagger_0 \left(1 - G \sum_q^{\mathcal{N}} \frac{w_q \hat{\Omega}_q / 2 \pm \hat{\hat{n}}_q}{2\epsilon_q - E_\nu} \right) \end{aligned} \tag{A.37}$$

Inserting (A.37) into Eq. (A.33), one obtains:

$$\begin{aligned}
\left[\hat{H}, \prod_{\nu=1}^{N_{\text{pair}}} \hat{S}_\nu^\dagger\right] &= \sum_{\nu=1}^{N_{\text{pair}}} \left(\prod_{\eta=1}^{\nu-1} \hat{S}_\eta^\dagger\right) \left[\hat{H}, \hat{S}_\nu^\dagger\right] \left(\prod_{\mu=\nu+1}^{N_{\text{pair}}} \hat{S}_\mu^\dagger\right) \\
&= \sum_{\nu=1}^{N_{\text{pair}}} \left(\prod_{\eta=1}^{\nu-1} \hat{S}_\eta^\dagger\right) E_\nu \hat{S}_\nu^\dagger \left(\prod_{\mu=\nu+1}^{N_{\text{pair}}} \hat{S}_\mu^\dagger\right) \\
&+ \sum_{\nu=1}^{N_{\text{pair}}} \left(\prod_{\eta=1}^{\nu-1} \hat{S}_\eta^\dagger\right) \hat{S}_0^\dagger \left(1 - G \sum_q^{\mathcal{N}} \frac{w_q \hat{\Omega}_q/2 \pm \hat{\tilde{n}}_q}{2\epsilon_q - E_\nu}\right) \left(\prod_{\mu=\nu+1}^{N_{\text{pair}}} \hat{S}_\mu^\dagger\right) \\
&= \sum_{\nu=1}^{N_{\text{pair}}} E_\nu \left(\prod_{\eta=1}^{N_{\text{pair}}} \hat{S}_\eta^\dagger\right) + \sum_{\nu=1}^{N_{\text{pair}}} \left(\prod_{\eta=1}^{N_{\text{pair}}} \hat{S}_\mu^\dagger\right) \hat{S}_0^\dagger \left(\prod_{\mu=\nu+1}^{N_{\text{pair}}} \hat{S}_\mu^\dagger\right) \\
&- \sum_{\nu=1}^{N_{\text{pair}}} \left(\prod_{\eta=1}^{\nu-1} \hat{S}_\eta^\dagger\right) \hat{S}_0^\dagger G \sum_q^{\mathcal{N}} \frac{w_q \hat{\Omega}_q/2 \pm \hat{\tilde{n}}_q}{2\epsilon_q - E_\nu} \left(\prod_{\mu=\nu+1}^{N_{\text{pair}}} \hat{S}_\mu^\dagger\right)
\end{aligned} \tag{A.38}$$

where the 2nd term can be expressed as:

$$\sum_{\nu=1}^{N_{\text{pair}}} \left(\prod_{\eta=1}^{\nu-1} \hat{S}_\eta^\dagger\right) \hat{S}_0^\dagger \left(\prod_{\mu=\nu+1}^{N_{\text{pair}}} \hat{S}_\mu^\dagger\right) = \sum_{\nu=1}^{N_{\text{pair}}} \hat{S}_0^\dagger \left(\prod_{\substack{\eta=1 \\ \neq\nu}}^{N_{\text{pair}}} \hat{S}_\eta^\dagger\right) \tag{A.39}$$

and the 3rd term :

$$\begin{aligned}
&\sum_{\nu=1}^{N_{\text{pair}}} \left(\prod_{\eta=1}^{\nu-1} \hat{S}_\eta^\dagger\right) \hat{S}_0^\dagger G \sum_q^{\mathcal{N}} \frac{w_q \hat{\Omega}_q/2 \pm \hat{\tilde{n}}_q}{2\epsilon_q - E_\nu} \left(\prod_{\mu=\nu+1}^{N_{\text{pair}}} \hat{S}_\mu^\dagger\right) \\
&= G \sum_{\nu=1}^{N_{\text{pair}}} \hat{S}_0^\dagger \left(\prod_{\eta=1}^{\nu-1} \hat{S}_\eta^\dagger\right) \sum_q^{\mathcal{N}} \frac{w_q \hat{\Omega}_q/2 \pm \hat{\tilde{n}}_q}{2\epsilon_q - E_\nu} \left(\prod_{\mu=\nu+1}^{N_{\text{pair}}} \hat{S}_\mu^\dagger\right) \\
&= G \sum_{\nu=1}^{N_{\text{pair}}} \frac{w_q \hat{\Omega}_q/2}{2\epsilon_q - E_\nu} \hat{S}_0^\dagger \left(\prod_{\substack{\eta=1 \\ \neq\nu}}^{N_{\text{pair}}} \hat{S}_\eta^\dagger\right) \\
&\pm G \sum_{\nu=1}^{N_{\text{pair}}} \left(\prod_{\eta=1}^{\nu-1} \hat{S}_\eta^\dagger\right) \sum_q^{\mathcal{N}} \frac{\hat{S}_0^\dagger \hat{\tilde{n}}_q}{2\epsilon_q - E_\nu} \left(\prod_{\mu=\nu+1}^{N_{\text{pair}}} \hat{S}_\mu^\dagger\right)
\end{aligned} \tag{A.40}$$

Now, let us derive the expression for $\left[\hat{\hat{n}}_q, \prod_{\mu=\nu+1}^{N_{\text{pair}}} \hat{S}_\mu^\dagger\right]$ using Eq. (A.36):

$$\begin{aligned}
\hat{\hat{n}}_q \left(\prod_{\mu=\nu+1}^{N_{\text{pair}}} \hat{S}_\mu^\dagger\right) &= f_q(E_{J_{\nu+1}}) \left(\prod_{\mu=\nu+2}^{N_{\text{pair}}} \hat{S}_\mu^\dagger\right) + \hat{S}_{J_{\nu+1}}^\dagger \hat{\hat{n}}_q \left(\prod_{\mu=\nu+2}^{N_{\text{pair}}} \hat{S}_\mu^\dagger\right) \\
&= f_q(E_{J_{\nu+1}}) \left(\prod_{\mu=\nu+2}^{N_{\text{pair}}} \hat{S}_\mu^\dagger\right) + f_q(E_{J_{\nu+2}}) \left(\prod_{\substack{\mu=\nu+1 \\ \neq \nu+2}}^{N_{\text{pair}}} \hat{S}_\mu^\dagger\right) + \hat{S}_{J_{\nu+1}}^\dagger \hat{S}_{J_{\nu+2}}^\dagger \hat{\hat{n}}_q \left(\prod_{\mu=\nu+3}^{N_{\text{pair}}} \hat{S}_\mu^\dagger\right) \\
&= f_q(E_{J_{\nu+1}}) \left(\prod_{\mu=\nu+2}^{N_{\text{pair}}} \hat{S}_\mu^\dagger\right) + f_q(E_{J_{\nu+2}}) \left(\prod_{\substack{\mu=\nu+1 \\ \neq \nu+2}}^{N_{\text{pair}}} \hat{S}_\mu^\dagger\right) + f_q(E_{J_{\nu+3}}) \left(\prod_{\substack{\mu=\nu+1 \\ \neq \nu+3}}^{N_{\text{pair}}} \hat{S}_\mu^\dagger\right) \\
&+ \hat{S}_{J_{\nu+1}}^\dagger \hat{S}_{J_{\nu+2}}^\dagger \hat{S}_{J_{\nu+3}}^\dagger \hat{\hat{n}}_q \left(\prod_{\mu=\nu+4}^{N_{\text{pair}}} \hat{S}_\mu^\dagger\right)
\end{aligned} \tag{A.41}$$

To simplify notation in the above expressions, we have defined:

$$\left[\hat{\hat{n}}_q, \hat{S}_\nu^\dagger\right] = \frac{2\hat{\hat{b}}_q^\dagger \sqrt{w_q}}{2\epsilon_q - E_\nu} = f_q(E_\nu) \tag{A.42}$$

Eq. (A.41) can be generalized as follows:

$$\hat{\hat{n}}_q \left(\prod_{\mu=\nu+1}^{N_{\text{pair}}} \hat{S}_\mu^\dagger\right) = \sum_{\ell=\nu+1}^{N_{\text{pair}}} f_q(E_{J_\ell}) \left(\prod_{\substack{\mu=\nu+1 \\ \neq \ell}}^{N_{\text{pair}}} \hat{S}_\mu^\dagger\right) + \left(\prod_{\mu=\nu+1}^{N_{\text{pair}}} \hat{S}_\mu^\dagger\right) \hat{\hat{n}}_q \tag{A.43}$$

and one obtains:

$$\left[\hat{\hat{n}}_q, \prod_{\mu=\nu+1}^{N_{\text{pair}}} \hat{S}_\mu^\dagger\right] = \sum_{\ell=\nu+1}^{N_{\text{pair}}} \frac{2\sqrt{w_q}\hat{\hat{b}}_q^\dagger}{(2\epsilon_q - E_{J_\ell})} \left(\prod_{\substack{\mu=\nu+1 \\ \neq \ell}}^{N_{\text{pair}}} \hat{S}_\mu^\dagger\right) \tag{A.44}$$

Consequently Eq. (A.40) becomes:

$$\begin{aligned}
&\sum_{\nu=1}^{N_{\text{pair}}} \left(\prod_{\eta=1}^{\nu-1} \hat{S}_\eta^\dagger\right) \hat{S}_0^\dagger G \sum_q^{\mathcal{N}} \frac{w_q \hat{\Omega}_q/2 \pm \hat{\hat{n}}_q}{2\epsilon_q - E_\nu} \left(\prod_{\mu=\nu+1}^{N_{\text{pair}}} \hat{S}_\mu^\dagger\right) \\
&= G \sum_{\nu=1}^{N_{\text{pair}}} \frac{w_q \hat{\Omega}_q/2}{2\epsilon_q - E_\nu} \hat{S}_0^\dagger \left(\prod_{\substack{\eta=1 \\ \neq \nu}}^{N_{\text{pair}}} \hat{S}_\eta^\dagger\right) \\
&\pm G \sum_{\nu=1}^{N_{\text{pair}}} \left(\prod_{\eta=1}^{\nu-1} \hat{S}_\eta^\dagger\right) \sum_q^{\mathcal{N}} \frac{\hat{S}_0^\dagger}{2\epsilon_q - E_\nu} \left(\prod_{\mu=\nu+1}^{N_{\text{pair}}} \hat{S}_\mu^\dagger\right) \hat{\hat{n}}_q \\
&\pm G \sum_{\nu=1}^{N_{\text{pair}}} \left(\prod_{\eta=1}^{\nu-1} \hat{S}_\eta^\dagger\right) \sum_{\ell=\nu+1}^{N_{\text{pair}}} \sum_q^{\mathcal{N}} \frac{2\sqrt{w_q}\hat{S}_0^\dagger \hat{\hat{b}}_q^\dagger}{(2\epsilon_q - E_\nu)(2\epsilon_q - E_{J_\ell})} \left(\prod_{\substack{\mu=\nu+1 \\ \neq \ell}}^{N_{\text{pair}}} \hat{S}_\mu^\dagger\right)
\end{aligned} \tag{A.45}$$

Inserting (A.39) and (A.45) into Eq. (A.38), one finds:

$$\begin{aligned}\left[\hat{H}, \prod_{\nu=1}^{N_{\text{pair}}} \hat{S}_\nu^\dagger\right] &= \sum_{\nu=1}^{N_{\text{pair}}} E_\nu \left(\prod_{\eta=1}^{N_{\text{pair}}} \hat{S}_\eta^\dagger\right) + \sum_{\nu=1}^{N_{\text{pair}}} \left(1 - \sum_q^{\mathcal{N}} \frac{G w_i \hat{\Omega}_q/2}{2\epsilon_q - E_\nu}\right) \hat{S}_0^\dagger \left(\prod_{\substack{\eta=1 \\ \neq\nu}}^{N_{\text{pair}}} \hat{S}_\eta^\dagger\right) \\ &\mp G \sum_{\nu=1}^{N_{\text{pair}}} \left(\prod_{\eta=1}^{\nu-1} \hat{S}_\eta^\dagger\right) \sum_q^{\mathcal{N}} \frac{\hat{S}_0^\dagger}{2\epsilon_q - E_\nu} \left(\prod_{\mu=\nu+1}^{N_{\text{pair}}} \hat{S}_\mu^\dagger\right) \hat{\tilde{n}}_q \\ &\mp G \sum_{\nu=1}^{N_{\text{pair}}} \left(\prod_{\eta=1}^{\nu-1} \hat{S}_\eta^\dagger\right) \sum_{\ell=\nu+1}^{N_{\text{pair}}} \sum_q^{\mathcal{N}} \frac{2\sqrt{w_q} \hat{S}_0^\dagger \hat{\tilde{b}}_q^\dagger}{(2\epsilon_q - E_\nu)(2\epsilon_q - E_{J_\ell})} \left(\prod_{\substack{\mu=\nu+1 \\ \neq\ell}}^{N_{\text{pair}}} \hat{S}_\mu^\dagger\right)\end{aligned} \tag{A.46}$$

Applying the commutator (A.46) on the vacuum state $|0\rangle$, and using: $\hat{H}|0\rangle = 0$, one obtains:

$$\begin{aligned}\hat{H}|\Psi_n\rangle &= E_n|\Psi_n\rangle + \sum_{\nu=1}^{N_{\text{pair}}} \left(1 - \sum_q^{\mathcal{N}} \frac{G w_q \left(\hat{\Omega}_q/2 \pm \nu_q\right)}{2\epsilon_q - E_\nu}\right) \hat{S}_0^\dagger \left(\prod_{\eta=1;\neq\nu}^{N_{\text{pair}}} \hat{S}_\eta^\dagger\right)|0\rangle \\ &\mp \sum_{\nu=1}^{N_{\text{pair}}} \left(\prod_{\eta=1}^{\nu-1} \hat{S}_\eta^\dagger\right) \sum_{\ell=\nu+1}^{N_{\text{pair}}} \sum_q^{\mathcal{N}} \frac{2G\sqrt{w_q} \hat{S}_0^\dagger \hat{\tilde{b}}_q^\dagger}{(2\epsilon_q - E_\nu)(2\epsilon_q - E_{J_\ell})} \left(\prod_{\substack{\mu=\nu+1 \\ \neq\ell}}^{N_{\text{pair}}} \hat{S}_\mu^\dagger\right)|0\rangle\end{aligned} \tag{A.47}$$

The summation over q in the last term can be rewritten as:

$$\begin{aligned}\frac{\hat{S}_\nu^\dagger - \hat{S}_{J_\ell}^\dagger}{E_\nu - E_{J_\ell}} &= \frac{1}{E_\nu - E_{J_\ell}} \sum_q^{\mathcal{N}} \left(\frac{\hat{\tilde{b}}_q^\dagger \sqrt{w_q}}{2\epsilon_q - E_\nu} - \frac{\hat{\tilde{b}}_q^\dagger \sqrt{w_q}}{2\epsilon_q - E_{J_\ell}}\right) \\ &= \sum_q^{\mathcal{N}} \frac{\hat{\tilde{b}}_q^\dagger \sqrt{w_q}}{(2\epsilon_q - E_\nu)(2\epsilon_q - E_{J_\ell})}\end{aligned} \tag{A.48}$$

Hence, the last term of Eq. (A.47) can be expressed as:

$$\begin{aligned}&\sum_{\nu=1}^{N_{\text{pair}}} \left(\prod_{\eta=1}^{\nu-1} \hat{S}_\eta^\dagger\right) \sum_{\ell=\nu+1}^{N_{\text{pair}}} \sum_q^{\mathcal{N}} \frac{2G\sqrt{w_q} \hat{S}_0^\dagger \hat{\tilde{b}}_q^\dagger}{(2\epsilon_q - E_\nu)(2\epsilon_q - E_{J_\ell})} \left(\prod_{\substack{\mu=\nu+1 \\ \neq\ell}}^{N_{\text{pair}}} \hat{S}_\mu^\dagger\right) \\ &= \sum_{\nu=1}^{N_{\text{pair}}} \left(\prod_{\eta=1}^{\nu-1} \hat{S}_\eta^\dagger\right) \sum_{\ell=\nu+1}^{N_{\text{pair}}} \frac{2G\hat{S}_0^\dagger \left(\hat{S}_\nu^\dagger - \hat{S}_\mu^\dagger\right)}{E_\nu - E_\mu} \left(\prod_{\substack{\mu=\nu+1 \\ \neq\ell}}^{N_{\text{pair}}} \hat{S}_\mu^\dagger\right)|0\rangle \\ &= \sum_{\nu=1}^{N_{\text{pair}}} \left(\sum_{\ell=\nu+1}^{N_{\text{pair}}} \frac{2G}{E_\nu - E_{J_\ell}}\right) \hat{S}_0^\dagger \left(\prod_{\substack{\eta=1 \\ \neq\ell}}^{N_{\text{pair}}} \hat{S}_\eta^\dagger\right)|0\rangle - \sum_{\nu=1}^{N_{\text{pair}}} \left(\sum_{\ell=\nu+1}^{N_{\text{pair}}} \frac{2G}{E_\nu - E_{J_\ell}}\right) \hat{S}_0^\dagger \left(\prod_{\substack{\eta=1 \\ \neq\nu}}^{N_{\text{pair}}} \hat{S}_\eta^\dagger\right)|0\rangle\end{aligned} \tag{A.49}$$

If we consider the Heavyside function $H(\nu - \mu)$ and the function $f(\mu, \nu)$, where μ and ν are two integer parameters, then:

$$\sum_{\mu=1;\neq\nu}^{N_{\text{pair}}} f(\mu,\nu) H(\nu-\mu) = \sum_{\mu=1}^{N_{\text{pair}}} \sum_{\nu=\mu+1}^{N_{\text{pair}}} f(\mu,\nu) = \sum_{\nu=1}^{N_{\text{pair}}} \sum_{\mu=1}^{\nu-1} f(\mu,\nu) \tag{A.50}$$

Using this property, one can do the following modification of indices involved in the sums in the first term of Eq. (A.49):

$$\begin{aligned}
&\sum_{\nu=1}^{N_{\text{pair}}}\left(\prod_{\eta=1}^{\nu-1}\hat{S}_\eta^\dagger\right)\sum_{\ell=\nu+1}^{N_{\text{pair}}}\sum_{q}^{\mathcal{N}}\frac{2G\sqrt{w_q}\hat{S}_0^\dagger\hat{\tilde{b}}_q^\dagger}{(2\epsilon_q-E_\nu)(2\epsilon_q-E_{J_\ell})}\left(\prod_{\substack{\mu=\nu+1\\ \neq\ell}}^{N_{\text{pair}}}\hat{S}_\mu^\dagger\right)\\
&=\sum_{\mu=1}^{N_{\text{pair}}}\left(\sum_{\nu=1}^{\mu-1}\frac{2G}{E_\nu-E_\mu}\right)\hat{S}_0^\dagger\left(\prod_{\substack{\eta=1\\ \neq\nu}}^{N_{\text{pair}}}\hat{S}_\eta^\dagger\right)|0\rangle-\sum_{\nu=1}^{N_{\text{pair}}}\left(\sum_{\mu=\nu+1}^{N_{\text{pair}}}\frac{2G}{E_{\nu-E_\mu}}\right)\hat{S}_0^\dagger\left(\prod_{\substack{\eta=1\\ \neq\nu}}^{N_{\text{pair}}}\hat{S}_\eta^\dagger\right)|0\rangle\\
&=\sum_{\nu=1}^{N_{\text{pair}}}\left(\sum_{\substack{\mu=1\\ \neq\nu}}^{N_{\text{pair}}}\frac{2G}{E_\mu-E_\nu}\right)\hat{S}_0^\dagger\left(\prod_{\substack{\eta=1\\ \neq\nu}}^{N_{\text{pair}}}\hat{S}_\mu^\dagger\right)|0\rangle
\end{aligned}\tag{A.51}$$

As $\hat{H}|\Psi\rangle = E|\Psi\rangle$, one obtains from (A.47) the generalized Richardson equations (A.52) for the pair energies of the discretized pairing Hamiltonian in the Berggren basis:

$$1\pm 2G\sum_{q}^{\mathcal{N}}\frac{w_q d_q}{2\epsilon_q-E_\nu}\mp\sum_{\mu\neq\nu}^{N_{\text{pair}}}\frac{2G}{E_\mu-E_\nu}=0\tag{A.52}$$

with $d_q = \Omega_q/4 \pm \nu_q/2$.

A.3 Initial conditions for solving the generalized Richardson equations

Initial conditions are essential to solve numerically the generalized Richardson equations (2.99). They are usually determined by considering the solution for pair energies in the weak coupling limit ($G \ll 1$):

$$\lim_{G\to 0} E_i = 2\epsilon_q \qquad i=1,\ldots,N_{\text{pair}}\ ; \qquad q=1,\ldots,\mathcal{N}\tag{A.53}$$

In the case of one pair per level ($\Omega = 2$) and $G << 1$, the generalized Richardson equations (2.99) become:

$$1\pm\frac{2Gd_q}{2\epsilon_q-E_q}=0 \qquad q=1,\ldots,\mathcal{N}\tag{A.54}$$

The solution of Eq. (A.54):

$$E_q = 2\epsilon_q \pm 2Gd_q w_q$$

provides a good starting point for solving the generalized Richardson equations (2.99) using the Newton-Raphson procedure in the case of one pair of particles (bosons or fermions) per level.

In the case of two pairs of particles ($i = 1, 2$) on a s.p. level q, the boundary conditions in the weak coupling limit $G \ll 1$ are:

$$\lim_{G\to 0} E_1 = \lim_{G\to 0} E_2 = 2\epsilon_q\tag{A.55}$$

where E_1 and E_2 are the energies of the two pairs being on the same s.p. level at $G = 0$. In such a case, generalized Richardson equations (2.99) become:

$$\begin{cases} 1 \pm \dfrac{2Gd_q}{2\epsilon_q - E_1} \mp \dfrac{2G}{E_2 - E_1} = 0 \\ 1 \pm \dfrac{2Gd_q}{2\epsilon_q - E_2} \mp \dfrac{2G}{E_1 - E_2} = 0 \end{cases} \tag{A.56}$$

One can rewrite them in the following form:

$$\begin{cases} -(E_1 - E_2)^2 \mp 2G(4\epsilon_q - E_1 - E_2) = 0 \\ (4\epsilon_q - E_1 - E_2) \pm 4Gd_q \pm 2G = 0 \end{cases} \tag{A.57}$$

Eqs. (A.57) can be linearized:

$$\begin{cases} \lambda_- \mp 2G\lambda_+ = 0 \\ \lambda_+ \pm 4Gd_q \pm 2G = 0 \end{cases} \tag{A.58}$$

in variables:

$$\lambda_+ = 4\epsilon_q - E_1 - E_2 \quad \text{and} \quad \lambda_- = (E_1 - E_2)^2 \ .$$

The solutions for λ_+ and λ_- are:

$$\begin{aligned} \lambda_+ &= \mp 4Gd_q \mp 2G \\ \lambda_- &= -8G^2 d_q - 4G^2 \end{aligned} \tag{A.59}$$

and hence the expression for E_1 and E_2 in the weak coupling limit is:

$$\begin{aligned} E_1 &= 2\epsilon_q - \frac{1}{2}(\lambda_+ - \sqrt{\lambda_-}) \\ E_2 &= 2\epsilon_q - \frac{1}{2}(\lambda_+ + \sqrt{\lambda_-}) \end{aligned} \tag{A.60}$$

A.4 Normalization of scattering states including the Coulomb potential

A.4.1 Partial overlap integral

The radial Schrödinger equation for a spherical non-local potential reads:

$$u''_k(r) = \left(\frac{\ell(\ell+1)}{r^2} + v(r) - k^2 \right) u_k(r) + \int_0^{+\infty} w(r, r') u_k(r') \, dr' \tag{A.61}$$

where ℓ is the orbital angular momentum, $v(r)$ is the local part of the potential and $w(r, r')$ its non-local part. In the asymptotic region, one demands:

$$v(r) = \frac{\alpha}{r} \qquad \text{for} \quad r > R_{\text{pot}} \tag{A.62}$$

$$w(r, r') = 0 \qquad \text{for} \quad r > R_{\text{pot}} \quad \text{or} \quad r' > R_{\text{pot}} \tag{A.63}$$

where α is real and $R_{\text{pot}} > 0$. These conditions are always satisfied in practice.

Let us consider two different linear momenta $k_a > 0$ and $k_b > 0$, and a radius $R > R_{\text{pot}}$. Eq. (A.61) provides the overlap of u_{k_a} and u_{k_b} in $[0:R]$. After simple manipulations, one obtains:

$$\int_0^R \left[u''_{k_b}(r)u_{k_a}(r) - u''_{k_a}(r)u_{k_b}(r)\right] dr = \\ (k_a^2 - k_b^2)\int_0^R u_{k_a}(r)u_{k_b}(r)dr + \int_0^R \int_0^R w(r,r')\left[u_{k_b}(r')u_{k_a}(r) - u_{k_a}(r')u_{k_b}(r)\right] dr'dr \tag{A.64}$$

As $w(r,r')$ is symmetric in r and r', the integral involving $w(r,r')$ in Eq. (A.64) vanishes identically. Hence, integrating the l.h.s. of Eq. (A.64) and using the fact that $u_{k_a}(0) = u_{k_b}(0) = 0$, one obtains:

$$I_{ab}(R) \equiv \int_0^R u_{k_a}(r)u_{k_b}(r)\ dr = \frac{u'_{k_b}(R)u_{k_a}(R) - u'_{k_a}(R)u_{k_b}(R)}{k_a^2 - k_b^2} \tag{A.65}$$

$I_{ab}(R)$ will be shown in Appendix A.4.3 and A.4.4 to converge weakly to a Dirac delta.

A.4.2 Asymptotic expression of partial overlap integral

From Eqs. (A.62) and (A.63), $u_{k(R)}$ is equal to a linear combination of incoming and outgoing Coulomb wave functions:

$$u_k(R) = C_k^+ H^+(\ell,\eta,kR) + C_k^- H^-(\ell,\eta,kR) \tag{A.66}$$

where $\eta = \alpha/k$ is the Sommerfeld parameter, and $C_k^\pm$ are fixed up to an overall factor to be determined.

$H^\pm(\ell,\eta,kR)$, $u_{k(R)}$ and its derivative have simple analytical form in the asymptotic region :

$$H^\pm(\ell,\eta,kR) = e^{\pm i(kR - \eta_k \ln(2kR) - \ell\frac{\pi}{2} + \sigma_\ell(\eta))} + O\left(\frac{1}{R}\right) \tag{A.67}$$

$$\left[\frac{dH^\pm(\ell,\eta,kr)}{dr}\right]_{r=R} = \pm ik\ e^{\pm i(kR - \eta_k \ln(2kR) - \ell\frac{\pi}{2} + \sigma_\ell(\eta))} + O\left(\frac{1}{R}\right) \tag{A.68}$$

where $\sigma_\ell(\eta)$ is the Coulomb phase shift. The asymptotic form of $u_k(R)$ and $u_{k'}(R)$ derive from Eqs. (A.66), (A.67),(A.68):

$$u_k(R) = C_k \sin(kR - \eta_k \ln(2kR) + \delta_k) + O\left(\frac{1}{R}\right) \tag{A.69}$$

$$u'_k(R) = C_k k \cos(kR - \eta_k \ln(2kR) + \delta_k) + O\left(\frac{1}{R}\right), \tag{A.70}$$

where $C_k^2 = 4C_k^+C_k^-$, and δ_k is the phase shift associated to $u_k(r)$, which verifies

$$e^{2i\delta_k} = -C_k^+/C_k^-$$

Note that C_k and δ_k are real.

Inserting Eqs. (A.69) and (A.70) in Eq. (A.65), one obtains:

$$\begin{aligned}
I_{ab}(R) &= C_{k_a}C_{k_b}\frac{k_b\sin(k_aR-\eta_{k_a}\ln(2k_aR)+\delta_{k_a})\cos(k_bR-\eta_{k_b}\ln(2k_bR)+\delta_{k_b})}{(k_a-k_b)(k_a+k_b)}\\
&- C_{k_a}C_{k_b}\frac{k_a\cos(k_aR-\eta_{k_a}\ln(2k_aR)+\delta_{k_a})\sin(k_bR-\eta_{k_b}\ln(2k_bR)+\delta_{k_b})}{(k_a-k_b)(k_a+k_b)}+O\left(\frac{1}{R}\right)\\
&= C_{k_a}C_{k_b}\frac{k_a\sin((k_b-k_a)R-\eta_{k_b}\ln(2k_bR)+\eta_{k_a}\ln(2k_aR)+\delta_{k_b}-\delta_{k_a})}{(k_b-k_a)(k_a+k_b)}\\
&- C_{k_a}C_{k_b}\frac{\sin((k_a+k_b)R-\eta_{k_a}\ln(2k_aR)-\eta_{k_b}\ln(2k_bR)+\delta_{k_a}+\delta_{k_b})}{2(k_a+k_b)}\\
&+ C_{k_a}C_{k_b}\frac{\sin((k_b-k_a)R-\eta_{k_b}\ln(2k_bR)+\eta_{k_a}\ln(2k_aR)+\delta_{k_b}-\delta_{k_a})}{2(k_a+k_b)}+O\left(\frac{1}{R}\right)\\
&= C_{k_a}C_{k_b}\frac{k_a\sin(\Delta_kR+\beta_{ab}\Delta_k\ln(R)+f_-(k_a,k_b))}{\Delta_k\ (k_a+k_b)}\\
&- C_{k_a}C_{k_b}\frac{\sin((k_a+k_b)R-(\eta_{k_a}+\eta_{k_b})\ln(R)+f_+(k_a,k_b))}{2(k_a+k_b)}\\
&+ C_{k_a}C_{k_b}\frac{\sin(\Delta_kR+\beta_{ab}\Delta_k\ln(R)+f_-(k_a,k_b))}{2(k_a+k_b)}+O\left(\frac{1}{R}\right)
\end{aligned}$$

and finally:

$$\begin{aligned}
I_{ab}(R) &= C_{k_a}C_{k_b}\frac{\sin(\Delta_kR+\beta_{ab}\Delta_k\ln(R))}{2\Delta_k}\\
&+ C_{k_a}C_{k_b}\sin(\Delta_kR+\beta_{ab}\Delta_k\ln(R))\left(k_a\frac{\cos(f_-(k_a,k_b))}{\Delta_k\ (k_a+k_b)}-\frac{1}{2\Delta_k}\right)\\
&+ C_{k_a}C_{k_b}\cos(\Delta_kR+\beta_{ab}\Delta_k\ln(R))\left(k_a\frac{\sin(f_-(k_a,k_b))}{\Delta_k\ (k_a+k_b)}\right)\\
&- C_{k_a}C_{k_b}\frac{\sin((k_a+k_b)R-(\eta_{k_a}+\eta_{k_b})\ln(R)+f_+(k_a,k_b))}{2(k_a+k_b)}\\
&+ C_{k_a}C_{k_b}\frac{\sin(\Delta_kR+\beta_{ab}\Delta_k\ln(R)+f_-(k_a,k_b))}{2(k_a+k_b)}+O\left(\frac{1}{R}\right),
\end{aligned}\tag{A.71}$$

where:

$$\begin{aligned}
\Delta_k &= k_b-k_a\\
\beta_{ab} &= \frac{\alpha}{k_ak_b}\\
f_\pm(k_a,k_b) &= \mp\eta_{k_a}\ln(2k_a)-\eta_{k_b}\ln(2k_b)+\delta_{k_b}\pm\delta_{k_a}.
\end{aligned}\tag{A.72}$$

The five terms which enter Eq. (A.71) are denoted respectively as $J^{(i)}_{ab}(\Delta_k,R)$, $i\in\{1,2,3,4,5\}$. Only $J^{(1)}_{ab}(\Delta_k,R)$ provides a Dirac delta if $R\to+\infty$. All the other terms will be shown to vanish in this limit.

A.4.3 Generalized Riemann-Lebesgue lemma

We will formulate the generalization of the Riemann-Lebesgue lemma in the case if R enters integrated functions logarithmically. The generalized lemma will be then used to prove that all terms not leading to a Dirac delta vanish for $R \to +\infty$.

Let us consider a differentiable function $f_R(k)$ defined for $k \in [k_{\min} : k_{\max}]$, and verifying:

$$\begin{aligned} &|f_R(k)| = O\left(\ln^n(R)\right) \qquad \forall k \\ &\int_{k_{\min}}^{k_{\max}} |f'_R(k)|\, dk = O\left(\ln^n(R)\right) \end{aligned} \tag{A.73}$$

where n is an integer which can be the same for $f_R(k)$ and $f_{R'}(k)$. Integration by parts provides:

$$\int_{k_{\min}}^{k_{\max}} f_R(k)\, e^{ikR}\, dk = \frac{1}{iR}\left(\left[f_R(k)\, e^{ikR}\right]_{k_{\min}}^{k_{\max}} - \int_{k_{\min}}^{k_{\max}} f'_R(k)\, e^{ikR}\, dk\right) \tag{A.74}$$

Thus, majoring Eq. (A.74), one obtains:

$$\begin{aligned} \left|\int_{k_{\min}}^{k_{\max}} f_R(k)\, e^{ikR}\, dk\right| &\leq \frac{1}{R}\left(|f_R(k_{\min})| + |f_R(k_{\max})| + \int_{k_{\min}}^{k_{\max}} |f'_R(k)|\, dk\right) \\ &= O\left(\frac{\ln^n(R)}{R}\right) \to 0 \end{aligned} \tag{A.75}$$

A.4.4 Weak convergence of the overlap to a Dirac delta

In order to show that $I_{ab}(R)$ converges to a Dirac delta, we will integrate $I_{ab}(R)$ with a smooth test function $F(\Delta_k)$ of a compact support: $\Delta_k \in [\Delta_{k_{\min}} : \Delta_{k_{\max}}]$, where $-k_a < \Delta_{k_{\min}} < 0$ and $\Delta_{k_{\max}} > 0$ (These conditions are consistent with the requirements $k_a > 0$ (fixed) and $k_b > 0$.):

$$I_F(R) = \int_{\Delta_{k_{\min}}}^{\Delta_{k_{\max}}} F(\Delta_k) I_{ab}(R)\, d\Delta_k = \sum_{i=1}^{5} \int_{\Delta_{k_{\min}}}^{\Delta_{k_{\max}}} F(\Delta_k) J^{(i)}(\Delta_k, R)\, d\Delta_k \tag{A.76}$$

Integrals involving $J_{ab}^{(i)}(\Delta_k, R)$ for $i \geq 2$ in Eq. (A.76) can be written as the real or imaginary part of $\int_{\Delta_{k_{\min}}}^{\Delta_{k_{\max}}} f_R^{(i)}(\Delta_k)\, e^{i\Delta_k R}\, d\Delta_k$, where:

$$\begin{aligned} f_R^{(2)}(\Delta_k) &= C_{k_a} C_{k_b} e^{i\beta_{ab}\Delta_k \ln(R)} \left(k_a \frac{\cos(f_-(k_a, k_b))}{\Delta_k\ (k_a + k_b)} - \frac{1}{2\Delta_k}\right) \\ f_R^{(3)}(\Delta_k) &= C_{k_a} C_{k_b} e^{i\beta_{ab}\Delta_k \ln(R)} \left(\frac{\sin(f_-(k_a, k_b))}{\Delta_k\ (k_a + k_b)}\right) \\ f_R^{(4)}(\Delta_k) &= C_{k_a} C_{k_b} e^{2ik_a R - i(\eta_{k_a} + \eta_{k_b})\ln(R)} \left(\frac{e^{if_+(k_a, k_b))}}{2(k_a + k_b)}\right) \\ f_R^{(5)}(\Delta_k) &= C_{k_a} C_{k_b} e^{i\beta_{ab}\Delta_k \ln(R)} \left(\frac{e^{if_-(k_a, k_b)}}{2(k_a + k_b)}\right) \end{aligned} \tag{A.77}$$

One can check from Eq. (A.77) that $f_R^{(i)}(\Delta_k)$ always verifies Eq. (A.73) for $i \geq 2$. Consequently, from the generalized Riemann-Lebesgue lemma (see Appendix A.4.3) one finds that integrals involving $J_{ab}^{(i)}(\Delta_k, R)$ for $i \geq 2$ in Eq. (A.76) vanish for $R \to +\infty$.

In the integral involving $J^{(1)}_{ab}(\Delta_k, R)$, let us expand the sine function in products of sine and cosine functions:

$$\begin{aligned}\int_{\Delta_{k_{\min}}}^{\Delta_{k_{\max}}} F(\Delta_k) J^{(1)}(\Delta_k, R)\, d\Delta_k &= \frac{C_{k_a} C_{k_b}}{2} \int_{\Delta_{k_{\min}}}^{\Delta_{k_{\max}}} F(\Delta_k) \sin(\Delta_k R)\ \cos(\beta_{ab} \Delta_k \ln(R))\ \frac{d\Delta_k}{\Delta_k} \\ &+ \frac{C_{k_a} C_{k_b}}{2} \int_{\Delta_{k_{\min}}}^{\Delta_{k_{\max}}} F(\Delta_k) \cos(\Delta_k R)\ \sin(\beta_{ab} \Delta_k \ln(R))\ \frac{d\Delta_k}{\Delta_k}\end{aligned} \tag{A.78}$$

The second integral of Eq. (A.78) is a real part of:

$$\int_{\Delta_{k_{\min}}}^{\Delta_{k_{\max}}} F(\Delta_k) e^{i\Delta_k R}\ \sin(\beta_{ab} \Delta_k \ln(R))\ \frac{d\Delta_k}{\Delta_k} \tag{A.79}$$

This integral vanishes if $R \to +\infty$:

$$f_R(\Delta_k) = F(\Delta_k) \sin(\beta_{ab} \Delta_k \ln(R))/\Delta_k$$

because the function $f_R(\Delta_k)$ verifies Eq. (A.73).

The first integral of Eq. (A.78) is a real part of the integral:

$$I^{(c)}_F(R) = \frac{C_{k_a} C_{k_b}}{2} \int_{\Delta_{k_{\min}}}^{\Delta_{k_{\max}}} F(\Delta_k) \sin(\Delta_k R)\ e^{i\beta_{ab} \Delta_k \ln(R)}\ \frac{d\Delta_k}{\Delta_k} \tag{A.80}$$

To determine the limit of $I^{(c)}_F(R)$ for $R \to +\infty$, we introduce the function $G_R(\Delta_k)$:

$$F(\Delta_k) = [F(0) U(\Delta_k) + \Delta_k G_R(\Delta_k)]\, e^{-i\beta_{ab} \Delta_k \ln(R)}\ , \tag{A.81}$$

where $U(\Delta_k) = 1$ for $\Delta_k \in [\Delta_{k_{\min}} : \Delta_{k_{\max}}]$, and $U(\Delta_k) = 0$ elsewhere. Then, from Eqs. (A.80), (A.81), one finds that $I^{(c)}_F(R)$ becomes:

$$\begin{aligned} I^{(c)}_F(R) &= \frac{C_{k_a} C_{k_b}}{2} \left(F(0) \int_{\Delta_{k_{\min}}}^{\Delta_{k_{\max}}} \sin(\Delta_k R)\ \frac{d\Delta_k}{\Delta_k} + \int_{\Delta_{k_{\min}}}^{\Delta_{k_{\max}}} G_R(\Delta_k)\ \sin(\Delta_k R)\ d\Delta_k \right) \\ &= \frac{C_{k_a} C_{k_b}}{2} \left(F(0) \int_{\Delta_{k_{\min}} R}^{\Delta_{k_{\max}} R} \sin(x)\ \frac{dx}{x} + \int_{\Delta_{k_{\min}}}^{\Delta_{k_{\max}}} G_R(\Delta_k)\ \sin(\Delta_k R)\ d\Delta_k \right) \end{aligned} \tag{A.82}$$

where a change of variable has been effected in the first integral.

The first integral of Eq. (A.82) clearly has π as a limit when $R \to +\infty$. The second integral in Eq. (A.82) equals:

$$\frac{1}{2i} \left(\int_{\Delta_{k_{\min}}}^{\Delta_{k_{\max}}} G_R(\Delta_k)\ e^{i\Delta_k R}\ d\Delta_k - \int_{\Delta_{k_{\min}}}^{\Delta_{k_{\max}}} G_R(\Delta_k)\ e^{-i\Delta_k R}\ d\Delta_k \right) \tag{A.83}$$

By reversing and deriving Eq. (A.81), we can show that the function $G_R(\Delta_k)$ has the same properties as the function $f_R(\Delta_k)$ in Eq. (A.73). Thus, the integrals in Eq. (A.83) vanish if $R \to +\infty$.

We can now evaluate the limit of $I_{ab}(R)$ (Eq. (A.71)) when $R \to +\infty$:

$$I_{ab}(R) \to \frac{\pi}{2} C^2_{k_a} \delta(k_a - k_b) \tag{A.84}$$

and obtain (see Eq. (A.65)):

$$\int_0^{+\infty} u_{k_a}(r)u_{k_b}(r)\ dr = \frac{\pi}{2}C_{k_a}^2\delta(k_a - k_b) = 2\pi C_{k_a}^+ C_{k_a}^-\delta(k_a - k_b) \tag{A.85}$$

The Dirac delta normalization arises from the following equality:

$$\int_0^{+\infty} u_{k_a}(r)u_{k_b}(r)\ dr = \delta(k_a - k_b) \Leftrightarrow 2\pi C_k^+ C_k^- = 1 \qquad \forall u_k \tag{A.86}$$

A.5 Solution of Faddeev equation using Berggren basis

Berggren basis, due to its completeness properties, can be used to solve the reaction problems represented by the Faddeev equation. Its Hamiltonian and Schrödinger equation read:

$$H\,|\Psi\rangle = E\,|\Psi\rangle \tag{A.87}$$

$$H = H_{\mathrm{P}} + \frac{\vec{P}^2}{2\mu_{\mathrm{T}}} + V_{\mathrm{S}} \tag{A.88}$$

where H_{P} is the intrinsic Hamiltonian of the projectile, $\vec{P}$ is the linear momentum of the c.m. of the projectile with respect to the target, μ_{T} is the reduced mass of the target and V_{S} is a potential describing the scattering of the projectile subsystems away from the target.

Let us consider Berggren basis associated with the intrinsic Hamiltonian H_{P} of the projectile:

$$H_{\mathrm{P}}\,|\Phi_{\mathrm{P}}\rangle = e_{\mathrm{P}}\,|\Phi_{\mathrm{P}}\rangle \tag{A.89}$$

In the case of a three-body problem, whereby the projectile bears two subsystems, H_{P} in Eq. (A.89) becomes a one-body Hamiltonian:

$$H_{\mathrm{P}} = \frac{\vec{p}^2}{2\mu_{\mathrm{P}}} + V_{\mathrm{P}}(r) \tag{A.90}$$

where r is the intrinsic radius, $\vec{p}$ the intrinsic linear momentum, μ_{P} the reduced mass of the projectile, and $V_{\mathrm{P}}(r)$ the intrinsic interaction of the projectile. In this case, $|\Phi_{\mathrm{P}}\rangle$ is a one-body Berggren basis state, which is straightforward to calculate.

In the continuum discretized CC method, the scattering states $|\Phi_{\mathrm{P}}\rangle$ are dealt with the bin states, obtained by integrating scattering states on finite energy interval. In this way, one obtains a basis of discrete bound states. It is however not necessary to use this procedure if one works with the Berggren basis, as one would consider scattering states $|\Phi_{\mathrm{P}}\rangle$ of a fixed energy. Such a method is already used in the mid point method, where one takes the middle energy of the considered bin to define $|\Phi_{\mathrm{P}}\rangle$. However, the energies would hereby be determined with a Gauss-Legendre quadrature, so that one would expect a much better precision for a fixed number of discretized scattering states.

The standard method of solving Eq. (A.87) is to expand $|\Psi\rangle$ in a basis of intrinsic and c.m. projectile states:

$$|\Psi\rangle = \sum_n |\Phi_{\mathrm{P}}^{(n)}\rangle\,|\Psi^{(n)}\rangle \tag{A.91}$$

where $|\Phi_{\rm P}^{(n)}\rangle$ is an eigenstate of $H_{\rm P}$ and $|\Psi^{(n)}\rangle$ is a c.m. projectile state verifying the equation:

$$\left(\frac{\vec{P}^2}{2\mu_{\rm T}} + V_{nn}(\vec{R}) - E_n\right)\Psi^{(n)}(\vec{R}) + \sum_{n'\neq n} V_{nn'}(\vec{R})\Psi^{(n')}(\vec{R}) = 0 \tag{A.92}$$

$$V_{nn'}(\vec{R}) = \langle\Phi_{\rm P}^{(n')}|V_{\rm S}|\Phi_{\rm P}^{(n)}\rangle \tag{A.93}$$

where $\vec{R}$ is the space coordinate of the c.m. of the projectile with respect to the target, and $E_n = E - e_n$. Expanding $\Psi^{(n)}(\vec{R})$ in partial waves, one obtains the set of CC equations which must be solved to obtain $|\Psi\rangle$:

$$\Psi^{(n)}(\vec{R}) = \sum_L i^L \chi_a(R) Y_L(\Omega_R) \tag{A.94}$$

$$\left[-\frac{\hbar^2}{2\mu_{\rm T}}\left(\frac{d^2}{dR^2} - \frac{L(L+1)}{R^2}\right) + V_{aa}^J(R) - E_n\right]\chi_a^J(R) + \sum_{a'\neq a} i^{L'-L} V_{aa'}(R)\chi_{a'}(R) = 0 \tag{A.95}$$

$$V_{aa'}(R) = \langle\left[\Phi_{\rm P}^{(n')}Y'_L\right]_J|V_{\rm S}|\left[\Phi_{\rm P}^{(n)}Y_L\right]_J\rangle \tag{A.96}$$

where J is the total angular momentum of the system and a represents different quantum numbers associated to the total system.

As Eq. (A.95) has the same form as Eq. (3.100), it can be solved with the Green's function method described in Sec. (3.3.5). As this method replaces the direct integration of CC equations by a linear system, it should be more efficient, insofar as the number of channels in Faddeev equations is usually very large. If we have more than two subsystems in the projectile, Eq. (A.89) becomes a many-body problem which can be solved by the GSM as well.

Bibliography

[1] E. Rutherford, Philosophical Magazine. Series 6, vol.**21** (1911) .

[2] P. Navrátil, J.P. Vary and B.R. Barrett, Phys. Rev. Lett. **84**, 5728 (2000) .

[3] P. Navrátil, J.P. Vary and B.R. Barrett, Phys. Rev. C **62**, 054311 (2000) .

[4] P. Navrátil et al., J. Phys. G : Nucl. Part. Phys. **36**, 083101 (2009) .

[5] N. Michel et al., Phys. Rev. Lett. **89**, 042502 (2002) .

[6] R. Id Betan et al., Phys. Rev. Lett. **89**, 042501 (2002) .

[7] N. Michel et al., J. Phys. G: Nucl. Part. Phys. **36**, 013101 (2009) .

[8] S. Quaglioni and P. Navrátil, Phys. Rev. Lett. **101**, 092501 (2008) .

[9] S. Quaglioni and P. Navrátil, Phys. Rev. C **79**, 044606 (2009) .

[10] G. Papadimitriou et al., Phys. Rev. C **88**, 044318 (2013) .

[11] S. Baroni et al., Phys. Rev. Lett. **110**, 022505 (2013) .

[12] S. Baroni et al., Phys. Rev. C **87**, 034326 (2013) .

[13] D. Lee, Prog. Part. Nucl. **63**, 117 (2009) .

[14] E. Epelbaum et al., Phys. Rev. Lett. **106**, 192501 (2011) .

[15] E. Epelbaum et al., Phys. Rev. Lett. **109**, 252501 (2012) .

[16] J. Dobaczewski, Journal of Physics: Conference Series **312**, section 9, 092002 (2011) .

[17] K. Bennaceur et al., Phys. Lett. B **488**, 75 (2000) .

[18] K. Bennaceur et al., Nucl. Phys. A **651**, 289 (1999) .

[19] K. Bennaceur et al., Nucl. Phys. A **671**, 203 (2000) .

[20] R. Chatterjee, J. Okołowicz and M. Płoszajczak, Nucl. Phys. A **764**, 528 (2006) .

[21] G. Hagen et al., Phys. Lett. B **656**, 169 (2007) .

[22] G. Hagen, T. Papenbrock and M. Hjorth-Jensen, Phys. Rev. Lett. **104**, 182501 (2010) .

[23] G. Hagen et al., Phys. Rev. Lett. **108**, 242501 (2012) .

[24] G. Hagen and N. Michel, Phys. Rev. C **86**, 021602(R) (2012) .

[25] G. Hagen et al., Rep. Prog. Phys. **77**, 096302 (2014) .

[26] J. Rotureau et al., Phys. Rev. Lett. **97**, 110603 (2006) .

[27] J. Rotureau et al., Phys. Rev. C **79**, 014304 (2009) .

[28] O. Legeza et al., Phys. Rev. C **92**, 051303 (2015) .

[29] R. Machleidt and D.R. Entem, Phys. Rep. **503**, 1 (2011) .

[30] S.K. Bogner, R.J. Furnstahl and R.J. Perry, Phys. Rev. C **75**, 061001 (2007) .

[31] K. Tsukiyama, S.K. Bogner and A. Schwenk, Phys. Rev. Lett. **106**, 222502 (2011) .

[32] K. Tsukiyama, S.K. Bogner and A. Schwenk, Phys. Rev. C **85**, 061304 (2012) .

[33] H. Hergert et al., Phys. Rep. **621**, 165 (2016) .

[34] H.W. Barz, I. Rotter and J. Höhn, Nucl. Phys. A **275**, 111 (1977) .

[35] I. Rotter, H.W. Barz and J. Höhn, Nucl. Phys. A **297**, 237 (1978) .

[36] R.J. Philpott, Nucl. Phys. A **289**, 109 (1977) .

[37] D. Halderson and R.J. Philpott, Nucl. Phys. A **321**, 295 (1979) .

[38] I. Rotter, Rep. Prog. Phys. **54**, 635 (1991) .

[39] H.W. Barz, I. Rotter and J. Höhn, Phys. Lett. B **37**, 4 (1971) .

[40] D. Halderson and R.J. Philpott, Nucl. Phys. A **359**, 365 (1981) .

[41] A. Volya and V. Zelevinsky, Phys. Rev. C **74**, 064314 (2006) .

[42] H. Feshbach, Ann. Phys. **5**, 357 (1958) .

[43] H. Feshbach, Ann. Phys. **19**, 287 (1962) .

[44] T. Berggren, Nucl. Phys. A **109**, 265 (1968) .

[45] T. Berggren, Phys. Lett. B **73**, 389 (1978) .

[46] T. Berggren, Phys. Lett. C **373**, 1 (1996) .

[47] I.M. Gel'fand et al., Generalized functions (New York : Academic, 1964).

[48] K. Maurin, Generalized eigenfunction expansions and unitary representations of topological groups (Warsaw: Polish Scientific Publishers, 1968).

[49] A. Böhm, M. Gadella and S. Maxson, Computers Math. Applic. **34**, 427 (1997) .

[50] G. Ortiz et al., Nucl. Phys. B **707**, 421 (2005) .

[51] R.W. Richardson, Phys. Lett. **3**, 277 (1963) .

[52] R.W. Richardson and N. Sherman, Nucl. Phys. **52**, 221 (1964) .

[53] W.M. Elsasser, J. Phys. Radium **4**, 549 (1933) .

[54] W.M. Elsasser, J. Phys. Radium **5**, 389 (1934) .

[55] W.M. Elsasser, J. Phys. Radium **5**, 635 (1934) .

[56] E. Gapon and D. Iwanenko, Naturwissenschaften **20**, 792 (1932) .

[57] H.A. Bethe and R.F. Bacher, Rev. Mod. Phys. **8**, 82 (1936) .

[58] M. Goeppert-Mayer, Phys. Rev. **74**, 235 (1948) .

[59] M. Goeppert-Mayer, Phys. Rev. **75**, 1969 (1949) .

[60] J.H.D. Jensen, O. Haxel and H.E. Suess, Phys. Rev. **75**, 1766 (1949) .

[61] A.M. Lane, Proc. Phys. Soc. A **68**, 189 (1955) .

[62] D. Kurath, Phys. Rev. **101**, 216 (1956) .

[63] D.H. Wilkinson, Proc. Robert A. Welsh Foundation Conf. Chemical Research. I. The Structure of the Nucleis (p.13, Houston, Texas, 1957).

[64] K.A. Brueckner, Phys. Rev. **96**, 508 (1954) .

[65] J.P. Eliott and A.M. Lane, Handbuch der Physik XXXIX (Springer Verlag, Berlin, 1957).

[66] E. Caurier et al., Rev. Mod. Phys. **77**, 427 (2005) .

[67] B.A. Brown, Prog. Part. Nucl. Phys. **47**, 517 (2001) .

[68] B.R. Barrett, P. Navrátil and J.P. Vary, Prog. Part. Nucl. Phys. **69**, 131 (2013) .

[69] D.J. Dean and M. Horth-Jensen, Phys. Rev. C **69**, 054320 (2004) .

[70] R.J. Bartlett and M. Musial, Rev. Mod. Phys. **79**, 291 (2007) .

[71] C. Barbieri and W.H. Dickhoff, Phys. Rev. C **63**, 034313 (2001) .

[72] C. Barbieri and W.H. Dickhoff, Phys. Rev. C **65**, 064313 (2002) .

[73] Y. Dewulf, D. van Neck and M. Waroquier, Phys. Rev. C **65**, 054316 (2002) .

[74] C. Barbieri and W.H. Dickhoff, Phys. Rev. C **68**, 014311 (2003) .

[75] Y. Dewulf et al., Phys. Rev. Lett. **90**, 152501 (2003) .

[76] D. van Neck, S. Rombouts and S. Verdonck, Phys. Rev. C **72**, 054318 (2003) .

[77] C. Barbieri, Phys. Lett. B **643**, 268 (2006) .

[78] C. Mahaux and H.A. Weidenmüller, Shell-model approach to nuclear reactions (North-Holland Pub. Co., 1969).

[79] V.I. Goldanskii, JETP **39**, 497 (1960) .

[80] B. Blank and M. Płoszajczak, Rep. Prog. Phys. **71**, 046301 (2008) .

[81] J. Giovinazzo et al., Phys. Rev. Lett. **89**, 102501 (2002) .

[82] M. Pfützner, Phys. J. A **14**, 279 (2002) .

[83] R.E. Azuma et al., Phys. Rev. Lett. **43**, 1652 (1979) .

[84] Z. Kohley et al., Phys. Rev. Lett. **110**, 152501 (2013) .

[85] I. Tanihata, Nucl. Phys. A **478**, 795c (1988) .

[86] M.V. Zhukov et al., Phys. Rep. **231**, 151 (1993) .

[87] P.G. Hansen and B. Jonson, EPL (Europhysics Letters) **4**, 409 (2013) .

[88] N. Auerbach and V. Zelevinsky, Rep. Prog. Phys. **74**, 106301 (2011) .

[89] N. Auerbach, J. Phys. Conf. Ser. **639**, 012010 (2015) .

[90] P. Kleinwächter and I. Rotter, Phys. Rev. C **32**, 1742 (1985) .

[91] J. Okołowicz, M. Płoszajczak and W. Nazarewicz, Prog. Theor. Phys. Supp. **196**, 230 (2012) .

[92] J. Okołowicz, W. Nazarewicz and M. Płoszajczak, Fortschr. Phys. **61**, 66 (2013) .

[93] K. Ikeda, N. Takigawa and H. Horiuchi, Prog. Theor. Phys. Suppl. (Extra number) **464**, (1968) .

[94] H. Feshbach, Theoretical nuclear physics : nuclear reactions (Wiley, New York, 1992).

[95] K. Bennaceur et al., J. Phys. G **24**, 1631 (1998) .

[96] B.A. Loiseau and Y. Nogami, Nucl. Phys. B **2**, 470 (1967) .

[97] R.B. Wiringa et al., Phys. Rev. C **62**, 014001 (2000) .

[98] S.C. Pieper, K. Varga and R.B. Wiringa, Phys. Rev. C **66**, 044130 (2002) .

[99] E. Epelbaum et al., Phys. Rev. C **66**, 064001 (2002) .

[100] P. Navrátil and W.E. Ormand, Phys. Rev. C **68**, 034305 (2003) .

[101] A.P. Zuker, Phys. Rev. Lett. **90**, 042502 (2003) .

[102] T. Otsuka et al., Phys. Rev. Lett. **105**, 032501 (2010) .

[103] G. Hagen et al., Phys. Rev. Lett. **108**, 242501 (2012) .

[104] J. Okołowicz, M. Płoszajczak and I. Rotter, Phys. Rep. **374**, 271 (2003) .

[105] A.M. Lane and R.G. Thomas, Rev. Mod. Phys. **30**, 257 (1958) .

[106] A.M. Lane, Nucl. Phys. **35**, 676 (1962) .

[107] P. Descouvemont and D. Baye, Rep. Prog. Phys. **73**, 036301 (2010) .

[108] P. Dirac, The principles of quantum mechanics (Oxford : Clarendon, 1958).

[109] J. von Neumann, Foundation of quantum mechanics (Princeton university press, Princeton, 1955).

[110] G. Gamow, Z. Phys. **51**, 204 (1928) .

[111] R.G. Newton, Scattering theory of waves and particles (Springer-Verlag, New York Heidelberg Berlin, second edition, 1982).

[112] H.M. Nussenzveig, Causality and dispersion relations (New York : Academic, 1972).

[113] J.R. Taylor, Scattering theory : The quantum theory on nonrelativistic collisions (John Wiley and Sons, Inc., New York, 1972).

[114] W. Domcke, J. Phys. B : At. Mol. Phys. **14**, 4889 (2009) .

[115] V.I. Kukulin, Theory of resonances : Principles and applications (John Wiley and Sons, Inc., New York, 1989).

[116] W.D. Heiss and R.G. Nazmitdinov, Eur. Phys. J. D. **63**, 369 (2011) .

[117] A.B. Migdal, A.M. Perelov and V.S. Popov, Sov. J. Nucl. Phys. **14**, 488 (1972) .

[118] H.M. Nussenzveig, Nucl. Phys. **11**, 499 (1959) .

[119] R. Zavin and N. Moiseyev, J. Phys. A : Math. Gen. **37**, 4619 (2004) .

[120] Z. Ya, Zh. Eksp. Theor. Fiz. **39**, 776 (1960) .

[121] N. Michel, W. Nazarewicz and M. Płoszajczak, Phys. Rev. C **70**, 064313 (2004) .

[122] N. Michel, J. Math. Phys. **49**, 022108 (2008) .

[123] T. Vertse et al., Acta. Phys. Hung. **65**, 305 (1989) .

[124] R.I. Betan et al., Phys. Lett. B **584**, 48 (2004) .

[125] N. Michel et al., Phys. Rev. C **74**, 054305 (2006) .

[126] R.I. Betan et al., Phys. Rev. C **72**, 054322 (2005) .

[127] A. Bürgers and J.M. Rost, J. Phys. B: At. Mol. Opt. Phys. **29**, 3825 (1996) .

[128] N. Hokkyo, Prog. Theor. Phys. **33**, 1116 (1965) .

[129] W.J. Romo, Nucl. Phys. A **116**, 617 (1968) .

[130] G. Garcia-Calderon and R. Peierls, Nucl. Phys. A **265**, 443 (1976) .

[131] B. Gyarmati, Int. Workshop on many-body open quantum systems : From atomic nuclei to quantum dots, (2007) .

[132] W.P. Reinhardt, Ann. Rev. Phys. Chem. **33**, 233 (1982) .

[133] J. Aguilar and J.M. Combes, Commun. Math. Phys. **22**, 269 (1971) .

[134] E. Balslev and J.M. Combes, Commun. Math. Phys. **22**, 280 (1971) .

[135] B. Simon, Commun. Math. Phys. **27**, 1 (1972) .

[136] D. Babbitt and E. Balslev, J. Func. Anal. **18**, 1 (1975) .

[137] B. Gyarmati and T. Vertse, Nucl. Phys. A **160**, 523 (1971) .

[138] B. Simon, Phys. Lett. A **71**, 211 (1979) .

[139] D.D. Lawson, Theory of the nuclear shell model (Clarendon Press, 1980).

[140] Y. Suzuki and K. Ikeda, Phys. Rev. C **38**, 410 (1988) .

[141] C. Lanczos, Journal of Research of the National Bureau of Standards **45**, 255 (1950) .

[142] N. Michel et al., Phys. Rev. C **67**, 054311 (2003) .

[143] E.R. Davidson, J. Comput. Phys. **17**, 87 (1975) .

[144] R.I. Betan et al., Phys. Rev. C **67**, 014322 (2003) .

[145] N. Michel et al., Revista Mexicana De Fisica **50**, 2 SUPPL. 74 (2004) .

[146] N. Michel, W. Nazarewicz and M. Płoszajczak, Nucl. Phys. A **794**, 29 (2007) .

[147] N. Michel, W. Nazarewicz and M. Płoszajczak, Phys. Rev. C **75**, 031301(R) (2007) .

[148] J. Okołowicz et al., Phys. Rev. C **85**, 064320 (2012) .

[149] G. Papadimitriou et al., Phys. Rev. C **84**, 051304(R) (2011) .

[150] R.I. Betan et al., Phys. Lett. B **584**, 48 (2004) .

[151] H. Masui et al., Phys. Rev. C **89**, 044317 (2014) .

[152] K. Suzuki and S.Y. Lee, Prog. Theor. Phys. **64**, 2091 (1980) .

[153] G. Hagen, M. Hjorth-Jensen and J.S. Vaagen, Phys. Rev. C **71**, 044314 (2005) .

[154] G. Hagen, M. Hjorth-Jensen and J.S. Vaagen, J. Phys. G: Nucl. Part. Phys. **31**, S1337 (2005) .

[155] G. Hagen, M. Hjorth-Jensen and N. Michel, Phys. Rev. C **73**, 064307 (2003) .

[156] E. Epelbaum, Prog. Part. Nucl. Phys. **57**, 654 (2006) .

[157] K. Fossez and J. Rotureau, private communication .

[158] N. Michel, G. Papadimitriou and M. Płoszajczak, private communication .

[159] G. Racah, Phys. Rev. **63**, 367 (1943) .

[160] J. Bardeen, L.N. Cooper and J.R. Schrieffer, Phys. Rev. **108**, 1175 (1957) .

[161] D.J. Dean and M. Hjorth-Jensen, Rev. Mod. Phys. **75**, 607 (2003) .

[162] M. Heritier, Nature (London) **414**, 6859 (2001) .

[163] G. Sierra et al., Phys. Rev B **61**, 11890 (2000) .

[164] J. von Delft and D.C. Ralph, Phys. Rep. **345**, 61 (2001) .

[165] J. Dukelsky and P. Schuck, Phys. Rev. Lett. **86**, 4207 (2001) .

[166] J. Dukelsky and S. Pittel, Phys. Rev. Lett. **86**, 4791 (2001) .

[167] J. Dukelsky, C. Esebbag and S. Pittel, Phys. Rev. Lett. **88**, 062501 (2002) .

[168] M. Hasegawa and K. Kaneko, Phys. Rev. C **67**, 024304 (2003) .

[169] M. Gaudin, J. Physique **37**, 1087 (1976) .

[170] J. Dukelsky, C. Esebbag and P. Schuck, Phys. Rev. Lett. **87**, 066403 (2001) .

[171] J. Dukelsky et al., Phys. Rev C **84**, 061301 (2011) .

[172] J. Dukelsky et al., Phys. Rev. Lett **96**, 072503 (2006) .

[173] S. Lerma H. et al., Phys. Rev. Lett. **99**, 032501 (2007) .

[174] R. Id Betan, Phys. Rev. C **85**, 064309 (2012) .

[175] C.N. Yang, Phys. Rev. Lett. **19**, 1312 (1967) .

[176] C.N. Yang, Phys. Rev. **168**, 1920 (1968) .

[177] R.J. Baxter, Exactly Solved Models in Statistical Mechanics (Academic Press, London, 1982).

[178] W. Heisenberg, Z. Phys. **49**, 619 (1928) .

[179] H.A. Bethe, Z. Phys. **71**, 205 (1931) .

[180] J.M. Luttinger, J. Math. Phys. **15**, 609 (1963) .

[181] S. Tomonaga, Prog. Theor. Phys. **5**, 544 (1950) .

[182] F. Calogero, J. Math. Phys. **10**, 2191 (1962) .

[183] B. Sutherland, J. Math. Phys. **12**, 246 (1971) .

[184] J.P. Elliott, Proc. Roy. Soc. (London) A **245**, 128 (1958) .

[185] F. Iachello and A. Arima, The Interaction Boson Model (Cambridge University Press, 1980).

[186] M. Gaudin, États propres et valeurs propres de l'Hamiltonien d'appariement (Les Éditions de Physique, 1995).

[187] M.C. Cambiaggio, A.M.F. Rivas and M. Saraceno, Nucl. Phys. A **624**, 157 (1997) .

[188] J. Dukelsky, J. Okołowicz and M. Płoszajczak, J. Stat. Mech. L07001 (2009) .

[189] S.M.A. Rombouts, J. Dukelsky and G. Ortiz, Phys. Rev. B **82**, 224510 (2010) .

[190] S.M.A. Rombouts, D.V. Neck and J. Dukelsky, Phys. Rev. C **69**, 061303(R) (2004) .

[191] R.W. Richardson, J. Math. Phys. **6**, 1034 (1965) .

[192] R.W. Richardson, Phys. Rev. **141**, 949 (1966) .

[193] J. Dukelsky et al., arXiv:0206016v2 [nucl-th] .

[194] P.W. Anderson, J. Phys. Chem. Solids **11**, 28 (1959) .

[195] D.C. Ralph, C.T. Black and M. Tinkham, Phys. Rev. Lett. **74**, 3241 (1995) .

[196] C.T. Black, D.C. Ralph and M. Tinkham, Phys. Rev. Lett. **76**, 688 (1996) .

[197] I. Giaever and H.R. Zeller, Phys. Rev. Lett. **20**, 1504 (1968) .

[198] J. von Delft et al., Phys. Rev. Lett. **77**, 3189 (1996) .

[199] F. Braun and J. von Delft, Phys. Rev. Lett. **81**, 4712 (1998) .

[200] A. Mastellone, G. Falci and R. Fazio, Phys. Rev. Lett. **80**, 4542 (1998) .

[201] S.D. Berger and B.I. Halperin, Phys. Rev. B **58**, 5213 (1998) .

[202] J. Dukelsky and G. Sierra, Phys. Rev. Lett. **83**, 172 (1999) .

[203] F. Braun and J. von Delft, Phys. Rev. B **59**, 9527 (1999) .

[204] K.A. Matveev and A.I. Larkin, Phys. Rev. Lett. **78**, 3749 (1997) .

[205] A.M. Mukhamedzhanov et al., Phys. Rev. C **84**, 024616 (2011) .

[206] H.A. Bethe, Phys. Rev. **57**, 1125 (1940) .

[207] S. Fernbach, R. Serber and R.B. Taylor, Phys. Rev. **75**, 1352 (1949) .

[208] S. Pasternack and H.S. Snyder, Phys. Rev. **80**, 921 (1950) .

[209] H. Feshbach, Ann. Phys. (N.Y.) **5**, 537 (1958) .

[210] G.E. Brown, Rev. Mod. Phys. **31**, 893 (1959) .

[211] A. Agodi and E. Eberle, Nuovo. Cimento **18**, 718 (1960) .

[212] C. Mahaux and R. Sartor, Adv. Nucl. Phys. **20**, 1 (1991) .

[213] W.H. Dickhoff, EPJ Web of Conferences **122**, 09003 (2016) .

[214] G. Breit, Phys. Rev. **69**, 472 (1946) .

[215] R.G. Newton, Ann. Phys. **4**, 29 (1958) .

[216] E. Rost, Phys. Rev. **154**, 4 (1967) .

[217] N. Bohr, Nature **137**, 344 (1936) .

[218] P.L. Kapure and R.E. Peierls, Proc. Roy. Soc. (London) A **166**, 277 (1938) .

[219] E.P. Wigner and L. Eisenbund, Phys. Rev. **72**, 29 (1947) .

[220] J. Humblet and L. Rosenfeld, Nucl. Phys. **26**, 529 (1961) .

[221] H. Feshbach, Ann. Phys. **43**, 410 (1967) .

[222] M.L. Goldberger and K.M. Watson, Collision theory (Wiley, New York, 1964).

[223] N. Austern, Direct nuclear reaction theories (Wiley, New York, 1970).

[224] J. Rotureau, J. Okołowicz and M. Płoszajczak, Nucl. Phys. A **767**, 13 (2006) .

[225] J.B. Faes and M. Płoszajczak, Nucl. Phys. A **800**, 21 (2008) .

[226] Y. Jaganathen, Thèse de doctorat, Université de Caen (2012) .

[227] Y. Jaganathen, N. Michel and M. Płoszajczak, Phys. Rev. C **89**, 034624 (2014) .

[228] F.D. Grancey et al., Phys. Letters. B **758**, 26 (2016) .

[229] K. Fossez et al., Phys. Rev. C **91**, 034609 (2015) .

[230] G.X. Dong et al., arXiv:1601.06660v1 [nucl-th] .

[231] P. Fröbrich and R. Lipperheide, Theory of nuclear reactions (Clarendon press, Oxford, 1996).

[232] J.A. Wheeler, Phys. Rev. **52**, 1107 (1937) .

[233] Y.C. Tang, M.L. Mere and D.R. Thompson, Phys. Rev. **47**, 167 (1978) .

[234] E.H. Moore, Bull. AMS. **26**, 394 (1920) .

[235] R. Penrose, Proceedings of the Cambridge Philosophical Society **51**, 406 (1955) .

[236] P. Ring and P. Schuck, The Nuclear Many-Body Problem (Springer-Verlag (New York), 1980).

[237] J. Suhonen, From Nucleons to Nucleus, Concepts of Microscopic Nuclear Theory (Springer, 2007).

[238] H. Furutani, H. Horiuchi and R. Tamagaki, Prog. Theor. Phys. **60**, 307 (1978) ; ibid. **62**, 981 (1979) .

[239] J.F. Dicello et al., Phys. Rev. C **4**, 1130 (1971) .

[240] D. Winterhalter, Zeitschrift für Physik **200**, 487 (1971) .

[241] M. Hjorth-Jensen, private communication .

[242] I. Fodor, I. Szentpétery and J. Zimányi, Nucl. Phys. **73**, 155 (1965) .

[243] G.J. KeKelis et al., Phys. Rev. C **17**, 1929 (1978) .

[244] W. Benenson et al., Phys. Rev. C **17**, 1939 (1978) .

[245] W. Peters et al., Phys. Rev. C **68**, 034607 (2003) .

[246] A. Lepine-Szily et al., Nucl. Phys. A **722**, 512c (2003) .

[247] A. Lepine-Szily et al., Nucl. Phys. A **734**, 331 (2004) .

[248] V.Z. Goldberg et al., Phys. Rev. C **69**, 031302(R) (2004) .

[249] F.Q. Guo et al., Phys. Rev. C **72**, 034312(R) (2005) .

[250] H.T. Fortune, Phys. Rev. C **74**, 054310 (2006) .

[251] D. Baye et al., Phys. Rev. C **72**, 024309 (2005) .

[252] A.M. Mukhamedzhanov et al., Phys. Rev. C **81**, 054314 (2010) .

[253] H.T. Fortune and R. Sherr, Phys. Rev. C **72**, 024319 (2005) .

[254] L.V. Grigorenko, T.A. Golubkova and M.V. Zhukov, Phys. Rev. C **91**, 024325 (2005) .

[255] H.T. Fortune, Phys. Rev. C **83**, 024311 (2011) .

[256] L. Canton et al., Phys. Rev. Lett. **96**, 072502 (2006) .

[257] H.T. Fortune and R. Sherr, Phys. Rev. Lett. **99**, 089201 (2007) .

[258] I. Mukha et al., Phys. Rev. C **79**, 031301 (2009) .

[259] F.D. Grancey, Thèse de doctorat, Université de Caen (2009) .

[260] M. Assié et al., Phys. Lett. B **712**, 198 (2012) .

[261] E. Berthoumieux et al., Nucl. Instr. and Meth. B, **55**, 136 (1998) .

[262] G. Hagen et al., Phys. Rev. Lett. **109**, 032502 (2012) .

[263] A. Ekström et al., Phys. Rev. C **91**, 051301(R) (2015) .

[264] S.R. Stroberg et al., Phys. Rev. C **93**, 051301(R) (2016) .

[265] Y. Luo et al., arXiv:0211068v1 [nucl-th] .

[266] A. Gade et al., Phys. Rev. Lett. **93**, 042501 (2004) .

[267] A. Gade et al., Phys. Rev. C **77**, 044306 (2008) .

[268] F. Flavigny et al., Phys. Rev. Lett. **110**, 122503 (2013) .

Titre : Réactions nucléaires dans le modèle en couches de Gamow et solutions de l'Hamiltonien d'appariement basées sur le modèle rationnel de Gaudin

Au voisinage de la limite de stabilité, ou à haute énergie d'excitation, l'influence du continuum devient de plus en plus importante, modifiant ainsi la structure des états faiblement liés. Dans cette région, les noyaux sont des systèmes quantiques ouverts qui peuvent être décrits correctement avec le *Gamow Shell Model* (GSM) offrant une description unifiée des états liés, des résonances et des états de diffusion.

La compréhension de propriétés nucléaires induites par certaines symétries du système à plusieurs corps, peut être approfondie en considérant des modèles exactement solubles. Dans la première partie, nous avons généralisé l'Hamiltonien d'appariement basé sur le modèle rationel de Gaudin aux états du continuum, et dérivé la solution algébrique qui généralise la solution exacte de Richardson initialement introduite pour les systèmes liés. Ces équations de Richardson généralisées ont ensuite été appliquées à l'étude des spectres et des énergies de liaison dans une chaîne d'isotopes de carbone.

Dans la deuxième partie, nous avons formulé une théorie des réactions basée sur le GSM. Dans ce but, le GSM est formulé dans une base de canaux de réaction pour les projectiles à plusieurs nucléons. Cette théorie des réactions prend en compte l'antisymétrisation des fonctions d'onde de cible et de projectile, ainsi que la fonction d'onde du système composé. Les applications de cette théorie sont présentées pour la réaction ^{14}O(p,p')^{14}O, où le système composé ^{15}F est un émetteur de proton, et pour la réaction ^{40}Ca(d,d)^{40}Ca.

Mots-clés : Structure nucléaire, réactions nucleaire, Gamow shell model, Hamiltonien d'appariement, réactions directes, sections efficaces.

Title : Nuclear reactions in the Gamow shell model and solutions of the pairing Hamiltonian based on the rational Gaudin model

Moving towards drip lines, or higher in excitation energy, the continuum coupling becomes gradually more important, changing the nature of weakly bound states. In this regime, atomic nuclei are open quantum systems which can be conveniently described using the Gamow shell model (GSM) which offers a fully symmetric treatment of bound, resonance and scattering states.

The understanding of specific nuclear properties is often improved by considering exactly solvable models, motivated by a symmetry of the many-body system. In the first part , we have generalized the rational Gaudin pairing model to include the continuous part of the single-particle spectrum, and then derived a reliable algebraic solution which generalizes the exact Richardson solution for bound states. These generalized Richardson solutions have been applied for the description of binding energies and spectra in the long chain of carbon isotopes.

In the second part, we have formulated the reaction theory rooted in GSM. For that the GSM is expressed in the basis of reaction channels and generalized for multi-nucleon projectiles. This reaction theory respects the antisymmetrization of target and projectile wave functions, as well as the wave function of the combined system. The application of this theory have been presented for the reaction ^{14}O(p,p')^{14}O, where the combined system ^{15}F is a proton emitter, and for ^{40}Ca(d,d)^{40}Ca.

Keywords : Nuclear structure, nuclear reactions, Gamow shell model, pairing Hamiltonian, direct reactions, cross sections.